UNIVERSIDAD DE JAÉN

ESCUELA POLITÉCNICA SUPERIOR DE JAÉN
DEPARTAMENTO DE INGENIERÍA ELECTRÓNICA Y AUTOMÁTICA

TESIS DOCTORAL

CONTRIBUCIÓN AL DESARROLLO DE SISTEMAS FOTOVOLTAICOS DE ALTA CONCENTRACIÓN. ANÁLISIS DE NUEVAS CONFIGURACIONES DE MÓDULOS

PRESENTADA POR:
JUAN PABLO FERRER RODRÍGUEZ

DIRIGIDA POR:
DR. D. PEDRO JESÚS PÉREZ HIGUERAS
DR. D. EDUARDO FERNÁNDEZ FERNÁNDEZ

JAÉN, 27 DE ABRIL DE 2018

ISBN 978-84-9159-206-8

Universidad de Jaén

TESIS DOCTORAL

CONTRIBUCIÓN AL DESARROLLO DE SISTEMAS FOTOVOLTAICOS DE ALTA CONCENTRACIÓN. ANÁLISIS DE NUEVAS CONFIGURACIONES DE MÓDULOS

AUTOR

JUAN PABLO FERRER RODRÍGUEZ

DIRECTORES

DR. PEDRO JESÚS PÉREZ HIGUERAS

DR. EDUARDO FERNÁNDEZ FERNÁNDEZ

CENTRO DE ESTUDIOS AVANZADOS EN ENERGÍA Y MEDIO AMBIENTE

GRUPO IDEA, INVESTIGACIÓN EN ENERGÍA SOLAR

DEPARTAMENTO DE INGENIERÍA ELECTRÓNICA Y AUTOMÁTICA

JAÉN, ABRIL 2018.

Universidad de Jaén

TESIS DOCTORAL

CONTRIBUCIÓN AL DESARROLLO DE SISTEMAS FOTOVOLTAICOS DE ALTA CONCENTRACIÓN. ANÁLISIS DE NUEVAS CONFIGURACIONES DE MÓDULOS

AUTOR

JUAN PABLO FERRER RODRÍGUEZ

DIRECTORES

DR. PEDRO JESÚS PÉREZ HIGUERAS

DR. EDUARDO FERNÁNDEZ FERNÁNDEZ

TRIBUNAL

Presidente: Dr. Pedro Manuel Rodrigo Cruz (Universidad Panamericana, México)
Secretaria: Dra. Florencia Almonacid Cruz (Universidad de Jaén)
Vocal: Dr. Antonio García Loureiro (Universidad de Santiago de Compostela)
Suplente: Dra. Natalia Seoane Iglesias (Universidad de Santiago de Compostela)
Suplente: Dr. Gustavo E. Nofuentes Garrido (Universidad de Jaén)

UNIVERSIDAD DE JAÉN

CENTRO DE ESTUDIOS AVANZADOS EN ENERGÍA Y MEDIO AMBIENTE

GRUPO IDEA, INVESTIGACIÓN EN ENERGÍA SOLAR

DEPARTAMENTO DE INGENIERÍA ELECTRÓNICA Y AUTOMÁTICA

TESIS DOCTORAL

La memoria titulada: “Contribución al desarrollo de los sistemas fotovoltaicos de alta concentración. Análisis de nuevas configuraciones de módulos” ha sido desarrollada en el Centro de Estudios Avanzados en Energía y Medio Ambiente (CEAEMA), en el Grupo IDEA, Investigación en Energía Solar, dentro del Departamento de Ingeniería Electrónica y Automática de la Universidad de Jaén, y es presentada por el aspirante al título de Doctor en Energías Renovables, Juan Pablo Ferrer Rodríguez, bajo la dirección del Dr. Pedro J. Pérez Higueras y el Dr. Eduardo Fernández Fernández.

Jaén, abril 2018

El doctorando

Fdo. Juan Pablo Ferrer Rodríguez

Los directores de la Tesis

Fdo. Dr. Pedro J. Pérez Higueras Fdo. Dr. Eduardo Fernández Fernández

AGRADECIMIENTOS

Agradezco a Eduardo Fernández y a Pedro Pérez que me dieran la oportunidad de realizar una investigación para una tesis doctoral en este campo tan interesante como es la energía solar fotovoltaica de alta concentración.

Agradezco a todos los profesores y compañeros del Departamento de Ingeniería Electrónica y Automática y del CEAEMA, ya que con ellos los que he podido colaborar gratamente.

Agradezco a mi familia todo el esfuerzo para conseguir la mejor formación desde la escuela hasta la Universidad.

Agradezco a Victoria su paciencia y apoyo durante la Tesis.

Agradezco a Alberto Soria el compartir la aventura por la energía solar cuando la comenzamos en el Fraunhofer ISE, donde aprendimos tanto e hicimos tan buenas amistades.

I also want to thank the colleagues in the University of Exeter (Penryn) for their support during my research stay.

ÍNDICE

CONTRIBUTION TO THE DEVELOPMENT OF HIGH CONCENTRATOR PHOTOVOLTAIC SYSTEMS. ANALYSIS OF NEW MODULE CONFIGURATIONS.

1. *Abstract*

The end of the fossil fuels era will be one of the biggest challenges of Humanity to be confronted. However, a lot of effort is currently ongoing worldwide to develop new renewable energy technologies (solar, wind, biofuels, etc.). Also, different technologies are being developed for energy carriers (hydrogen), energy storage (flow batteries, supercapacitors, etc.) and "e-mobility" (electric vehicle network). All of these efforts are aimed at a new era free of fossil fuels. The Photovoltaic (PV) technology is expected to play an important role in this scenario.

The PV technology diversifies in many different technologies (Silicon, Thin Film, Organic PV, Concentrator PV, etc.). Among all the PV technologies, the High Concentrator Photovoltaics (HCPV, with concentrations higher than 100 suns) retains the highest solar-to-electrical conversion efficiencies. Additionally, the HCPV modules are recognised for their potential for a significant efficiency growth –especially due to the increase in the efficiency of the concentrator solar cells. This Doctoral Thesis is intended to be a contribution to the development of the HCPV technology by focusing on the HCPV modules and on the improvement of their configurations, especially from the point of view of the concentrator optics.

Firstly, the analysis of the HCPV modules technology is addressed. The most important performance parameters of the HCPV modules, i.e. efficiency and acceptance angle are analysed for the current commercial HCPV modules. The evolution of the efficiency of the HCPV modules in the last 20 years is compared to other PV technologies (crystalline-Silicon and Thin Film). This is found to be maximal for the HCPV modules, with a growth of +0.83%/year. Although efficiency records of HCPV modules are around 43%, current commercial HCPV modules present efficiencies up to around 34%. Regarding the acceptance angle, current commercial HCPV modules present values of $\pm 0.9^{o}$ on average. Their geometrical concentrations are in the range between 500× and 1000×. In order to compare datasheet values of commercial HCPV modules with experimental ones, a total of 24 commercial HCPV modules were characterised indoors in a CPV Solar Simulator at the University of Jaén. The experimental results matched those provided by the manufacturers for both efficiency and acceptance angle values.

HCPV modules were also analysed from the point of view of their electrical behaviour with respect to the incoming light, specifically with respect to the irradiance level. Two commercial Fresnel-based HCPV modules were indoors characterised in the CPV Solar Simulator under controlled conditions for different irradiance levels in the range 700−1000 W/m^2, while the spectral conditions of the simulated light were maintained constant and equivalent to the reference spectrum. The irradiance (*DNI*) was demonstrated to be the main driver of the I-V characteristics of the HCPV modules: all the characteristic parameters of the I-V curve can be approximated by simple functions of the *DNI*. The parameters of the current-voltage (I-V) characteristics, as well as the five characteristic parameters of the single exponential model (SEM) were analysed as a function of the irradiance. SEM parameters showed that the photogenerated current (I_{ph}) increased linearly with the irradiance. In the cases of the ideality factor (m) and the saturation current (I_o), both resulted stable with *DNI*. On the other hand, both parasitic resistances, series and shunt resistance (R_s y R_{sh}), decreased with *DNI*.

Economic aspects related to the HCPV installations were analysed. The feasibility of the investments in HCPV systems (of 1 MWp) were analysed through the calculation of the levelised cost of electricity (*LCOE*), since the *LCOE* is a common parameter to compare different energy generation systems. The $LCOE_{HCPV}$ (for a HCPV system) was estimated for a total of 133 countries for the year 2014. The regions with lowest $LCOE_{HCPV}$, in the range 5-10 c€/kW·h, were: North America, Chile, Australia, North and South Africa, and South of Europe. The $LCOE_{HCPV}$ was compared to the price of the electricity in the domestic segment in order to analyse the grid parity. The results showed that grid parity was already achieved in Spain, Italy, Greece, France, or even in Sweden, Denmark or Ireland, among other countries. In addition, a forecast for the year 2020 related to the *LCOE* of both HCPV and conventional systems was performed, showing the investment in HCPV systems was more favourable than in conventional PV systems in the MENA region (Middle East and North Africa), the South of Africa and South America.

Regarding the improvement of the concentrator optical systems, a powerful optical modelling was developed. This optical modelling included many wavelength-dependent material properties, such us refractive index, absorption coefficient, spectral response of solar cell, etc. Solar spectrum and angular distribution were also considered. It was applied to four Fresnel-based HCPV units equipped with refractive secondary optical elements (SOEs). These SOEs were: (i) DCCPC (*dielectric-cross compound-parabolic-concentrator*), (ii) SILO-Pyramid, (iii) RTP (*refractive truncated pyramid*), and (iv) Trumpet. As output of the optical modelling, the short-circuit current density of each subcell ($J_{sc,subcell}^{conc}$) was obtained, and using that, the optical polychromatic efficiency of

each HCPV was calculated. Using the $J_{sc,subcell}^{conc}$ values of each HCPV unit, an analysis in terms of *SMR* (spectral matching ratio) was conducted. It was concluded that in any situation, none of the HCPV units produced concentrated light with a spectral distribution equivalent to the reference spectrum. Concerning the optical efficiencies, all the SOEs resulted in 81-83.4%, and the acceptance angles in ±0.96-1.13º. Regarding the $J_{sc,subcell}^{conc}$ distributions, the SOEs RTP and Trumpet performed best. Considering all the simulation results, the RTP unit showed the best trade-off among them all.

Four Fresnel-based HCPV units were mounted for their characterisation in the CPV Solar Simulator. The four modelled SOEs were fabricated in PMMA (through precision machining), whereas Fresnel lens and concentrator solar cells were commercial products. I-V curves were acquired for different conditions of irradiance, spectrum and incoming angle of the light. The measured electrical efficiencies, under reference conditions, were in the range 25.5-28.2%, with effective concentrations of 403-427 suns. The SOE RTP presented the best trade-off of results considering efficiency and acceptance angle. In general, experimental results were similar to simulated ones, especially for the optical efficiencies of the SOEs. The main divergences between experiment and simulation were found in the case of the (commercial) Fresnel lens (with 8% less optical efficiency) and the acceptance angle curves of some HCPV units, specifically in the case of the DCCPC SOE. Analysing the influence of spectrum and irradiance in the acceptance angle of the HCPV units, these performed in a stable way. Among the electrical parameters of the I-V characteristics in relation to the irradiance, only V_{oc} showed a clear tendency (logarithmic). In relation to spectral changes of the incoming light, only the efficiency exhibited a slight reduction up to 3.7% for blue-rich spectra.

Finally, an ultra-high CPV (UHCPV, with concentrations higher than 1000 suns) module optical design was presented. It consisted in a modification of the Cassegrain design, by using four different and independent optical units that focus sunlight onto a central common receiver. Each unit consisted of a paraboloid-hyperboloid pair whose optical axes were not parallel. The geometrical concentration was fixed to 2304×. The optical simulation results were similar to those of conventional Cassegrain designs. The optical efficiency was 73% (without considering antireflective coatings), resulting in an effective concentration ratio of 1682 suns. By removing the glass cover, the optical efficiency was 79%. The acceptance angle was simulated to be 0.61º, with a *CAP* value of 0.51.

2. Introducción

En el sistema energético mundial, actualmente, las principales fuentes de energía primaria son los llamados combustibles fósiles (petróleo, carbón, gas natural…). Dichos combustibles fósiles no se consideran una fuentes de energía renovable, pues su formación se produjo hace millones de años. Ello implica una futura escasez de recursos energéticos a medio y largo plazo, dada su limitación. Por otro lado, la utilización energética de los combustibles fósiles supone la principal fuente de emisiones de dióxido de carbono a la atmósfera. Dichas emisiones han aumentado el llamado efecto invernadero hasta el punto de provocar un cambio climático mundial por causa antropogénica [1]. Además, los gases emitidos por la combustión de los recursos energéticos fósiles son muy tóxicos para los seres vivos, provocando numerosas enfermedades en las personas, especialmente en las grandes ciudades [2].

Como solución a dichos problemas inherentemente asociados a los combustibles fósiles, se presentan las energías renovables (solar, eólica, hidráulica, etc.). Dichas fuentes de energía son obtenidas, principalmente, como consecuencia del vasto flujo de energía del Sol que globalmente incide en la superficie de la Tierra. Por tanto, la fuente inicial energética es un recurso no agotable.

Dentro de las energías renovables, la energía solar fotovoltaica supone el aprovechamiento de un recurso ampliamente disponible en casi todas las regiones del mundo, lo cual contribuye, además, a eliminar tensiones territoriales por el acceso al recurso energético. Más aún, supone una conversión directa de la radiación solar en electricidad, sin necesidad de usar máquinas grandes o complejas (como turbinas). Actualmente se trata de una fuente de energía que puede ser competitiva, si bien su implantación no se ha generalizado ampliamente a nivel mundial aún (cubre un 1.3% de la demanda eléctrica global [3]).

La tecnología de alta concentración fotovoltaica (HCPV, *High Concentrator PhotoVoltaics*) es una variante de la tecnología fotovoltaica que se basa en aumentar la irradiancia sobre las células solares. Se entiende por HCPV cuando el sistema óptico es capaz de concentrar al menos 100 veces la luz sobre la célula solar [4, 5]. Ello conlleva una reducción del área de semiconductor necesaria, que debe propiciar el abaratamiento de costes de producción para instalaciones en lugares con altas irradiancias anuales.

El potencial de la tecnología HCPV se basa en dos aspectos fundamentales, por un lado, la eficiencia de las células solares de concentración no ha parado de aumentar en

los últimos años [6], por otro lado, los sistemas ópticos concentradores siguen mejorando sus prestaciones (concentración, compacidad, etc.) [7, 8].

Atendiendo a la realidad de la tecnología HCPV, su implantación mundial tan solo llega a unos 370 MWp de instalaciones conectadas a red [9], mientras que, por ejemplo, en el año 2016 solo se instalaron algo más de 15 MWp a nivel mundial. Ello es debido, principalmente, a la competencia por parte de la tecnología fotovoltaica convencional. El coste nivelado de la producción de electricidad (*LCOE*) de una instalación, en este caso de tipo HCPV, es un parámetro utilizado para comparar diferentes tipos de instalaciones productoras de electricidad. El *LCOE* es el coste teórico constante de producción de cada unidad de energía (1 kW·h) de la instalación de producción de energía durante toda su vida útil. Actualmente el *LCOE* para instalaciones HCPV en lugares con valores altos de irradiancia (>2000 kW·h/kWp·año) y con reducidos costes de financiación es alrededor de 5-10 c€/kW·h [10]. Sin embargo, este valor debe ser reducido para propiciar una mayor implantación de la tecnología HCPV.

Con respecto a las instalaciones HCPV, éstas suelen utilizar sistemas de seguimiento a dos ejes para garantizar el continuo apuntamiento de los módulos HCPV hacia los rayos solares. Los seguidores solares son un componente fundamental de una instalación HCPV y están basados en sistemas electro-mecánicos, aunque no participan activamente de la conversión de energía solar en electricidad [11, 4]. Su coste está relacionado con las exigencias impuestas por las necesidades de precisión de apuntamiento de los módulos HCPV. Es por ello que los módulos HCPV, con mayores tolerancias de desapuntamiento (mayor aceptancia angular), y menores peso y tamaño, requerirán seguidores solares de menor coste.

En cuanto a los módulos HCPV, son muy diversos en su diseño, aunque básicamente consisten en una caja cerrada que contiene las pequeñas células fotovoltaicas de concentración, los sistemas ópticos concentradores, y el resto de componentes eléctricos, térmicos y mecánicos necesarios para evacuar la electricidad y el calor, y alojar todos los elementos de forma segura y protegida de los fenómenos atmosféricos (lluvia, granizo, polvo…) [4]. Con respecto de los elementos eléctricos, además de los cables de conexión entre células solares y los terminales del módulo HCPV, también suelen usarse diodos de paso para evitar el sobrecalentamiento de células. Además, el exterior del módulo HCPV debe estar suficientemente aislado eléctricamente de los componentes interiores. En relación a los elementos térmicos, los módulos HCPV suelen disponer de elementos pasivos de refrigeración de las células solares, como por ejemplo, radiadores de aletas. En la Figura 1 puede verse un esquema de un módulo HCPV.

Para propiciar la implantación a mayor escala de la tecnología de HCPV es necesario mejorar los módulos HCPV. Éstos, en comparación con los módulos fotovoltaicos

convencionales, tienen una profundidad y peso muy superiores, ya que tienen que albergar los sistemas ópticos concentradores, además de las células solares, cableado, etc. El análisis de los módulos HCPV se realiza fundamentalmente a través de sus características I-V (corriente-voltaje), mientras que para analizar las células fotovoltaicas, el modelo SEM (*single exponential model*) proporciona cinco parámetros que se relacionan con los de las características I-V [12]. Estos modelos circuitales describen el comportamiento de las células solares a nivel de propiedades fundamentales de los semiconductores, como p.ej. la corriente de saturación, o las resistencias parásitas.

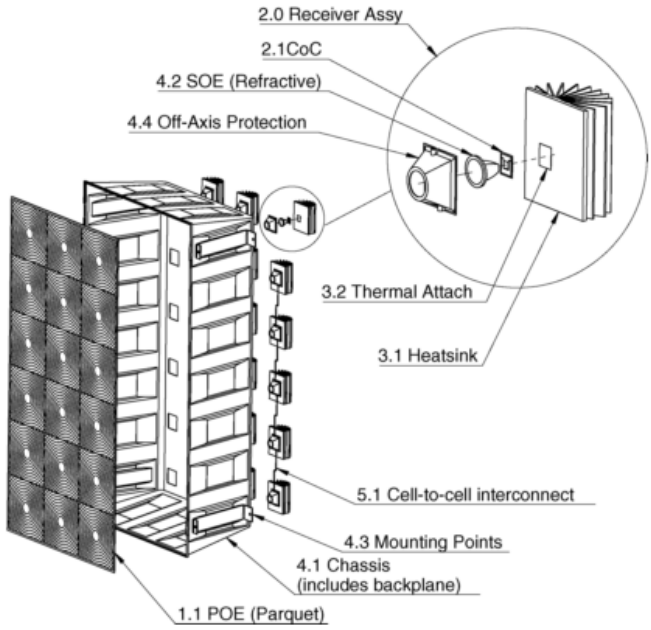

Figura 1. Esquema de componentes de un módulo HCPV [5].

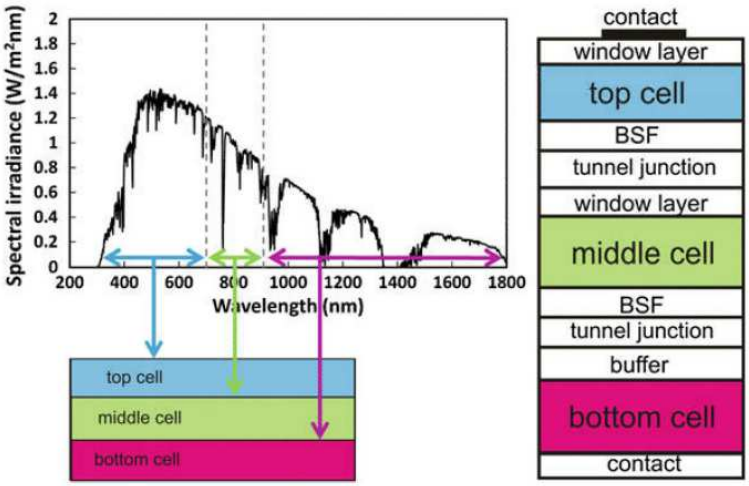

Figura 2. A la izquierda, espectro de radiación solar terrestre y rangos típicos de longitud de onda para cada subcélula de una célula solar de triple-unión (TJ). A la derecha, esquema típico de capas que forman una célula solar TJ [4].

Las células solares empleadas en los módulos HCPV son típicamente de triple-unión (TJ, *triple-junction*). Dichas células alcanzan un 44.4% de eficiencia, aunque incluso ese valor es superado por células de cuatro uniones p-n, llegando a un 46.0% de eficiencia [6]. Para el caso de las células TJ, se muestran en la Figura 2 los rangos de longitud de onda para los que es sensible cada subcélula (‘*top*’, superior; ‘*mid*’, media; ‘*bot*’, inferior) [4]. También se muestra el esquema de capas que forman una célula TJ típica. Las células solares TJ de los módulos HCPV suelen ser cuadradas y de entre 5 mm y 10 mm de lado.

La luz debe ser concentrada sobre dichas células TJ, ya que el precio de las mismas es demasiado elevado como para no utilizar un sistema óptico concentrador. Los sistemas ópticos concentradores consiguen focalizar los rayos solares sobre las células TJ. Para ello se pueden utilizar tanto lentes convergentes como espejos cóncavos, es decir, sistemas con un foco real. En el caso de las lentes, las más utilizadas son las lentes de Fresnel. Las lentes de Fresnel se utilizan con la idea de eliminar material interior de la lente, el cual no es necesario para la focalización de los rayos solares, ya que esto es solamente una consecuencia de la forma de las superficies exteriores de la lente [13, 14]. En la Figura 3 se puede ver un corte transversal de una lente de Fresnel con simetría rotacional. Los dientes resultan en anillos de sección cónica al revolucionar con respecto del eje focal de la lente. Las lentes de Fresnel suelen ser de, o bien de PMMA (polimetilmetacrilato), o bien de silicona adherida a vidrio (SoG, ‘*silicon on glass*’) [15]. En cualquiera de los casos, las lentes producen, en general, aberraciones cromáticas, las cuales reducen las posibilidades de concentración de la luz [7].

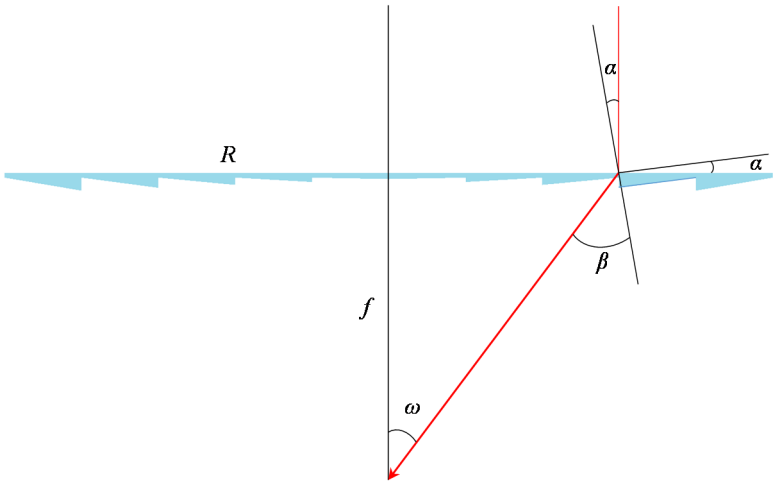

Figura 3. Esquema para el cálculo bidimensional de los dientes de una lente de Fresnel. Aplicando trigonometría y la ley de Snell, se puede determinar el ángulo α *de cada diente para una distancia focal* f *y un radio* R *de lente determinados. En rojo, un rayo solar incidente y focalizado posteriormente.*

En el caso de los concentradores basados en espejos, el ejemplo más básico lo constituye el espejo parabólico, el cual concentra los rayos solares en su punto focal [16]. Los sistemas basados en espejos no producen aberraciones cromáticas, aunque no

están exentos de producir otros tipos de aberraciones ópticas. Los sistemas más típicos basados en espejos son los de tipo Cassegrain, los cuales combinan un espejo primario parabólico cóncavo con un espejo secundario hiperbólico convexo [17, 18]. En la Figura 4 puede verse un esquema típico de un concentrador HCPV de tipo Cassegrain, en donde se tiene un espejo primario, un espejo secundario y una célula solar. Los concentradores basados en espejos son propicios para alcanzar concentraciones ultra-altas (UHCPV, más de 1000 soles, 1 sol = 1000 W/m^2) ya que no presentan aberraciones cromáticas.

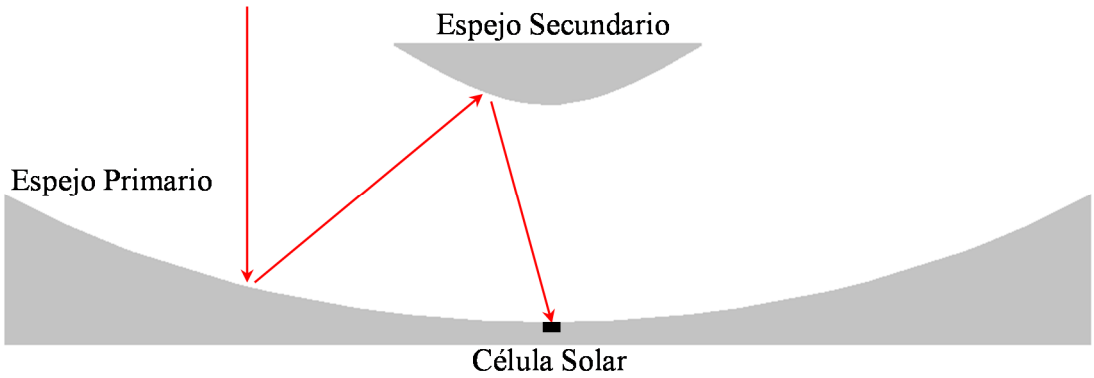

Figura 4. Esquema básico de un concentrador Cassegrain. En rojo, un rayo solar incidente en el módulo HCPV y focalizado posteriormente sobre la célula solar.

3. Justificación

Como se ha comentado en la Introducción, la tecnología fotovoltaica de alta concentración (HCPV) es un tipo de tecnología solar fotovoltaica con un alto potencial de implantación. No obstante, esta tecnología no ha cumplido con las expectativas de mercado en los últimos años (la mayoría de las empresas fabricantes han cesado la actividad), debido a la competencia de la tecnología solar fotovoltaica convencional. Sin embargo, para localizaciones con abundante radiación solar directa, la tecnología HCPV puede ser competitiva [10]. Esta Tesis pretende ser una contribución al desarrollo de la tecnología HCPV desde el enfoque de los módulos fotovoltaicos.

Para lograr dicha finalidad, es necesario, en primer lugar hacer un análisis detallado de la tecnología actual de los módulos HCPV. La información disponible sobre los módulos HCPV es limitada, en gran parte, debido al secreto industrial de las empresas fabricantes (las hojas de especificaciones técnicas no aportan todos los datos útiles sobre su funcionamiento). Además, la información disponible en publicaciones (libros, revistas científicas, etc.) suele ser específica de algunos aspectos del funcionamiento de los módulos HCPV. Es por ello que el análisis propuesto permitirá conocer las características principales de los módulos HCPV de forma general y además servirá para poder comparar los diferentes diseños comerciales bajo los mismos criterios.

No solamente es necesario analizar los módulos HCPV desde un punto de vista técnico, sino también desde un punto de vista económico. De esta forma, será posible obtener una visión más completa de la tecnología de módulos HCPV que propicie así aumentar su implantación mundialmente. Un parámetro económico clave para comparar diversas fuentes de energía según su coste es el *LCOE* [10]. Así, el cálculo del coste nivelado de la producción energía solar HCPV tiene que ser analizado en detalle. Ello es debido a que no solamente influyen en el *LCOE* de una instalación HCPV los costes asociados a la tecnología en sí (como el coste total de los módulos, de los seguidores solares, etc.), sino que también son cruciales parámetros relacionados con el recurso solar y con los condicionantes económicos de cada país. Aparte de estos condicionantes económicos, el conocimiento sobre el *LCOE* aporta las claves sobre qué es necesario mejorar de la tecnología de módulos HCPV para reducirlo.

Desde el punto de vista de los sistemas ópticos, se encuentran tres características necesarias para propiciar la reducción del *LCOE*. En primer lugar, es necesario aumentar la energía total anual producida por una instalación HCPV, y ello es posible mediante el aumento de la eficiencia y de la aceptancia angular de los sistemas ópticos concentradores. Por otro lado, es necesario aumentar el nivel de concentración de los

módulos HCPV, pues ello permite reducir la cantidad empleada de semiconductor y el coste en módulos fotovoltaicos.

En cuanto a la mejora de la eficiencia y aceptancia angular de los módulos HCPV, es necesario optimizar los diseños de los elementos ópticos secundarios (SOE, *secondary optical element*, comúnmente denominados 'secundarios'). Dichos SOEs típicamente son de tipo refractivo y están en contacto con la célula solar, o muy próximos a la misma. Los SOEs, por un lado, aumentan la concentración captando más rayos solares concentrados (funcionando como lentes y/o guías de luz), y por otro lado, aumentan la tolerancia óptica del concentrador con respecto al alineamiento con los rayos solares incidentes. Para poder realizar la optimización de los SOEs, es necesario tener en cuenta las no idealidades más importantes en cuanto a la interacción de la luz con los materiales. Ello permitirá realizar diseños más realistas. Dichos efectos no ideales, especialmente aquellos basados en las propiedades dependientes de la longitud de onda (índice de refracción, coeficiente de absorción, respuesta espectral de la célula, etc.), no suelen ser tenidos en cuenta en la mayoría de publicaciones científicas relacionadas. El desarrollo de un modelado óptico con esas características para los típicos sistemas concentradores ha de servir de base para el diseño optimizado de diferentes SOEs. Además ello provee de los elementos para el modelado más exhaustivo de las características de los módulos HCPV.

Asimismo, es necesario un desarrollo experimental basado en tal modelado óptico que permita verificar los supuestos del análisis teórico de los módulos HCPV. La fabricación, ensamblaje y caracterización de los SOEs formando parte de diferentes unidades HCPV, bajo las mismas condiciones controladas y repetitivas era un trabajo aún pendiente de desarrollar con una profundidad de detalle como en la de esta Tesis. Para obtener resultados de los módulos HCPV a condiciones constantes de irradiancia sin variar sus condiciones espectrales, y viceversa, para condiciones constantes espectrales variando la irradiancia, es necesario utilizar un simulador solar para módulos de concentración, como lo es el del Centro de Estudios Avanzados en Energía y Medio Ambiente (CEAEMA).

Con respecto al aumento de los niveles de concentración como estrategia para reducir el *LCOE* de las instalaciones HCPV, una estrategia es superar la barrera de los 1000 soles de concentración de las típicas lentes de Fresnel, alcanzando las concentraciones ultra-altas (UHCPV). Nuevos diseños basados en otro tipo de sistemas concentradores son necesarios, ya que los actuales no alcanzan concentraciones ultra-altas. En concreto, se dispone una posibilidad manifiesta para conseguirlo con el uso de ópticas reflexivas. Los sistemas basados en el diseño tipo Cassegrain, con un espejo primario parabólico y otro secundario hiperbólico, permiten alcanzar tales

concentraciones. Por otro lado, es necesario explorar diseños basados en la focalización de haces de luz provenientes de diferentes unidades ópticas para alcanzar niveles superiores de concentración. Aunque hay diversos diseños publicados con esas características para concentradores con óptica primaria de lentes de Fresnel, no se habían desarrollado tales concentradores mediante elementos reflexivos.

4. Objetivos

El objetivo de esta Tesis Doctoral es realizar una aportación para el avance de la fotovoltaica de alta concentración, haciendo énfasis en nuevos diseños de módulos HCPV para mejorar la tecnología. Este objetivo general se desarrolla a través de varios objetivos específicos, realizando contribuciones a la tecnología HCPV bien a nivel de módulo HCPV, bien a nivel de costes de los sistemas HCPV, bien a nivel de mejoras de los sistemas ópticos concentradores convencionales (elementos ópticos secundarios), o bien a nivel de diseños ópticos de sistemas concentradores no convencionales (alcanzando concentraciones ultra-altas). Los objetivos específicos son los siguientes:

1. Analizar el estado de la tecnología de módulos fotovoltaicos de alta concentración.
2. Analizar la viabilidad económica de la tecnología fotovoltaica de alta concentración a nivel mundial.
3. Modelar, diseñar y caracterizar elementos ópticos secundarios.
4. Realizar un diseño óptico para concentraciones ultra-altas.

Los objetivos específicos se desarrollan a continuación:

Objetivo nº1. Analizar el estado de la tecnología de módulos fotovoltaicos de alta concentración

Debido a la escasez de información sistemática sobre las características fundamentales de los módulos HCPV comerciales actuales, tanto a nivel de literatura científica como a nivel de hojas comerciales con características técnicas de los módulos HCPV, resulta necesario hacer un estudio sobre los mismos. La finalidad principal de este Objetivo nº1 es aportar información detallada sobre la eficiencia y aceptancia angular de los módulos HCPV comerciales actuales. Asimismo se pretende hacer un análisis histórico de la evolución de los módulos HCPV.

Por otro lado, para complementar la información recopilada, se aportarán datos experimentales sobre una serie de módulos HCPV comerciales disponibles en la Universidad de Jaén, que serán caracterizados bajo condiciones controladas en el Simulador Solar CPV 'Helios 3198'. El objetivo de dicha caracterización será, entre otros, cotejar la información comercial de dichos módulos HCPV con datos reales.

Dentro del Objetivo nº1, se plantea también el análisis de los parámetros eléctricos de las características corriente-voltaje (I-V) de los módulos HCPV comerciales. En

concreto, se espera encontrar las relaciones de los parámetros más importantes en función de la irradiancia, ya que se trataba de un análisis poco explorado en la literatura. Además, se estudiará la aplicación de algún modelo circuital, como es el modelo SEM (*single exponential model*), para aplicarlo al funcionamiento de los módulos HCPV. Para conseguir este objetivo se utilizarán datos experimentales de módulos HCPV obtenidos bajo condiciones controladas en el Simulador Solar CPV.

Objetivo nº2. Analizar la viabilidad económica de la tecnología fotovoltaica de alta concentración a nivel mundial

El objetivo fundamental de la tecnología HCPV es reducir el coste de generación de electricidad solar fotovoltaica, disminuyendo la cantidad de semiconductor empleada. El parámetro convencional para evaluar el coste de generación de electricidad es el *LCOE* (*Levelised Cost of Electricity*), en español, coste nivelado de la electricidad. Este parámetro hace referencia al coste teórico constante de producción de cada unidad de energía (1 kW·h), de una instalación de producción de energía durante toda su vida útil.

Debido a la drástica disminución de los precios de los módulos fotovoltaicos convencionales (con células solares de silicio y sin sistemas ópticos de concentración), el mercado de la tecnología HCPV ha quedado muy reducido en los últimos años. No obstante, se analizarán las posibles oportunidades de la tecnología HCPV para ser competitiva (a través del *LCOE*) en diferentes regiones del planeta.

En este Objetivo nº2 se pretende realizar un estudio a nivel mundial sobre la factibilidad de la inversión en los sistemas HCPV (de 1 MWp) a través del cálculo del *LCOE* de los sistemas HCPV. En ese marco, además se analizará la paridad de red en los países considerados. Con toda la información obtenida, se presentarán diversos mapas mundiales por países que aporten información directa relevante sobre la factibilidad de los sistemas HCPV, para utilidad de futuros inversores, propietarios y entidades financieras.

Objetivo nº3. Modelar, diseñar y caracterizar elementos ópticos secundarios

Los sistemas ópticos concentradores de los módulos HCPV necesitan del uso de elementos ópticos secundarios (SOE), acoplados a la célula solar, para lograr dos requisitos fundamentales: (a) mejorar la tolerancia a desapuntamientos (aceptancia angular) del módulo y, (b) mejorar la uniformidad de la luz concentrada que ilumina la célula solar. Por tanto, la utilización de SOEs repercute en la disminución del *LCOE*, ya que permite incrementar la energía anual producida.

En este objetivo específicamente se pretende desarrollar un modelado óptico de distintas unidades HCPV de tipo Fresnel con óptica secundaria, que tenga en cuenta propiedades dependientes de la longitud de onda. El modelado óptico deberá tener en cuenta que la célula solar no es un absorbente perfecto de luz y que además está compuesta por tres uniones p-n típicamente. Para ello se recurrirá a conceptos como la respuesta espectral y la eficiencia óptica policromática, entre otros. Se quiere determinar, además, qué tipo de SOE, entre varios diseños típicos, es el más adecuado para un sistema HCPV de tipo Fresnel.

Posteriormente, se procederá al estudio experimental (caracterización en el Simulador Solar CPV) de diferentes SOEs diseñados y fabricados, integrando diferentes unidades HCPV. El objetivo es determinar cuál SOE funciona mejor desde el punto de vista de las propiedades eléctricas medidas de cada unidad HCPV. Para ello se realizará una caracterización tanto a condiciones de referencia como a condiciones muy alejadas de las mismas. Se determinarán los parámetros eléctricos característicos de las curvas I-V de cada unidad HCPV, así como la aceptancia angular para las diferentes condiciones espectrales y de irradiancia. Los resultados se compararán con aquellos de las simulaciones ópticas.

Objetivo nº4. Realizar un diseño óptico para concentraciones ultra-altas

Otra estrategia para reducir el *LCOE* de la tecnología HCPV es aumentar los niveles de concentración solar del módulo, alcanzando lo que se denomina, concentraciones ultra-altas ("*ultra-High"* CPV, UHCPV) de más de 1000 soles. De esta forma, se reduciría aún más la cantidad usada de semiconductor en cada módulo UHCPV, por tanto, abaratando su coste de fabricación.

El objetivo de este trabajo es realizar un diseño óptico de un dispositivo concentrador UHCPV que dirija la luz concentrada, desde varias unidades ópticas independientes entre sí. Así se conseguiría multiplicar la concentración geométrica del módulo UHCPV según el número de unidades ópticas cuyos haces de luz concentrada convergen hacia un mismo receptor común.

Además, dicho concentrador UHCPV debe ser compacto, garantizar una aceptancia angular mínima (lo cual es más difícil a medida que se aumenta la concentración geométrica) e iluminar la célula solar de forma uniforme (para evitar problemas de punto caliente, etc.).

5. Publicaciones de la Tesis

5.1. Relación de publicaciones

Artículo nº 1	"**Efficiency and acceptance angle of High Concentrator Photovoltaic Modules: Current Status and Indoor Measurements**"
Autores	P. Pérez-Higueras, **J.P. Ferrer-Rodríguez**, F. Almonacid y E.F. Fernández
Revista	*Renewable and Sustainable Energy Reviews*
Volumen, etc.	(En revisión)
Clasificación JCR	ENERGY AND FUELS: 5/89 (Q1)
Índice de impacto	8.050 (2016)
DOI	

Artículo nº 2	"**Current-voltage dynamics of multi-junction CPV modules under different irradiance levels**"
Autores	E.F. Fernández, **J.P. Ferrer-Rodríguez**, F. Almonacid y P. Pérez-Higueras
Revista	*Solar Energy*
Volumen, etc.	155, 39–50, (2017)
Clasificación JCR	ENERGY AND FUELS: 21/89 (Q1)
Índice de impacto	4.018 (2016)
DOI	dx.doi.org/10.1016/j.solener.2017.06.012

Artículo nº 3	"**A worldwide assessment of levelised cost of electricity of HCPV systems**"
Autores	D.L. Talavera, **J.P. Ferrer-Rodríguez**, P. Pérez-Higueras, J. Terrados y E.F. Fernández.
Revista	*Energy Conversion and Management*
Volumen, etc.	127, 679–692, (2016)
Clasificación JCR	ENERGY AND FUELS: 10/89 (Q1)
Índice de impacto	5.589 (2016)
DOI	dx.doi.org/10.1016/j.enconman.2016.09.054

Artículo nº 4	"**Optical modeling of four Fresnel-based high-CPV units**"
Autores	**J.P. Ferrer-Rodríguez**, H. Baig, E.F. Fernández, F. Almonacid, T. Mallick y P. Pérez-Higueras.
Revista	*Solar Energy*
Volumen, etc.	155, 805–815, (2017)
Clasificación JCR	ENERGY AND FUELS: 21/89 (Q1)
Índice de impacto	4.018 (2016)
DOI	dx.doi.org/10.1016/j.solener.2017.07.027

Artículo nº 5	"**Development, indoor characterisation and comparison to optical modelling of four Fresnel-based high-CPV units equipped with refractive secondary optics**"
Autores	**J.P. Ferrer-Rodríguez**, E.F. Fernández, H. Baig, F. Almonacid, T. Mallick y P. Pérez-Higueras.
Revista	*Solar Energy Materials and Solar Cells*
Volumen, etc.	(En revisión)
Clasificación JCR	ENERGY AND FUELS: 13/89 (Q1)
Índice de impacto	4.784 (2016)
DOI	

Artículo nº 6	"**Optical design of a 4-off-axis-unit Cassegrain ultra-high concentrator photovoltaics module with a central receiver**"
Autores	**J.P. Ferrer-Rodríguez**, E.F. Fernández, F. Almonacid y P. Pérez-Higueras.
Revista	*Optics Letters*
Volumen, etc.	41(9), 1985–1988, (2016)
Clasificación JCR	OPTICS: 15/92 (Q1)
Índice de impacto	3.416 (2016)
DOI	dx.doi.org/10.1364/OL.41.001985

5.2. Conexión de las publicaciones con Objetivos de la Tesis

5.2.1. Objetivo nº1: Analizar el estado de la tecnología de módulos fotovoltaicos de alta concentración

Artículo nº 1:	"**Efficiency and acceptance angle of High Concentrator Photovoltaic Modules: Current Status and Indoor Measurements**"
Artículo nº 2:	"**Current-voltage dynamics of multi-junction CPV modules under different irradiance levels**"

El objetivo primero, "**Analizar el estado de la tecnología de módulos fotovoltaicos de alta concentración**", se desarrolló entre los **artículos número 1 y 2**, arriba citados.

En el artículo número 1 ("*Efficiency and acceptance angle of High Concentrator Photovoltaic Modules: Current Status and Indoor Measurements*") se realizó un análisis de los módulos de alta concentración fotovoltaica (HCPV).

El objetivo principal de este artículo es hacer una revisión de los módulos HCPV actuales, ya que la información disponible en la literatura es escasa y no abarca los principales aspectos de los módulos HCPV de forma global. Además, la información detallada de los módulos HCPV, proporcionada por los fabricantes, suele ser incompleta. Este artículo pretende aportar información detallada sobre dos aspectos clave de los módulos HCPV, eficiencia y aceptancia angular, y así cubrir la ausencia de la misma en la literatura. Para completar la información recopilada, se propone como objetivo aportar datos de medidas experimentales en simulador solar de un total de 24 módulos HCPV comerciales. Dichos datos, además, son comparados con aquellos dados por los fabricantes.

Para propiciar una mejor comprensión del análisis presentado en este artículo, las principales magnitudes eléctricas fueron definidas: eficiencia del módulo HCPV (η_{MOD}) y de la célula solar (η_{CELL}), eficiencia óptica del sistema concentrador (η_{OPT}), concentración geométrica (C_g), aceptancia angular (ϑ) y producto concentración-aceptancia angular (*CAP*).

Previo al análisis de los módulos HCPV actuales, se presenta un análisis histórico, desde 1990 hasta la actualidad, de la evolución de los valores récord de eficiencia de los módulos de las principales tecnologías fotovoltaicas: HCPV, c-Si (silicio cristalino) y '*Thin Film*' (lámina delgada). El mayor incremento de eficiencia corresponde a los módulos HCPV, con un crecimiento que llega al +1.43%/año entre 2010 y 2017 [9, 6].

Se detallan los cinco módulos fotovoltaicos con mayor eficiencia medida por laboratorios de prestigio. Sus eficiencias son alrededor de 40% y además sus C_g son, en general, menores de 400×. Los valores de estos módulos contrastan con aquellos de los módulos HCPV comerciales, que son presentados en una tabla con los valores de eficiencia de 15 módulos HCPV actuales de diferentes fabricantes. Se comprueba que los módulos HCPV comerciales presentan eficiencias alrededor de 30% y su C_g está entre 500× y 1000×. En la tabla, además se incluyen los valores de potencia, aceptancia angular, *CAP*, y el tipo de óptica de los módulos HCPV. Utilizando dichos valores de eficiencia, se presenta un histograma de frecuencias centrado en 30% con poca dispersión (3%). Usando los valores mencionados, la aceptancia angular resulta típicamente entre ±0.7º y ±1.0º, con un promedio de ±0.9º. El valor *CAP* promedio resulta 0.46. Se comprueba que ningún módulo HCPV comercial consigue simultáneamente altos valores de eficiencia, aceptancia angular y C_g.

Complementando a los valores comerciales, se presentan valores medidos de eficiencia, en el Simulador Solar CPV de la Universidad de Jaén, de un total de 24 módulos HCPV comerciales correspondientes a tres fabricantes distintos. El promedio de los valores medidos de los módulos HCPV comerciales resulta no desviarse más de un ±3.5% respecto de los valores dados por los fabricantes. Considerando 21 de los 24 módulos, correspondientes a dos fabricantes distintos, sus valores de eficiencia mantienen solo un 2% de desviación alrededor de sus respectivos valores promedio. En cuanto a la aceptancia angular caracterizada de 16 módulos HCPV comerciales, se obtiene una muy baja dispersión de los resultados, 0.05%, con un valor promedio entre ±0.77º y ±0.82º. Por consiguiente, tanto en eficiencia como en aceptancia angular, se verifica muy poca dispersión en los resultados medidos.

En este artículo se **concluye** que las principales características de los módulos HCPV comerciales son analizadas, especialmente: eficiencia, aceptancia angular, concentración geométrica. En cuanto a la evolución de la eficiencia de los módulos HCPV, ésta es la mayor entre todas las tecnologías fotovoltaicas. Los valores récord de eficiencia de módulos HCPV alcanzan valores alrededor del 40%. En el caso de los módulos HCPV comerciales, sus eficiencias están alrededor del 30%, con concentraciones geométricas entre 500× y 1000×, y valores de aceptancia angular entre ±0.7º y ±1.0º. Complementando al análisis, se realizó la caracterización en Simulador Solar CPV de un total de 24 módulos HCPV de tres fabricantes distintos. Las eficiencias medidas se ajustaron a los valores dados por los fabricantes. Igualmente, los valores de aceptancia angular (de 16 módulos) se ajustaron a los de los fabricantes, fueron repetitivos y resultaron entre ±0.77º y ±0.82º.

En el artículo número 2 ("*Current-voltage dynamics of multi-junction CPV modules under different irradiance levels*") se analizaron las propiedades de los módulos HCPV respecto de la irradiancia.

El funcionamiento de los módulos fotovoltaicos de alta concentración (HCPV) es mucho más complejo que el de los módulos fotovoltaicos convencionales. Aunque la literatura es extensa en cuanto a los análisis de módulos HCPV a nivel de célula, módulo y sistema, resulta indispensable estudiar el comportamiento de corriente-voltaje (I-V) de los módulos HCPV en función de un parámetro esencial como es la irradiancia directa. Para ello, se puede utilizar el modelo de la exponencial simple (SEM, *single exponential model*), que relaciona la curva I-V de un dispositivo fotovoltaico con cinco parámetros característicos: la corriente fotogenerada (I_{ph}), la corriente de saturación del diodo (I_o), el factor de idealidad del diodo (m) y las resistencias parásitas, en serie (R_s) y en paralelo (R_{sh}). Este método ha de ser adaptado a nivel de módulo HCPV, para estudiar la dependencia con la irradiancia, debido a que la óptica puede afectar a la uniformidad, y los *mismatch* eléctricos y ópticos pueden afectar a la curva I-V y al aumento de la resistencia serie por el conexionado entre células.

El objetivo fundamental de este artículo es mejorar el conocimiento del comportamiento de los módulos HCPV, específicamente, en función de la irradiancia. Para ello, se pretende determinar (en condiciones totalmente controladas) la dependencia de la curva I-V y de los parámetros del modelo SEM con la irradiancia en los módulos HCPV basados en células multi-unión.

Para realizar el estudio planteado, se realiza la caracterización controlada, de dos módulos HCPV comerciales, en el Simulador Solar CPV de la Universidad de Jaén, a condiciones de referencia (temperatura 25^{o} C, *SMR(top/mid)* = 1 ± 0.05, *spectral matching ratio*, y a diferentes irradiancias (700-1000 W/m^2). Ambos módulos HCPV tienen óptica primaria de Fresnel y secundaria de pirámide truncada refractiva de vidrio. La lente primaria del módulo A es de tipo SoG (*silicon on glass*) mientras que la del B es de PMMA (polimetilmetacrilato). El módulo A tiene una concentración geométrica de 500× y el B de 820×. Las células solares de ambos son '*lattice-matched*' (parámetro reticular ajustado) de triple-unión (GaInP/GaInAs/Ge).

Utilizando las curvas I-V obtenidas en el Simulador Solar, los cinco parámetros del modelo SEM son extraídos a nivel de una célula solar, para cada valor de irradiancia. Se obtienen los siguientes resultados: I_{ph} crece linealmente con la irradiancia, como es esperado; m e I_o no muestran dependencia con la irradiancia; mientras que las resistencias parásitas, R_s y en R_{sh}, decrecen al aumentar la irradiancia, debido al incremento de los portadores de carga en el material semiconductor. Los parámetros claves de las curvas I-V, es decir, I_{sc}, I_{mpp}, V_{oc} y V_{mpp}, se pueden obtener tras una serie de

aproximaciones dentro del modelo SEM. Estos parámetros resultan expresados por funciones relativamente simples y con diversos coeficientes que pueden ser obtenidos mediante análisis de regresión de datos monitorizados de los módulos HCPV, por tanto, sin necesidad de conocer la curva I-V en condiciones de referencia. En el caso de estos parámetros clave de la curva I-V de ambos módulos HCPV caracterizados, se observa que, por un lado, I_{sc} e I_{mpp} aumentan linealmente con la irradiancia, mientras que V_{oc} crece con el logaritmo de la irradiancia. Por otro lado, V_{mpp} aumenta hasta un cierto valor de irradiancia (alrededor de 800 W/m^2) y luego decrece. Ello es debido al aumento de las pérdidas por resistencia en serie a irradiancias mayores. A su vez, esta disminución de V_{mpp} produce una reducción de la eficiencia a partir de cierta irradiancia. Esto implica que, por un lado, para optimizar el funcionamiento de un módulo HCPV, es necesario ajustar el nivel de concentración del sistema óptico con aquél del máximo de eficiencia de la célula. Por otro lado, para aumentar el valor de irradiancia a la cual la eficiencia de la célula es máxima, es necesario reducir su resistencia en serie. Además, dado que normalmente solo se dispone de valores a condiciones de referencia, se calculan las curvas I-V teóricas a diferentes irradiancias. De esta forma, resulta un error relativo en la estimación de la potencia menor del 0.3% para irradiancias en el rango 750-1000 W/m^2.

En este artículo se **concluye** que se han caracterizado, en condiciones controladas de laboratorio Simulador Solar CPV, dos módulos comerciales HCPV basados en óptica primaria Fresnel y en óptica secundaria de tipo refractivo, y en células de triple-unión. Variando la irradiancia (*DNI*, entre 700-1000 W/m^2), se han analizado las características de las curvas I-V así como los parámetros del modelo SEM (*single exponential model*) aplicado a cada módulo HCPV. Con respecto a los parámetros eléctricos de las curvas I-V, los resultados muestran que la corriente de cortocircuito (I_{sc}) y la corriente del punto de máxima potencia (I_{mpp}) aumentan linealmente con la *DNI*. Además, el voltaje a circuito abierto (V_{oc}) aumenta con el logaritmo de la *DNI*. Por otro lado, el voltaje en el punto de máxima potencia (V_{mpp}) presenta un crecimiento hasta cierto valor de *DNI* (unos 800 W/m^2), a partir del cual disminuye debido al incremento de las pérdidas por resistencia en serie en las células. Entre los parámetros SEM, los resultados muestran que la corriente fotogenerada (I_{ph}) aumenta linealmente con la *DNI*. El factor de idealidad (m) y la corriente de saturación (I_o) no muestran dependencia frente a la *DNI*. Por otro lado, las resistencias parásitas en serie y en paralelo (R_s y R_{sh}) disminuyen al aumentar la *DNI*. A partir de los valores de referencia, se estiman las curvas I-V con buena aproximación hasta irradiancias de 750 W/m^2.

Para futuros trabajos se destaca el modelado del impacto de la temperatura en los parámetros SEM y en las características I-V en función de la irradiancia, y la aplicación de correcciones espectrales.

5.2.2. Objetivo nº2: Analizar la viabilidad económica de la tecnología fotovoltaica de alta concentración a nivel mundial

Artículo nº 3:	"**A worldwide assessment of levelised cost of electricity of HCPV systems**"

El objetivo número 2, "**Analizar la viabilidad económico de la tecnología fotovoltaica de alta concentración a nivel mundial**", se llevó a cabo en el **artículo número 3** ("*A worldwide assessment of levelised cost of electricity of HCPV systems*").

El aspecto económico de las instalaciones de energía solar fotovoltaica (PV) es tan importante como la tecnología PV en sí. Los estudios económicos relacionados con la energía solar PV son útiles para evaluar la factibilidad de una inversión, así como para apoyar regulaciones que fomenten la implantación de las energías renovables (EERR). No obstante, se observa escasez tanto de estudios económicos precisos sobre los sistemas HCPV, como de análisis que indiquen las regiones potenciales óptimas para los sistemas HCPV a nivel mundial. En este artículo se utiliza el parámetro *LCOE* (*Levelised Cost of Electricity*, coste nivelado de la electricidad) como el parámetro que indica la factibilidad de una inversión económica para realizar una instalación PV. El *LCOE* representa el coste teórico constante de un sistema de producción de electricidad durante toda su vida útil. Este parámetro es típicamente utilizado para comparar diferentes sistemas de producción de electricidad, especialmente en los basados en EERR. Además, el parámetro *LCOE* se puede relacionar con el precio de la electricidad a través del concepto de paridad de red (*grid parity*) [19]. La paridad de red se alcanza cuando el *LCOE* de una fuente de EERR es igual o menor al precio de la electricidad. Se observa que no hay estudios anteriores sobre la paridad de red de los sistemas HCPV.

Por todo lo expuesto, se pretende realizar un estudio a nivel mundial sobre la factibilidad de la inversión en los sistemas HCPV (de 1 MWp) a través del cálculo del *LCOE* de los sistemas HCPV, en un total de 133 países. En ese marco, además se pretende analizar la paridad de red en los países analizados. Con toda la información analizada, se pretende presentar diversos mapas mundiales por países que aporten información directa relevante sobre la factibilidad de los sistemas HCPV, para utilidad de futuros inversores, propietarios y entidades financieras.

El cálculo del *LCOE*, para el año 2014, se realiza en función de los siguientes parámetros de entrada: $HCPV_I$ (€), coste inicial de la inversión; $HCPV_{AOM}$ (€), coste anual de operación y mantenimiento; *DEP* (€), amortización anual del sistema HCPV; N_d, el número de años de amortización del sistema HCPV; Y_f (kW·h/kWp·año), la producción anual de energía; *d* (%), el tipo de descuento nominal; *N,* el número de años de vida útil;

T (%), el impuesto; r_d (%), la degradación anual de la eficiencia del sistema HCPV; y, $r_{O\&M}$ (%), el incremento anual de los gastos de operación y mantenimiento del sistema HCPV. Es importante destacar el cálculo de Y_f, que se realiza a través del método de basado en el *PR* (*Performance Ratio*, coeficiente de rendimiento), definido por la norma IEC-61724 como la energía eléctrica producida en AC (corriente alterna) por un sistema PV por unidad de potencia instalada, expresado en kW·h/kWp·año. Se asume un *PR* = 0.82 común para las instalaciones HCPV. Con estas premisas, se genera un mapa mundial coloreado según el valor de $Y_{f\,HCPV}$, que resulta en el rango 1100-2000 kW·h/kWp·año. Otro concepto importante para determinar el *LCOE* es la curva de aprendizaje de la tecnología, que sirve para determinar $HCPV_I$ (€) y, en general, determina la evolución en la reducción del coste de una tecnología como consecuencia de la experiencia acumulada en su producción. En este análisis se asume un coste inicial de la instalación HCPV de 1700 €/kWp para el año 2014.

Además, se asume una serie de suposiciones para realizar los cálculos económicos, como por ejemplo que el 70% de los costes iniciales se financian y el 30% corresponde a capital propio, o que el préstamo se devuelve en un plazo de 20 años. Con los resultados se genera un mapa con el valor de *LCOE* (c€/kW·h) a nivel mundial (año 2014). Resulta mínimo para EAU (Emiratos Árabes Unidos) con 6.7 c€/kW·h y máximo en Vietnam, con 62 c€/kW·h. Las zonas con menor *LCOE* (< 10 c€/kW·h) son: Norte América, Chile, Australia, Norte y Sur de África, y Sur de Europa.

Comparando con el precio de la electricidad en el segmento doméstico, se alcanza la paridad de red mediante la tecnología HCPV (año 2014), entre otros países, en: España, Italia, Grecia, Francia, e incluso en países nórdicos como Irlanda, Suecia y Dinamarca. El motivo es el alto precio de la electricidad y los reducidos costes de financiación.

Por último se realiza un pronóstico sobre el *LCOE* para las tecnologías HCPV y PV para el año 2020 para determinar en qué países sería más rentable una instalación HCPV que una convencional PV. Entre las suposiciones incluidas, por ejemplo, se asume un valor de 900€/kWp para ambas tecnologías como coste inicial de la instalación. El resultado muestra que en 99 países, el $LCOE_{HCPV}$ es menor que el $LCOE_{PV}$, destacando la región MENA (Oriente Medio y Norte de África) y Sur de África y Sur de América. Con los análisis realizados, se dibujan respectivos mapas mundiales, marcando los países con un color según el valor de la magnitud correspondiente.

En este artículo se **concluye** que se ha realizado un estudio de la factibilidad de las inversiones en instalaciones HCPV de 1 MW mediante el cálculo del $LCOE_{HCPV}$ mundial. Las regiones con menor $LCOE_{HCPV}$ (menor de 10 c€/kW·h), son Norte América, Chile, Australia, Norte y Sur de África, y Sur de Europa. Por otro lado, se utiliza el concepto de paridad de red para analizar la viabilidad de las inversiones HCPV. Para ello se compara

el $LCOE_{HCPV}$ con el precio de la electricidad doméstica, y se obtiene que para el año 2014 en, entre otros países, España, Italia, Gracia, Francia, Irlanda, Suecia y Dinamarca se consigue la paridad de red. Además, se realiza una previsión para el año 2020 de la factibilidad de los sistemas HCPV en comparación con los convencionales. Según el pronóstico, la inversión en HCPV resultará más favorable en la región MENA (Oriente Medio y Norte de África), Sur de África y Sur de América. Para facilitar la consulta rápida de los resultados, se elaboran diferentes mapas mundiales marcando los países más propicios para las inversiones en sistemas HCPV.

5.2.3. Objetivo nº3: Modelar, diseñar y caracterizar elementos ópticos secundarios

Artículo nº 4:	"**Optical modeling of four Fresnel-based high-CPV units**"
Artículo nº 5:	"**Development, indoor characterisation and comparison to optical modelling of four Fresnel-based high-CPV units equipped with refractive secondary optics**"

El objetivo número 3, "**Modelar, diseñar y caracterizar elementos ópticos secundarios**" engloba dos **artículos**, el **número 4** ("*Optical modeling of four Fresnel-based high-CPV units*") y el **número 5** ("*Development, indoor characterisation and comparison to optical modelling of four Fresnel-based high-CPV units equipped with refractive secondary optics*").

Como se comentó anteriormente, una forma de propiciar la reducción del *LCOE* es aumentar la energía producida por los sistemas HCPV. Teniendo en cuenta las exigencias de tolerancia óptica (focalización, apuntamiento…) necesarias para el buen funcionamiento de un concentrador HCPV, la utilización de elementos ópticos próximos o acoplados a la célula solar permite incrementar considerablemente dicha tolerancia óptica. Este incremento de tolerancia óptica podría repercutir en pequeñas pérdidas ópticas bajo condiciones de alineamiento perfecto respecto de la luz incidente, pero, sin embargo, supone una ganancia considerable de producción de energía bajo condiciones reales de operación.

En el **artículo número 4** se expuso el desarrollo de un nuevo modelado óptico (superando a los que había disponibles) para la simulación óptica de unidades (o monomódulos) HCPV basadas en lentes de Fresnel y óptica secundaria (SOEs). Las ventajas de usar SOEs se resumen en el aumento de: (a) la eficiencia óptica al captar más rayos concentrados, (b) la aceptancia angular, la cual sirve para incrementar la producción de energía y para reducir costes de fabricación, instalación y de sistemas de seguimiento, y (c) la uniformidad espacial y espectral de la luz concentrada sobre la célula multi-unión (MJ). Numerosos estudios anteriores realizan un modelado óptico de los sistemas concentradores Fresnel con SOEs, pero la mayoría no incluyen la dependencia de la longitud de onda de la luz en las propiedades ópticas de los materiales.

El objetivo de este artículo es desarrollar un modelado óptico de distintas unidades HCPV de tipo Fresnel con óptica secundaria, que tenga en cuenta propiedades dependientes de la longitud de onda y se aproxime a los fenómenos ópticos reales, para aplicarlo al diseño y análisis de los distintos SOEs. Para ello, el modelado óptico debe

incluir: (i) espectro solar estándar para la superficie de la Tierra, (ii) la distribución angular de los rayos solares, (iii) óptica primaria (POE) de tipo Fresnel, (iv) dependencia con la longitud de onda del índice de refracción y del (v) coeficiente de absorción, y (vi) respuesta espectral de cada subcélula de una célula solar de triple-unión (TJ). Este modelado óptico permitirá determinar qué subcélula está limitando en corriente, así como calcular la eficiencia óptica policromática y los parámetros *SMR* (*spectral matching ratio*) [20, 21].

El modelado óptico descrito es aplicado a cuatro unidades HCPV distintas, formadas todas por la misma lente de Fresnel (POE) e igual célula TJ de concentración, aunque con un SOE, de PMMA (polimetilmetacrilato), distinto en cada una de ellas. Los cuatro SOEs son: (i) DCCPC (*dielectric-cross compound-parabolic-concentrator*, concentrador parabólico compuesto cuadrado dieléctrico), (ii) SILO-Pyramid, (iii) RTP (*refractive truncated pyramid*, pirámide truncada (e invertida) refractiva), y (iv) Trumpet ('trompeta'). El SOE SILO-Pyramid, una adaptación del SILO con la base piramidal, es una lente cuya superficie de entrada corresponde a un óvalo cartesiano de revolución calculado analíticamente. En el caso de los otros SOEs, éstos responden al principio de la reflexión total interna (TIR) y funcionan como guías de luz, conduciendo los rayos concentrados hacia la célula solar. Estos SOEs se diferencian básicamente en la geometría de las aristas. Las aristas del RTP son rectas, las del DCCPC son parabólicas y las del Trumpet son hiperbólicas. En cada una de las cuatro unidades HCPV, la lente de Fresnel es cuadrada de 130 mm de lado y tiene 152 mm de distancia focal. La célula TJ simulada está compuesta por los materiales GaInP/GaInAs/Ge y es cuadrada de 5.5 mm de lado, resultando cada unidad HCPV en una concentración geométrica de 559×. Atendiendo al modelado de las propiedades ópticas, destaca, por ejemplo, la aplicación de la ley de Beer-Lambert mediante el coeficiente de absorción, para la transmisión de luz a través de un material. Las simulaciones ópticas de cada unidad HCPV se realizan mediante trazado de rayos, situando la superficie de entrada de cada SOE a la distancia focal de la lente de Fresnel.

A partir de la típica respuesta espectral para una célula TJ y con los resultados de la simulación óptica, se calcula la densidad de corriente de cortocircuito (J_{sc}^{conc}) de cada subcélula (top, mid y bot) tanto para incidencia normal de luz solar como para diferentes inclinaciones, hasta un valor de 2º. De estos valores se calcula la eficiencia óptica policromática, $\mu_{opt,policrom}$, (que tiene en cuenta qué subcélula está limitando en corriente) así como los valores *SMR(top/mid)*, *SMR(top/bot)* y *SMR(mid/bot)*. Se encuentra que, por ejemplo, para incidencia normal, en las unidades HCPV DCCPC y SILO-Pyramid limita la subcélula top, mientras que para las unidades RTP y Trumpet, la subcélula bot limita en corriente, probablemente debido a la absorción en el rango IR

(infrarrojo) del espectro en el material PMMA. Se tiene que los valores de $\mu_{opt,policrom}$ resultan entre 81-83.4%, mientras que la aceptancia angular resulta entre ±0.96-1.13º para las diferentes unidades HCPV. En términos de $\mu_{opt,policrom}$, el comportamiento angular de las cuatro unidades HCPV es similar hasta los 1.4º de inclinación de los rayos solares.

Otros resultados de las simulaciones ópticas, son las distribuciones espaciales de $J_{sc,subcél}^{conc}$ de la luz concentrada tanto para incidencia normal como para incidencia con 1º de inclinación para cada una de las subcélulas. Aunque para incidencia normal, todas las unidades HCPV presentan patrones muy uniformes en general, para 1º de inclinación se tiene que los SOEs RTP y Trumpet proporcionan una uniformidad visiblemente superior a las unidades DCCPC y SILO-Pyramid. De forma global, es decir, valorando la eficiencia óptica policromática, la aceptancia angular y la uniformidad de la densidad de corriente de cortocircuito para incidencia normal y de 1º de inclinación, el SOE RTP presenta el mejor resultado.

Se **concluye** que se ha desarrollado un modelado óptico que incluye un amplio número de no idealidades: espectro solar y su distribución angular, índice de refracción, coeficiente de absorción, etc. También se considera la respuesta espectral de cada subcélula que compone una célula de triple-unión y el cálculo de la eficiencia óptica policromática. Se realiza un análisis espectral de la luz concentrada en términos de *SMR* (utilizando las densidades de corriente de corto-circuito simuladas de cada subcélula), y se encuentra que en ningún caso se obtiene una distribución espectral de la luz concentrada equivalente al espectro de referencia. Entre los resultados, los SOEs diseñados presentan valores de eficiencia y aceptancia angular similares entre ellos, en los rangos 81-83.4% y ±0.96-1.13º, respectivamente. En cuanto a las distribuciones espaciales de densidad de corriente de corto-circuito para cada subcélula, los SOEs RTP y Trumpet presentan las distribuciones más uniformes. En términos globales, el SOE RTP presenta el mejor compromiso entre los valores simulados.

El desarrollo futuro de este trabajo es introducir los patrones de $J_{sc,subcél}^{conc}$ en un modelo eléctrico tridimensional de la célula TJ, el cual emule los efectos de no uniformidad de la iluminación concentrada, tanto para cada subcélula como en la célula TJ en conjunto.

Para el **artículo número 5** ("*Development, indoor characterisation and comparison to optical modelling of four Fresnel-based high-CPV units equipped with refractive secondary optics*") se procedió a la fabricación de los SOEs analizados teóricamente con anterioridad. En el anterior artículo número 4, se estableció la necesidad de la utilización de elementos ópticos secundarios en los módulos fotovoltaicos de alta concentración

para aumentar la producción de energía y reducir los costes de generación de la misma. Sin embargo, una caracterización experimental comparativa, bajo condiciones controladas y repetitivas, de la influencia de diferente SOEs refractivos en dispositivos Fresnel HCPV estaba ausente en la literatura.

El objetivo de este artículo es determinar cuál SOE funciona mejor desde el punto de vista de las propiedades eléctricas de la unidad HCPV. Para ello se realiza una caracterización tanto a condiciones de referencia como a condiciones muy alejadas de las de referencia. Por un lado, se mantienen constantes las condiciones espectrales variando la irradiancia. Por otro lado, se varían las condiciones espectrales a una irradiancia fijada. Para las diferentes condiciones espectrales y de irradiancia, se determinan los parámetros eléctricos característicos de las curvas I-V de cada unidad HCPV así como sus valores de aceptancia angular. Los resultados sirven también para compararlos con aquellos obtenidos mediante simulación óptica.

En este artículo se realiza una caracterización experimental (utilizando el Simulador Solar CPV 'Helios 3198') de cuatro unidades HCPV, las mismas que fueron modeladas ópticamente en el artículo número 4. Tanto la lente de Fresnel como las células TJ utilizadas corresponden a las características descritas en el artículo número 4. Los cuatro SOEs, fabricados en PMMA, son: (i) DCCPC (*dielectric-cross compound-parabolic-concentrator*, concentrador parabólico compuesto cuadrado dieléctrico), (ii) SILO-Pyramid, (iii) RTP (*refractive truncated pyramid*, pirámide truncada (e invertida) refractiva), y (iv) Trumpet ('trompeta').

Para formar las diferentes unidades HCPV, se utilizan receptores del mismo modelo, equipados con células TJ comerciales (AZUR SPACE Solar Power GmbH). También se utiliza una lente de Fresnel comercial (ORAFOL Fresnel Optics GmbH). Cada SOE es fabricado a bajo coste mediante tallado CNC (control numérico por computador) de bloques de PMMA y posterior pulido. Cada SOE es montado sobre una célula mediante un adhesivo óptico (Norland 68TH). Con estos elementos se consigue cada unidad HCPV, utilizando una mesa óptica para colocar los mismos. En el Simulador Solar CPV se realiza una caracterización para diferentes condiciones espectrales y de irradiancia mediante la utilización de distintos filtros, tanto neutros como no neutros.

Las correspondientes curvas I-V de todas las unidades HCPV son obtenidas. Los valores de eficiencia resultan entre 25.5-28.2%, mientras la concentración efectiva resulta entre 403-427 soles. La eficiencia óptica de la lente de Fresnel resulta casi un 8% menor que en la simulación óptica, aunque las eficiencia ópticas de los SOEs resultan entre 90.3-95.7%, similares a las simulaciones ópticas. Con respecto de la caracterización de la aceptancia angular, solamente en el caso del SOE RTP se obtuvo un valor (±1.09^{o}) similar al simulado mediante trazado de rayos. Para el resto de SOEs se

obtienen valores inferiores, especialmente para el DCCPC (probablemente debido a las tolerancias de fabricación y al montaje sobre la célula). En la comparación de la eficiencias ópticas medidas con las simuladas para diferentes ángulos (entre 0-2^{o}), se observa en general un comportamiento similar de las unidades HCPV en ambos análisis, excepto para el SOE DCCPC.

Analizando el comportamiento de las unidades HCPV para diferentes irradiancias, manteniendo similares condiciones espectrales, se encuentra que los valores de aceptancia angular son, en general, estables. En cuanto a la eficiencia y el factor de forma (*FF*), ambos no presentan variaciones con la irradiancia. En el caso del voltaje a circuito abierto (V_{oc}), éste aumenta con el logaritmo de la irradiancia, como es esperado. Variando las condiciones espectrales (en función de *SMR(top/mid)*), manteniendo constante la irradiancia, se encuentra que los valores de aceptancia angular son, en general, también estables. V_{oc} y *FF* no muestran dependencia espectral para las unidades HCPV caracterizadas. Sin embargo, en el caso de la eficiencia, todas las unidades HCPV, incluyendo la unidad sin SOE, presentan una ligera disminución de eficiencia (hasta un 3.7%) para valores *SMR(top/mid)* mayores de 1 (espectro 'azul').

Se **concluye** que, para las unidades HCPV de tipo Fresnel caracterizadas, el SOE RTP presenta el mejor compromiso de eficiencia y aceptancia angular. Las eficiencias eléctricas medidas están en el rango 25.5-28.2%, con concentraciones efectivas entre 403-427 soles. Los valores medidos de eficiencia óptica son similares a los simulados en general. Por el contrario, el SOE DCCPC presenta un comportamiento angular anómalo que habrá de ser estudiado. Comparando con las simulaciones ópticas, las eficiencias ópticas de los SOEs son similares a éstas. Sin embargo, ello no ocurre con la lente de Fresnel (8% menos de eficiencia óptica), ni en el caso de la aceptancia angular de algunos SOEs. Al variar las condiciones experimentales, se comprueba que la aceptancia angular no es sensible a los cambios espectrales ni de irradiancia. Por otro lado, frente a cambios de irradiancia, solo V_{oc} presenta una dependencia clara (logarítmica) respecto de la misma. Considerando los cambios espectrales, solo la eficiencia es ligeramente sensible, disminuyendo hasta un 3.7% para espectros denominados 'azules'.

Para futuros trabajos experimentales, la caracterización de la uniformidad de la luz concentrada por los SOEs sobre la célula aportará una información muy útil para una mejor comprensión del funcionamiento de estas unidades HCPV. Además, las divergencias encontradas entre las simulaciones y la caracterización experimental deben ser investigadas.

5.2.4. Objetivo nº4: Realizar un diseño óptico para concentraciones ultra-altas

Artículo nº 6:	"**Optical design of a 4-off-axis-unit Cassegrain ultra-high concentrator photovoltaics module with a central receiver**"

Otra estrategia para reducir el *LCOE* es reducir la cantidad usada de semiconductor (costoso), sustituyéndolo por materiales convencionales (vidrio, plástico, etc.), que conforman los sistemas ópticos concentradores. Ello implica aumentar drásticamente el nivel de concentración. Se denomina concentración ultra-alta (UH, *ultra-high*, UHCPV) cuando la irradiancia promedio sobre la célula solar es de más de 1000 soles (1 sol = 1000 W/m^2).

Este objetivo número 4 ha sido desarrollado en el **artículo número 6**: "*Optical design of a 4-off-axis-unit Cassegrain ultra-high concentrator photovoltaics module with a central receiver*".

Diferentes autores han señalado las ventajas, y el potencial para la reducción de costes, que tienen los sistemas de ultra-alta concentración fotovoltaica (UHCPV), con concentraciones por encima de 1000 soles [5]. Sin embargo, diversas barreras tecnológicas deben ser superadas para poder desarrollo la tecnología UHCPV, como: la obtención de células con máximos de eficiencia a concentraciones de al menos 1000 soles, o la obtención de adecuados sistemas de refrigeración de las células solares. Desde el punto de vista de la óptica, los sistemas basados en lentes de Fresnel de un solo material están limitados a concentraciones de alrededor de 1000 soles, debido a las aberraciones cromáticas. No obstante, los espejos están exentos de este tipo de aberraciones, aunque son caros y difíciles de fabricar.

El objetivo de este trabajo es realizar un diseño óptico de un dispositivo concentrador UHCPV que dirija la luz concentrada, desde varias unidades ópticas independientes entre sí, hacia una única célula solar. Además, dicho concentrador UHCPV debe ser compacto, garantizar una aceptancia angular mínima e iluminar la célula solar de forma uniforme.

En este trabajo, se diseña un concentrador UHCPV que utiliza cuatro unidades ópticas independientes entre sí que concentran la luz solar sobre un receptor central, donde se encuentra la célula solar. Por un lado, se modela cada unidad óptica como una modificación del diseño típico Cassegrain, aprovechando la acromaticidad y la alta compacidad del mismo. Por otro lado, para asegurar una distribución de luz concentrada relativamente uniforme sobre la célula, se emplea la técnica de la iluminación Köhler [22].

De esta forma, cada unidad óptica está formada por un espejo POE (elemento primario) paraboloide y un espejo SOE (elemento secundario) hiperboloide, con el eje óptico de éste no paralelo al del POE (de ahí el nombre '*off-axis*'). Nótese que en este contexto, SOE no hace referencia a un elemento óptico sobre la célula, como era el caso de las unidades HCPV basadas en sistemas Fresnel. El punto focal del POE y el punto focal cercano del SOE son coincidentes, de forma que los rayos solares se focalizan en el foco lejano del SOE tras las dos respectivas reflexiones. Cada espejo POE está recortado con forma cuadrada, mientras que cada SOE es recortado por el contorno de los rayos reflejados en el POE. En el foco lejano del SOE se coloca un óvalo cartesiano de revolución de tipo refractivo convenientemente calculado. Este óvalo está orientado hacia el vértice más lejano del SOE, proyectando así una imagen del SOE sobre la célula solar. El ensamblaje de las cuatro unidades ópticas resulta en un mono-módulo cuadrado con simetría por cada 90º, siendo el homogeneizador o TOE (elemento terciario), la unión de los volúmenes de los cuatro óvalos cartesianos de cada unidad óptica.

El mono-módulo UHCPV diseñado tiene una concentración geométrica de 2304×, ya que cada uno de los cuatro espejos cuadrados POE tiene un lado de 120 mm, y la célula solar, de 5 mm. Cada espejo POE tiene una distancia focal de 150 mm, mientras que cada espejo SOE tiene una distancia focal cercana (lado cóncavo) de 35 mm y una distancia focal lejana (lado convexo) de 120 mm. La altura del mono-módulo es de 123 mm. En las simulaciones ópticas se tienen en cuenta diferentes no idealidades como: (i) la dispersión angular de los rayos solares, (ii) así como su distribución espectral, y (iii) dispersión de luz en las superficies de los espejos ('ABg *scatter model*'). El TOE es simulado de vidrio B270 y la cubierta protectora externa, de vidrio común. La célula solar se considera un absorbente perfecto.

La eficiencia óptica simulada es 73%, resultando una concentración efectiva sobre la célula solar de 1682 soles. La aceptancia angular se determina en ±0.61º, siendo el valor *CAP* = 0.51. Se obtiene sobre la célula un máximo de irradiancia a incidencia normal de 5480 soles, 3.3 veces mayor que el valor promedio de la distribución de irradiancia.

Se **concluye** en este trabajo la factibilidad de un diseño UHCPV (con concentración geométrica de 2304× y concentración efectiva de 1682 soles) basado en la concentración de luz solar desde diferentes e independientes unidades ópticas compactas, que en este caso son de tipo Cassegrain no convencionales. Además se obtienen valores similares de eficiencia, aceptancia angular y *CAP* a los de otros diseños Cassegrain convencionales. Entre los resultados, se tiene que la eficiencia óptica es del 73%, con una aceptancia angular de 0.61º y un valor *CAP* de 0.51. Resulta una

distribución de iluminación sobre la célula relativamente uniforme, cuyo máximo es 3.3 veces superior al mínimo.

Para aumentar la eficiencia óptica, se podrían considerar tratamientos antirreflectantes (AR) en las superficies del TOE y del vidrio protector. Otra posibilidad sería reducir el tamaño de los espejos SOE, los cuales producen un 7.5% de pérdidas por sombreado. Por otra parte, el ajuste de la posición del foco lejano del SOE de cada unidad óptica en relación con el TOE es un grado de libertad de diseño, útil para una futura optimización del sistema.

5.3. Otras publicaciones relacionadas con la Tesis

1) K. Shanks, N. Sarmah, **J.P. Ferrer-Rodríguez**, S. Senthilarasu, K. S. Reddy, E. F. Fernández, and T. Mallick, "Theoretical investigation considering manufacturing errors of a high concentrating photovoltaic of cassegrain design and its experimental validation," Solar Energy, vol. 131, pp. 235–245, 2016. DOI: dx.doi.org/10.1016/j.solener.2016.02.050

2) **J.P. Ferrer-Rodríguez**, P. Pérez-higueras, F. Almonacid, and E. F. Fernández, "Global Annual Final AC Yield Comparison between HCPV and c-Si PV," Journal of Solar Energy, vol. 2015, 2015. DOI: dx.doi.org/10.1155/2015/603608

5.3.1. Publicaciones de congresos

1) **J. P. Ferrer-Rodríguez**, H. Baig, A. Riverola, E. F. Fernández, D. Chemisana, F. Almonacid, T. K. Mallick, and P. Pérez-Higueras, "Design and characterization of refractive secondary optical elements for a point-focus Fresnel lens-based high CPV system," AIP Conf. Proc., vol. 1881, pp. 30003-1-30003–6, 2017. DOI: dx.doi.org/10.1063/1.5001414

2) **J. P. Ferrer-Rodríguez**, E.F. Fernández, F. Almonacid, and P. Pérez-higueras, "Investigating the Optical Performance of Cassegrainian Systems at Ultra-High Concentrations," AIP Conf. Proc., vol. 50003, pp. 9–14, 2016. DOI: dx.doi.org/10.1063/1.4962085

3) P. Pérez-Higueras, **J. P. Ferrer-Rodríguez**, K. Shanks, F. Almonacid, and E. F. Fernández, "Thin photovoltaic modules at ultra high concentration," AIP Conf. Proc., vol. 1679, p. 130004, 2015. DOI: dx.doi.org/10.1063/1.4931564

6. *Conclusions and future work*

This Doctoral Thesis supposes a contribution to the development of the High Concentrator Photovoltaics (HCPV) technology from different points of view, which are connected to each other. This Thesis provides knowledge about the current status of commercial HCPV modules, as well as about the fundamentals of their working performance through the characteristic electrical parameters. Complementary to the technical knowledge of the HCPV modules, an economic analysis is carried out worldwide, at country level, in order to calculate the levelised cost of electricity (*LCOE*) of HCPV. This last allows a connection between the HCPV technology with the economic reality of each country analysed. The necessity of reducing *LCOE* is detected, and in this Thesis, this reduction is contemplated through the improvement of the concentrator optics with two different strategies: on the one hand, to improve the secondary optical elements (homogenisers), and on the other hand, to increase the concentration levels beyond 1000 suns (ultra-high CPV, UHCPV).

The main conclusions can be summarised as follows:

- The main characteristics of the commercial HCPV modules are analysed: efficiency, acceptance angle, geometrical concentration and concentration-acceptance angle product (*CAP*).
- The evolution in the efficiency of commercial HCPV modules is the fastest one compared to the rest of PV technologies (c-Si, Thin Film, etc.). It reaches a growth rate up to +1.43%/year between 2010 and 2017.
- Record efficiency HCPV modules, certified by renowned laboratories, achieve around 40% and, in general, they have geometrical concentrations no higher than 400×.
- 15 commercial HCPV modules were analysed from their datasheets. Their efficiencies are around 30%, whereas their geometrical concentrations are spread between 500× y 1000×. Their acceptance angle values are typically between ±0.7º y ±1.0º and their *CAP* values between 0.3-0.5.
- Two commercial Fresnel-based HCPV modules have been characterised indoors in the CPV Solar Simulator for irradiances (*DNI*) between 700-1000 W/m^2. Both their I-V characteristics as well as the SEM (*single exponential model*) model parameters are analysed.
- Results showed that both short circuit current (I_{sc}) and current at maximum power point (I_{mpp}) increased linearly with *DNI*. The voltage at open-circuit (V_{oc}) grew logarithmically with *DNI*. On the other hand, the voltage at maximum

power point (V_{mpp}) showed a maximum at a certain value of *DNI* (ca. 800 W/m^2).

- SEM parameters showed that the photogenerated current (I_{ph}) increased linearly with *DNI*. Both ideality factor (*m*) and saturation current (I_o) were stable with *DNI*. On the other hand, both parasitic resistances, series and shunt (R_s y R_{sh}), decreased with *DNI*.
- I-V curves of both HCPV modules were predicted from the reference values, showing a good fitting until 750 W/m^2 of irradiance.
- The economic feasibility for the investments in HCPV installations of 1 MWp has been analysed through the worldwide calculation of the $LCOE_{HCPV}$ (*levelised cost of electricity*) in 133 countries. The lowest $LCOE_{HCPV}$ regions were North America, Chile, Australia, North and South of Africa, and South Europe, with values lower than 10 c€/kW·h.
- Calculated $LCOE_{HCPV}$ values were compared to the electricity prices in the domestic segment in order to analyse the grid parity. The result was that grid parity is already achieved, among other countries, in Spain, Italy, Greece, France, Ireland, Sweden and Denmark for the year 2014.
- Forecasts for $LCOE_{HCPV}$ and *LCOE* of conventional PV were conducted for 2020. The investment in HCPV resulted more favourable than using conventional PV in the following regions: MENA (Middle East and North Africa), the South of Africa and South America.
- An optical modelling that included many non-ideal effects has been developed. This optical modelling took into account wavelength-dependent optical properties of materials. It also included the spectral response of each subcell within a triple-junction solar cell.
- This optical modelling was applied to four different Fresnel-based HCPV units equipped with the correspondent dielectric (PMMA) SOEs (secondary optical units). These SOEs were: (i) DCCPC (*dielectric-cross compound-parabolic-concentrator*), (ii) SILO-Pyramid, (iii) RTP (*refractive truncated pyramid*), and (iv) Trumpet.
- From the simulated short-circuit current density ($J_{sc,subcell}^{conc}$) values of each subcell, a spectral analysis of the concentrated illumination in terms of *SMR* (*spectral matching ratio*) was performed. It was found that, in any situation, the spectral distribution of the concentrated light was never equivalent to the reference spectrum.

- All the designed SOEs presented efficiency and acceptance angle values similar to each other, being in the ranges 81-83.4% and ±0.96-1.13º, respectively.
- The HCPV units with SOEs RTP and Trumpet showed the most uniform distributions of $J_{sc,subcell}^{conc}$. The SOE RTP achieved the best trade-off among the results.
- Those four SOEs were fabricated in PMMA and the correspondent HCPV units were characterised in the CPV Solar Simulator. Their I-V curves were acquired, with efficiencies of 25.5-28.2% and effective concentrations of 403-427 suns under reference conditions.
- Regarding the experimental results of the HCPV units, the SOE RTP presented the best trade-off between experimentally measured efficiency and acceptance angle, moreover, those values were similar to the simulated ones. On the other hand, the SOE DCCPC exhibited a bad angular performance whose reasons are to be investigated.
- The experimental results were, in general, similar to those of the optical simulations except for the optical efficiency of the Fresnel lens (8% lower) and in the acceptance angle of some SOEs.
- It was found that the acceptance angle was stable under spectral and irradiance variations.
- Under irradiance variations, only V_{oc} exhibited a clear trend (logarithmic). Under spectral variations, only the efficiency was (slightly) sensitive, decreasing up to 3.7% for 'blue-rich' spectra.
- A UHCPV design based on the sunrays concentration from different and compact optical units (non-conventional Cassegrain-based), while achieving similar values of optical efficiency, acceptance angle and *CAP* (*concentration-acceptance angle product*) to conventional Cassegrain-based designs, was demonstrated.
- The simulated optical efficiency was of 73%, reaching an effective concentration of 1682 suns over the solar cell (with a geometrical concentration of 2304×). Removing the glass cover, the optical efficiency rose up to 79%. Concerning the angular properties, the acceptance angle was ±0.61º, whereas the *CAP* value was 0.51. Regarding the illumination distribution over the solar cell, it reached a maximum value of 5480 suns, 3.3 times over the minimum, assuring the uniformity.

The main future work to be developed are:

- To analyse the impact of temperature in the SEM parameters as well as in the I-V characteristics as a function of the irradiance. Moreover, spectral corrections in the I-V characteristics are to be developed.
- To input the $J_{sc,subcell}^{conc}$ distributions in a three-dimensional electrical model of a triple-junction solar cell, in order to simulate non-uniformity effects at subcell level and also for the entire solar cell as a device.
- For future experimental work, the spectral uniformity characterisation of the concentrated illumination over the solar cell is to be developed. In addition, the divergences found between simulation and experimental results are to be investigated.
- In order to increase the optical efficiency of the UHCPV design, antireflective coatings may be applied to the entrance surfaces of both TOE and glass cover. Another possibility is to reduce the size of the SOE mirrors, which incur 7.5% of optical losses by shading, by changing the correspondent focal distances of both POE and SOE. On the other hand, the adjustment of the position of the far focal point of the SOE of each optical unit in relation to the TOE, is a degree of freedom in the optical design, which can be useful for a future optimisation.

7. Referencias

[1] Pachauri, R.K.; Meyer, L.A.;, "IPCC, 2014: Climate Change 2014: Synthesis Report. Contribution of Working Groups I, II and III to the Fifth Assessment Report of the Intergovernmental Panel on Climate Change," IPCC, Geneva, Switzerland, 2014.

[2] "Air quality guidelines for particulate matter, ozone, nitrogen dioxide and sulfur dioxide. Summary of risk assessment," World Health Organization, Geneva, Switzerland , 2005.

[3] Fraunhofer Institute for Solar Energy, "Photovoltaics Report," Freiburg, 2017.

[4] Pérez-Higueras, P; Fernández, EF;, High Concentrator Photovoltaics: Fundamentals, Engineering and Power Plants, Springer International Publishing, 2015.

[5] Algora, C; Rey-Stolle, I;, Handbook on Concentrator Photovoltaic Technology, John Wiley & Sons, 2016.

[6] M. Green, K. Emery, Y. Hishikawa, W. Warta, E. Dunlop, D. Levi and A. Ho-Baillie, "Solar cell efficiency tables (version 50)," *Prog. Photovolt: Res. Appl.,* vol. 25, p. 668–676.

[7] K. Shanks, S. Senthilarasu and T. Mallick, "High-Concentration Optics for Photovoltaic Applications," in *High Concentrator Photovoltaics: Fundamentals, Engineering and Power Plants*, Springer International Publishing, 2015, p. 85–113.

[8] M. Buljan, J. Mendes-Lopes, P. Benítez and J. Miñano, "Recent trends in concentrated photovoltaics concentrators' architecture," *Journal of Photonics for Energy,* vol. 4, 2014.

[9] M. Wiesenfarth, S. Philipps, A. Bett, K. Horowitz and S. Kurtz, "Current Status of Concentrator Photovoltaic (CPV) Technology," Fraunhofer Institute for Solar Energy Systems ISE - National Renewable Energy Laboratory, 2017.

[10] D. Talavera, J. Ferrer-Rodríguez, P. Pérez-Higueras, J. Terrados and E. Fernández, "A worldwide assessment of levelised cost of electricity of HCPV systems," *Energy Conversion and Management,* vol. 127, p. 679–692, 2016.

[11] Luque, A.; Andreev, V, Concentrator Photovoltaics, Springer-Verlag, 2007.

[12] E. Fernández, J. Ferrer-Rodríguez, F. Almonacid and P. Pérez-Higueras, "Current-voltage dynamics of multi-junction CPV modules under different irradiance levels," *Solar Energy,* vol. 39–50, no. 155, 2017.

[13] R. Leutz and A. Suzuki, Nonimaging Fresnel Lenses: Design and Performance of Solar Concentrators, Springer, 2001.

[14] A. Davis and F. Kühnlenz, "Optical Design using Fresnel Lenses Basic Principles and some Practical Examples," *Optik and Photonik, Wiley,* no. 4, p. 52–55, 2007.

[15] D. Miller and S. R. Kurtz, "Durability of Fresnel lenses: A review specific to the concentrating photovoltaic application," *Solar Energy Materials and Solar Cells,* vol. 95, p. 2037–2068, 2011.

[16] K. Lovegrove, G. Burgess and J. Pye, "A new 500m2 paraboloidal dish solar concentrator," *Sol. Energy,* vol. 85, no. 4, p. 620–626, 2011.

[17] R. Winston and J. Gordon, "Planar concentrators near the étendue limit," *Optics Letters,* vol. 30, no. 19, p. 2617–2619, 2005.

[18] K. Shanks, N. Sarmah, J. P. Ferrer-Rodríguez, S. Senthilarasu, K. S. Reddy, E. F. Fernández and T. Mallick, "Theoretical Investigation Considering Manufacturing Errors of a High Concentrating Photovoltaic of Cassegrain design and its Experimental Validation," *Solar Energy,* vol. 131, p. 235–245, 2016.

[19] D. Talavera, J. de la Casa, E. Muñoz-Cerón and G. Almonacid, "Grid parity and self- consumption with photovoltaic systems under the present regulatory framework in Spain: the case of the University of Jaén Campus," *Renew Sustain Energy Rev,* vol. 33, p. 752–771, 2014.

[20] P. Benitez, J. Miñano, P. Zamora, R. Mohedano, A. Cvetkovic, M. Buljan, J. Chaves and M. Hernández, "High performance Fresnel-based photovoltaic concentrator," *Optics Express,* vol. 18, no. S1, pp. A25-A40, 2010.

[21] C. Domínguez, G. Antón and S. Askins, "Current-matching estimation for multijunction cells within a CPV module by means of component cells," *Prog. Photovoltaics: Res. Appl.,* vol. 21, no. 7, p. 1478–1488, 2013.

[22] J. Minano, P. Benitez, P. Zamora, M. Buljan, R. Mohedano and A. Santamaria, "Free-form optics for Fresnel-lens-based photovoltaic concentrators," *Optics Express,* vol. 21, p. A494–A502, 2013.

[23] Azure Space Solar Power GmbH, "Enhanced Fresnel Assembly - EFA Type: 3C42A – with 5.5x5.5mm2 CPV TJ Solar Cell Application: Concentrating Photovoltaic (CPV) Modules," 2014. [Online]. Available: www.azurspace.com/images/products/DB_3987-00-00_3C42_AzurDesign_EFA_10x10_2014-03-27.pdf. [Accessed 12 10 2016].

8. Copias de las publicaciones JCR

Efficiency and Acceptance Angle of High Concentrator Photovoltaic Modules: Current Status and Indoor Measurements

Pedro Pérez-Higueras, Juan P. Ferrer-Rodríguez*, Florencia Almonacid and Eduardo F. Fernández

*IDEA Solar Research Group, Centre for Advanced Studies in Energy and Environment (CEAEMA), Electronics and Automation Department, Universidad de Jaén, Las Lagunillas Campus, Jaén, 23071, Spain, *jferrer@ujaen.es*

Abstract

High Concentrator Photovoltaic (HCPV) modules (with concentrations higher than 300 times) have increased their conversion efficiency records up to more than 43% in the last years. This represents the maximum conversion efficiency by any type of photovoltaic (PV) module. Moreover, HCPV modules still have a theoretical potential for a significant efficiency growth. This work analyses the current status of efficiency records of HCPV modules and their evolution in the last 20 years, as well as the most efficient commercial HCPV modules, these last with up to around 34% efficiency nowadays. It is found that the efficiency growth of HCPV modules in the last years is considerably greater than that of other PV technologies like crystalline silicon (c-Si) or Thin Film. The values of efficiency, acceptance angle, geometrical concentration and power of current HCPV modules are gathered. Current efficiency values are typically centred in the range between 27% and 33%, whereas the current average of acceptance angle values is ±0.9º. Regarding the geometrical concentration of the efficiency record HCPV modules, it is typically lower than 400× whereas current commercial HCPV modules work in the range of 500-1000×. Moreover, a total of 24 commercial HCPV modules were characterised indoors at the CPV solar simulator at the University of Jaén in order to compare the datasheets with the experimental data. The measurement results, including the efficiency and acceptance angle characteristics, are presented and compared with datasheet values.

Keywords: High Concentrator Photovoltaics. Modules. Efficiency. Acceptance angle.

1. Introduction

A High Concentrator Photovoltaic (HCPV) module is made up of solar cells, optical devices and peripheral components necessary to generate electricity. The most industrialised HCPV module is typically a closed box containing a series of interconnected concentrator photovoltaic solar cells and their respective concentrator optical systems. The solar cells inside the HCPV module are interconnected through a circuit with typically only two terminals exiting it. This circuit is isolated to prevent current leakages and, in addition, all the components in the HCPV module are protected from different meteorological phenomena. A HCPV module also incorporates others elements such as bypass diodes to avoid the overheating of cells, mainly due to mismatch among cells and the shading that may take place when HCPV systems are working under real operating conditions. Among the basic requirements needed by a HCPV module from the point of view of its operation, it has to be capable of permanently concentrating sunrays onto the solar cells when mounted on a

2-axis tracker, and collecting their generated current. These functions are to be performed without incurring in high losses and removing enough heat in order to maintain the solar cells at controlled working temperatures.

Regarding to the terminology, HCPV modules are designed to concentrate sunlight more than 300-500 times over the solar cell [1]. Broadly speaking, HCPV technology can be considered in the concentration range between 100 to 2000 times [2]. Other authors refer to the HCPV technology to concentration ratios over 400 times [3] or even over 500 times [4]. The authors of this work find more convenient to use the definition of most than 300 times of concentrated sunlight over the solar cell since, as it will be described later, most of efficiency records of HCPV modules are measured under concentrated light between 300 and 400 times.

In relation to the use of the HCPV modules in energy production plants, the worldwide cumulative installed capacity of the HCPV technology is approximately 370 MW [5]. **Figure 1** shows the cumulative installed capacity of HCPV technology detailed by manufacturer. It can be seen that the highest installed capacity by a manufacturer (Suncore) is around 140 MW, a value that is around twice as high as for the second highest manufacturer in terms of installed capacity (Soitec, formerly Concentrix). The third company with more installed capacity is Arzon Solar (formerly Amonix) with a total of 40 WM. Despite more than 10 manufacturers have been installing HCPV plants in the last years, only three manufacturers installed the majority of the total HCPV capacity. The contribution of the other manufacturers to the total cumulative installed capacity is marginal.

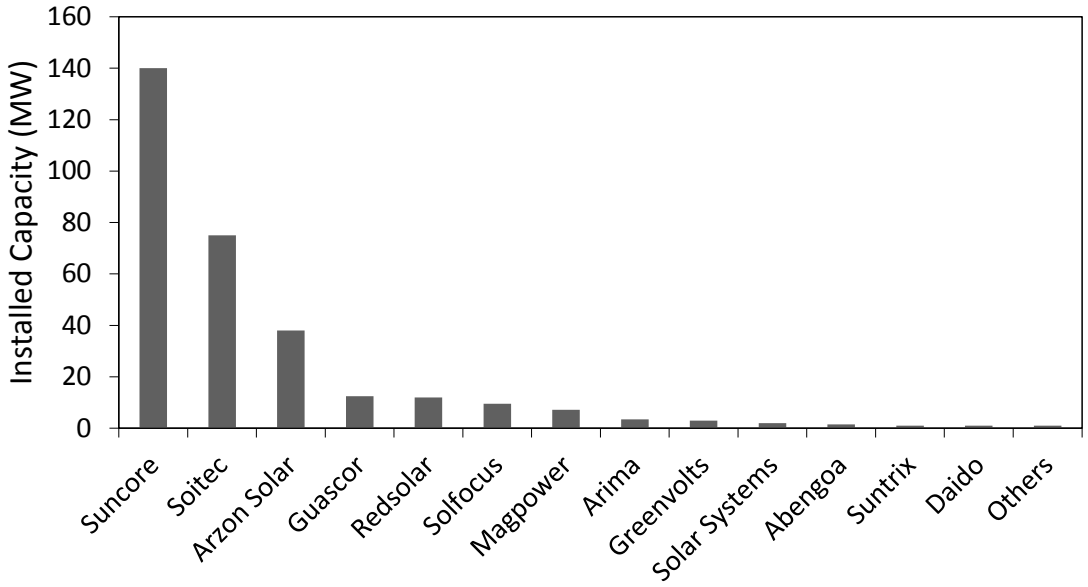

Figure 1. Global installed capacity of HCPV technology by companies [5-7].

Although the CPV technology has been developed some decades ago, current CPV (especially HCPV) is a relative new technology with a smaller market than conventional PV. This is mainly due to the higher electricity generation costs of the HCPV respect to the conventional PV systems [8]. In order to make HCPV more competitive and increase the market, the costs associated to the HCPV systems need to diminish. One way to lower costs is to reduce the total amount of material involved in the HCPV systems, particularly, reducing the quantity of most expensive materials and also replacing them by less expensive materials as far as possible. In order to achieve this costs decrease, among other possibilities, the next improvements are indicated:

i. To increase the concentration since the total amount of expensive semiconductor material is decreased by replacing it with less expensive concentrator optics.
ii. To increase the efficiency since, in this way, HCPV modules can be smaller while maintaining their generated power. Therefore, less material will be needed for a HCPV module, also smaller tracker systems, less wire connections, less land area, etc.
iii. To increase the misalignment tolerance, or acceptance angle of HCPV modules, since less accurate and expensive tracker systems will be needed.

Therefore, to increase concentration, efficiency and acceptance angle it is needed to reduce the cost of electricity generated by HCPV systems. Moreover, these three parameters can be considered as merit figures from the point of view of costs, besides economical parameters.

Thus, this work is intended to serve as a review of current HCPV modules, placing an emphasis on their efficiency and acceptance angle characteristic. Moreover, indoor characterization results (using a CPV Solar Simulator) of different commercial HCPV module technologies, including the measurement of the efficiency and the acceptance angle characteristic, are presented. These measurement results will be useful to validate the data given by the manufacturers and also to provide more information about the HCPV modules.

The literature concerning different aspects related to HCPV modules is extensive. For instance, there are many publications about multi-junction solar cells [9] and optical concentrator systems [10, 2]. In those works, a lot of information dealing with concentrator solar cells efficiency and with the acceptance angle of the concentrator optical systems is delivered. Nevertheless they rarely provide much information concerning efficiency and acceptance angle of HCPV modules. It is possible also to find in the literature many works about different theoretical models that calculate electrical parameters of the HCPV modules under different conditions [11-14]. Nevertheless, those theoretical models allow to estimate efficiency only of the specific HCPV module used for validating the model. However, some works can be found in which some efficiency and/or acceptance angle data of HCPV modules are given [1,7,15], although those data are either limited or not up-to-date. Additionally, some works include information related to prototypes of HCPV modules [16] but those have been not considered in this work since this is limited to commercial ones.

Besides, detailed information about commercial HCPV modules is limited since manufacturers usually consider it as confidential, and therefore, e.g. less precise data are given in company brochures, or even HCPV modules' datasheets are absent in manufacturer's websites. Moreover, many manufacturers have ceased their activity and closed their websites. Considering the information related to HCPV modules, it is very limited in quantity, despite HCPV market still exists. In fact, nowadays, some of the referred companies in **Figure 1** do not manufacture HCPV modules since they either have closed down, or moved their business to conventional PV, or transferred their technology to other companies –like in the case of Soitec to Stace (Saint-Augustin Canada Electric Inc.) and Daido to BSQ Solar. Nevertheless, this work includes the HCPV modules of those companies in order to provide a global vision of the HCPV modules technology. Thus, there is currently a lack of information on module specifications, features, performance, designs, etc. In addition, most of the published data are incomplete. For all those reasons, it is worthy to compile some useful information about HCPV modules like in this work.

This Paper is structured as follows. In the second section, the key definitions for this current status analysis, related to HCPV modules, are described, namely, efficiency, acceptance angle and concentration-acceptance angle product (*CAP*). In the third section, the evolution of efficiency values of HCPV modules in the last 25 years is presented and also record measurement values are

analysed. In the fourth section, the current status of commercial HCPV modules is shown and analysed in terms of efficiency and acceptance angle. In the fifth section, indoor measurement results are presented and analysed, as well as the experimental setup is described. In the sixth section, the summary and conclusions are exposed.

2. Definitions

In this section, the definitions involving the key magnitudes, needed for understanding the performance of HCPV modules, are described.

2.1. Efficiency

In order to have a deep view of the efficiency, it is worthy to analyse its definition. The efficiency of a HCPV module, η, is defined as the relation between the electric power produced by the module, P_{output}, and the incoming irradiance, P_{input}, (Eq. 1):

$$\eta = \frac{P_{output}}{P_{input}} \tag{1}$$

Concerning the energy conversion process, concentrator solar cells are the only elements in a HCPV module that generate electrical energy. The efficiency of a solar cell, η_{CELL}, can be expressed in terms of the global irradiance, G, impinging on its surface, the solar cell's area, A_{cell}, and the electrical power provided by the cell, P_{cell} (Eq. 2):

$$\eta_{CELL} = \frac{P_{cell}(W)}{G\left(\frac{W}{m^2}\right)\cdot A_{cell}\left(m^2\right)} \tag{2}$$

Applying this definition to HCPV modules, the overall module efficiency, η_{MOD}, is related to the electrical power generated, P_{mod}, when an incoming direct normal irradiance, DNI, is collected at the module's surface, A_{mod} (Eq. 3):

$$\eta_{MOD} = \frac{P_{\mathrm{mod}}(W)}{DNI\left(\frac{W}{m^2}\right)\cdot A_{\mathrm{mod}}\left(m^2\right)} \tag{3}$$

From the point of view of the optics, the efficiency of the concentrator optical system, η_{OPT}, is referred to its capability of collecting and focusing sunrays onto the relative small solar cell area. For a monomodule, it can be defined by the next equation, using the concept of geometrical concentration, $C_g=A_{mod}/A_{cell}$ (Eq. 4):

$$\eta_{OPT} = \frac{I_{sc,concentrated}(A)}{I_{sc,ref}(A)}\cdot\frac{1}{C_g} \tag{4}$$

where $I_{sc,ref}$ is the short-circuit current of the solar cell under reference conditions (reference spectrum ASTM G173-03 and an irradiance level of 1000 W/m^2 [17]) and $I_{sc,concentrated}$ is the short-circuit current of the HCPV monomodule under the same reference conditions, thus when the solar cell is converting concentrated sunlight into electricity. Taking into account the previous definitions, the total efficiency of a HCPV module can be stated as (Eq. 5):

$$\eta_{MOD} = \eta_{CELL} \cdot \eta_{OPT} \cdot \left(1 - L_{\text{mod}}\right) \quad (5)$$

where L_{mod} represents all the electrical losses of the rest of elements in the HCPV module (diodes, wires, etc.). Note that the contribution of the optical efficiency to the module efficiency is as important as the solar cell efficiency, since it is modelled as a linear factor in (Eq. 5). Thus, the HCPV module efficiency can be understood as the product of three partial efficiency factors (cell, optical system, and rest of electrical connections).

2.2. Acceptance angle

Although the efficiency of a HCPV module is a crucial parameter, its acceptance angle is also very important in relation to the electrical energy that can produce such kind of modules in real operating conditions. The acceptance angle of the HCPV module has to be considered when designing a HCPV installation, since the accuracy requirements of the tracker systems for the HCPV modules will be relaxed by increasing the misalignment tolerance of the HCPV modules.

The acceptance angle, θ, of a HCPV module can be defined as the angle of misalignment respect to the incoming sunlight for which its short-circuit current is 90% of the value under perfect alignment to the incoming sunlight (Eq. 6):

$$\frac{I_{sc}(\theta)}{I_{sc}(0)} = 0.9 \quad (6)$$

where $I_{SC}(0)$ the short-circuit current of the HCPV module under normal alignment respect to the incoming sunlight and $I_{SC}(\theta)$ is that by the acceptance angle. Another possibility is to define the acceptance angle in terms of power generated instead of the short-circuit current. Both definitions may lead to different angular values. Commonly, the first definition (short-circuit current) is used. Although different acceptance angle characteristics may have the same value of acceptance angle, this last represents a useful parameter for characterising the angular behaviour of the HCPV modules.

2.3. Concentration-Acceptance angle product (*CAP*)

High acceptance angle values are difficult to achieve with very high concentration levels. Therefore, when working with HCPV modules, it is common to utilize the concept of concentration-acceptance angle product (*CAP*). This figure of merit (*CAP*) [18], can be defined as (Eq. 7):

$$CAP = \sqrt{C_g} \cdot \sin\theta \,. \quad (7)$$

The concentration-acceptance angle product is a measurement of how much near the concentrator system is to the ideal maximum concentration.

3. Evolution of HCPV module efficiency and efficiency records

In this section, the efficiency values of the HCPV modules within around the last 25 years are analysed and compared with other PV technologies. In addition, the five HCPV modules with highest efficiencies are discussed.

In order to have a look to the evolution of the HCPV modules' efficiency in the last decades, HCPV modules record efficiency data versus the year of appearance are shown in **Figure 2**. These values are connected with a straight line to make easier the visualization of the efficiency growth trend, and they are mainly based on the data of Green et al [19] through all the versions of the solar cell efficiency tables and from data of Fraunhofer ISE [6]. Also, efficiency values corresponding to HCPV sub- and minimodules are presented. In order to compare the efficiency growth of the HCPV technology with other photovoltaic technologies, the efficiency evolution lines for c-Si (crystalline silicon) and Thin Film modules are added. These last two module technologies present a slower efficiency growth than that of HCPV modules, as can be seen in **Figure 2**. More in detail, on one hand, HCPV modules efficiency has increased from around 19% in 1992 to around 39% in 2017 which results in an annual increment of +0.83%. It is remarkable that the increase in the efficiency of HCPV modules is even greater (+1.43%/year) from 2010 to present time than in the period from 1992 to 2010 (+0.56%/year). On the other hand, c-Si modules efficiency has grown from around 21% in the year 1992 to around 24% in 2017, which supposes a yearly efficiency increment of +0.12%. Whereas in the case of Thin Film modules, their efficiency has changed from around 12% in 1992 to around 20% in 2016, with a yearly efficiency increment of +0.3%. It can be seen in **Figure 2** that HCPV modules' efficiency evolution has substantially overtaken the growth of other photovoltaic technologies.

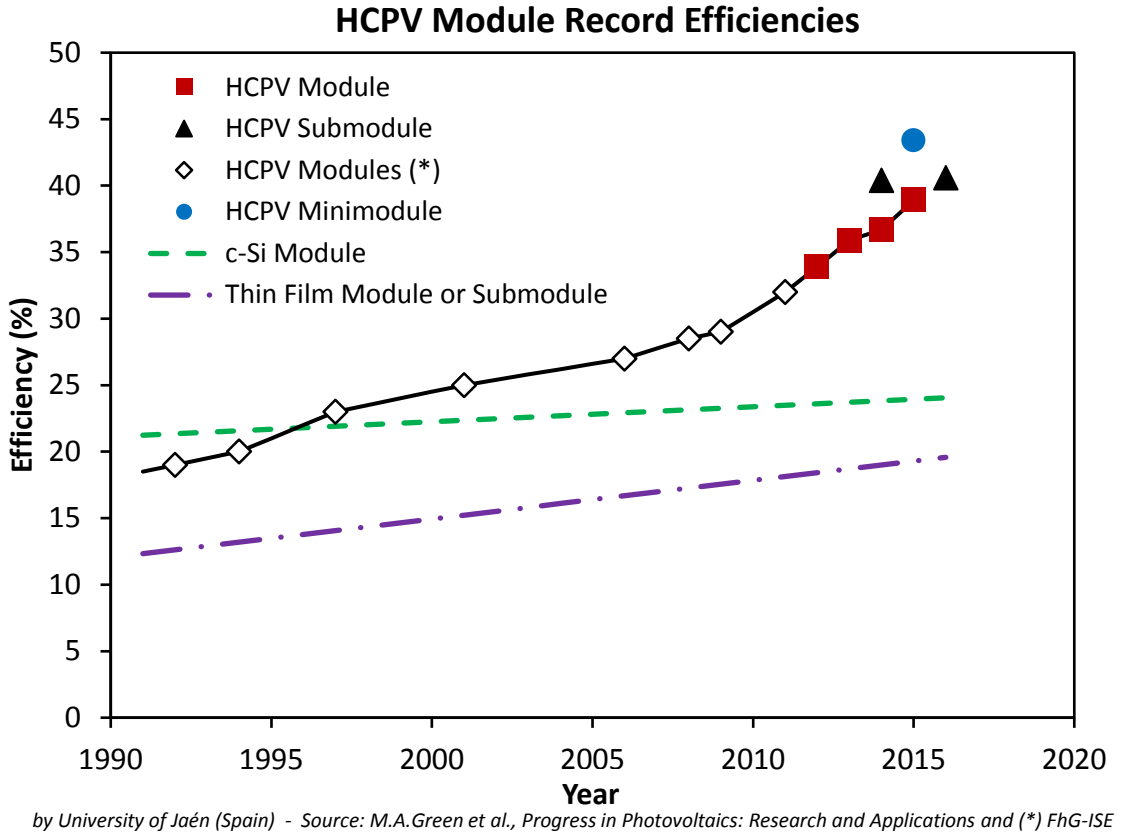

Figure 2. Efficiency evolution of HCPV Modules and other photovoltaic technologies [6,19].

According to the efficiency record data collected by Green et al., the list of the five record efficiencies (certified by renowned laboratories) of HCPV modules, minimodules or submodules is shown in **Table 1**, when considering only geometrical concentrations above 300×, at conditions of DNI=1000 W/m^2 and solar cell temperature of 25 ˚C [20]. Moreover, the geometrical

concentration, manufacturer, date of measurement, solar cell type and optics used are detailed in **Table 1**. All these devices were measured in different experienced and renowned test centres. The efficiencies of these five record HCPV module devices range from 33.9% (Semprius [21]) up to 43.4% (Fraunhofer ISE), and up to 38.9% (Soitec) if no minimodule or submodule are considered. It is remarkable that among these five HCPV module devices, different concentrator solar cell technologies are involved, like microtransfer triple-junction solar cells (Semprius), triple-junction solar cells (Amonix), four-junction solar cells (Fraunhofer ISE and Soitec) or triple-junction plus a Si solar cell (University of New South Wales). Considering the optical concentrator systems, distinct strategies from the conventional Fresnel lens (Soitec and Amonix) are present among these record devices such, e.g., central tower plus spectrum splitting (University of New South Wales), achromatic full-glass lens (Fraunhofer ISE) or solid lenses (Semprius). The geometrical concentrations related to these HCPV efficiency record modules are mostly near 350× (Soitec, Fraunhofer ISE and University of New South Wales), being the maximum one the case of Semprius with 1111×–around triple than in the other cases. Concerning the date of measurement, it is remarkable that two of the efficiency records were achieved some years ago, i.e. Semprius in 2012 and Amonix in 2013, while the other ones are more recent.

Table 1 Record efficiencies of HCPV modules, minimodules and submodules measured in test centres. Note that all the measurements are rated to DNI=1000 W/m^2 and cell temperature of 25 ºC.

	Efficiency (%)	**Geometrical concentration (×)**	**Manufacturer**	**Date**	**Cell type**	**Optics**
1 [19]	43.4[a]	340	Fraunhofer ISE	2015	Four-junction	Achromatic full-glass lens
2 [19]	40.6[b]	365	University of New South Wales	2016	Triple-junction plus Si-cell	Central tower plus spectrum splitting
3 [19]	38.9	333	Soitec	2015	Four-junction	Fresnel
4 [19]	35.9	N/A	Amonix	2013	Triple-junction	Fresnel
5 [21]	33.9	1111	Semprius	2012	Microtransfer. Triple-junction	Lens

[a]Minimodule. [b]Submodule

4. Current status of commercial HCPV modules

In this section, current commercial HCPV modules are analysed in terms of efficiency, concentration and acceptance angle.

4.1. Current efficiency and concentration values

Current commercial HCPV modules have increased significantly their efficiency in the last years until reaching record values near to 34%, which is directly influenced with the fact that, nowadays, manufacturers provide commercial concentrator solar cells with efficiencies over 40%. Also, the geometrical concentration ratio of some current HCPV modules is greater than 1000× (between 1100× and 1300×), more than double than some years ago. It has been achieved either by increasing the size of the primary optics or by reducing the size of the solar cells used. In addition, secondary optics are typically used in HCPV modules, since they are convenient to homogenize the concentrated light onto the solar cell at high concentrations. In terms of heat removing, this increase in the concentration ratio may lead to higher solar cell temperatures. Nevertheless, nowadays HCPV modules can manage heat removing only through passive cooling.

In order to have an idea of the performance and main characteristics of different commercial HCPV modules, a list of the extracted parameters, from the available published information, is showed in both **Table 2** and in the Annex I (data of previous models of HCPV modules) with the next items: geometrical concentration ratio, the kind of optical device used, the power of the HCPV module and its efficiency, the acceptance angle and *CAP* value. The concentration-acceptance angle product values are calculated from the data provided by the manufacturers. Note that power and efficiency data are relative to the conditions of cell temperature T_{cell}=25 ºC and direct normal irradiation DNI=1000 W/m^2. For composing the tables, available data of cell operating temperature and power are translated to the aforementioned conditions [12, 22-26].

Table 2. HCPV Modules data from their datasheets at T_{cell}=25 ºC and under DNI=1000 W/m^2 [7,15].

HCPV Module	C_g **(×)**	**Optics**	**Power (W)**	**Efficiency (%)**	**Half Acceptance angle (º)**	***CAP* (-)**
Abengoa M300S	1300	Fresnel	234[a]	32.5	1.0	0.63
Arima CPV-G2-140	1000	Fresnel	142.5	34.0	1.0	0.55
Arzon Solar	n/a	Fresnel	2700	31.7[a]	n/a	n/a
Daido 280 W	820	Fresnel	280	28.0	0.9	0.45
Emcore G3-1090	1090	Fresnel	455	28.0	0.7	0.40
Guascor	700	Fresnel	345[a]	33.0	n/a	n/a
Isofoton GEN-2	500[a]	Fresnel	95	27.7	0.8	0.31
Magpower TRK60	800	Fresnel	8336[a]	25.0[a]	1.9	0.94
Redsolar	500	Fresnel	n/a	32.0	n/a	n/a
Semprius SM-U01	1111	Lens	87.5	33.9	0.8	0.47
Soitec CX-M500	500	Fresnel	2450	31.8	0.4	0.16
Solfocus SF-1100P	650	Mirror	390[a]	27.0[a]	1.0	0.44
Soliant SE-1000X	1000	Fresnel	554[a]	27.0[a]	n/a	n/a
Suncore DDM-090X	1090	Fresnel	490[a]	31.0[a]	0.7	0.40
Suntrix SCPV-500	594[a]	Fresnel	266	28.0	0.75	0.32
mean	***833***	***n/a***	***1202***	***30.0***	***0.90***	***0.46***

[a] Calculated from modules' datasheets.

From the data of the HCPV modules of **Table 2**, the following analysis can be done.

In relation to the concentration ratio values, the average is 833×, with 40% of the HCPV modules with higher concentrations and 60% of them with lower concentrations. In one case, a concentration ratio much greater than the other HCPV modules is shown: Abengoa with 1300× −beyond the theoretical limit imposed by chromatic aberrations of stand-alone lenses [2]. Apart from that case, five of the HCPV modules work at concentration ratios higher than 1000×: Arima, Emcore, Semprius, Soliant and Suncore. There are also some examples of concentration ratios around 500× (Isofoton, Redsolar, Soitec and Solfocus), which is the minimum value found.

Concerning the optics, on one hand, many of the concentrator designs are based on Fresnel lenses plus secondary optics. On the other hand, mirror-based designs were also available in the market, like in the case of Solfocus, but working at relative lower concentration ratios (650×) than the typical maximum concentration of lens-based ones. Some other less typical designs, like dome-shaped Fresnel lens (Daido), or based on light-guides (Sun Simba^{TM} of Morgan Solar) are also used.

Regarding to the power of the HCPV modules, their mean value is 1202 W, and these values vary in a wide range, from 87.5 W (Semprius) to 8336 W (Magpower). Excepting for the cases of Magpower (with 8336 W), Arzon Solar (with 2700 W) and Soitec (with 2450 W), most of the HCPV modules have a maximum power no higher than around 550 W. The dispersion in the power values is a direct consequence of the wide variety of number of cells used in the HCPV modules.

Finally, the available efficiency values show an average of 30% and range from a minimum of 25% (Magpower) to a maximum of 34% (Arima). Note that this maximum efficiency of the module of Arima was not certified by a renowned laboratory and therefore it is not included in **Table 1** (efficiency record modules). From all the analysed HCPV modules, seven different manufacturers assure to provide HCPV modules with more than 30% efficiency (Abengoa, Amonix, Arima, Redsolar, Semprius, Soitec and Suncore).

Considering now only the five highest efficiency HCPV commercial modules (Abengoa, Amonix, Arima, Redsolar and Semprius), they show efficiency values logically lower than the record values of **Table 1** and range from 32.0% (Redsolar) up to 34% (Arima). Most of these highest efficiency HCPV modules utilise Fresnel lenses as primary optic elements with the only exception of Semprius, using small solid plano-convex lenses. Two of these five modules overtake the geometrical concentration ratio of 1000× (Abengoa and Semprius). The lowest geometrical concentration value correspond to Resolar, with only 500×. In relation to the type of solar cell used, all of these HCPV modules incorporate multi-junction solar cells. Concerning the manufacturers by countries, two of them are from USA (Amonix and Semprius), other two of them are Asiatic (Arima in Taiwan and Redsolar in China), and Abengoa is European (Spain). It can be also observed that most of the record efficiency values of **Table 1** correspond to concentration ratios no higher than 400×, which is much lower than comparing with the highest efficiency commercial HCPV modules.

Using the 15 efficiency values of **Table 2**, the histogram of **Figure 3** is built. This figure shows that most efficiency values are in the range between 27% and 33% and they present a normal distribution with a mean value of 30%. In contrast, the normal distribution corresponding to the

efficiency values for the year 2010 [1] has a mean value of 24%. This shows a clear increase in the HCPV modules efficiency in the last years.

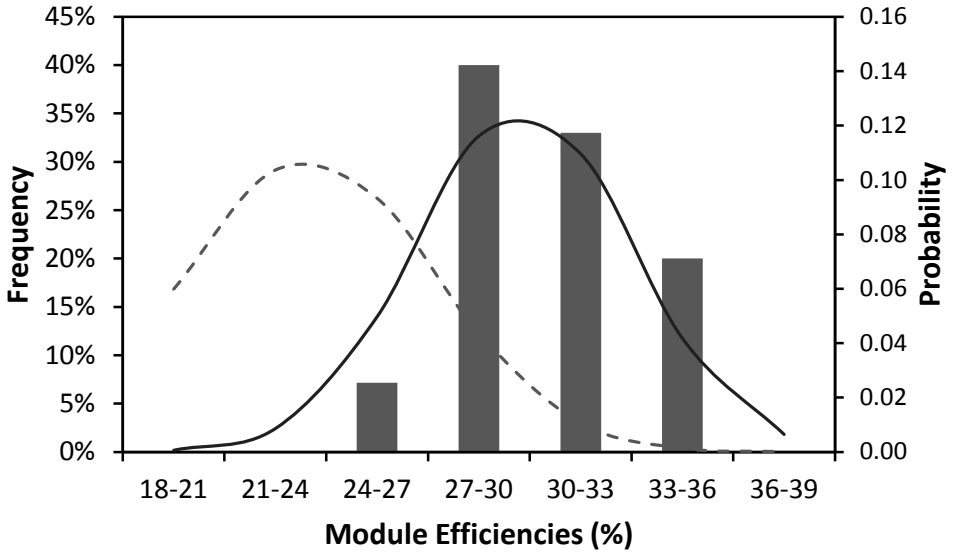

Figure 3. Histogram and probability density functions of HCPV module efficiencies. The solid line represents the normal distribution of current efficiency values, N(30,3), whereas the dashed line represents the normal distribution, N(24,4) of efficiency values for the year 2010 [1].

For commercial HCPV modules, their efficiency values can be plotted (see **Figure 4**) versus their geometrical concentrations. As it was previously commented, from the point of view of reducing the cost of producing electricity through the HCPV technology, those modules with simultaneously high efficiency and high geometrical concentration levels are desired in principle, since they will produce more energy per unit of area, and also less photovoltaic material will be required, respectively. In the case of the modules represented in **Figure 4**, those points in the upper-right zone, i.e. more than 1000× as geometrical concentration and above 30% of module efficiency, correspond to the more competitive designs in principle. In this figure, also data of year 2010 are included (hollow points). These are centred in around 500× of geometrical concentration and with efficiency no higher than 28%. It can be observed that the efficiency and geometrical concentration of current HCPV modules have dramatically increased in the last years. Some data corresponding of year 2010 used for both **Figure 3** and **Figure 4** are taken from Pérez-Higueras et al [1].

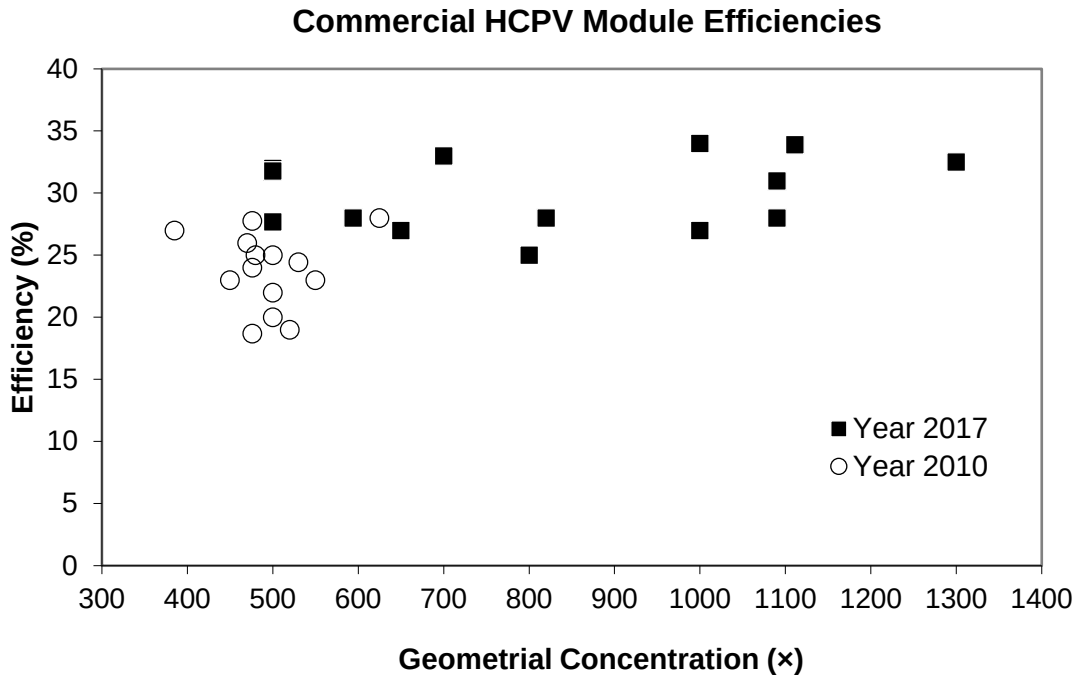

Figure 4. Current module efficiencies of different commercial HCPV technologies (datasheets) versus geometrical concentration. Also values corresponding to the year 2010 [1] are plotted.

4.2. Current acceptance angle values and *CAP*

The acceptance angle values of current HCPV modules (**Table 2**) range from ±0.4º (Soitec) to ±1.9º (Magpower), although they are typically in the range of ±0.7º to ±1.0º (Arima, Emcore, Semprius, Solfocus and Suncore), being the average around ±0.9º. The concentration-acceptance angle product, *CAP*, values have an average of 0.46, and are of a minimum of 0.16 (Soitec) and a maximum of 0.94 (Magpower).

In **Figure 5** current values of acceptance angle of commercial HCPV modules versus geometrical concentration are plotted. Most half acceptance angle values are between 0.7º and 1.0º and are spread relatively uniformly versus the geometrical concentration values. As it was commented before, the HCPV modules with best optical systems are those with highest both concentration and acceptance angle. It can be observed in **Figure 5** that the maximum acceptance angle value (1.9º) corresponds to a HCPV module with a medium geometrical concentration ratio, whereas the HCPV module with highest concentration (1111×) has an acceptance angle value not much higher than the average. Therefore, from the point of view of the optics, none of the commercial HCPV modules can be considered as the best. This last is equivalent to the observation that none of the points of acceptance angle of **Figure 5** are in the upper-right zone.

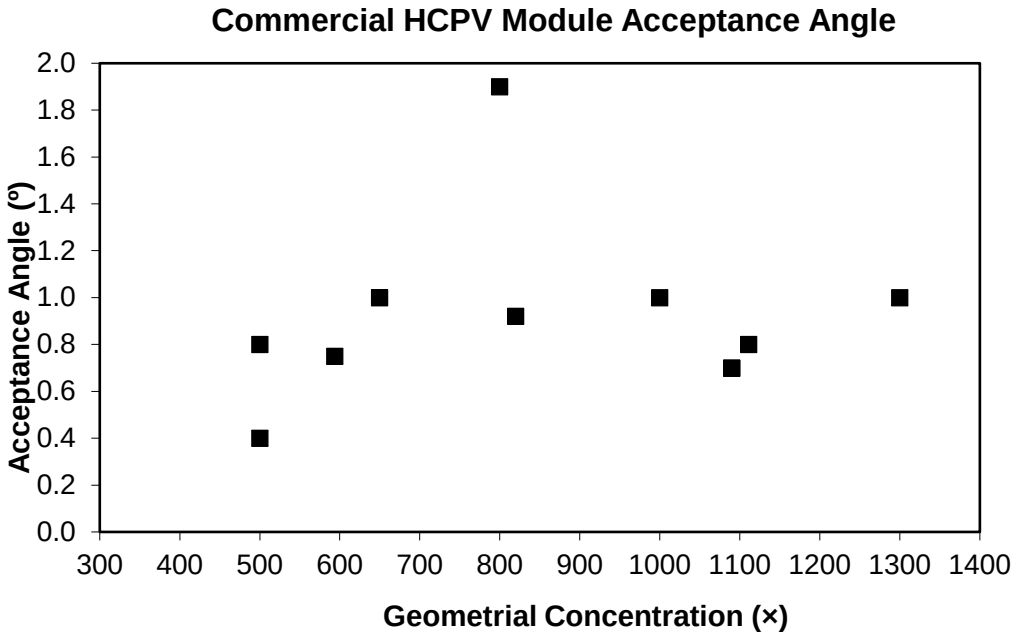

Figure 5. Current acceptance angle and efficiency values of HCPV modules versus their geometrical concentration.

4.3. Combined analysis of C_g, efficiency and acceptance angle

As it was previously commented, among other possibilities, concentration, efficiency and acceptance angle of a HCPV module are needed to be increased in order to lower the cost of the generated electricity of a HCPV system.

From the data of **Table 2**, the best HCPV modules concerning the three categories, geometrical concentration, efficiency and acceptance angle, are selected and gathered in **Table 3**. This will inform if it is possible to find a HCPV module with best values simultaneously in those three categories. The three selected HCPV modules are: Abengoa, Arima and Magpower. Their geometrical concentration values range from 800× (Magpower) to 1300× (Abengoa). Their efficiency values range from 25% (Magpower) to 32.5% (Abengoa). Finally, their acceptance angle values range from 1º (Abengoa and Arima) to 1.9º (Magpower). It can be observed that none of those selected HCPV modules simultaneously reaches the maximum value of these paremeters. Moreover, each of the three HCPV modules only has as maximum value one of the three parameters. For instance, the module Abengoa is that with highest C_g (1300×) but it has lowest efficiency (32.5%). Also, the module Arima is the best in one category (with 34% efficiency) but with the worst acceptance angle (1º). Finally, the module Magpower has the highest acceptance angle (1.9º) but also the lowest geometrical concentration (800×). Note that *CAP* values are added in this table to complete the information.

Table 3. Geometrical concentration, efficiency and acceptance angle of the three HCPV modules with highest values of one of these parameters. *CAP* values are also added.

	C_g (×)	**Efficiency (%)**	**Acceptance Angle (º)**	***CAP* (-)**
Abengoa M300	1300	32.5	1.0	0.47
Arima CPV-G2-140	1000	34.0	1.0	0.55
Magpower TRK60	800	25.0	1.9	0.94
Mean value	***1033***	***30.5***	***1.3***	***0.65***

That idea can be graphically shown as in the radial plot of **Figure 6**, in where each HCPV module of **Table 3** is represented with a non-equilateral triangle (which would be the case of a HCPV module with the three parameters in a maximum simultaneously).

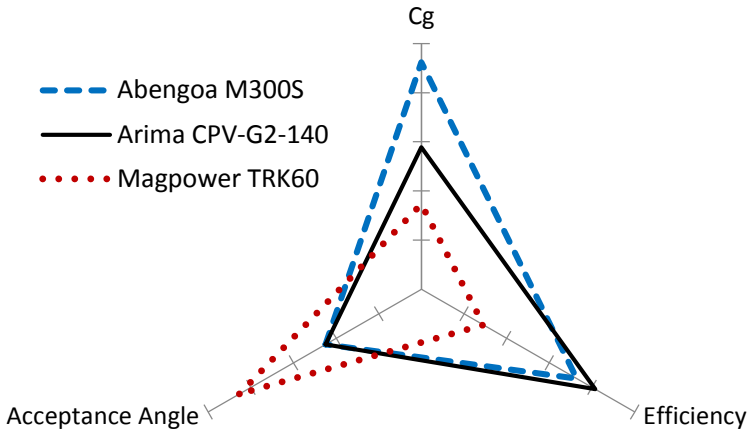

Figure 6. Radial plot of the three best HCPV modules in terms of the next parameters: geometrical concentration, acceptance angle and efficiency.

5. Indoor Measurements

In order to obtain real measurement data of the parameters of the HCPV modules analysed in the previous sections, a series of indoor measurements of a total of 24 HCPV modules were performed in a CPV Solar Simulator under controlled and repeatable conditions. These measurement data are useful to be compared with the data given in datasheets or in any other kind of publication. Thus, in this section, first, the experimental indoor measurement setup is described, then, efficiency and acceptance angle indoor measurement results are presented, discussed and compared with datasheets.

5.1. Experimental Setup

As mention above, controlled indoor measurements in a CPV Solar Simulator were performed in order to measure HCPV modules with guaranteed repeatability in terms of incoming irradiance, spectral distribution, ambient temperature, etc. The details of the indoor test laboratory "Helios 3198" CPV Solar Simulator are described below.

The "Helios 3198" CPV Solar Simulator uses a xenon flash bulb for simulating the solar radiation and a parabolic mirror as a collimator [27]. Light collimation is needed in order to perform the electrical characterization of HCPV modules, since they only utilise direct normal irradiation [15]. For this purpose, the flash tube (light source) is located at the focal point of the parabolic mirror, then the light rays are reflected parallel to the parabola's optical axis. The parabolic mirror has a focal distance of 6 m and a diameter of 2 m and its surface is capable of reflecting light coming from the lamp with relative good uniformity (less than ±5% intensity deviation from average) [27]. The angular size of the lamp seen from the parabolic mirror's surface is similar to that of the sun (±0.3º) and is conserved after reflection on the mirror. The spectral distribution of the light emitted by the Xenon flash bulb is similar enough to that of the AM1.5D low AOD spectrum [28]. Since this is a multi-flash simulator, a series of current-voltage points, preceded each one by a flash pulse, are measured. A reference irradiance sensor is used in order to measure the I-V

curve for a determined irradiation level. For that, the short-circuit current of a previously calibrated monomodule is registered during the light pulse in order to measure each I-V point at the desired irradiance level. Moreover, it is possible to characterise the HCPV module at different irradiance levels, or DNI, (e.g. from 700 to 1000 W/m^2) during the decay of each light pulse [29]. For this interval of DNI, the spectral matching ratio, *SMR(top/mid)* [30], is 1 ±0.05, as measured using a spectro-heliometer ICU-3J25 [31, 32]. Concerning the temperature, it is maintained at 25 ºC during the whole characterisation.

For the calculation of the HCPV module efficiency, only the primary optics area is considered (without frames). Each HCPV module under test is mounted on a 2-axis adjustable support structure that permits to search for an optimum alignment of the module. All these characteristics assure the indoor measurement of HCPV modules under controlled and repeatable conditions.

5.2. Results and discussion

5.2.1. Measurement of Efficiency

A total of 24 HCPV modules of three different manufacturers, being of a total of four different models, are indoors characterised using the described experimental setup. From these 24 HCPV modules, twelve modules are of the same model of a Manufacturer A; nine modules are of the model B1 of a Manufacturer B; two modules are of the model B2 of the Manufacturer B too; and, one module is of the Manufacturer C. Due to the difficulty of obtaining commercial HCPV modules, only those ones have been characterised. Although these HCPV modules are not completely representative, their characterisation provide useful data, since the related published information is limited.

The HCPV modules are characterised for irradiance values from 700 W/m^2 to 1000 W/m^2 in steps of 50 W/m^2, and for standard test conditions of DNI=1000 W/m^2, the measured efficiency values range from 23.1% up to 27.7%.

The measured average efficiency of the 12 HCPV modules of the Manufacturer A is around 3% lower than the data given in the manufacturer's datasheet. In the case of the 9 HCPV modules of model B1 of Manufacturer B, the measured average efficiency is around 3.5% higher than in the manufacturer's datasheet. For the group of two HCPV modules B2 of the Manufacturer B, the measured average efficiency is around 3% lower than in the manufacturer's datasheet. For the HCPV module of Manufacturer C, the efficiency measured is around 2% lower than in the datasheet. It is observed that those average efficiency values are within around ±3.5% deviation from their respective manufacturers' datasheets, thus, they are within the typical tolerances for HCPV modules.

For the cases of the B2 HCPV modules of Manufacturer B and that of Manufacturer C, the low number of samples gives a less representative measurement. However, in the cases of the HCPV modules of Manufacturer A and those B1 of Manufacturer B, the measurements can be considered as representative enough. Moreover, for those last groups of HCPV modules, a histogram with the measured efficiency values can be plotted (see **Figure 7**). In this figure, also efficiency results of Abengoa HCPV modules (Manufacturer D) from [7] are included, in order to complete the analysis. These histograms are built using the normalized efficiency data to allow a comparison. The dashed line represents a normal distribution that fits the frequency histogram, resulting in this particular case approximately the same normal distribution for both experimental series of data,

characterised by N(100,2), i.e. with a standard deviation of only 2%. This assures a low dispersion of the indoors measured efficiencies. From the histogram of **Figure 7**, it also can be concluded that these three types of HCPV modules are manufactured with a good repeatability in terms of efficiency and with centred values around their respective average ones.

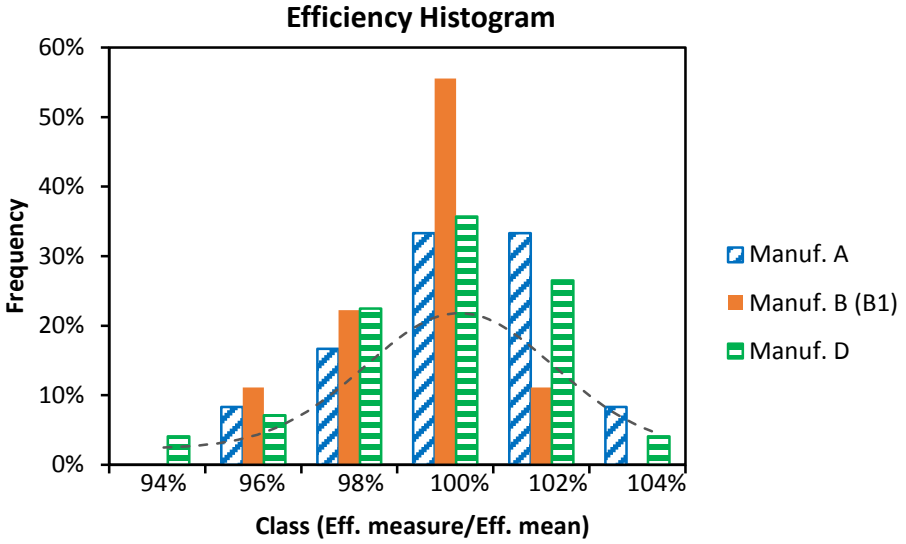

Figure 7. Normalized efficiency histogram of HCPV modules measured indoors with the CPV solar simulator "Helios 3198" at the University of Jaén and of data published in [7].

In addition to this analysis of the indoor measured efficiencies at standard test conditions, an analysis of the behaviour of the efficiency respect to the irradiance can be conducted. For that, the efficiency of the modules measured indoors can be plotted versus the DNI in the range of 700-1000 W/m^2.

The results are shown in **Figure 8** for four different models HCPV modules, one module of Manufacturer A, one module of the group B1 and another of group B2, both of Manufacturer B, and the module of Manufacturer C. There is an efficiency decrease for increased DNI for the four HCPV modules, which is of a maximum of 1.3% (for Manufacturer A) in absolute value, when analysing the efficiency between 700 and 1000 W/m^2 of DNI. This decrease is expected, since the most concentrator solar cells utilised by the HCPV modules manufactures, present a maximum efficiency at 500×. Thus, for increased concentrations, the efficiency of the HCPV modules is expected to decrease.

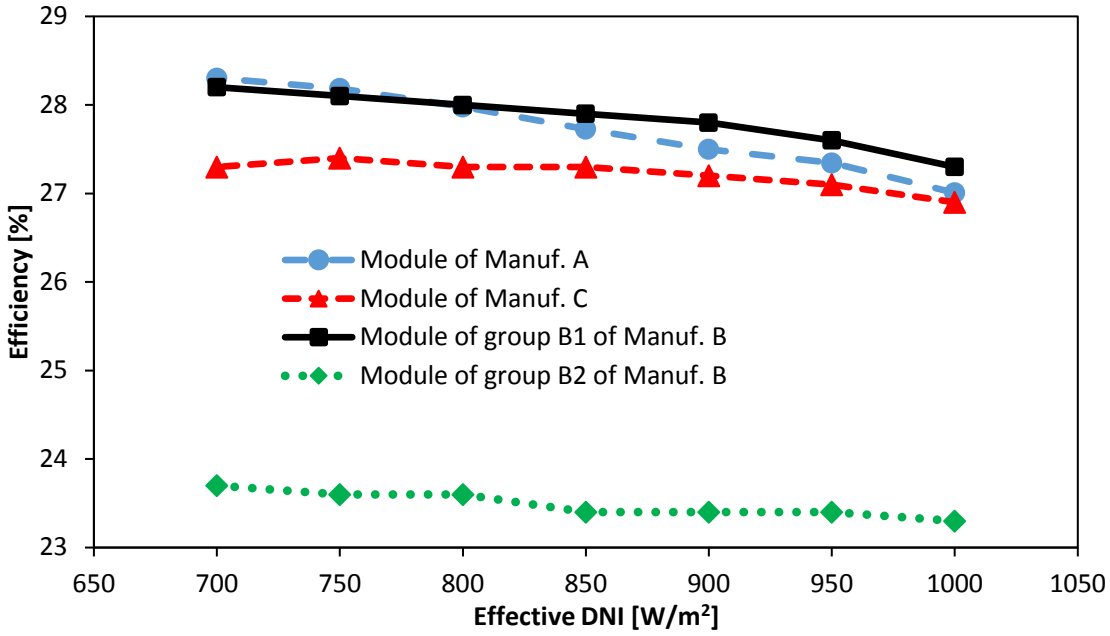

Figure 8: Efficiency measured indoors versus DNI.

5.2.2. Measurement of the acceptance angle characteristic

The procedure of measuring indoor acceptance angle characteristics of HCPV modules consists in acquiring a series of I-V curves corresponding to different and controlled tilted positions of the HCPV module. This is possible since the HCPV module under test is mounted on the 2-axis adjustable support structure. This support structure is similar to that of a tracker system with the difference that the mechanism manually is actioned. A laser pointer is fixed to the support structure in such a way that its light impacts on a screen at around 7 m distance creating a spot of around 2 mm diameter. For every I-V curve measurement, the position of the laser spot on the screen is registered. Tilt angles of I-V measurements are known by measuring the distances among the laser spots on the screen.

The angular characterisation is performed for a total of 16 HCPV modules. These HCPV modules are: the 12 modules of Manufacturer A; one of the modules of the group B1 and the two modules of the group B2, all of Manufacturer B; and, the module of the Manufacturer C.

The acceptance angle measurement results are useful to be compared with those ones of the respective datasheets and they range from a minimum of ±0.51º to a maximum of ±0.97º. In the case of the HCPV modules of Manufacturer A, their measured average of I_{SC} acceptance angle matches that of their datasheet. The module of the group B1 presents an acceptance angle 7.4% higher than in its datasheet. The average of acceptance angle values of the two modules of the group B2 matches that of their datasheet.

Only in the case of the HCPV modules of the Manufacturer A, there are enough acceptance angle values for building a histogram as in **Figure 9**. It shows a symmetric distribution of the half acceptance angle centred in the range 0.77º-0.82º, with 50% percent of the total frequency distribution for that group. The distribution can be adjusted by a normal distribution with mean

value 0.80º and a dispersion of 0.05º, N(0.80º,0.05º). This histogram takes account of the small dispersion in the acceptance angle values of this kind of HCPV modules.

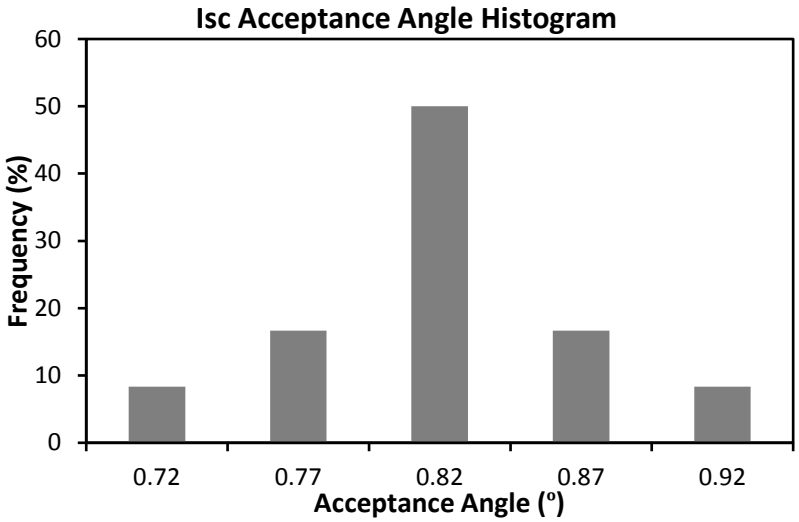

Figure 9. I_{SC} acceptance angle histogram corresponding to the indoor measurements of the HCPV modules of Manufacturer A.

In order to compare the I_{SC} acceptance angle characteristics of the five different types of HCPV modules indoors measured, these are plotted in **Figure 10** corresponding to five representative examples of modules. Most of these kinds of HCPV modules present similar angular behaviour until a misalignment angle of around ±1º (corresponding to around 90% of the maximum).

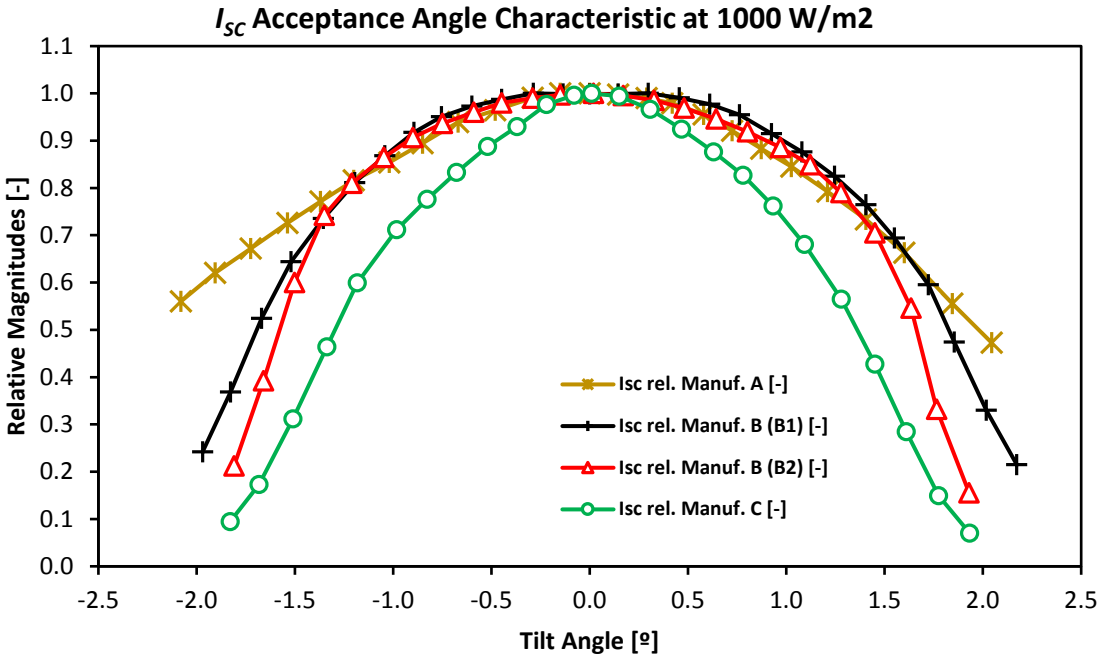

Figure 10. Normalised I_{SC} acceptance angle characteristics of each type of HCPV module measured indoors.

Appart from the I_{SC} acceptance angle, other electrical parameters like P_{MAX} and V_{OC} can also be plotted versus the tilt angle, like in the example of **Figure 11**, which corresponds to a HCPV module of the group B2 of Manufacturer B. For simplicity, only normalised magnitudes to their maximum values are represented for plotting the characteristic acceptance angle curves, which

were measured indoors for a DNI of 1000 W/m^2. As it is exposed in the example of **Figure 11**, it is commonly observed for HCPV modules that the P_{MAX} acceptance angle characteristic is typically lower than that of I_{SC}, whereas V_{OC} is much less sensitive to misalignments. Both I_{SC} and P_{MAX} characteristic curves are typically bell-shaped with relative good symmetry around the maximum value, as can be seen in the example of **Figure 11**. In this case, the I_{SC} acceptance angle value is of ±0.91º while I_{SC} decreases to around 20% of the maximum I_{SC} value for around ±1.8º tilt angle, whereas P_{MAX} acceptance angle value is 0.73º and decreases to less than 10% of the maximum value of power for around ±1.8º of tilt angle.

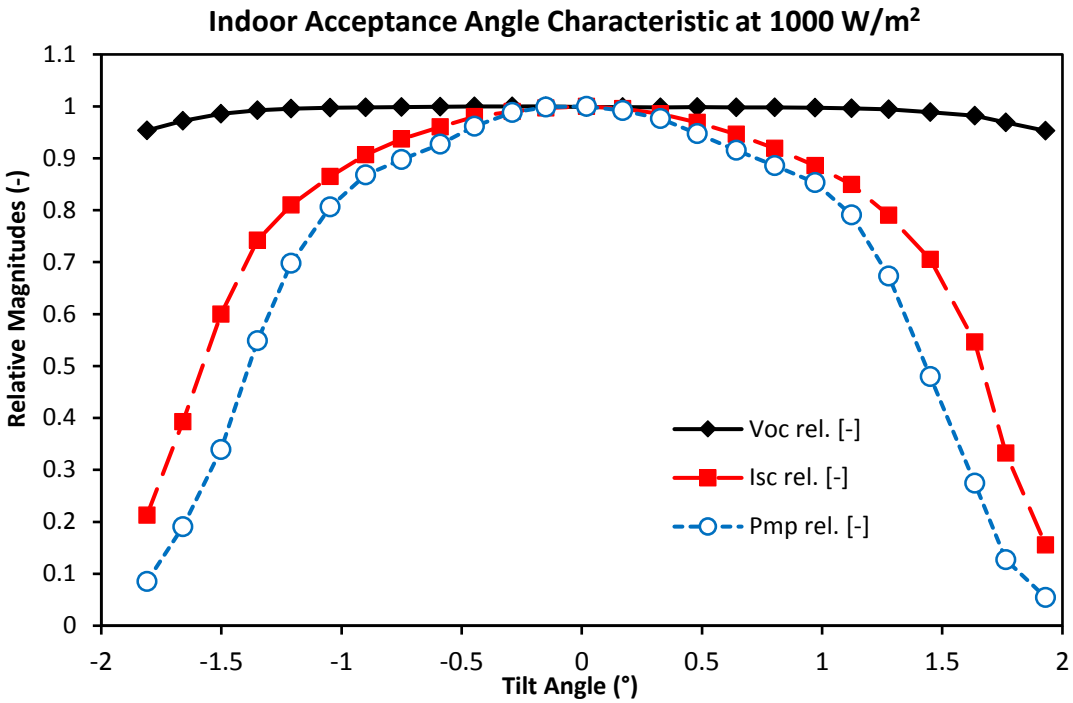

Figure 11. Example of acceptance angle characteristics of a commercial HCPV module measured indoors at the University of Jaén.

Derived from the measurement of the I_{SC} acceptance angle values, *CAP* values can be estimated. Note that since the geometrical concentration values of the modules measured are given by the manufacturers, they may be not exact, and therefore, these *CAP* values are approximate. Bearing this in mind, these *CAP* values result in a range from 0.24 to 0.46.

6. Summary and conclusions

An analysis of the main characteristics of the current HCPV modules has been presented in this work. The key performance definitions (efficiency, acceptance angle and concentration-acceptance angle product) have been detailed for a better understanding of the current status of the HCPV modules. Then, the evolution of the efficiency of the HCPV modules from around the year 1990 to the year 2017 was presented for different PV technologies, being the HCPV modules those with highest efficiency yearly growth (+0.83%/year, and +1.43%/year in the period 2010 to 2017). Moreover, the five highest efficiency record HCPV modules, measured in renowned laboratories, were compared. They reach efficiency values up to around 40% and geometrical concentrations lower than 400×.

Concerning current commercial HCPV modules, their characteristic were detailed and analysed: a table with the geometrical concentration, efficiency, power, acceptance angle and *CAP* value for 15 modules was built. In terms of efficiency, commercial HCPV modules are usually around 30%, and with low dispersion (standard deviation of 4%). It was found that commercial HCPV modules usually work with geometrical concentrations between 500× and 1000×. Current commercial HCPV modules were analysed simultaneously respect to their efficiency and geometrical concentration. A small group of them maintain highest efficiency values (more than 30%) and, at the same time, geometrical concentrations of 1000× or greater. These last HCPV modules may represent the most favourable conditions to produce cheapest energy in principle. Concerning the acceptance angle values and concentration-acceptance angle product (*CAP*), they are typically in the range of ±0.7º and ±1.0º, and in the range of 0.3 and 0.5, for current commercial HCPV modules, respectively. Note that none of the commercial HCPV modules presented simultaneously best performance values in efficiency, geometrical concentration and acceptance angle.

Complementary to the review analysis commented above, a series of indoor measurements of HCPV modules in a CPV solar simulator were taken in order to compare them with those data provided by the manufacturers. A total of 24 HCPV modules of three different manufacturers, and with a total of four different models of HCPV modules, were indoor characterised.

The average of the measured efficiency of each type of HCPV module was within a tolerance range of ±3.5%, acceptable for this technology, and also matched the datasheet values. The measured efficiencies of a total of 21 HCPV modules (identical twelve of one manufacturer and other identical nine of other manufacturer) were used for building a histogram. Both group of data were centred on their average values and with low dispersion (2% of standard deviation). Additionally, the efficiency of four different models of HCPV modules was proven to decrease a maximum of absolute 1.3% in the range of DNI between 700 and 1000 W/m^2.

Finally, the acceptance angle characteristics of 16 of those HCPV modules were also acquired. For each type of HCPV module, the measured average of I_{sc} acceptance angle values matched the correspondent one of the datasheet. Additionally, with the I_{sc} acceptance angle values of 12 HCPV modules of one of the manufacturers, a histogram was built. It resulted centred in the range of ±0.77º and ±0.82º and with low dispersion (±0.05º of standard deviation), assuring good repeatability.

7. Funding and acknowledgments

European Regional Development Fund (ERDF) and Spanish Economy Ministry (ENE2016-78251-R); Universidad de Jaén (UJA) and Caja Rural de Jaén (UJA2015/07/01). Financial support provided by the Universidad de Jaén Doctoral School.

Annex I: Previous models of HCPV modules

In this section, the information about the previous models of HCPV modules is presented in **Table 4**. These data were not used in this work, although they are here gathered to fill out the information about HCPV modules.

Table 4. Data of previous models of HCPV modules from their datasheets at T_{cell}=25 ºC and under DNI=1000 W/m^2 [7,15].

HCPV Module	C_g (×)	Optics	Power (W)	Efficiency (%)	Half Acceptance angle (º)	*CAP* (-)
Abengoa M300	1000	Fresnel	406[a]	32.0	1.3	0.72
Arima CPV M010	476	Fresnel	151[a]	24.0[a]	0.5	0.19
Arima CPV-G1	476	Fresnel	500	27.0	0.3	0.11
Daido DACPV 150W25	550	Fresnel	150	23.0[a]	0.9	0.37
Soitec CX-M400	530	Fresnel	95	29.9	0.4	0.14
Solfocus SF-CPV-205	500	Mirror	259[a]	18.0[a]	1.0	0.39
Suncore LMT-Alpha	625	Fresnel	1168	30.5[a]	0.8	0.35
Mean value	***594***		***390***	***26.3***	***0.74***	***0.32***

[a] Calculated from modules' datasheets.

8. References

[1] P. Pérez-Higueras, E. Muñoz, G. Almonacid and P. G. Vidal, "High Concentrator PhotoVoltaics efficiencies: Present status and forecast," *Renewable and Sustainable Energy Reviews,* no. 15(4), p. 1810–1815, 2011.

[2] K. Shanks, S. Senthilarasu and T. K. Mallick, "Optics for concentrating photovoltaics: Trends, limits and opportunities for materials and design," *Renewable and Sustainable Energy Reviews,* vol. 60, pp. 394-407, 2016.

[3] S. Kurtz, "Opportunities and Challenges for Development of a Mature Concentrating Photovoltaic Power Industry Opportunities and Challenges for Development of a Mature Concentrating Photovoltaic Power Industry," *NREL,* 2012.

[4] A. Cristóbal López, A. Martí Vega and A. Luque López, Next Generation of Photovoltaics, Springer, 2012.

[5] M. Wiesenfarth, S. Philipps, A. Bett, K. Horowitz and S. Kurtz, "Current Status of Concentrator Photovoltaic (CPV) Technology," Fraunhofer Institute for Solar Energy Systems ISE - National Renewable Energy Laboratory, 2017.

[6] M. Wiesenfarth, H. Helmers, S. Philipps, M. Steiner and A. Bett, "Advanced concepts in concentrating photovoltaics (CPV)," *Proceedings of 27th Eur. PV Sol. Energy Conf. Exhib,* 2012.

[7] C. Algora and I. Rey-Stolle, Handbook on Concentrator Photovoltaic Technology, John Wiley & Sons Ltd, 2016.

[8] D. Talavera, J. Ferrer-Rodríguez, P. Pérez-Higueras, J. Terrados and E. Fernández, "A worldwide assessment of levelised cost of electricity of HCPV systems," *Energy Conversion and Management,* vol. 127, p. 679–692, 2016.

[9] E. Fernández, G. Siefer, F. Almonacid, A. Loureiro and P. Pérez-Higueras, “A two subcell equivalent solar cell model for III-V triple junction solar cells under spectrum and temperature variations,” *Solar Energy,* vol. 92, p. 221–229, 2013.

[10] M. Buljan, J. Mendes-Lopes, P. Benítez and J. Miñano, “Recent trends in concentrated photovoltaics concentrators’ architecture,” *Journal of Photonics for Energy,* vol. 4, 2014.

[11] M. Steiner, G. Siefer, T. Hornung, G. Peharz and A. Bett, “YieldOpt, a model to predict the power output and energy yield for concentrating photovoltaic modules,” *Prog. Photovolt: Res. Appl.,* vol. 23, p. 385–397, 2015.

[12] P. Rodrigo, E. Fernández, F. Almonacid and P. Pérez-Higueras, “Review of methods for the calculation of cell temperature in high concentration photovoltaic modules for electrical characterization,” *Renew. Sustain. Energy Rev.,* vol. 38, p. 478–488, 2014.

[13] E. Fernández, J. Ferrer-Rodríguez, F. Almonacid and P. Pérez-Higueras, “Current-voltage dynamics of multi-junction CPV modules under different irradiance levels,” *Solar Energy,* vol. 39–50, no. 155, 2017.

[14] D. Talavera, P. Pérez-Higueras, F. Almonacid and E. Fernández, “A worldwide assessment of economic feasibility of HCPV power plants: Profitability and competitiveness,” *Energy,* vol. 119, pp. 408-424, 2017.

[15] Pérez-Higueras, P; Fernández, EF, High Concentrator Photovoltaics: Fundamentals, Engineering and Power Plants, Springer International Publishing, 2015.

[16] A. Pereira et al, “Electro-optical study of a x1024 concentrator photovoltaic system,” *Prog. Photovolt: Res. Appl,* vol. 22, no. 383–393, 2014.

[17] IEC 60904-3:2016 RLV. Photovoltaic devices - Part 3: Measurement principles for terrestrial photovoltaic (PV) solar devices with reference spectral irradiance data, ISBN 978-2-8322-3335-1, 2016.

[18] P. Benitez, J. Miñano, P. Zamora, R. Mohedano, A. Cvetkovic, M. Buljan, J. Chaves and M. Hernández, “High performance Fresnel-based photovoltaic concentrator,” *Optics Express,* vol. 18, no. S1, pp. A25-A40, 2010.

[19] M. Green, K. Emery, Y. Hishikawa, W. Warta, E. Dunlop, D. Levi, J. Hohl-Ebinger and A. Ho-Baillie, “Solar cell efficiency tables (version 50),” *Prog. Photovolt: Res. Appl.,* vol. 25, p. 668–676, 2017.

[20] E. F. Fernández, A. J. García-Loureiro and G. P. Smestad, “Multijunction concentrator solar cells: Analysis and fundamentals,” in *High Concentrator Photovoltaics: Fundamentals, Engineering and Power Plants*, Pérez-Higueras, Pedro and Fernández, Eduardo F. (Eds.) Springer, 2015, pp. 9-37.

[21] K. Ghosal, D. Lilly, J. Gabriel, M. Whitehead, S. Seel, B. Fisher, J. Wilson and S. Burroughs, "Semprius field results and progress in system development," *IEEE J. Photovoltaics,* vol. 4, no. 2, p. 703–708, 2014.

[22] F. Almonacid, P. Pérez-Higueras, E. Fernández and P. Rodrigo, "Relation between the cell temperature of a HCPV module and atmospheric parameters," *Solar Energy Materials and Solar Cells,* vol. 105, p. 322–327, 2012.

[23] J. Jaus, G. Peharz, A. Gombert, J. Ferrer-Rodríguez, F. Dimroth, F. Eltermann, O. Wolf, M. Passig, G. Siefer, A. Hakenjos, S. Van Riesen and A. Bett, "Development of FLATCON® modules using secondary optics," *Conf. Rec. IEEE Photovolt. Spec. Conf,* p. 001931–001936, 2009.

[24] R. Dows and E. Gough, "PVUSA procurement, acceptance, and rating practices for photovoltaic power plants," Report number 95-30910000.1;, 1995.

[25] D. King, W. Boyson and J. Kratochvill, "Photovoltaic array performance model," SAND2004-3535, Albuquerque, New Mexico: Sandia National Laboratories, 2004 .

[26] P. Pérez-Higueras et al, "High-Concentrator Photovoltaic Power Plants: Energy Balance and Case Studies," in *High Concentrator Photovoltaics*, Springer, 2015.

[27] C. Domínguez, I. Antón and G. Sala, "Solar simulator for concentrator photovoltaic systems," *Optics Express,* vol. 16, no. 19, p. 14894–14901, 2008.

[28] C. Gueymard, D. Myers and K. Emery, "Proposed reference irradiance spectra for solar energy systems testing," *Solar Energy,* vol. 73, no. 6, p. 443–467, 2002.

[29] I. Antón, M. Domínguez, M. Victoria, R. Herrero, S. Askins and G. Sala, "Characterization capabilities of solar simulators for concentrator photovoltaic modules," *Jpn. J. Appl. Phys,* vol. 51, no. 10 PART 2, 2012.

[30] P. Rodrigo, E. Fernández, F. Almonacid and P. Pérez-Higueras, "Quantification of the spectral coupling of atmosphere and photovoltaic system performance: Indexes, methods and impact on energy harvesting," *Solar Energy Materials and Solar Cells,* vol. 163, p. 73–90, 2017.

[31] " Solar Added Value," [Online]. Available: solaraddedvalue.com/en.

[32] C. Domínguez, I. Antón, G. Sala and S. Askins, "Current-matching estimation for multijunction cells," *Prog. in Photovoltaics: Research and Applications,* vol. 21, no. 7, pp. 1478-1488, 2013.

[33] IEC 62108:2007 Concentrator photovoltaic (CPV) modules and assemblies—design qualification and type approval, ISBN 2-8318-9430-1.

[34] IEC 62670-1:2013 Concentrator Photovoltaic (CPV) Modules and Assemblies Performance Testing - Part 1: Standard Conditions, ISBN 978-2-8322-1120-5.

[35] IEC 62670-2:2013 Concentrator Photovoltaic (CPV) Modules and Assemblies Performance Testing - Part 2: Energy Measurement, ISBN 978-2-8322-2627-8.

[36] IEC TS 62789:2014 Photovoltaic Concentrator Cell Documentation, ISBN 978-2-8322-1944-7.

[37] K. Ghosal, D. Lilly, J. Gabriel, S. Seel, E. Menard, S. Burroughs, R. Daniel, S. Lowe and C. Kudija, “Performance of a micro-cell based transfer printed HCPV system in the South Eastern US,” *AIP Conf. Proc.,* no. 1477, p. 327–330, 2012.

[38] "http://www.nrel.gov/ncpv/images/efficiency_chart.jpg," National Renewable Energy Laboratory, 2016. [Online].

[39] "NREL Press Release NR-4514," 16 December 2014.

[40] N. Ekins-Daukes and e. al, "What does CPV need to achieve in order to succeed?," *AIP Publishing Articles,* no. 020004.

[41] M. Renzi, L. Egidi and G. Comodi, “Performance analysis of two 3.5kWp CPV systems under real operating conditions,” *Applied Energy,* vol. 160, p. 687–696, 2015.

[42] C. Cancro et al., “Characterization and performance analysis of Ecosole HCPV system first prototype Prototype,” *AIP Conf. Proc.,* vol. 1766, p. 40001–1–40001–6, 2016.

[43] Globaldata, “Concentrated Photovoltaics (CPV) - Global Market,” *Renewable Energy World Magazine,* p. 45, 2014.

Solar Energy 155 (2017) 39–50

Contents lists available at ScienceDirect

Solar Energy

journal homepage: www.elsevier.com/locate/solener

Current-voltage dynamics of multi-junction CPV modules under different irradiance levels

Eduardo F. Fernández *, Juan P. Ferrer-Rodríguez, Florencia Almonacid, Pedro Pérez-Higueras

Centro de Estudios Avanzados en Energía y Medio Ambiente (CEAEMA), IDEA Solar Energy Research Group, Universidad de Jaén, Las Lagunillas Campus, Jaén 23071, Spain

ARTICLE INFO

Article history:
Received 6 April 2017
Received in revised form 1 June 2017
Accepted 6 June 2017

Keywords:
I-V characteristics
SEM model parameters
Light intensity variations
Multi-junction CPV modules

ABSTRACT

The current-voltage output of concentrator photovoltaic (CPV) modules shows a complex behaviour under irradiance variations due to the use of multi-junction solar cells and optical elements. The single exponential model (SEM) relates the I-V curve of a PV device and its five characteristic parameters. Hence, it is fundamental to understand the dependence of the SEM model and I-V parameters of CPV modules with irradiance. In this paper, two samples of concentrator modules were characterized under fully controlled conditions by using a CPV solar simulator for light intensities within 700–1000 W/m^2. Results show that the photo-generated current increases linearly with irradiance, the diode ideality factor and saturation current present a stable behaviour under irradiance variations while the parasitic resistances, i.e. series and shunt, trend to decrease as the intensity increases. In addition, different approximations are carried out in the SEM model equation to explain the dependence of the performance of the concentrators with light intensity. Finally, the prediction of the I-V curves and key electrical parameters from reference values is discussed. Results show a good fitting of the I-V curves until 750 W/m^2 and a high accuracy in the estimations of the electrical parameters with a MAPE lower than 1.2%, a MRE within 1% and a R^2 equal of higher than 0.9.

1. Introduction

Concentrator photovoltaics (CPV) is considering as one of the most promising research avenues to reduce the cost of solar electricity and for large scale implementation (Talavera et al., 2016, 2017). The CPV module is the fundamental unit of this technology to convert the non-concentrated sunlight into electricity. Nowadays, these modules are largely based on multi-junction (MJ) solar cells made up of several p-n junctions interconnected in series, usually a GaInP/GaInAs/Ge structure, to improve the absorption of the spectral irradiance (Cotal et al., 2009; Fernández et al., 2015a). The most widely used optical configuration is based on a primary optical element (POE) and a secondary optical element (SOE) per receiver (Shanks et al., 2016). The aim of the POE, usually a Fresnel lens, is to collect and concentrate the direct light received from the sun (Xie et al., 2011). On the other hand, the SOE, e.g. pyramid, CPC, SILO, etc., is intended to homogenize the luminous power on the solar cell surface and to improve the acceptance angle of the system (Victoria et al., 2009). A passive cooling mechanism for avoiding overheating of the solar cells consisting of a flat back plate or finned heat-sink is used in the majority of the cases due to its simplicity and reliability (Micheli et al., 2016; Rodrigo et al., 2014).

The assembly of the elements above makes the electrical performance of CPV technology more complex and inherently different than conventional photovoltaics (PV) (Rodrigo et al., 2013). Hence, important efforts have been made within last years to analyse the behaviour and to develop models tailored to the special features of this technology at cell (Theristis and O'Donovan, 2015; Fernández et al., 2013a; Domínguez et al., 2010), module (Fernández et al., 2013b; Theristis et al., 2017; Steiner et al., 2015) and system level (Fernández et al., 2015b; Kim et al., 2013; Strobach et al., 2015). This is crucial to gain a better understanding of the current-voltage output of concentrator devices as a function of the relevant input parameters, and therefore, to promote the market expansion of CPVs (Kurtz et al., 2015; Leloux et al., 2014; Fernández et al., 2016a).

The single exponential model (SEM) relates the I-V curve of a PV device and its five characteristic parameters, namely, the photo-generated current, the diode saturation current, the diode ideality factor, the series resistance and the shunt (or parallel) resistance. The extraction and study of the SEM model parameters of PV devices have been under study for decades (Cotfas et al., 2013; Ciulla et al., 2014; Humada et al., 2016; Li et al., 2013, 2016;

* Corresponding author.
E-mail address: fenandez@ujaen.es (E.F. Fernández).

http://dx.doi.org/10.1016/j.solener.2017.06.012
0038-092X/

Ghani et al., 2014). Last years, several authors have also applied different methods for extracting the five parameters of multi-junction CPV devices (Segev et al., 2012; Ben Or and Appelbaum, 2013; Appelbaum and Peled, 2014; Almonacid et al., 2016; Fernández et al., 2016b). A semi-empirical method was applied to extract the parameters of InGaP/InGaAs/Ge solar cells under different concentrations and temperatures (Segev et al., 2012). The Newton-Raphson method, the Levenberg-Marquardt method combined with Lambert-W function and a Genetic-Algorithm have been applied to the same structure under different concentration levels (Ben Or and Appelbaum, 2013; Appelbaum and Peled, 2014). More recently, numerical and analytical methods have been applied for the electrical characterization of a whole CPV module under real working conditions (Almonacid et al., 2016; Fernández et al., 2016b; Ghani et al., 2017).

The direct irradiance is the main driver of the current-voltage output of CPV systems (Fernández et al., 2013c). Because of this, it is fundamental to investigate the behaviour of the parameters of the SEM model and the I-V characteristics of concentrator modules as a function of this variable. However, only few studies, and mainly at cell level, have been conducted regarding the dependence of these magnitudes (Ben Or and Appelbaum, 2014; Khan et al., 2014). Nevertheless, the dynamics of the current-voltage characteristics of CPV modules cannot be completely understood from the simply analysis of the concentrator cells employed. First, the use of optical devices could affect the uniformity over the solar cell surface, and therefore, the I-V characteristics of the concentrator (Baig et al., 2012). Second, the interconnection of several receivers produces optical and electrical mismatches that could modify the performance of the system with light intensity (Rodrigo et al., 2016; Peharz et al., 2011a). Finally, the wiring among the cells is expected to produce additional series resistance losses that could affect the evolution of the electrical characteristics with light intensity.

Bearing the above in mind, this paper aims to analyse and elucidate the behaviour of the SEM model and I-V parameters of multi-junction CPV modules with irradiance variations under fully controlled conditions. To the knowledge of the authors, this has not been addressed in any previous research work and is, therefore, still pending. In order to achieve this issue, two different CPV modules were characterized under laboratory controlled conditions by using the Helios 3198 CPV solar simulator for light intensities within 700–1000 W/m^2. Based on the experimental data, the SEM model parameters of the modules are extracted and their dependence with intensity discussed in relation to the physical properties of the multi-junction solar cells. Based on the extracted values, different approximations are carried out in the I-V characteristic equation to explain the electrical performance of the concentrators under irradiance variations. The accuracy in the modelling of the I-V curves and key electrical parameters with irradiance from the measured and extracted parameters at reference conditions is also investigated. The final goal is to contribute to the understanding and modelling of the performance of CPV modules as a function of the input direct irradiance.

2. Materials and experimental procedure

To carry out this study, two samples of commercial CPV modules from different manufactures have been selected i.e. module A and B. Both modules are based on triple-junction lattice-matched GaInP/GaInAs/Ge solar cells. The primary optics of the modules consists of point-focus flat Fresnel lenses. The module A uses silicone-on-glass (SoG) lenses, while the module B uses poly (methylmethacrylate) (PMMA) lenses. The modules also include a secondary optics based on refractive truncated pyramids made up of glass. The geometric concentration of the modules is 500x, module A, and 820x, module B. Both concentrators use a passive cooling mechanism to remove the heat generated by the cells. The cooling system of the module A is based on aluminium finned heat-sinks, while is based on a simple aluminium flat back plate for the module B. Additional information about the main characteristics of each module can be found in Table 1. In addition, Table 2 shows the rated values of the main electrical parameters of the two concentrators under reference conditions. The features of the modules selected represent the most wide-spread multi-junction concentrator PV system nowadays. Because of this, it is worth mentioning that the conclusions of this work can be considered representative of the current CPV technology (Rodrigo et al., 2015).

The multi-junction CPV modules were tested with the Helios 3198 solar simulator from Solar Added Value Company at the Centro de Estudios Avanzados en Energía y Medio Ambiente (CEAEMA) of the University of Jaen. This solar simulator uses a Xenon flash lamp for simulating the solar radiation and a parabolic mirror as a collimator. The spectral irradiance distribution is close to the AM1.5D reference spectrum, and the collimation angle is around ±0.3°. Hence, this set-up represents a useful tool for the electrical characterization of CPV modules and systems under controlled conditions, see Fig. 1. Additional detailed information about the features of the simulator can be found in (Domínguez et al., 2008).

The modules were mounted on the support structure of the solar simulator. After that, the Fresnel lenses were cleaned and examined to avoid any distortion of the data caused by soiling or damaged optical elements. Later on, the modules were aligned to the continuous light, a halogen lamp located in the centre of the Xenon flash tube, by changing the azimuth and elevation angles of the adjustable support structure to diminish the possible effect of optical mismatches. The correct alignment of both systems is

Table 1
Main features of the multi-junction concentrator PV modules used to carry out this study.

Parameter	Module A	Module B
Geometric concentration	500x	820x
Primary optics	Silicone-on-glass (SoG)	Poly (methylmethacrylate) (PMMA)
Lens area	23.9 cm × 23.9 cm = 571 cm^2	20 cm × 20 cm = 400 cm^2
F-number	~0.90	~0.80
Secondary optics	Refractive pyramid	Refractive pyramid
Type of solar cells	Lattice-matched GaInP/GaInAs/Ge	Lattice-matched GaInP/GaInAs/Ge
Number of solar cells	6	25
Area of solar cells	~1 cm^2	~0.5 cm^2
Bypass diodes	1 per cell	1 per cell
Cooling type	Passive (finned heat-sink)	Passive (flat heat-sink)
Number of fins	10	–
Length of fin	9 cm	–

Table 2
Rated values of the main electrical parameters of the concentrator PV modules used in this study obtained with the Helios 3198 CPV solar simulator at the CEAEMA in the University of Jaen at 1000 W/m^2, spectral irradiance similar to AM1.5D reference spectrum, SMR (top/mid) = 1 ± 0.05 and room temperature of 25 °C ± 0.5 °C.

Parameter	Module A	Module B
I_{sc} (A)	5.84	4.29
I_{mpp} (A)	5.55	4.00
V_{oc} (V)	18.9	77.5
V_{mpp} (V)	16.8	68.3
FF (%)	84.5	82.2
η (%)	27.3	27.4

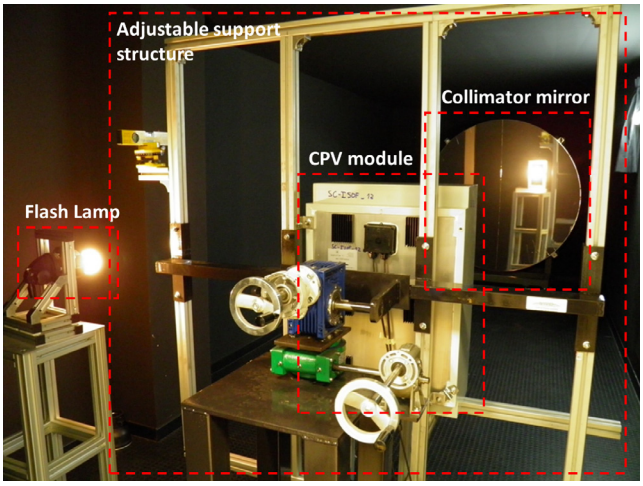

Fig. 1. Photo of the Helios 3198 CPV solar simulator at the Centro de Estudios Avanzados en Energía y Medio Ambiente (CEAEMA) of the University of Jaen.

later verified by measuring the acceptance angle profile of the CPV modules in steps of around 0.15° by using the adjustment controls of the structure, see Fig. 2.

The modules were tested under light intensities from 700 to 1000 W/m^2, see Fig. 3, which can be considered as a representative range of irradiance under actual conditions (Soria-Moya et al., 2015). Each I-V curve was measured in steps of 50 W/m^2 by measuring a set of 20–25 current-voltage points spread relatively uniformly excepting in the "knee" of the curves, where a more density of measurement points was fixed. The room temperature was maintained at 25 ± 0.5 °C to avoid thermal effects in the results (Peharz et al., 2011b). Also, the Spectra Matching Ratio (SMR) (Domínguez et al., 2013) for the top and middle subcells was monitored through the measurements of component cells from Solar Added Value Company with an equivalent structure than the MJ solar cells of the modules:

$$SMR(top/mid) = \frac{I_{sc,top}^{c.c.}}{I_{sc,top,ref}^{c.c.}} \frac{I_{sc,mid,ref}^{c.c.}}{I_{sc,mid}^{c.c.}} \quad (1)$$

where $I_{sc,top}^{c.c.}$ and $I_{sc,mid}^{c.c.}$ are, respectively, the measured short-circuit currents of the top and middle components cells; the subscript "ref" refers to the values at reference conditions. This index has been recorded to ensure the adequate input spectrum for each light intensity due to the high spectral sensitivity of CPV modules caused by the use of multi-junction solar cells made up of various subcells with different band gaps (Fernández et al., 2014, 2016c). The value of SMR (top/mid) was kept constant at 1 ± 0.05 for all the irradiance values, so that, the spectral effects are not expected to play an important role in the results (Muller et al., 2015; Theristis et al., 2016; Fernández et al., 2015c).

3. Dependence of SEM model parameters with irradiance

In this section, first, the methodology used to extract the parameters of the SEM model is described and experimentally validated. After that, the impact of irradiance changes on the extracted parameters is discussed.

3.1. Methodology

The equivalent circuit shown in Fig. 4 has recently demonstrated to be valid for the electrical characterization of multi-junction CPV modules (Almonacid et al., 2016). Based on this circuit, the relation between the parameters of a concentrator module and its current-voltage electrical output can be expressed by the so-called single exponential model (SEM) as:

$$I = I_{ph} - I_o\left(\exp\left(\frac{V + IR_s}{mV_T}\right) - 1\right) - \frac{V + IR_s}{R_{sh}} \quad (2)$$

where I_{ph} is the photo-generated current, I_o is the diode saturation current, m is the diode ideality factor, R_s is the series resistance and R_{sh} is the shunt (or parallel) resistance of the modules. V_T in Eq. (1) is defined as the thermal voltage, given by $V_T = kT/q$; being k the Boltzmann constant with a value of 1.38E−23 J/K and q the elementary charge with a value of 1.60E−19C.

The five parameters of Eq. (2) can be extracted from the measured I-V characteristics of the photovoltaic device under study. Several methods for extracting the five parameters of the SEM model for the electrical characterization of multi-junction CPV modules were evaluated in (Fernández et al., 2016b). Among the different approaches analysed, the method of Phang et al. (1984) has been selected in this study due to its accuracy and simplicity. First, the initial values of R_{so} and R_{sho} are estimated by performing a linear fit of the I-V curve around the open-circuit voltage and the short-circuit current as:

$$R_{so} = -\left(\frac{dV}{dI}\right)_{V=V_{oc}} \quad (3)$$

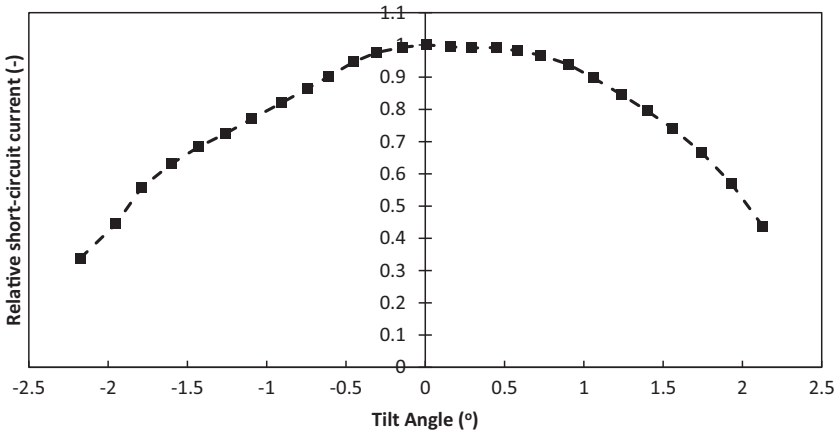

Fig. 2. Acceptance angle profile of the CPV module A measured with the Helios 3198 CPV solar simulator at the CEAEMA in the University of Jaen at 1000 W/m^2, spectral irradiance similar to AM1.5D reference spectrum, SMR (top/mid) = 1 ± 0.05 and room temperature of 25 °C ± 0.5 °C. The optimum alignment is considered at the point 0 of the *x*-axis.

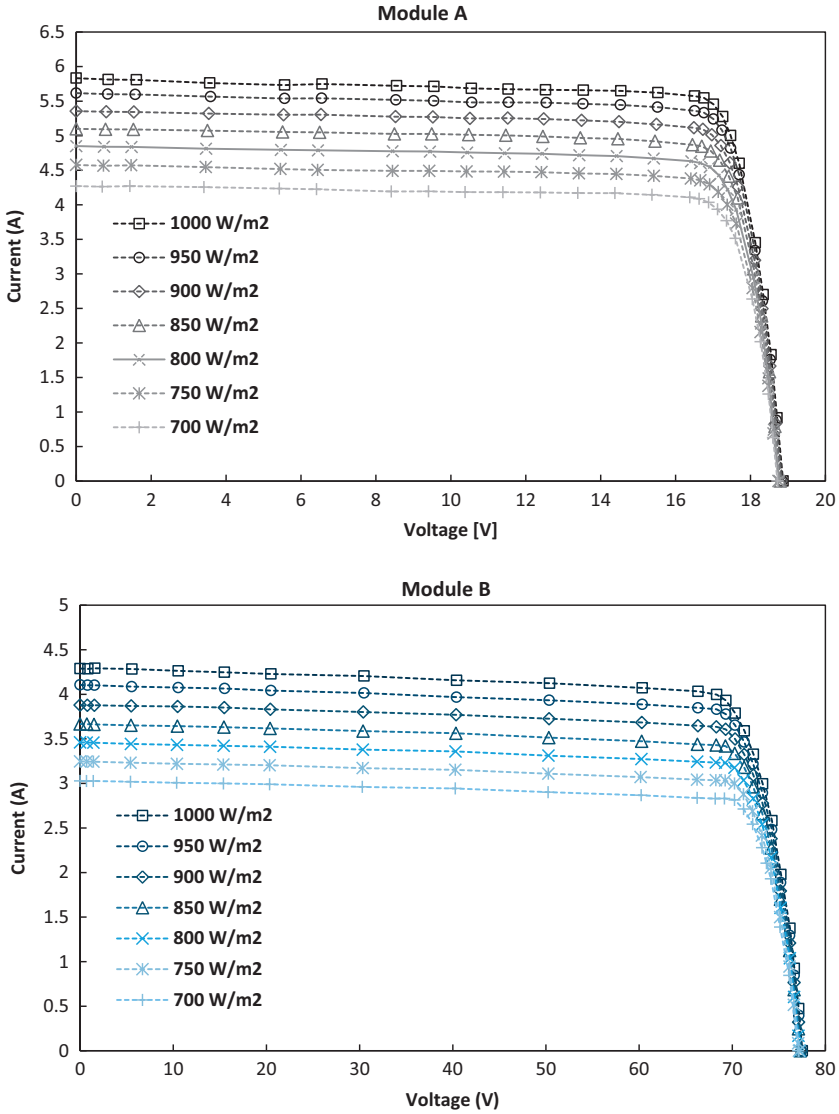

Fig. 3. Current-voltage curves of the CPV modules used in this study measured with the Helios 3198 CPV solar simulator at irradiance levels within 700–1000 W/m^2, spectral irradiance similar to AM1.5D reference spectrum, SMR (top/mid) = 1 ± 0.05 and room temperature of 25 °C ± 0.5 °C.

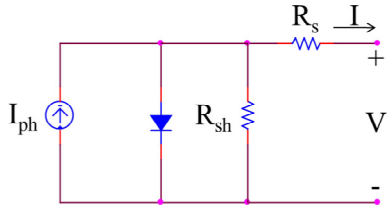

Fig. 4. Equivalent circuit of the single exponential model of a photovoltaic device.

$$R_{sho} = -\left(\frac{dV}{dI}\right)_{I=I_{sc}} \tag{4}$$

After that, the parameters of Eq. (1) are estimated from the measure values of I_{sc}, V_{oc}, I_{mpp}, V_{mpp}, R_{so} and R_{sho} according to:

$$I_{ph} = I_{sc}\left(1 + \frac{R_s}{R_{sh}}\right) + I_o\left(\exp\left(\frac{I_{sc}R_s}{mV_T}\right) - 1\right) \tag{5}$$

$$I_o = \left(I_{sc} - \frac{V_{oc}}{R_{sh}}\right)\exp\left(-\frac{V_{oc}}{mV_T}\right) \tag{6}$$

$$m = \frac{V_{mpp} + R_{so}I_{mpp} - V_{oc}}{V_T\left[ln(I_{sc} - \frac{V_{mpp}}{R_{sh}} - I_{mpp}) - ln\left(I_{sc} - \frac{V_{oc}}{R_{sh}}\right) + \frac{I_{mpp}}{I_{sc} - \frac{V_{oc}}{R_{sh}}}\right]} \tag{7}$$

$$R_s = R_{so} - \frac{mV_T}{I_o}\exp\left(-\frac{V_{oc}}{mV_T}\right) \tag{8}$$

$$R_{sh} = R_{sho} \tag{9}$$

In order to give a sense of the accuracy of the method, Fig. 5 shows the measured and modelled I-V curves for the modules under study at reference conditions. As can be seen, the method estimates the electrical output with a high quality. In particular, the maximum, minimum and average absolute percentage errors between actual and predicted power are, respectively, 0.12%, 0.01% and 0.05% for module A, and 0.10%, 0.01% and 0.07% for module B. This accuracy is important to be confident with the results obtained and discussed below.

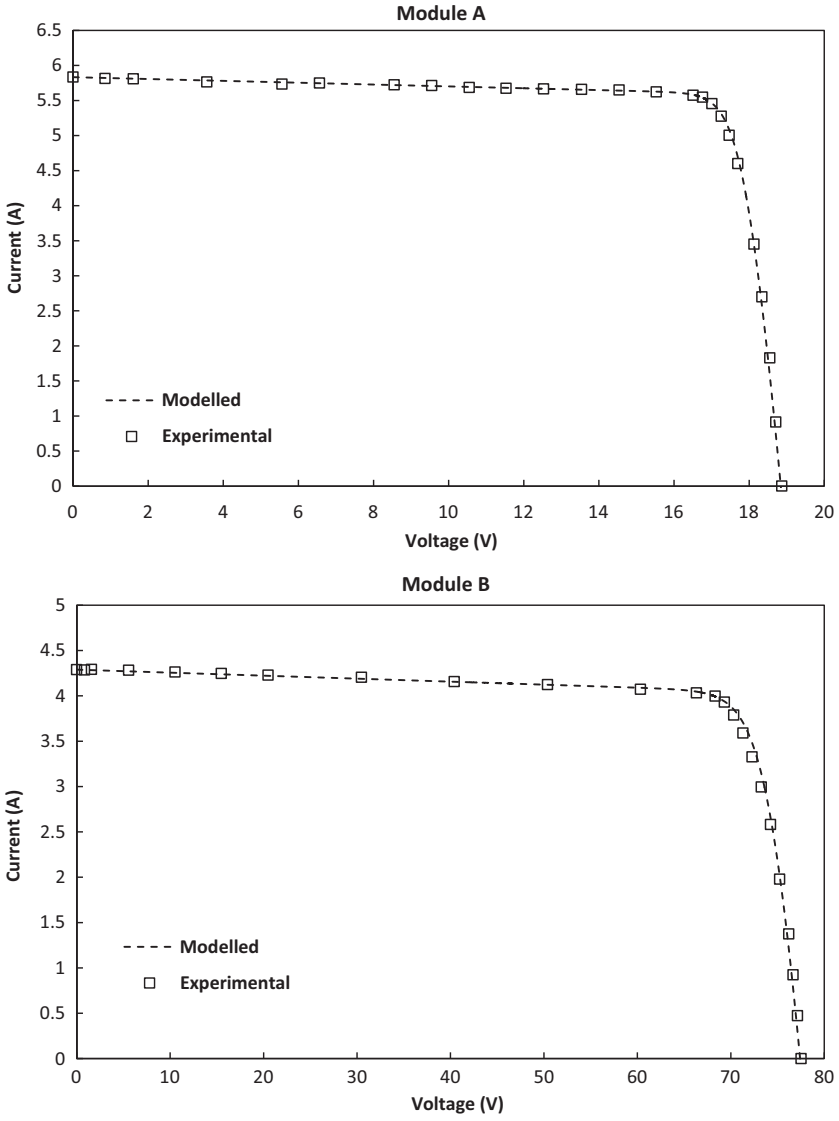

Fig. 5. Experimental and modelled current-voltage curve of the CPV modules used in this study at 1000 W/m^2, spectral irradiance similar to AM1.5D reference spectrum, SMR (top/mid) = 1 ± 0.05 and room temperature of 25 °C ± 0.5 °C.

3.2. Results

In this section, the dependence of the SEM model parameters of the modules with light intensity is discussed. It should be noted that the parameters are given and discussed at one-cell level by considering the electrical configuration of the modules as:

$$I_{ph,c} = I_{ph} \quad (10)$$

$$I_{o,c} = I_o \quad (11)$$

$$m_c = \frac{m}{N_s} \quad (12)$$

$$R_{s,c} = \frac{R_s}{N_s} \quad (13)$$

$$R_{sh,c} = R_{sh} \quad (14)$$

where the subscript "c" refers to the values at cell level and N_s the number of cells in series of each module. The use of normalized values is more appropriate since allows the extracted values of both modules to be directly compared. In addition, this also allows the results to be discussed based on previous studies concerning MJ solar cells. Moreover, the values provided can be easily translated to other modules by considering the specific number of cells in series of the specific concentrator considered.

Table 3 shows the extracted parameters of the CPV modules under study at reference conditions. As can be seen, the module A has a higher value of $I_{ph,c}$ than the module B, around 1.35 times greater, due to the its larger cell area. On the contrary, the module

Table 3
Single exponential model parameters of the CPV modules used in this study at 1000 W/m^2, spectral irradiance similar to AM1.5D reference spectrum, SMR (top/mid) = 1 ± 0.05 and room temperature of 25 °C ± 0.5 °C. The values of the parameters are given at one-cell level by considering the electrical configuration of the modules.

Parameter	Module A	Module B
$I_{ph,c}$ (A)	5.84	4.30
$I_{o,c}$ (A)	9.43E−25	4.11E−19
m_c	3.14	3.76
$R_{s,c}$ (Ω)	1.91E−02	1.93E−02
$R_{sh,c}$ (Ω)	75.9	302.5

A presents a much lower value of $I_{o,c}$ than the module B, an order of magnitude around 4E+5 times. Regarding the ideality factor, the module B has a higher value, around 1.20 times greater than module A. Both modules present a similar value of $R_{s,c}$, while they present a significant difference for $R_{sh,c}$, a value around 4 times greater for the module B.

Fig. 6-top shows the evolution of $I_{ph,c}$ with light intensity for the two modules considered. Under uniform irradiance, the photogenerated current of multi-junctions solar cells is expected to have a linear behaviour with intensity (Kinsey et al., 2008). However, the assembly of concentrator optics affects the spatial and spectral distribution of the irradiance over the solar cells surface (Victoria et al., 2013) and produce intrinsic electrical mismatches among the receivers (Vorster and Van Dyk, 2005), which can affect the behaviour of $I_{ph,c}$. Despite the possible effect of these phenomena, the extracted values of $I_{ph,c}$ are largely dominated by intensity and show a clear linear tendency with irradiance for both modules. They range from a value of 4.27 A (700 W/m^2) to 5.84 A (1000 W/m^2) for the module A, and from a value of 3.03 A (700 W/m^2) to 4.30 A (1000 W/m^2) for the module B. It should be noted that this linear behaviour, $R^2 = 0.99$ for both modules, also verifies the negligible effect on the results of the narrow spectral variations commented in Section 2.

Fig. 6-mid shows the values of $\ln(I_{o,c})$ and m_c as a function of the input irradiance for the two sample modules. These two parameters provided information about the rate and type of recombination mechanism that occurs in the solar cells (i.e. Radiative, Auger and Shockley-Read-Hall) (Nelson, 2014). Hence, they are expected to be sensible to the incident irradiance since this affects the injection level. As is shown, the extracted values of $\ln(I_{o,c})$ and m_c present a similar behaviour and do not show any particular trend with irradiance. The $\ln(I_{o,c})$ range from a value of −58.4 A (900 W/m^2) to −51.3 A (800 W/m^2) for the module A, and from a value of −50.5 A (800 W/m^2) to −42.6 A (700 W/m^2) for the module B. Also, the m_c values range from a minimum of 3.0 (900 W/m^2) to a maximum of 3.3 (800 W/m^2) for the module A, and from a minimum of 3.3 (800 W/m^2) to a maximum of 3.8 (700 W/m^2) for the module B. Based on these results, it can be concluded that the recombination processes of the solar cells are not significantly affected by intensity variations. In addition, the module A shows an average value of m_c of 3.2, around 1.0 per subcell, and the module B shows an average value of m_c of 3.6, around 1.2 per subcell. So, the

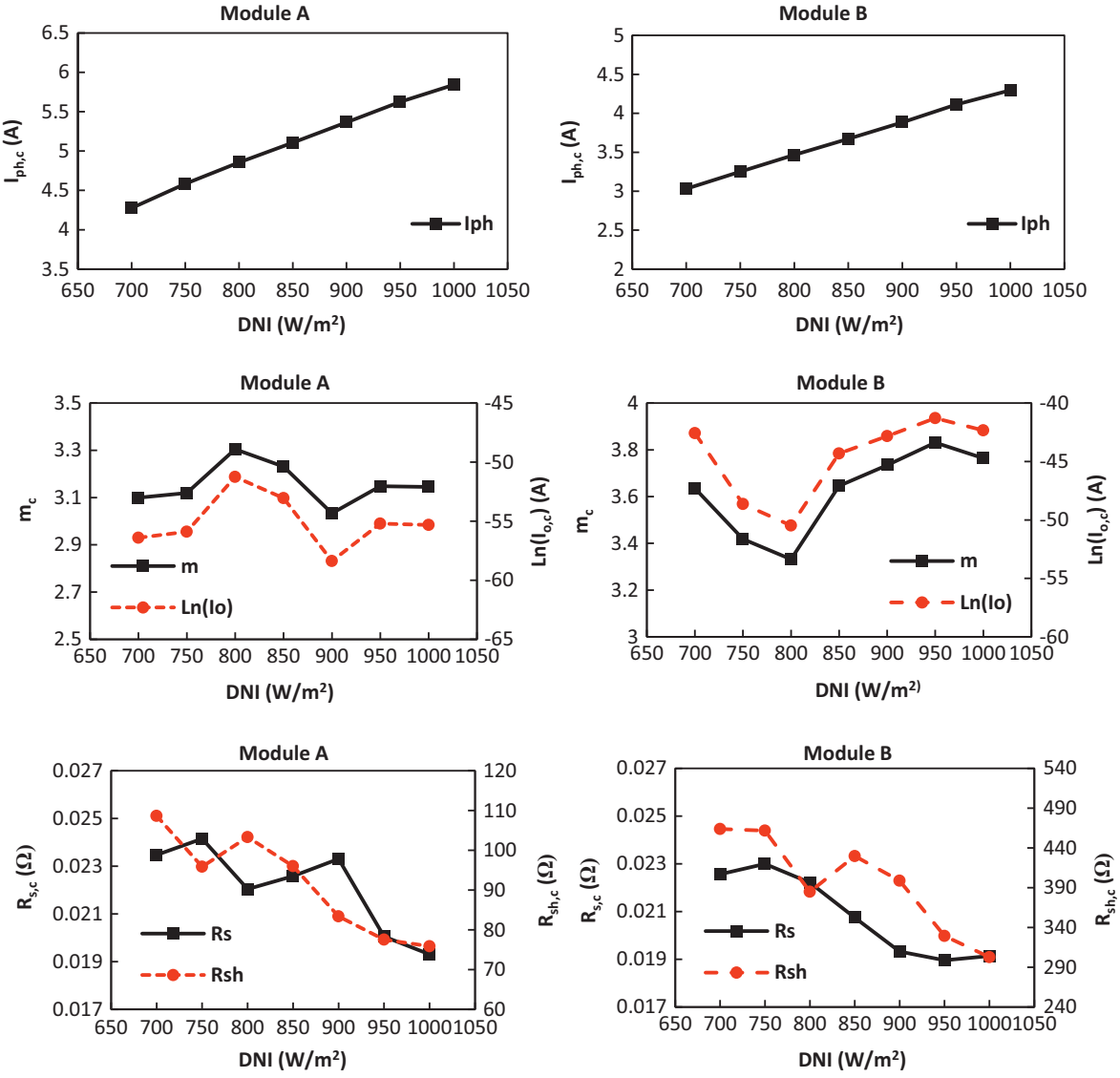

Fig. 6. Dependence of single exponential model parameters with input irradiance of the CPV modules under study. The values of the parameters are given at one-cell level by considering the electrical configuration of the module.

conversion of photons into electricity of the multi-junction solar cells of both modules, for the irradiance levels considered, seems to be dominated by radiative recombination in the surface and bulk region (Siefer and Bett, 2014).

Fig. 6-bottom shows the dependence of parasitic resistances, i.e. $R_{s,c}$ and $R_{sh,c}$, with irradiance variations. The $R_{s,c}$ of a solar cell is mainly determined by the resistance of the semiconductor layers, by the front metal grid resistance and by the metallic contact resistance (Vossier et al., 2012). In this case, the $R_{s,c}$ is also going to be affected by the resistance of the wires of the CPV modules. As can be seen, the $R_{s,c}$ trends to decrease with intensity for both modules. It ranges from a value of around 0.023 Ω (700 W/m^2) to 0.019 Ω (1000 W/m^2). This tendency can be understood by considering the increase of the conductivity of the semiconductor layers with the number of charge carriers, and therefore, with the input irradiance (Grundmann, 2010). This trend can be approximated with the following equation:

$$R_{s,c} = a_{Rs}\exp(-b_{Rs}DNI) \tag{15}$$

with an R^2 around 0.80 for both modules. The $R_{s,c}$ of a GaInP/GaAs/Ge solar cell has previously proven to decrease with concentration and ranges from a value of around 0.016 Ω (350 suns) to 0.009 Ω (900 suns) at 25 °C (Ben Or and Appelbaum, 2014). As expected, these values are slightly lower than the reported for the two CPV modules, probably due to the contribution of the resistance of the wires. Despite of this, it can be stated that the evolution of $R_{s,c}$ with light intensity is dominated by the dependence of the properties of the semiconductor materials.

On the other hand, the $R_{sh,c}$ is usually attributed to manufacturing defects that produce a leakage current flowing through the solar cell and around the edges of the semiconductor device (Nelson, 2014). In the case of concentrator modules, the extracted values of $R_{sh,c}$ are also going to be affected by possible optical and electrical mismatches among the receivers. As shown in Fig. 6-bottom, the $R_{sh,c}$ shows a clear tendency for diminishing with irradiance for both modules. It ranges from a value of 108.6 (700 W/m^2) to 75.9 (1000 W/m^2) for the module A, and from a value of 463.7 (700 W/m^2) to 302.5 (1000 W/m^2) for the module B. This trend can be explained due to the increase of the conductivity commented above, as well of the higher shunt leakage current as a function of the growing irradiance (Grundmann, 2010; Khan et al., 2014). As in the previous case, this behaviour can be approximated with the following equation:

$$R_{sh,c} = a_{Rsh}\exp(-b_{Rsh}DNI) \tag{16}$$

with an R^2 around 0.85 for both modules. The same tendency has been found for a GaInP/GaAs/Ge solar cell with $R_{sh,c}$ values raging from around 450 Ω (350 suns) to 160 Ω (900 suns) at 25 °C (Ben Or and Appelbaum, 2014). The results obtained for the module B are in agreement with these values, however, the module A presents significantly lower $R_{sh,c}$ values. This could be explained due to the possible decrease of the slope of the I-V curves near short-circuit current by the presence of optical mismatches(Vorster and Van Dyk, 2005). Despite of this effect, the dependence of $R_{sh,c}$ with irradiance has demonstrated to be dominated by the changes of the properties of the semiconductors materials.

4. Dependence of I-V parameters with irradiance

Fig. 7 shows the evolution of the key parameters of the I-V curves of both modules as a function of the input irradiance, namely, short-circuit current (I_{sc}), current at maximum power point (I_{mpp}), open-circuit voltage (V_{oc}) and voltage at maximum power point (V_{mpp}). Based on the results obtained in the previous section, different approximations are carried out in the SEM model to explain the results found.

As shown in Fig. 7-top, I_{sc} presents a clear linear tendency with irradiance for both modules. This can be explained by setting V = 0 in Eq. (1) at reference conditions, "*", as follows:

$$I^*_{sc} = I^*_{ph} - I^*_o\left(\exp\left(\frac{I^*_{sc}R^*_s}{m^*V_T}\right) - 1\right) - \frac{I^*_{sc}R^*_s}{R^*_{sh}} \approx I^*_{ph} \tag{17}$$

Then, under different irradiance levels, I_{sc} can be expressed with the following:

$$I_{sc} \approx \frac{I^*_{ph}}{DNI^*}DNI \approx \frac{I^*_{sc}}{DNI^*}DNI \tag{18}$$

As in the previous case, I_{mpp} shows a linear dependence with light intensity, see also Fig. 7-top. This can be understood by setting V = V_{mpp} and I = I_{mpp} and rearranging Eq. (1) at reference conditions as:

$$I^*_{ph} = I^*_{mpp} + I^*_o\left(\exp\left(\frac{V^*_{mpp} + I^*_{mpp}R^*_s}{m^*V_T}\right) - 1\right) + \frac{V^*_{mpp} + I^*_{mpp}R^*_s}{R^*_{sh}} \tag{19}$$

With light intensity, I_{mpp} can be expressed as follows:

$$I_{mpp} = \frac{I^*_{ph}}{DNI^*}DNI - I_o\left(\exp\left(\frac{V_{mpp} + I_{mpp}R_s}{mV_T}\right) - 1\right) - \frac{V_{mpp} + I_{mpp}R_s}{R_{sh}} \tag{20}$$

After substituting I^*_{ph} in this equation, I_{mpp} can be simplified to the following expression:

$$I_{mpp} \approx \frac{I^*_{mpp}}{DNI^*}DNI \tag{21}$$

Based on the above, it could be stated that I_{sc} and I_{mpp} present the same behaviour than I_{ph} with intensity variations and that are not significantly affected by the presence of parasitic resistances.

Fig. 7-bottom shows the evolution of V_{oc} with the intensity of the light. As shown, V_{oc} grows with a logarithmic dependence as the irradiance increases. According to Eq. (1), at reference conditions, V_{oc} (I = 0) can be expressed as:

$$V^*_{oc} = m^*V_T ln\left(\frac{I^*_{ph}}{I^*_o} - \frac{V^*_{oc}}{R^*_{sh}I^*_o} + 1\right) \approx m^*V_T ln\left(\frac{I^*_{ph}}{I^*_o}\right) \tag{22}$$

Based on this, under irradiance variations, V_{oc} can be approximated to the following expression:

$$V_{oc} \approx mV_T ln\left(\frac{DNI}{DNI^*}\frac{I^*_{ph}}{I^*_o}\right) \approx V^*_{oc} + mV_T \ln\left(\frac{DNI}{DNI^*}\right) \tag{23}$$

Hence, it could also be considered independent of parasitic resistances. In addition, the slope of V_{oc} as a function of ln(DNI) shows a constant behaviour. This confirms the narrow dependence of the ideality factor of the modules with irradiance commented in the previous section.

Fig. 7-bottom also shows the evolution of V_{mpp} with light intensity. This parameter has proven a more complex dependence than the previous. It trends to grow with ln(DNI) until a certain level and then starts to decrease gradually due to series resistance losses. This can also be explained from Eq. (1) following different approximations. At maximum power, V_{mpp} at reference conditions can be expressed as:

$$V^*_{mpp} = m^*V_T ln\left(\frac{I^*_{ph} - I^*_{mpp}}{I^*_o} - \frac{V^*_{mpp} + I^*_{mpp}R^*_s}{R^*_{sh}I^*_o} + 1\right) - I^*_{mpp}R^*_s \approx m^*V_T ln\left(\frac{I^*_{ph} - I^*_{mpp}}{I^*_o}\right) - I^*_{mpp}R^*_s \tag{24}$$

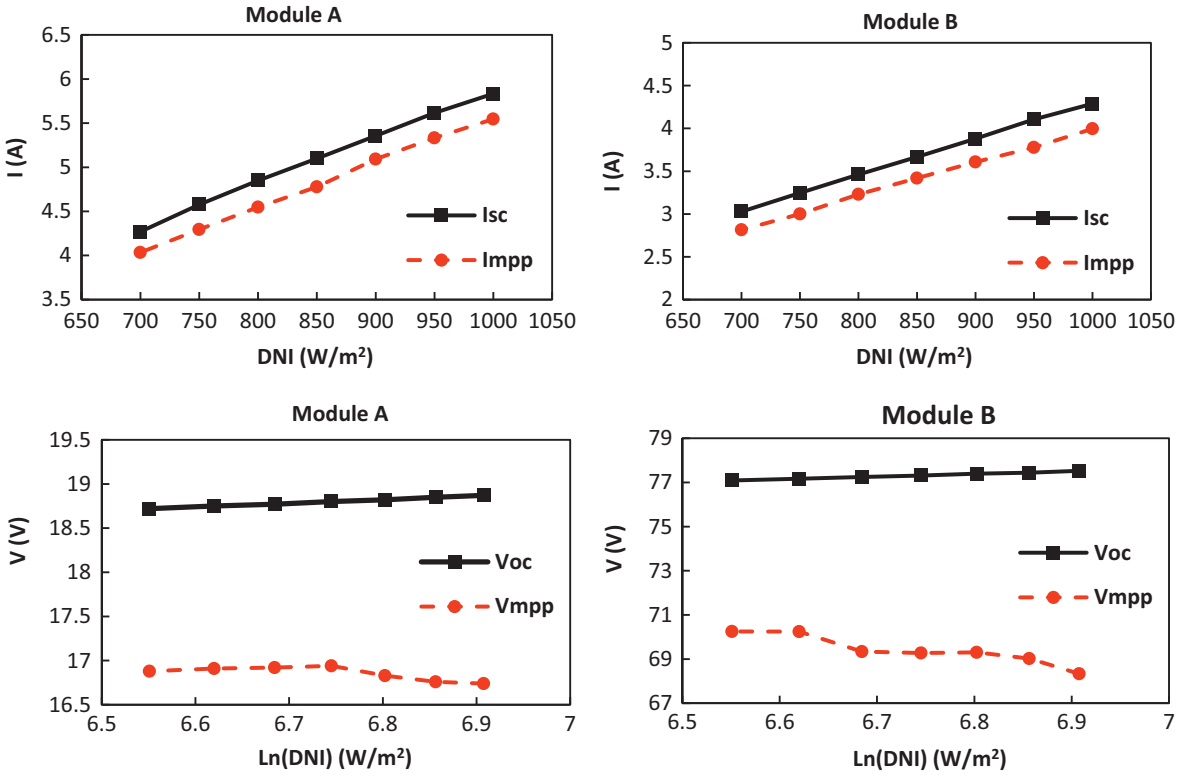

Fig. 7. Dependence of current-voltage parameters with input irradiance of the CPV modules under study.

So, with light intensity, V_{mpp} can be approximated to the following equation:

$$V_{mpp}(DNI) \approx mV_T ln\left(\frac{DNI}{DNI^*}\frac{I^*_{ph}-I^*_{mpp}}{I^*_o}\right) - \frac{DNI}{DNI^*}I^*_{mpp}R_s \approx V^*_{mpp} + mV_T ln\left(\frac{DNI}{DNI^*}\right) - I^*_{mpp}R_s\left(\frac{DNI}{DNI^*}-1\right) \quad (25)$$

This analysis demonstrates that the behaviour of V_{oc} and V_{mpp} is dominated by ln(DNI) variations. However, despite the reduction of R_s with irradiance, it causes V_{mpp} to decrease above a certain irradiance level. The presence of R_{sh} does not play a relevant role on the performance of these two parameters.

It should be noted that, based on the experimental data and relationships described above, the behaviour of the parameters with irradiance shown in Fig. 7 can be approximated with the following simple expressions:

$$I_{sc} \approx a \cdot DNI \quad (26)$$

$$I_{mpp} \approx b \cdot DNI \quad (27)$$

$$V_{oc} \approx c_1 ln(DNI) + c_2 \quad (28)$$

$$V_{mpp} \approx d_1 ln(DNI) - d_2 \cdot DNI + d_3 \quad (29)$$

with a high quality – a R^2 within 0.95–0.99 for both modules. In order show an example of the high accuracy of these approximations, Fig. 8 shows the measured and modelled V_{mpp}, the parameter with the more complex behaviour, for the module A. These approximations are useful since avoid the SEM model parameters and the I-V characteristics under reference conditions to be known. Hence, they offer a simple and accurate way for predicting the main electrical parameters as a function of the irradiance by performing simple regression analysis from monitored data.

The outcome of this study also indicates that the performance of the CPV modules is going to be limited by the effect of R_s on V_{mpp}. The fill factor (FF) of a photovoltaic device can be written as:

$$FF = \frac{I_{mpp}V_{mpp}}{I_{sc}V_{oc}} \quad (30)$$

By combining Eqs. (18), (21), (23) and (25), FF can be rewritten as:

$$FF = \frac{I^*_{mpp}}{I^*_{sc}}\frac{V^*_{mpp} + mV_T ln\left(\frac{DNI}{DNI^*}\right) - I^*_{mpp}R_s\left(\frac{DNI}{DNI^*}-1\right)}{V^*_{oc} + mV_T \ln\left(\frac{DNI}{DNI^*}\right)} \quad (31)$$

So, FF trends to unity as the irradiance increases without considering the effect of series resistance. However, for real concentrators, it tends to diminish above a determined irradiance level due to the increase of $R_s \cdot DNI/DNI^*$.

The efficiency (η) of a concentrator module can be expressed by means of the following equation:

$$\eta = \frac{P_{mpp}}{A_{module}DNI} \quad (32)$$

where P_{mpp} is the maximum power and A_{module} is the area of the concentrator. By combining Eqs. (18), (23) and (30), η can be rewritten as:

$$\eta = \frac{I^*_{sc}}{A_{module}DNI^*}\left(V^*_{oc} + mV_T \ln\left(\frac{DNI}{DNI^*}\right)\right)FF \quad (33)$$

Hence, the efficiency of the modules trends to grow due to the logarithmic increase of V_{oc} with the intensity of the light. However, as the irradiance increases, this effect is counterbalanced by the decrease of FF due to series losses. As a result, η of the modules decreases above a certain level.

The effect of the series resistance on FF and η with the increase of the intensity of the light is shown in Fig. 9. The FF decreases around 1% and 3% for the module A and B respectively. Regarding

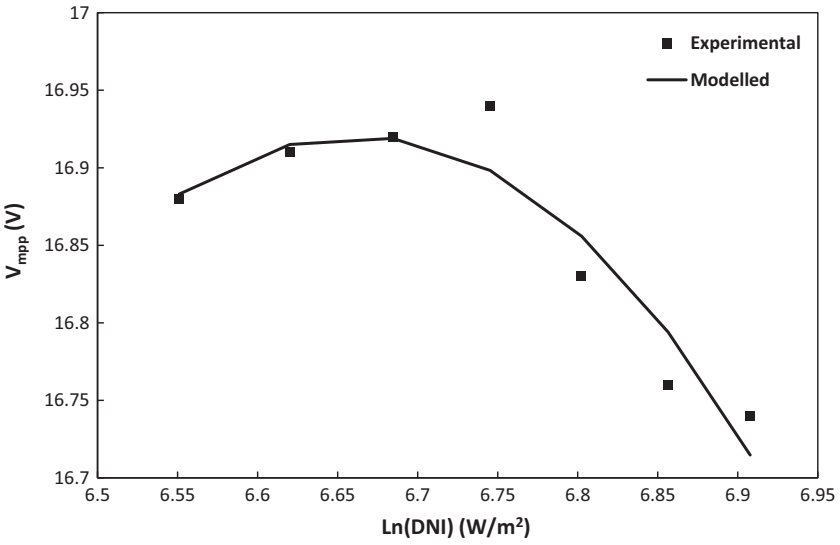

Fig. 8. Experimental versus modelled voltage at maximum power point (V_{mpp}) as a function of the incident irradiance for the module A.

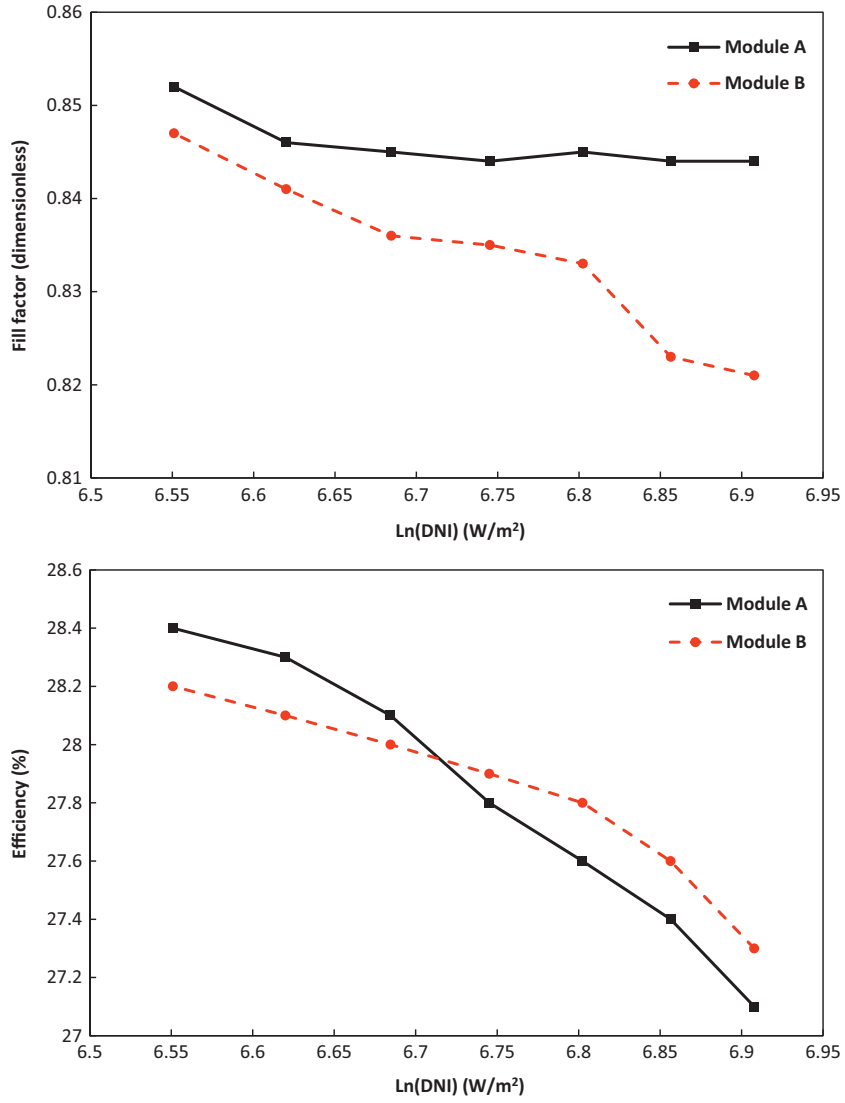

Fig. 9. Dependence of fill factor and efficiency with input irradiance of the CPV modules under study.

η, it is reduced approximately 1% for both modules. It is worth mentioning that the maximum of FF and η with irradiance cannot be clearly identified since it could happen at lower irradiance levels than the considered in this study. This highlights the importance of the coupling between the concentration of the modules and the peak of efficiency of the cells. The geometry and properties of the optical elements need to be carefully selected and designed to ensure multi-junction solar cells to operate around their maximum efficiency for the typical irradiance levels in outdoors. In addition, the reduction of the series resistance of the modules seems to be a crucial concern to have a peak efficiency at higher irradiance levels, and therefore, to maximize the energy harvested by CPV systems under real working conditions.

5. Modelling the electrical characteristics from reference values

The analysis and relationships discussed in the previous sections allow the electrical characteristics of concentrator PV modules as a function of the incident irradiance to be understood. For electrical modelling purposes, it is interesting to evaluate the accuracy in the estimation of the I-V curve and key parameters from the values of the concentrators at reference conditions. This is useful since the electrical characteristics under standard conditions are the variables provided by the manufacturers and testing laboratories in the majority of the cases. Hence, they are the only magnitudes available when is not possible to perform long-term outdoor measurements or to use a solar simulator able to change the input irradiance.

Fig. 10 shows an example of the measured and modelled I-V curve for the module A and the relative error between actual and predicted maximum power as a function of the input intensity for both modules. The photo-generated current at each light intensity has been estimated from the reference values, considering the linear dependency discussed in Section 3, with the following equation:

$$I_{ph} \approx \frac{I^*_{ph}}{DNI^*} DNI \tag{34}$$

The rest of the parameters of the SEM model equation have been kept constant at the values given in Table 3 and considering the number of cell in series of each module. As can be seen, the error in the fitting of the I-V curves increases as the irradiance

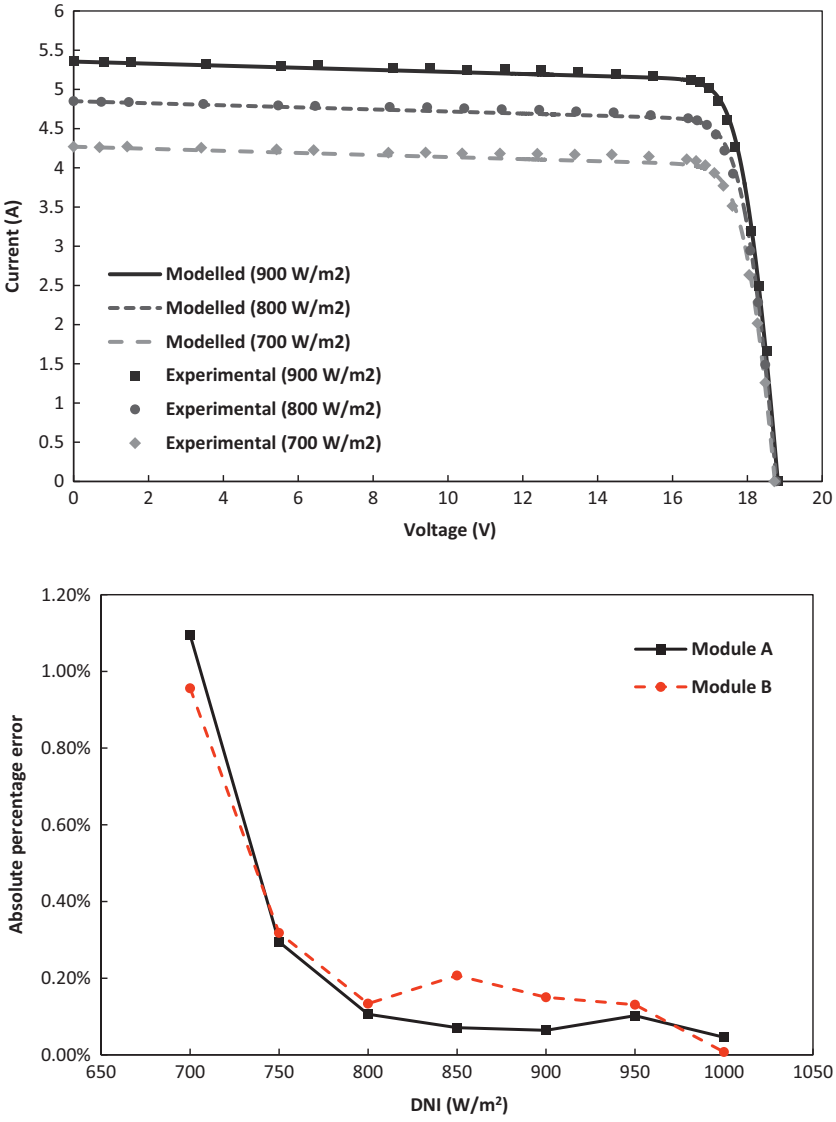

Fig. 10. Top: Experimental and modelled current-voltage curve by using the reference values of the CPV module A at three different irradiance levels, spectral irradiance similar to AM1.5D reference spectrum, SMR (top/mid) = 1 ± 0.05 and room temperature of 25 °C ± 0.5 °C. Bottom: Absolute percentage error between actual and estimated maximum power by using the reference values as a function of the direct normal irradiance (DNI) of the CPV modules used in this study.

Table 4
Mean absolute percentage error (MAPE), mean absolute error (MRE) and determination coefficient (R^2) between actual and predicted electrical parameters of the CPV modules under study using Eqs. (11), (14), (16) and (18) and the values at reference conditions.

Parameter	Module A			Module B		
	MAPE (%)	MRE (%)	R^2	MAPE (%)	MRE (%)	R^2
I_{sc}	1.2	0.4	0.98	0.4	0.4	0.99
I_{mpp}	1.1	1.0	0.99	0.3	0.2	0.99
V_{oc}	0.0	0.0	0.99	0.0	0.0	0.99
V_{mpp}	0.1	0.0	0.90	0.3	0.0	0.90

decreases. Despite of this, this approximation offers a good quality for both modules until irradiance values around 750 W/m^2 due to the fact that the absolute percentage error in the estimation of the maximum power is below 0.3%. So, it can be considered as a good first approximation to predict the I-V curve of concentrator modules for the typical operating irradiance levels in outdoors when the dependencies of the parameters of the SEM equation are unknown.

For the same reasons above, it is interesting to evaluate the accuracy in the estimation of the key electrical parameters of the modules from the reference values. These parameters have been estimated by means of Eqs. (18), (21), (23) and (25) and the reference values provided in Tables 2 and 3. Different statistical parameters have been calculated: the mean absolute percentage error (MAPE), the mean relative error (MRE) and the determination coefficient (R^2). These magnitudes have been calculated by means of the following expressions:

$$MAPE\ (\%) = \frac{100}{N}\sum_{i=1}^{N}\left|\frac{Z_{modelled} - Z_{measured}}{Z_{measured}}\right| \tag{35}$$

$$MRE\ (\%) = \frac{100}{N}\sum_{i=1}^{N}\frac{Z_{modelled} - Z_{measured}}{Z_{measured}} \tag{36}$$

$$R = \frac{\sum_{i=1}^{N}(Z_{measured} - \overline{Z_{measured}})(Z_{modelled} - \overline{Z_{modelled}})}{\sqrt{\sum_{i=1}^{N}(Z_{measured} - \overline{Z_{measured}})^2 \sum_{i=1}^{N}(Z_{modelled} - \overline{Z_{modelled}})^2}} \tag{37}$$

where N is the number of samples and Z represents the electrical parameter considered.

As can be seen in Table 4, the proposed approximations present a low variation of the estimated data around the experimental with a maximum MAPE of 1.2%. Also, the MRE is within 1%, which indicates that the approximations neither overestimate nor underestimate the electrical parameters significantly. Finally, a close match between actual and predicted data has been found – an R^2 equal of higher than 0.9.

Bearing the above in mind, the use of the reference values offer a simple way to predict the I-V curve and main electrical parameters of multi-junction CPV modules for the typical irradiance levels with a low margin of error. Obviously, under real operating conditions, thermal and spectral corrections need to be incorporated to model the electrical output with a satisfactory degree of accuracy. This should be the topic of next research activities concerning this issue.

6. Conclusions

This paper is focused on the analysis of the current-voltage output of multi-junction CPV modules under different irradiance levels. To carry out this study, two samples of concentrator modules were experimentally characterized in indoor laboratory at the CEAEMA of the University of Jaen by using the Helios 3198 CPV solar simulator. The I-V curves of both systems were recorded for light intensities within 700–1000 W/m^2, spectral irradiance similar to AM1.5D reference spectrum, SMR (top/mid) = 1 ± 0.05 and room temperature of 25 °C ± 0.5 °C. Based on these data, the single exponential model (SEM) parameters and I-V characteristics of the modules as a function of the input irradiance were extracted and discussed.

Results show that the photo-generated current increases linearly with irradiance. The diode ideality factor and saturation current have proven a noteworthy stable behaviour under irradiance variations. On the contrary, the parasitic resistances, i.e. series and shunt, of both concentrators have shown a clear tendency to decrease as the intensity increases. The fundamentals behind the behaviour of the SEM model parameters of the CPV modules are also discussed in relation to the physical properties of the multi-junction solar cells of the concentrators. In addition, different approximations are carried out in the I-V characteristic equation to explain the dependence of the electrical output of the devices with light intensity. Results show that the short-circuit current (I_{sc}) and current at maximum power point (I_{mpp}) are not affected by parasitic resistances and increase with a linear behaviour with irradiance. On the other hand, the open-circuit voltage (V_{oc}) and voltage at maximum power point (V_{mpp}) have proven to grow with a logarithmic dependence as the irradiance increases. However, while V_{oc} can be considered independent of parasitic resistances, V_{mpp} has demonstrated to decrease above a certain light intensity due to the increase of series resistance losses. Finally, the accuracy in the estimation of I-V curves and key electrical parameters of the concentrators from reference values are investigated. Results show that the I-V curves can be modelled with a good quality until irradiance values of around 750 W/m^2 due to an error in the estimation of the maximum power below 0.3%. The modelling of the main electrical parameters, i.e. I_{sc}, I_{mpp}, V_{oc} and V_{mpp}, present a high quality with a mean percentage absolute error (MAPE) lower than 1.2%, a mean relative error (MRE) within 1% and a determination coefficient (R^2) equal of higher than 0.9.

Future works should study the impact of temperature on the performance of the SEM model parameters and the I-V characteristics under different irradiance levels. This is a crucial next step to leverage our understanding of the electrical output of CPV modules under real working conditions. In addition, the validation of the relationships to predict the electrical parameters should be extended to a wider irradiance range to ensure their accuracy for low irradiance conditions. Thermal and spectral corrections have to be also incorporated with the aim of modelling the current-voltage output under the relevant time-varying atmospheric variables in outdoors.

Acknowledgments

Eduardo F. Fernández acknowledges the Spanish Ministry of Economy and Competitiveness for the Juan de la Cierva 2013 and 2015 fellowships. The authors also thank the Spanish Ministry of Economy and Competitiveness and FEDER funds for the projects ENE2013-45242-R and ENE2016-78251-R, and the "Plan de Apoyo

a la Investigación de la Universidad de Jaén y la Caja Rural de Jaén" (UJA2015/07/01).

References

Almonacid, F., Rodrigo, P., Fernández, E.F., 2016. Determination of the current-voltage characteristics of concentrator systems by using different adapted conventional techniques. Energy 101, 146–160.

Appelbaum, J., Peled, A., 2014. Parameters extraction of solar cells – a comparative examination of three methods. Sol. Energy Mater. Sol. Cells 122, 164–173.

Baig, H., Heasman, K., Mallick, T., 2012. Non-uniform illumination in concentrating solar cells. Renew. Sustain. Energy Rev. 16 (8), 5890–5909.

Ben Or, A., Appelbaum, J., 2013. Estimation of multi-junction solar cell parameters. Prog. Photovoltaics Res. Appl. 21 (4), 713–723.

Ben Or, A., Appelbaum, J., 2014. Dependence of multi-junction solar cells parameters on concentration and temperature. Sol. Energy Mater. Sol. Cells 130, 234–240.

Ciulla, G., Lo Brano, V., Di Dio, V., Cipriani, G., 2014. A comparison of different one-diode models for the representation of I-V characteristic of a PV cell. Renew. Sustain. Energy Rev. 32, 684–696.

Cotal, H. et al., 2009. III-V multijunction solar cells for concentrating photovoltaics. Energy Environ. Sci. 2 (2), 174–192.

Cotfas, D.T., Cotfas, P.A., Kplanis, S., 2013. Methods to determine the dc parameters of solar cells: a critical review. Renew. Sustain. Energy Rev. 28, 588–596.

Domínguez, C., Antón, I., Sala, G., 2008. Solar simulator for concentrator photovoltaic systems. Opt. Express 16 (19), 14894–14901.

Domínguez, C., Antón, I., Sala, G., 2010. Multijunction solar cell model for translating I-V characteristics as a function of irradiance, spectrum, and cell temperature. Prog. Photovoltaics Res. Appl. 18 (4), 272–284.

Domínguez, C., Antón, I., Sala, G., Askins, S., 2013. Current-matching estimation for multijunction cells within a CPV module by means of component cells. Prog. Photovoltaics Res. Appl. 21 (7), 1478–1488.

Fernández, E., Almonacid, F., Rodrigo, P., Pérez-Higueras, P., 2013b. Model for the prediction of the maximum power of a high concentrator photovoltaic module. Sol. Energy 97, 12–18.

Fernández, E., Almonacid, F., Ruiz-Arias, J., Soria-Moya, A., 2014. Analysis of the spectral variations on the performance of high concentrator photovoltaic modules operating under different real climate conditions. Sol. Energy Mater. Sol. Cells 127, 179–187.

Fernández, E., Almonacid, F., Soria-Moya, A., Terrados, J., 2015c. Experimental analysis of the spectral factor for quantifying the spectral influence on concentrator photovoltaic systems under real operating conditions. Energy 90, 1878–1886.

Fernández, E.F., García-Loureiro, A.J., Smestad, G.P., 2015a. Multijunction concentrator solar cells: analysis and fundamentals. In: Pérez-Higueras, Pedro, Fernández, Eduardo F. (Eds.)., High Concentrator Photovoltaics: Fundamentals, Engineering and Power Plants, Springer, s.l., pp. 9–37.

Fernández, E.F. et al., 2016b. Comparative study of methods for the extraction of concentrator photovoltaic module parameters. Sol. Energy 137, 413–423.

Fernández, E.F., Talavera, D.L., Almonacid, F.M., Smestad, G.P., 2016a. Investigating the impact of weather variables on the energy yield and cost of energy of grid-connected solar concentrator systems. Energy 106, 790–801.

Fernández, E. et al., 2015b. Model for estimating the energy yield of a high concentrator photovoltaic system. Energy 87, 77–85.

Fernández, E., Pérez-Higueras, P., Garcia Loureiro, A., Vidal, P., 2013c. Outdoor evaluation of concentrator photovoltaic systems modules from different manufacturers: first results and steps. Prog. Photovoltaics Res. Appl. 21 (4), 693–701.

Fernández, E. et al., 2013a. A two subcell equivalent solar cell model for III-V triple junction solar cells under spectrum and temperature variations. Sol. Energy 92, 221–229.

Fernández, E., Soria-Moya, A., Almonacid, F., Aguilera, J., 2016c. Comparative assessment of the spectral impact on the energy yield of high concentrator and conventional photovoltaic technology. Sol. Energy Mater. Sol. Cells 147, 185–197.

Ghani, F., Fernandez, E., Almonacid, F., O'Donovan, T., 2017. The numerical computation of lumped parameter values using the multi-dimensional Newton-Raphson method for the characterisation of a multi-junction CPV module using the five-parameter approach. Sol. Energy 149, 302–313.

Ghani, F., Rosengarten, G., Duke, M., Carson, J., 2014. The numerical calculation of single-diode solar-cell modelling parameters. Renew. Energy 72, 105–112.

Grundmann, M., 2010. The Physics of Semiconductors. Springer Berlin Heidelberg, s. l..

Humada, A., Hojabri, M., Mekhilef, S., Hamada, H., 2016. Solar cell parameters extraction based on single and double-diode models: a review. Renew. Sustain. Energy Rev. 56, 494–509.

Khan, F., Baek, S., Kim, J., 2014. Intensity dependency of photovoltaic cell parameters under high illumination conditions: an analysis. Appl. Energy 133, 356–362.

Kim, Y., Kang, S.-M., Winston, R., 2013. Modeling of a concentrating photovoltaic system for optimum land use. Prog. Photovoltaics Res. Appl. 21 (2), 240–249.

Kinsey, G. et al., 2008. Concentrator multifunction solar cell characteristics under variable intensity and temperature. Prog. Photovoltaics Res. Appl. 16 (6), 503–508.

Kurtz, S. et al., 2015. Key parameters in determining energy generated by CPV modules. Prog. Photovoltaics Res. Appl. 23 (10), 1250–1259.

Leloux, J. et al., 2014. A bankable method of assessing the performance of a CPV plant. Appl. Energy 118, 1–11.

Li, W. et al., 2016. Six-parameter electrical model for photovoltaic cell/module with compound parabolic concentrator. Sol. Energy 137, 551–563.

Li, Y. et al., 2013. Evaluation of methods to extract parameters from current-voltage characteristics of solar cells. Sol. Energy 90, 51–57.

Micheli, L. et al., 2016. Performance, limits and economic perspectives for passive cooling of high concentrator photovoltaics. Sol. Energy Mater. Sol. Cells 153, 164–178.

Muller, M., Kurtz, S., Steiner, M., Siefer, G., 2015. Translating outdoor CPV I-V measurements to a CSTC power rating and the associated uncertainty. Prog. Photovoltaics Res. Appl. 23 (11), 1557–1571.

Nelson, J., 2014. The Physics of Solar Sells. Imperial College Press, London.

Peharz, G., Ferrer-Rodríguez, J., Siefer, G., Bett, A., 2011a. A method for using CPV modules as temperature sensors and its application to rating procedures. Sol. Energy Mater. Sol. Cells 95 (10), 2734–2744.

Peharz, G., Ferrer-Rodríguez, J., Siefer, G., Bett, A., 2011b. Investigations on the temperature dependence of CPV modules equipped with triple-junction solar cells. Prog. Photovoltaics Res. Appl. 19 (1), 54–60.

Phang, J.C.H., Chan, D.S.H., Phillips, J.R., 1984. Accurate analytical method for the extraction of solar cell model parameters. Electron. Lett. 20 (10), 406–408.

Rodrigo, P., Fernández, E., Almonacid, F., Pérez-Higueras, P., 2013. Models for the electrical characterization of high concentration photovoltaic cells and modules: a review. Renew. Sustain. Energy Rev. 26, 752–760.

Rodrigo, P., Fernández, E., Almonacid, F., Pérez-Higueras, P., 2014. Review of methods for the calculation of cell temperature in high concentration photovoltaic modules for electrical characterization. Renew. Sustain. Energy Rev. 38, 478–488.

Rodrigo, P., Micheli, L., Almonacid, F., 2015. The high-concentrator photovoltaic module. In: Perez-Higueras, P., Fernández, Eduardo F., (Eds)., High Concentrator Photovoltaics: Fundamentals, Engineering and Power Plants. Springer, s.l., pp. 115–151.

Rodrigo, P. et al., 2016. Analysis of electrical mismatches in high-concentrator photovoltaic power plants with distributed inverter configurations. Energy 107, 374–387.

Segev, G., Mittelman, G., Kribus, A., 2012. Equivalent circuit models for triple-junction concentrator solar cells. Sol. Energy Mater. Sol. Cells 98, 57–65.

Shanks, K. et al., 2016. Theoretical investigation considering manufacturing errors of a high concentrating photovoltaic of cassegrain design and its experimental validation. Sol. Energy 131, 235–245.

Siefer, G., Bett, A., 2014. Analysis of temperature coefficients for III-V multi-junction concentrator cells. Prog. Photovoltaics Res. Appl. 22 (5), 515–524.

Soria-Moya, A. et al., 2015. Performance analysis of models for calculating the maximum power of high concentrator photovoltaic modules. IEEE J. Photovoltaics 5 (3), 947–955.

Steiner, M. et al., 2015. YieldOpt, a model to predict the power output and energy yield for concentrating photovoltaic modules. Prog. Photovoltaics Res. Appl. 23 (3), 385–397.

Strobach, E. et al., 2015. Modeling a grid-connected concentrator photovoltaic system. Prog. Photovoltaics Res. Appl. 23 (5), 582–592.

Talavera, D. et al., 2016. A worldwide assessment of levelised cost of electricity of HCPV systems. Energy Convers. Manage. 127, 679–692.

Talavera, D.L., Perez-Higueras, P.J., Almonacid, F., Fernández, E.F., 2017. A worldwide assessment of economic feasibility of HCPV power plants: profitability and competitiveness. Energy 119, 408–424.

Theristis, M., Fernández, E., Stark, C., O'Donovan, T., 2016. A theoretical analysis of the impact of atmospheric parameters on the spectral, electrical and thermal performance of a concentrating III-V triple-junction solar cell. Energy Convers. Manage. 117, 218–227.

Theristis, M., Fernández, E., Sumner, M., O'Donovan, T., 2017. Multiphysics modelling and experimental validation of high concentration photovoltaic modules. Energy Convers. Manage. 129, 122–134.

Theristis, M., O'Donovan, T., 2015. Electrical-thermal analysis of III-V triple-junction solar cells under variable spectra and ambient temperatures. Sol. Energy 118, 533–546.

Victoria, M., Domínguez, C., Antón, I., Sala, G., 2009. Comparative analysis of different secondary optical elements for aspheric primary lenses. Opt. Express 17 (9), 6487–6492.

Victoria, M. et al., 2013. Characterization of the spatial distribution of irradiance and spectrum in concentrating photovoltaic systems and their effect on multi-junction solar cells. Prog. Photovoltaics Res. Appl. 21 (3), 308–318.

Vorster, F., Van Dyk, E., 2005. Current-voltage characteristics of high-concentration, photovoltaic arrays. Prog. Photovoltaics Res. Appl. 13 (1), 55–66.

Vossier, A., Chemisana, D., Flamant, G., Dollet, A., 2012. Very high fluxes for concentrating photovoltaics: considerations from simple experiments and modeling. Renew. Energy 38, 31–39.

Xie, W.T., Dai, Y., Wang, R., Sumathy, K., 2011. Concentrated solar energy applications using Fresnel lenses: a review. Renew. Sustain. Energy Rev. 15 (6), 2588–2606.

Energy Conversion and Management 127 (2016) 679–692

Contents lists available at ScienceDirect

Energy Conversion and Management

journal homepage: www.elsevier.com/locate/enconman

A worldwide assessment of levelised cost of electricity of HCPV systems

D.L. Talavera *, J.P. Ferrer-Rodríguez, P. Pérez-Higueras, J. Terrados, E.F. Fernández

IDEA Research Group, University of Jaén, Campus Lagunillas, 23071 Jaén, Spain

ARTICLE INFO

Article history:
Received 26 April 2016
Received in revised form 8 September 2016
Accepted 17 September 2016

Keywords:
Levelised cost of electricity
High concentrator photovoltaic
Grid parity

ABSTRACT

Numerous works of exhaustive analysis of the economic assessment of PV systems are available in the literature. However, there is a lack of this kind of studies concerning High Concentrator Photovoltaic (HCPV) technology. In this work, a worldwide economic feasibility analysis of HCPV systems is performed through the LCOE estimation, since it is a commonly method to assess and compare energy generation systems of different technologies. The LCOE of HCPV grid-connected systems is estimated and analysed for 133 countries. The analysis and detection of the optimal zones for HCPV technology is conducted in terms of the LCOE, and in addition, an innovative global map of the LCOE of HCPV is presented. Moreover, the grid parity in the domestic market segment for the year 2014 is analysed and found to be a reality for several developed countries. Finally, a prospective scenario comparing the LCOE of HCPV and conventional PV systems for the year 2020 is analysed and plotted in a global map, in which many countries have found to be preferable for the HCPV technology in terms of the LCOE. As an important result, although the Annual Final Yield, Y_f, and LCOE are apparently inversely proportional, when comparing both parameters, Y_f and LCOE, on one hand, it is obtained that some countries with relative high Y_f values are also of relative high LCOE values (e.g. Iran and Sudan), and, on the other hand, some other countries with relative low Y_f values are also of relative low LCOE values (e.g. Canada and France).

1. Introduction

Electrical generation systems based on conventional Photovoltaic (PV) modules, either crystalline or thin film ones, have proved to be a sound technology thoroughly deployed around the world. That implies the existence of a significant number of studies, and research, concerning different economic aspects related to conventional PV systems [1,2]. Such studies are quite useful to assess, on one hand, the feasibility of the investments and, on the other hand, to support policy makers in order to outline renewable energy promotion policies.

Economical assessment of PV systems can be performed by means of the analysis of different methods such as: net present value (*NPV*), discounted payback time (*DPBT*), internal rate of return (*IRR*) and levelised cost of electricity (LCOE) [3–7]. The later one, LCOE, represents the constant and theoretical cost of every kW h produced by an energy generation system along its useful life [8] and it is a commonly used method to assess and compare energy generation systems of different technologies [9–16] and, in particular, in the economical assessment of conventional PV systems [5,9,13,14,17–20].

High Concentrator Photovoltaic (HCPV) systems are based on the use of optical devices able to concentrate solar radiation, usually in a range from 500 up to 1000 times, onto small and high efficient multi-junction solar cells. Currently the main strengths of HCPV systems are: (a) high efficiency, with MJ cells that have currently reached a 46% efficiency and with HCPV modules showing efficiencies up to 36.7%, they have potential for further efficiency increase; (b) technological maturity; (c) cost reduction potential by means of the optimization of the semiconductor materials used; (d) higher energy yield per square meter than other renewable energies; (e) high potential deployment; (f) high potential market growth rate as shown by the last years market progress when CPV accumulated power installed have increased around 330 MWp [21,22] in 2014. On the other hand, HCPV systems still have weaknesses such as: (a) higher costs than conventional PV systems; (b) lack of operational experience which implies higher technological risks; (c) suitability restricted to locations with high direct solar irradiation levels; (d) difficult architectural integration; (e) requirement of highly precise solar trackers.

Another weakness of HCPV technology is the lack of precise studies related with its economic aspects and we can only find a few studies concerning LCOE for CPV [10,23,24]. In [10] Fraunhofer ISE analysed different renewable energy technologies and estimated LCOE for CPV for two specific locations: (a) a location

* Corresponding author.
E-mail address: dlopez@ujaen.es (D.L. Talavera).

http://dx.doi.org/10.1016/j.enconman.2016.09.054
0196-8904/

Nomenclature

$[HCPV_{AOM}]_{kWp}$ normalized per-kWp annual operation and maintenance cost of the HCPV system (€)
$[HCPV_I]_{kWp}$ normalized per-kWp initial investment cost of HCPV(€/kWp)
$[PV_{AOM}]_{kWp}$ normalized per-kWp annual operation and maintenance cost of the PV system (€)
$[PV_I]_{kWp}$ normalized per-kWp initial investment cost of PV (€/kWp)
d nominal discount rate (%)
d_{ec} annual dividend the equity capital –return on equity- (%)
DEP annual tax depreciation (€)
DNI_A annual direct normal irradiation (kW h/(m^2 year))
DNI_{STC} direct normal irradiation in standard test condition (1 kW h/m^2)
G_{STC} global irradiance in standard test condition (1 kW/m^2)
$HCPV_{AOM}$ annual operation and maintenance cost of the HCPV system (€)
$HCPV_{ec}$ amount equal to the portion of the initial investment financed with equity capital (€)
$HCPV_I$ initial investment cost on the HCPV system (€)
$HCPV_l$ amount equal to the portion of the initial investment financed with loan (€)
$H_{opt\ A}$ annual Global Irradiation on optimally inclined plane (kW h/(m^2 year))
i annual inflation rate (%)
i_l annual loan interest (%)
LCC life cycle cost of the HCPV system (€)
$LCOE$ levelised cost of electricity (€/kW h)
LR learning rate
N life cycle of the HCPV system, equal to analysis period (years)
N_d tax life for depreciation (years)
N_l amortization of loan (years)
PR performance ratio (%)
$PW\ [DEP]$ present worth of the tax depreciation (€)
$PW[HCPV_{OM}\ (N)]$ present worth of the HCPV system operation and maintenance cost (€)
q factor equal to 1/(1 + d)
Q_{HCPV} HCPV world cumulative installed capacity
Q_A annual growth installed capacity (%)
r_d annual degradation rate in the efficiency of the HCPV panels (%)
$r_{O\&M}$ annual escalation rate of the operation and maintenance cost of the HCPV system (%)
S_V salvage value of the system at the end of their life cycle (€)
T income tax rate (%)
$WACC$ weighted average cost of capital (%)
$Y_{f\ HCPV}$ annual final yield of a HCPV system (kW h/(kWp year)
$Y_{f\ PV}$ annual final yield of a conventional PV system kW h/(kWp year)

with an annual Direct Normal Irradiation (DNI_A) of 2000 kW h/(m^2 year), typical in southern Spain and, (b) another one with DNI_A = 2500 kW h/(m^2 year), typical in the MENA region, where the initial investment cost is considered between 1400 and 2200 €/kWp. LCOE calculation for CPV systems with DNI_A = 2000 kW h/(m^2 year) in year 2013 results in the range of 0.10–0.15 €/kW h and with DNI_A = 2500 kW h/(m^2 year) it varies in the range of 0.08 €/kW h to 0.12 €/kW h. In a prospective scenario and assuming an initial investment cost for CPV system between 700 and 1100 €/kWp, LCOE for CPV would range between 0.045 €/kW h and 0.075 €/kW h. In [23] LCOE is evaluated by SolFocus for both CPV systems and conventional fixed PV for the locality of Phoenix, Arizona (USA). The results of this last study showed that LCOE for CPV was able to compete with PV in year 2009 and to reach the lowest LCOE in 2011 in locations with relative high values of DNI like Phoenix and south west USA. In [24] Talavera et al. perform an exhaustive analysis of the economic feasibility of HCPV systems in Spain using the LCOE. LCOE calculation for HCPV systems with DNI from 2221 to 982 kW h/(m^2 year) can reach LCOE values ranging from 0.081 to 0.184 €/kW h respectively, when assuming an initial investment cost for HCPV of 1800 €/kWp. Also, in a prospective scenario and assuming an initial investment cost for HCPV system of 700 €/kWp, LCOE for HCPV would range between 0.035 €/kW h and 0.080 €/kW h.

Except for that exposed above, no LCOE for HCPV studies are available in up-to-date literature. Thus, due to the lack of exhaustive worldwide studies of the HCPV technology and with the existing demand of economic feasibility information of HCPV systems, rigorous and detailed worldwide LCOE for HCPV studies are needed. Those studies should include potential regions for HCPV systems to be installed.

It is important to remark that LCOE is also utilized for comparing different electricity generation technologies in terms of grid parity. By definition, grid parity takes place when the LCOE for a renewable energy source is less or equal to the electricity price. Some specific studies use the model LCOE to analyse PV technology grid parity [19,25], but there are no previous studies in the literature about HCPV grid parity.

For those reasons, a worldwide analysis of economic feasibility of HCPV systems is carried out in this paper, using the LCOE as a feasibility indicator. In this document, firstly, the methodology is described and the data used for the calculations are explained and justified. Next, an economic feasibility analysis of HCPV systems for 133 countries is performed in terms of the LCOE. For determining LCOE values, specific parameters of each country like: DNI, financial cost (cost of capital) or tax rate and inflation have been taking into account. However, other parameters like the initial investment cost have been considered of the same value for every location. After that, a study concerning the grid parity of HCPV technology in the domestic market segment is conducted. Finally, the comparison of the LCOE of HCPV and conventional PV systems for a future year 2020 scenario is carried out.

The methodology shown here is definitively useful to identify countries where HCPV technology can be a feasible technology to generate electricity, and it means an original contribution regarding HCPV electrical generation costs in a global basis, not covered by previous literature. Furthermore, the map-based methodology proposed in the paper is easy to handle and can be consulted by future owners, investors and financial entities involved in HCPV systems.

Moreover, for applying this methodology, some assumptions have been made. First, on one hand, in this work, we define a HCPV system as a grid-connected system composed of HCPV modules with the characteristics commented above. On the other hand, we define a conventional PV system as a grid-connected system composed of c-Si fixed PV modules optimally inclined and oriented southwards in the North hemisphere or northwards in the South hemisphere. Second, concerning the data, since this work is a global analysis and the values of the parameters can be obtained from different sources, then the results obtained may differ slightly if other different sources of data (like Meteonorm, PWATTS, PVGIS, etc.) are used. Third, inside a single country, different electricity

prices are possible, since many of the electrical markets are liberalized and different operators may exist in the same country, but for the purpose of this study an average value for the domestic electricity price in a determined country has been taken.

2. Methodology and input factors

In this section, the model LCOE utilized for the feasibility analysis of the HCPV systems is presented. A review of the parameters used as inputs for the equations presented below is conducted. This review will lead to identify the parameter values for the analysis of the HCPV for a scenario in the year 2014 and prospective scenario 2020. Furthermore, in the Appendix A, all the parameter values used for the calculations are available. It should be noted that the figures presented here referring to costs and electricity yields are all normalized-per-kWp. The symbols used for these factors are the same for those not normalized, except that they are shown in brackets and with the subscript 'kWp'.

2.1. Model LCOE

The method utilized for the feasibility analysis is the LCOE and will be shown below. The calculation procedures are similar to those presented in previous works [6,24]. Levelised cost of electricity can be defined as the constant and theoretical cost of production of electricity of a HCPV system over its total life time expressed as:

$$\mathrm{LCOE} = \frac{HCPV_I + \sum_{n=1}^{N} \frac{HCPV_{AOM\,n}(1-T)}{(1+d)^n} - \sum_{n=1}^{N_d} \frac{DEP_n \cdot T}{(1+d)^n}}{\sum_{n=1}^{N} \frac{E_n}{(1+d)^n}} \quad (1)$$

where $HCPV_I$ (€) is the initial investment cost of the HCPV system, $HCPV_{AOM}$ (€) are the annual operation and maintenance costs, DEP (€) is the annual tax depreciation for the HCPV system, N_d (years) is the tax life for depreciation, E (kW h/(kWp year)) is the Annual Final Yield (it will be later defined and denoted as Y_f according to the IEC 61724 standard), d (%) is the nominal discount rate, N (years) is the useful life of the HCPV system and T (%) is the tax rate.

Assuming that r_d (%) is the annual degradation rate in the efficiency of the HCPV system and $r_{O\&M}$ (%) is the annual escalation rate of the operation and maintenance costs of the system, the LCOE may be estimated by:

$$\mathrm{LCOE} = \frac{HCPV_I + \sum_{n=1}^{N} \frac{HCPV_{AOM\,n}(1+r_{O\&M})^n \cdot (1-T)}{(1+d)^n} - \sum_{n=1}^{N_d} \frac{DEP_n \cdot T}{(1+d)^n}}{\sum_{n=1}^{N} \frac{E_n (1-r_d)^n}{(1+d)^n}} \quad (2)$$

Defining the parameters $K_d = (1 - r_d)/(1 + d)$, $K_P = (1 + r_{O\&M})/(1 + d)$, and $q = (1/(1 + d))$. Taking constant the annual HCPV electricity yield (E) and annual operation and maintenance costs ($HCPV_{AOM}$) over the life-cycle, using the parameters r_d and $r_{O\&M}$, and considering that the annual tax depreciation (DEP) is calculated as lineal over the period time (N_d) for the HCPV system, the Eq. (2) can be expressed:

$$\mathrm{LCOE} = \frac{HCPV_I + HCPV_{AOM}(1-T) \cdot \frac{K_P \cdot (1-K_P^N)}{1-K_P} - DEP \cdot \frac{q \cdot (1-q^{N_d})}{1-q} T}{E \cdot \frac{K_d (1-K_d^N)}{1-K_d}} \quad (3)$$

The numerator of Eq. (3) represents the life cycle cost of the HCPV system (LCC):

$$LCC = HCPV_I + HCPV_{AOM}(1-T) \cdot \frac{K_P \cdot (1-K_P^N)}{1-K_P} - DEP \cdot T \frac{q \cdot (1-q^{N_d})}{1-q} \quad (4)$$

Besides, Eq. (4), may be written as:

$$LCC = HCPV_I + \mathrm{PW}[HCPV_{OM}(N)] - \mathrm{PW}[DEP(N_d)] \quad (5)$$

where $PW[HCPV_{OM}(N)]$ is the present worth of operation and maintenance cost of the system and $PW[DEP(N_d)]$ is the present worth of the tax depreciation.

The weighted average cost of capital ($WACC$) over the discounting factor (nominal discount rate) allows for including explicitly the share of external financing and equity financing. $HCPV_I$ (€) is the initial investment cost of the HCPV system which may be financed through long-term debt or/and equity capital. $HCPV_I$ is financed through of a loan ($HCPV_l$) and equity capital ($HCPV_{ec}$), so that $HCPV_I = HCPV_l + HCPV_{ec}$. Then, this can be written as:

$$HCPV_I = \left(HCPV_l \cdot \frac{i_l(1-T)}{1-(1+i_l(1-T))^{-N_l}} \cdot \frac{q \cdot (1-q^{N_l})}{1-q} \right) + \left((d_{ec} \cdot HCPV_{ec}) \cdot \frac{q \cdot (1-q^N)}{1-q} + HCPV_{ec} \cdot q^N \right) \quad (6)$$

The loan is represented by the first addend of Eq. (6): $HCPV_l$ is borrowed at an annual loan interest (i_l) to be repaid in N_l years. The second term represents the equity capital, with an annual payback in the form of dividends (d_{ec}), which is, the return on equity, and it is amortized at the end of the life cycle of the system. It is remarkable that the left-hand side of Eq. (6) only equals its right-hand side if the selected value of d is equal to the weighted average cost of capital ($WACC$) of the investment.

$WACC$ is the cost that the owner or investor of the project must pay for the use of capital sources in order to finance the investment. Organizations typically use the value of the organization's weighted average cost of capital as nominal discount rate (d) [8]. In this paper, the nominal discount rate is assumed to be equal to $WACC$ in order to calculate the LCOE. LCOE values are highly location-specific, because factors like annual normal irradiation (DNI_A), cost of capital, tax rate and inflation are specific of each country.

2.2. Average HCPV electricity yields per country

As it was previously pointed, the Annual Final Yield of a HCPV system is a key parameter for the LCOE estimation. There are different methods to calculate the generated energy [26,27]. We use in this work the method based on the Performance Ratio (PR), which is established in the IEC 61724 standard [28]. In this standard, the Annual Final Yield is defined (Y_f) as the output electrical energy (AC electricity) generated by a photovoltaic system per unit of power installed, and is expressed in kW h/(kWp·year).The energy yield for a conventional PV system, Y_{fPV}, can be estimated through the Eq. (7):

$$Y_{fPV} = PR \frac{H_{OPTA}}{G_{STC}} \quad (7)$$

where $HOTP_A$ (kW h/(m^2·year)) is the annual global irradiation on the optimal inclined plane and G_{STC} the global irradiance at Standard Test Conditions (1 kW/m^2). The value of PR for conventional PV systems is typically in the range from 0.70 to 0.80. In our study, we take a value of PR = 0.75, based on the experience of this kind of systems [29–33].For the case of HCPV technology, the Annual Final Yield can be estimated using the following Eq. (8):

$$Y_{f\ HCPV} = PR \frac{DNI_A}{DNI_{STC}} \quad (8)$$

where $Y_{f\ HCPV}$ is the Annual Final Yield of a HCPV system (kW h/(kWp year)), DNI_A is the annual direct normal irradiation (kW h/(m^2 year)) and DNI_{STC} is the direct normal irradiance at Standard Test Conditions (1 kW/m^2). The value of PR in an HCPV system typically ranges from 0.76 to 0.91 [34–44]. In this case, we have used an intermediate value of 0.82.

Fig. 1 represents a novel map for the HCPV Annual Final Yield in 133 countries. The values here represented have been calculated from Eq. (8) taking an average value of DNI_A for each country and

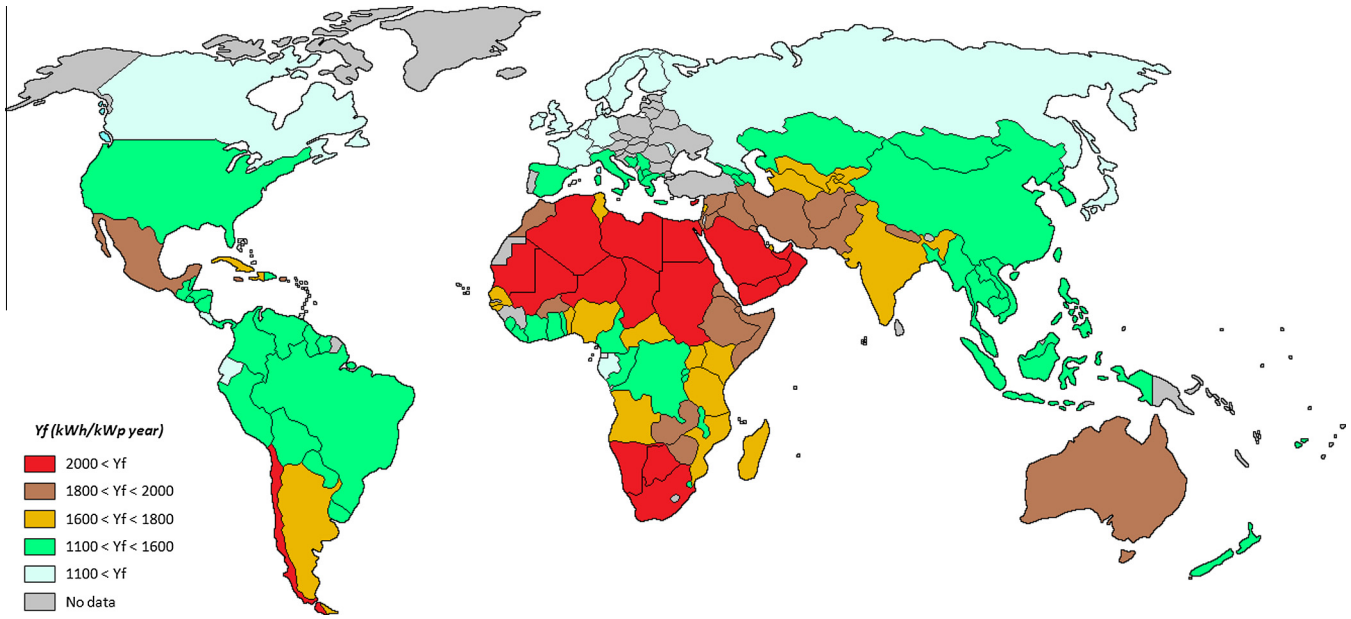

Fig. 1. Global map of HCPV systems annual final yield, $Y_{f\ HCPV}$.

assuming a fixed value of *PR = 0.82* for all the countries. NASA data [45], with a resolution of 1° for latitude and 1° for longitude, were utilized for calculating the average DNI_A for each country.

The results of the map of Fig. 1 show five different categories according to the level of the Annual Final Yield from lower than 1100 kW h/(kWp year) to greater than 2000 kW h/(kWp year). Each country is marked in a corresponding colour as a function on its level of energy yield. Analysing this map, three groups of countries can be made. There is a group of countries (Mexico, Chile, Australia, and those in North and South of Africa and Near East) where the annual energy production is over 1800 kW h/(kWp year). In principle, these countries may be considered as the most suitable for HCPV technology. There is another group of countries, where $1100 < Y_{f\ HCPV} < 1800$ kW h/(kWp year), those marked in green and light brown. For those countries, it is necessary to realise a more detailed study, since some regions of those countries may have relative high values of $Y_{f\ HCPV}$ and be suitable for HCPV technology. And finally, there is a last group of countries with $Y_{f\ HCPV}$ values lower than 1100 kW h/(kWp year) that, in principle, might seem to be not of interest for HCPV. However, it will later explained that some of these countries are really of interest for HCPV technology, as in the case of Canada and some other European countries.

2.3. Experience curve approach and HCPV initial investment cost

To determine the costs and the market that a new technology, as in the case of HCPV, will reach in next years is a difficult task. This is due to different causes that are, on one hand, inherent to the technology, an on the other hand, external to the technology. In relation to inherent causes, the costs may undergo strong variations in the initial stages of this technology development because of the incorporation of technological improvements on the products (increase of the efficiency, incorporation of new materials and new manufacturing processes). In relation to external causes, the evolution of the market is highly conditioned by the price of fossil fuels, the cost of other renewable energies and by the renewable energy policies dictated by the different governments.

Several market analysis [46–50] indicate that the HCPV world cumulative installed capacity in 2013 was between 160 and 275 MWp, 330 MWp in the year 2014 [22], and that this could be between 1100 and 1800 MWp in the year 2020 [51]. Based on the available information, an annual growth, Q_A (%), scenario of this capacity can be assumed to be of 40%. This growth rate, although high, is nevertheless lower than the historical annual growth rate of 88% during the period 2007–13 and have a possibility of being achieved in the coming years [52].

The learning curve can be used to estimate the evolution of the initial investment cost of HCPV systems for upcoming years. This curve describes the cost reduction as a function of the accumulated experience in the manufacturing and in the use of a particular technology. The learning curve of a HCPV system can be expressed as:

$$HCPV_{I\ year} = HCPV_{I\ 2014}\left(\frac{Q_{HCPV\ year}}{Q_{HCPV\ 2014}}\right)^{\log_2^{(1-LR)}} \quad (9)$$

where $HCPV_{I\ year}$ (€/kWp) is the HCPV initial investment cost in the year under review, $HCPV_{I\ 2014}$ is the HCPV initial investment cost in 2014, $Q_{HCPV\ year}$ (MW) is the HCPV world cumulative installed capacity in the year under review, $Q_{HCPV\ 2014}$ (MW) is the HCPV world cumulative installed capacity in 2014 and *LR* (0-1) is the Learning Rate. Based on an industry and literature survey in 2014, the typical initial investments cost per kWp of a HCPV system of a capacity larger than 1 MW may be taken at 1700 €/kWp with a variation ranging from 1400 to 2200 €/kWp [10,11,22]. Moreover, and based on survey literature, a learning ratio within 0.14 and 0.22 with a 90% confidence value was found Hayson et al. [52]

In this work, three scenarios have been considered, a low one where $HCPV_{I\ 2014}$ is 2000 €/kWp and *LR* is 18%, a conservative one where $HCPV_{I\ 2014}$ is 1800 €/kWp and *LR* is 20% and an accelerated one where $HCPV_{I\ 2014}$ is 1600 €/kWp and *LR* is 21%. Fig. 2 shows both proposed scenarios and the forecast of the company GTM Research Inc [53] Yole [54] and IHS [47]. Fig. 2 shows also the values of the scenario proposed by Hayson et al., where a $HCPV_{I\ 2013}$ of 2.8 $/Wp and a *LR* of 18% are assumed.

These results depend on multiple variables that may change over time and, therefore, modify the data obtained. For the year 2020, both scenarios predict that $HCPV_{I\ 2020}$ will be between 800 and 1000 €/kWp approximately. In this work it is assumed a Normalized-per-kWp initial investment cost of HCPV, $[HCPV_I]_{kWp}$, equal to 900 €/kWp for the prospective scenario of 2020, what is around the mean value between both scenarios and also close to the prediction of GTM Research Inc.

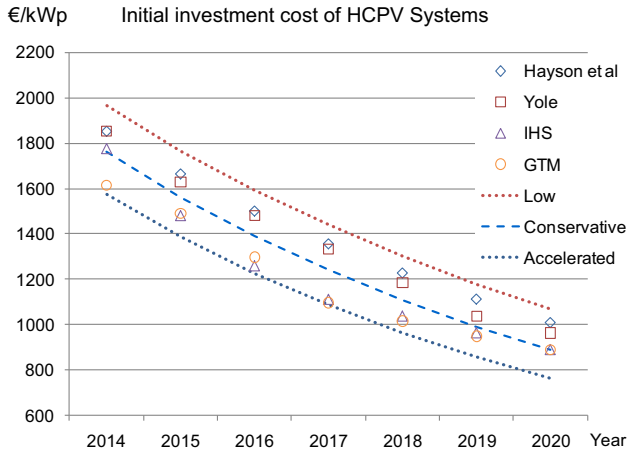

Fig. 2. Learning curves of the initial investment cost of HCPV systems. Also, initial investment cost of HCPV forecast estimated by Hayson et al. and the private company Yole, IHS and GTM Research Inc. Note: An exchange rate of 1,34 $/€ for the year 2014 has been considered.

2.4. Values of remain factors

The averages of historical data of the inflation rate (i) for each country in the period 2009–2013 [55,56] have been reviewed and the resulting data of this analysis are shown in Appendix A.

Initial investment cost may be financed by means of debt or/and equity capital. In this paper, we have selected the proportion between long-term loans and equity capital. On one hand, it has been assumed that 70% of this amount is borrowed at a loan –debt–, while the remaining investment amount, 30%, is contributed from equity capital; taking into account that commercial banks are generally accepting higher leverage in stable economies with secure property rights [57]. On the other hand, for remaining countries, the share of equity and debt in the project is assumed to be 50%, which is in line with the recommendations of the CDM Executive Board [58]. Regarding HCPV systems, the loan, i_l, is specific for each country (see Appendix A), N_l is equal to 20 years, and also equity capital, d_{ec}, is assumed specific for each country (see Appendix A) and being amortized at the end of the life cycle of the system.

The income tax rate (T) for the organization or taxpayer, changes depending on each country's regulations. In this analysis, the value of corporate income tax rate is assumed specific for each country, as shown in Appendix A. The method used in the tax depreciation is based on general method, using a maximum linear coefficient of 5%, with a tax life for depreciation of 20 years [59,60].

The HCPV Annual Final Yield is assumed to decrease every year. The annual degradation rate, r_d (%/year), in the efficiency of the HCPV System is 0.5%/year [9,61]. The analysis period is equal to the life time of the HCPV system, therefore N = 30 years. Nowadays, conventional PV systems have a life cycle of around more than 30 years. Salvage value of the system at the end of their life-cycle (S_V) is taken as equal to zero.

The nominal discount rate (d) is assumed to be equal to the weighted average capital of cost in order to calculate the LCOE [8,10]. This cost of capital will vary depending on how the capital resources are chosen to finance the initial investment cost. The after-tax WACC values are shown in Appendix A.

Normalized-per-kWp annual operation and maintenance costs, $[HCPV_{AOM}]_{kWp}$, are taken at 28 €/(kW year) for the HCPV systems [11,62], while for conventional PV systems they are estimated to be 20 €/(kW year) [62,63]. Moreover, there are estimations that consider an annual fixed percentage of the normalized-per-kWp initial investment cost of 2% for HCPV systems [50], while for conventional PV systems it is assumed to be 1.5% for the annual operation and maintenance costs [25]. The latter approach has been chosen in this paper. The annual escalation rate of the operation and maintenance costs ($r_{O\&M}$) is set equal to the value of the annual inflation rate, so $r_{O\&M} = i$.

Table 1
Values of the factors assumed for the calculation of LCOE on HCPV systems in the scenario for 2014.

Factors	Case base values	Units
Y_{HCPV}	According Fig. 1	kW h/(kWp year)
$[HCPV_I]_{kWp}$	1700	€/kWp
$[HCPV_{AOM}]_{kWp}$	2	%
r_d	0.5	%/year
$r_{O\&M}$	Equal to i	%/year
T	According Appendix A	%
i	According Appendix A	%
d	According Appendix A	%
i_l	According Appendix A	%
N_l	20	years
d_{ec}	According Appendix A	%
N	30	years

Table 1 summarizes the previous analysis by showing the figures chosen and assumed for each factor defining the HCPV system in each country. The LCOE estimation for each country is realised by solving the equations presented in Section 2.1 in combination with the figures shown in Table 1 in a spreadsheet.

3. Analysis and results

The LCOE for HCPV systems in 133 countries in the year 2014 has been estimated through solving the equations presented in Section 2. The parameters and the input data used in this study are shown in Table 1, including the next factors: Annual Final Yield (Y_{HCPV}), Normalized-per-kWp initial investment cost of HCPV ($[HCPV_I]_{kWp}$), Normalized-per-kWp annual operation and maintenance costs ($[HCPV_{AOM}]_{kWp}$), annual degradation rate (r_d), annual escalation rate of the operation and maintenance costs ($r_{O\&M}$), income tax rate (T), inflation (i), nominal discount rate (d), loan interest rate (i_l), repaying loan (N_l), dividends (d_{ec}) and life time of the HCPV system (N). The worldwide maps shown in Figs. 3–5 represent the output results of the analysis conducted. Moreover, in the Appendix A, the detailed numeric results of each country are available. Below, the levelised cost of electricity for the HCPV technology systems has been estimated.

In this work, the average value of DNI_A is taken for each country. However, those countries with highest area, or such area that LCOE variations are significant inside the own territory, are divided in two partitions North-South or West-East. Although these partitions are not shown in Fig. 3, they have been considered for obtaining the results shown in Section 3.1.

The global LCOE map of Fig. 3 has also five categories with the same colours as in Fig. 1, being the most favourable cases for HCPV in terms of LCOE those countries marked in red colour too. Some ideas can be pointed from this global LCOE map: (i) LCOE values range from 6.7 c€/kW h, in the case of United Arab Emirates, to 62 c€/kW h, in Vietnam. (ii) The zones that present lowest LCOE are: North America, Chile, Australia, North and South of Africa and the South of Europe. (iii) Although there is an inverse relation between Y_f and LCOE, as it was defined in Eq. (1), when comparing both maps of Figs. 1 and 3, on one hand, it can be observed that some countries with relative high Y_f values are also of relative high LCOE values (e.g. Iran and Sudan). On the other hand, some other countries with relative low Y_f values are also of relative low LCOE values (e.g. Canada and France).

It is important to point out that, concerning the LCOE estimation, countries in geographical zones with similar DNI_A values may not have similar economic parameters, like in the case of

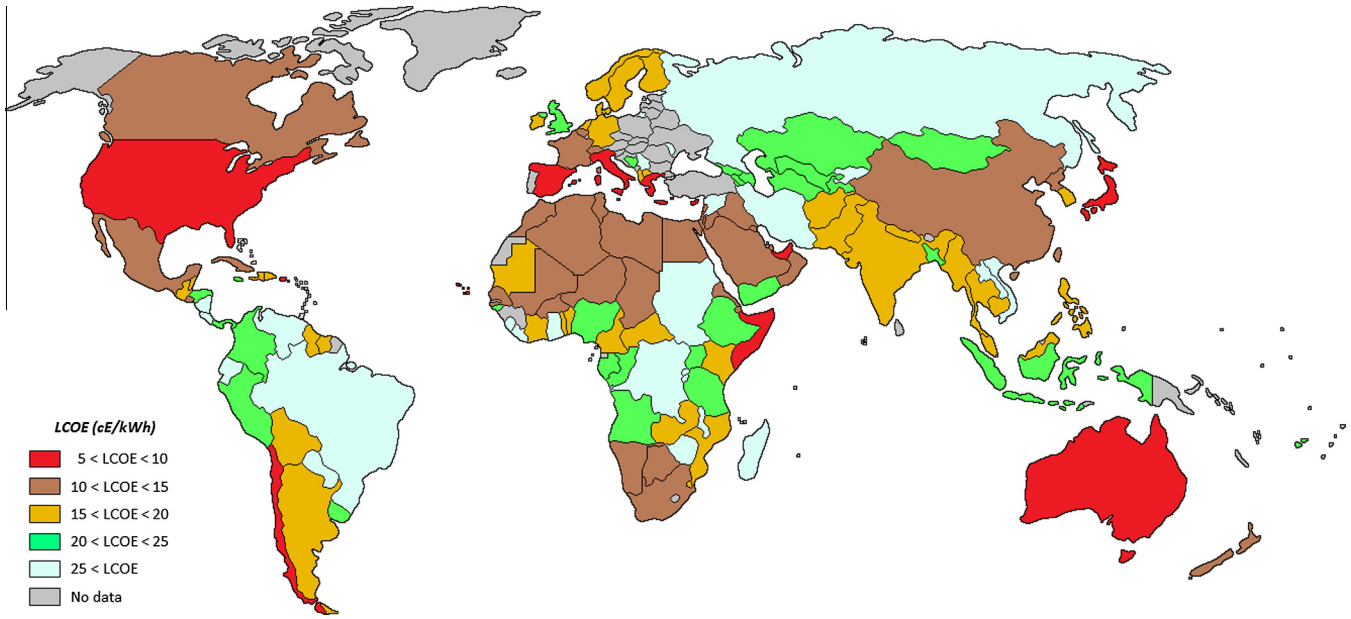

Fig. 3. Global map of LCOE for the year 2014.

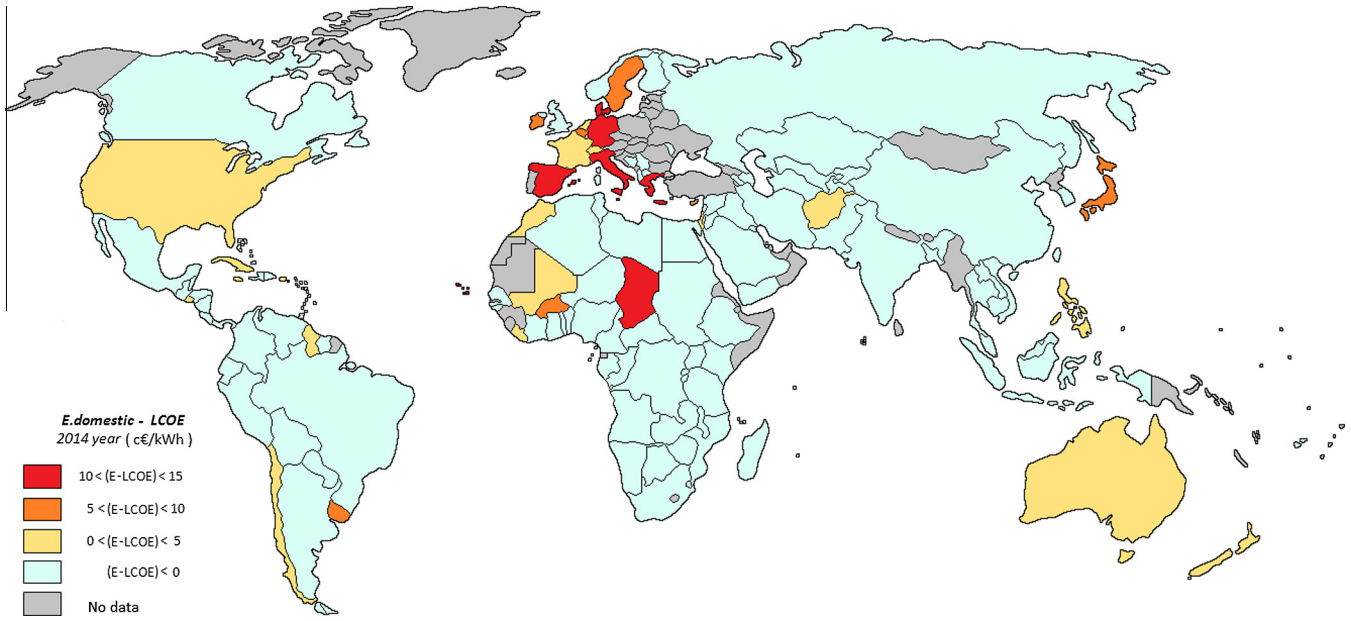

Fig. 4. Global map of difference between domestic electricity price and LCOE of the HCPV Systems.

Egypt and Sudan, or in South America, etc. The importance of the economic parameters is quite evident in the next two examples. On one hand, the study performed in countries like Algeria, South Africa and Mauritania, with relative high average values of DNI_A of 2490, 2493 and 2441 kW h/(m^2 year) respectively, provides values of LCOE of 13, 11 and 15 c€/kW h respectively. On the other hand, for some other countries like USA, Spain, Italy, Greece and Japan with average values of DNI_A, 1834, 1892, 1730, 1844 and 1325 kW h/(m^2 year) respectively, lesser than those of above countries, the values of LCOE obtained are 8, 7, 9, 7 and 10 c€/kW h respectively. Although the factors with more impact on the LCOE are the initial investment costs and the direct normal irradiation, others like the financing costs and the operation and maintenance costs, that exert a lower effect on the LCOE [24], are also important. From the cases studied above, it can be observed that the group of countries of Algeria, South Africa and Mauritania, with higher DNI_A than the group of USA, Spain, Italy, Greece and Japan, has higher values of LCOE. This is due to the fact that financing cost (cost of capital) is greater in the African countries than in USA, Euro Zone or Japan.

Although an average LCOE for each country is shown in the map of Fig. 3, for relative large countries like USA, Brazil, Australia and China, the analysis has been carried out considering two partitions of them by separating the most and the less sunny regions. In the case of Brazil, eastern Brazil (longitude > -50°) and western Brazil (longitude $\leqslant$ -50°) have been considered obtaining a LCOE value of 25 c€/kW h y 27 c€/kW h respectively. Similarly, we have for USA, eastern USA (longitude $\geqslant$ -97°) and western USA (longitude < -97°) with values of 9 c€/kW h and 7 c€/kW h respectively. For eastern Australia (longitude $\geqslant$ 135°) and western Australia

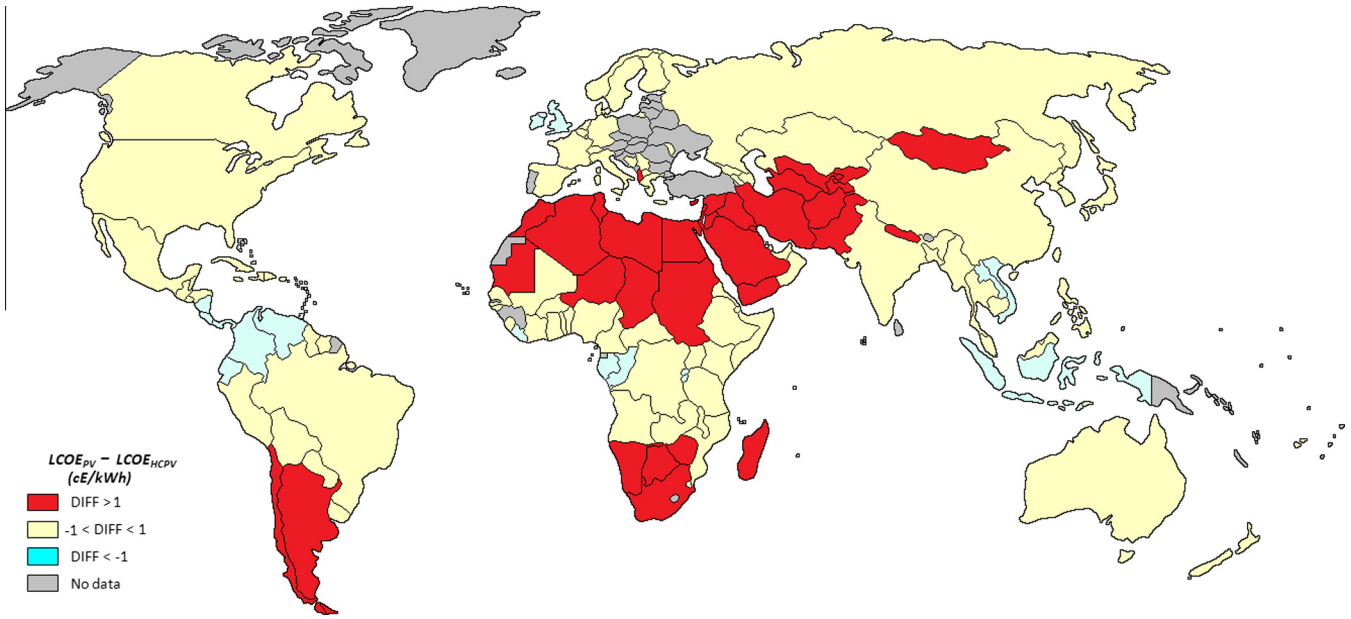

Fig. 5. Global map of difference between LCOE of conventional PV and HCPV systems in the prospective scenario (2 0 2 0).

(longitude < 135°), we have calculated LCOE of 9 c€/kW h y 8 c€/kW h respectively. Considering Chile, it is for northern Chile (latitude ⩾ -33°) and southern Chile (latitude < -33°) LCOE equal to 9 c€/kW h and 11 c€/kW h respectively. In the case of China, eastern China (longitude ⩾ 100°) and western China (longitude < 100°) correspond to LCOE of 15 c€/kW h y 11 c€/kW h respectively.

In other countries like Canada, the indicated value of LCOE in the map is only representative for locations with latitude lower than 60°, as well as for Norway and Sweden, the LCOE value corresponds only for locations above a latitude of 65°. For other countries like Syria, Iraq, and Sudan that are involved in different wars, or Venezuela and Zimbabwe, with political instability, some economic parameters like inflation and the financing cost are relatively very high. Therefore, for those countries, the values will not be representative for future stable periods.

3.1. Comparison between the LCOE of HCPV and domestic electricity price

In this section, an analysis of the grid parity for the HCPV technology in the domestic market segment is made. This analysis is done by comparing HCPV LCOE values with electricity price values in the domestic market segment. Below, some considerations assumed to fix electricity price values in the domestic market segment are explained.

Average electricity prices (€/kW h) in the domestic segment for some selected countries in 2014 with all taxes and levies included [64,65] are shown in Appendix A. There are significant variations in the electricity price depending on the quantity of the electricity consumption and even on the location within the same country. For instance, there are different ranges of annual domestic electricity consume for the countries in the European Union: (a) band DA, consumption < 1000 kW h; (b) band DB, 1000 kW h < consumption < 2500 kW h; (c) band DC, 2500 kW h < consumption < 5000 kW h; (d) band DD, 5000 kW h < consumption <15,000 kW h; (e) band DE, consumption >15,000 kW h [65]. In the case of Africa, each electricity supplier company has its own list of tariffs even those that operate in similar socio-economic and political environments. Some companies apply the same tariff for all their clients while others set different tariffs depending on the annual consume. As an example, as described in a comparative study [66], there are three categories in the domestic segment of electricity consume in Africa: (a) social consumers, with a consumption of 100 kW h/month; (b) single phase domestic consumer, with a consumption of 200 kW h/month; and (c) three-phase domestic consumer, with a consumption of 600 kW h/month.

In order to simplify the analysis, domestic electricity prices (€/kW h) considered in this document are a representative average of an annual consumption between 2400 kW h and 7200 kW h for the whole country, even when there are different categories or types of tariff.

In the case of USA, the average electricity prices (€/kW h) in the domestic segments in 2014 do not include the taxation [67] because of the different tax rates among the states. For some countries, electricity price has not been found in the literature no in data bases available for the authors. Therefore, data of previous years have been taken. A correction to these data has been applied consisting of an annual increment rate equal to the mean value of the annual increment of the electricity price in the period 2009–2013, otherwise an annual increment rate equal to the mean value of the inflation rate for the country in the same period 2009–2013.

In Fig. 4, it can be observed that some countries have already achieved HCPV grid parity (in 2014), corresponding to the scenario considered whose values are shown in Table 1. Grid parity is already achieved in countries like Spain, Italy and Greece, due to the relative high electricity price and DNI and to the relative low financial costs. Grid parity is even achieved in countries with moderate DNI values like Germany, Belgium, Denmark, Ireland, Sweden or Japan since their relative high electricity prices and relative lower financial costs. In other countries like USA, with moderate electricity prices, relative low financial costs and relative high DNI values, grid parity is achieved. In Chile and Morocco, with moderate electricity prices, moderate financial costs and relative high values of DNI, grid parity is also achieved. Finally, in countries with relative low electricity prices, moderate financial costs and relative high DNI values, like Algeria, Libya, Saudi Arabia, Iraq, etc., grid parity is not achieved. Therefore, an appropriate parameters combination is needed in order to make HCPV systems competitive in the domestic market segment. The results show that most countries, that have achieved grid parity, are developed countries. For the light blue coloured countries in Fig. 4, the LCOE of the HCPV systems is higher than the domestic electricity price.

3.2. Comparison between the LCOE of HCPV and conventional PV

In order to improve the analysis of this paper, a LCOE estimation in a prospective scenario in the year 2020 of conventional PV and HCPV systems has been also carried out. The LCOE for both technologies has been estimated following the method described in Section 2, and is analogous to the procedure previously used for estimating the LCOE of HCPV systems in the year 2014. In this case, the energy yield of conventional PV systems has been calculated according to Eq. (7) and considering a fixed value of PR = 0.75, as also discussed in Section 2. As for the case of HCPV systems, NASA data with a resolution of 1° for latitude and 1° for longitude, were utilized for calculating the average $HOTP_A$ for each country. In this prospective scenario, a normalized-per-kWp initial investment cost of 900 €/kWp has been considered for both technologies. This value has been taken from the learning curves shown in Fig. 2 for HCPV systems, while it has been taken from the analysis conducted in [68] for PV systems. The rest of the techno-economic variables involved in the estimation of the LCOE of both technologies remain constant to the values previously considered in the estimation of the LCOE of HCPV systems in the year 2014 since this can be considered a short-term forecast analysis. Table 2 summarizes the main variables used for estimating the LCOE of both technologies in the year 2020.

Fig. 5 shows the difference between LCOE for conventional PV and for HCPV systems in the prospective scenario of the year 2020. From this map, the next analysis can be realised. First, the HCPV technology is more suitable than conventional PV technology in terms of LCOE for those countries in red colour. In those countries, the values of DNI_A range from 1853 and 2804 kW h/(m^2 year), that corresponds respectively to Mongolia and Niger. Moreover, the irradiation ($HOTP_A$) is those countries in red colour is between 1616 and 2461 kW h/(m^2 year), that corresponds respectively to Albania and Niger. LCOE for HCPV is of 12.8 c€/kW h in Mongolia and of 5.9 c€/kW h in Niger, whereas LCOE for conventional PV for these two same countries is respectively 14 c€/kW h and 7.2 c€/kW h. Second, a more detailed regional study in the countries in yellow colour is necessary, since it is probable to find regions in which the HCPV technology presents lower costs of producing and vice versa. For these countries, DNI_A is between 944 and 2538 kW h/(m^2 year), that corresponds respectively to Norway and Oman. Irradiation values ($HOTP_A$) for the countries in yellow colour is between 966 and 2300 kW h/(m^2 year), that also correspond respectively to Norway and Oman, whereas LCOE for conventional PV is of 10 c€/kW h in Norway and of 6.7 c€/kW h in Oman. Third, for the countries in blue colour, conventional PV technology is preferable to the HCPV one in terms of LCOE. In these countries, the irradiation values ($HOTP_A$) are between 977 and 1946 kW h/(m^2 year), that correspond respectively to Ireland and Venezuela. DNI_A values for the countries in blue colour range between 811 and 1782 kW h/(m^2 year), that also correspond respectively to Ireland and Venezuela. LCOE of HCPV systems, is of 10.3 c€/kW h in Ireland and of 24.1 c€/kW h in Venezuela, whereas LCOE for conventional PV is 8.7 c€/kW h in Ireland and of 22.5 c€/kW h in Venezuela.

Considering those results comparing LCOE for both HCPV and conventional PV, HCPV systems are more attractive investments than conventional PV for those countries where DNI_A is near or higher to $HOTP_A$, when maintaining constant all the other calculation parameters except for the operation and maintenance costs.

Table 2
Values of the factors assumed for the calculation of the LCOE on the prospective scenario (2 0 2 0) for HCPV and conventional PV Systems.

Factors	Case base values	Units
$Y_{f\ HCPV}$	According (Fig. 1)	kW h/(kWp year)
$Y_{f\ PV}$	According (Eq. (7))	kW h/(kWp year)
$[HCPV_I]_{kWp}$	900	€/kWp
$[PV_I]_{kWp}$	900	€/kWp
$[HCPV_{AOM}]_{kWp}$	2	%
$[PV_{AOM}]_{kWp}$	1.5	%
r_d	0.5	%/year
$r_{O\&M}$	Equal to i	%/year
T	According Appendix A	%
i	According Appendix A	%
d	According Appendix A	%
i_l	According Appendix A	%
N_l	20	years
d_{ec}	According Appendix A	%
N	30	years

4. Conclusions

The market of solar photovoltaic energy and, specifically, that of the HCPV systems, is continuously growing, mainly due to the economies of scale and to the effects of learning curves. This growing will result in the extension of the number of countries where HCPV technology will be competitive in relation with other sources of electricity generation.

One of the methods used for the study of PV or HCPV systems' economic viability is the levelised cost of electricity (LCOE), with the purpose of comparing those systems with other technologies of electricity generation. This is a vital issue from the point of view of industrial planning, given that it is a way to analyse the potential of this young technology. In the work here presented an analysis of the LCOE of HCPV systems has been carried out in 133 countries, together with the comparison between LCOE and domestic electricity price in those countries. Besides, the LCOE of HCPV systems has been compared with the LCOE of conventional photovoltaic systems, for a mid-term scenario at 2020. The results obtained are shown in a set of innovative maps. These maps are easy to handle and can be consulted by future owners, investors and financial entities involved in HCPV systems.

Future owners and potential investors in HCPV systems demand information relating to the economic feasibility of their investment. That is why one of the objectives of this document is to provide information about the LCOE in HCPV systems. Besides, government organizations of each one of the countries that have been studied here, which participate either in the design or the selection of support mechanisms for HCPV, can be guided by the results obtained in this work.

On the other hand, LCOE values obtained in countries like USA, Spain, Greece, Australia and Japan, which were lower than LCOE values obtained in countries with higher DNI_A values, make evident the relevant effect that parameters like loan interest rate, dividends (return on equity) and inflation produce. Results suggest that, from a worldwide economic perspective, current growth pattern will continue, in large part concentrated in countries with low financing cost for HCPV projects and low inflation rates, instead of those ones with high DNI values and high project financing cost. Therefore, it would be an advantageous achievement for renewable energies and particularly for HCPV technology to reduce the financing cost of this type of projects in developing countries.

Regarding HCPV technology parity in relation with the domestic market segment, already at 2014 there are some countries were LCOE in HCPV plants is cheaper than the kW h price that domestic consumer pays to the electricity supplier. Besides, the upward trend in the price of domestic electricity will increase the number of countries where parity will be achieved.

According to the results obtained and represented in maps of Figs. 3 and 4, red colour countries are today's [1]most favourable ones

[1] For interpretation of color in Figs. 3 and 4, the reader is referred to the web version of this article.

for investments in HCPV systems. Likewise if we have to decide between investing in HCPV technology or in conventional PV in a mid-term prospective scenario, red colour countries depicted in the map of Fig. 5 will be the most favourable ones for receiving investments in HCPV technology.

It is also remarkable that in a future year 2020 scenario, in 92 countries out of the analysed 133 the cost of electric generation represented by LCOE (c€/kW h) in HCPV technology plants will be lower than that of conventional PV technology electric generation plants, provided that the predicted parameter values of the 2020 scenario finally occur.

Appendix A

Input data and results (see Tables A1 and A2).

Table A1
Input data.

Country	Average Lending interest rate (i_l) 2009–2013[a] (%)	Average Inflation (i) 2009–2013[b] (%)	Nominal Dividends (d_{ec}) (return on equity)[c] (%)	WACC (%)	Tax[d] (%)	Electricity price for domestic segment 2014 (c€/kW h)[f]
Afghanistan	15.2	3.5	18.5	15.6	20.0	16.6
Albania	11.7	2.7	16.0	13.3	15.0	11.6
Algeria	8.0	5.3	18.8	13.4	19.0	2.4
Angola	17.9	12.1	26.7	19.5	35.0	4.5
Argentina	14.3	9.5	25.4	17.9	35.0	5.0
Armenia	17.8	5.5	18.7	16.6	20.0	6.8
Australia	6.8	2.5	11.8	7.6	30.0	12.1
Azerbaijan	19.3	4.3	16.0	15.7	20.0	2.4
Bangladesh	13.4	7.6	21.4	16.1	27.5	10.7
Belgium	3.9	1.9	7.1	4.6	34.0	22.4
Belize	13.1	0.5	15.1	12.8	25.0	15.6
Benin	16.8	3.0	16.7	14.4	30.0	13.6
Bolivia	11.1	5.2	19.7	14.6	25.0	7.8
Bosnia and Herzegovina	7.4	1.5	15.5	11.8	10.0	8.1
Botswana	11.5	7.4	19.0	14.5	22.0	7.0
Brazil	38.5	5.6	18.1	21.7	34.0	19.0
Burkina Faso	16.8	1.8	15.8	14.0	30.0	20.3
Burundi	13.8	10.6	26.7	18.7	30.0	3.5
Cambodia	13.0	2.9	17.1	14.1	20.0	17.3
Cameroon	15.2	2.4	15.7	12.9	38.5	10.3
Canada	2.8	1.5	8.9	5.1	26.0	8.4
Central African Rep.	15.2	2.7	17.6	14.4	30.0	0.0
Chad	15.2	3.7	18.0	14.0	40.0	21.7
Chile	8.1	2.0	12.5	10.0	20.0	14.0
China	5.9	2.7	13.4	9.8	25.0	11.9
Colombia	11.4	3.0	15.4	12.4	25.0	10.3
Congo. Dem. Rep.	42.7	7.3	22.9	27.4	25.0	3.7
Congo. Rep.	15.2	4.3	17.9	14.4	33.0	6.1
Costa Rica	17.3	5.6	18.3	15.4	30.0	12.6
Cote d'Ivoire	16.8	2.3	15.9	14.4	25.0	16.4
Cuba	18.0	0.0	15.5	14.2	30.0	18.0
Cyprus	6.7	1.6	12.1	9.6	12.5	18.5
Denmark	7.1	1.9	8.9	6.8	24.5	30.2
Djibouti	11.0	3.6	17.0	13.2	25.0	–
Dominican Republic	15.0	5.0	19.4	15.5	28.0	17.8
Ecuador	12.4	4.2	21.9	16.3	22.0	8.9
Egypt	11.7	9.9	23.1	16.6	25.0	2.2
El Salvador	14.0	1.9	14.1	12.2	30.0	15.8
Eritrea	14.2	0.0	14.5	12.5	30.0	–
Ethiopia	7.5	16.1	33.0	20.3	30.0	5.1
Fiji	7.2	4.8	18.5	13.0	20.0	16.8
Finland	2.4	1.8	11.2	6.0	20.0	16.1
France	3.7	1.3	7.1	4.6	33.3	15.9
Gabon	15.2	1.6	13.5	12.0	35.0	14.7
Georgia	15.4	3.2	16.5	15.0	15.0	–
Germany	4.3	1.4	9.6	5.9	29.6	30.1
Ghana	25.6	11.9	26.8	23.1	25.0	7.3
Greece	6.2	2.0	2.0	2.8	26.0	17.4
Guatemala	13.5	4.0	17.0	13.8	28.0	15.5
Guinea Bassau	19.4	1.7	16.4	14.7	35.0	7.7
Guyana	14.2	2.9	11.0	12.6	35.0	22.1
Haiti	12.8	5.2	18.9	14.4	30.0	17.4
Honduras	19.1	5.5	20.0	16.9	30.0	12.7
India	10.3	10.4	23.4	16.0	34.0	9.9
Indonesia	12.7	5.2	18.3	14.4	25.0	6.6
Iran. Islamic Rep.	11.4	22.2	37.9	24.1	25.0	5.3
Iraq	13.7	4.7	14.7	13.3	15.0	1.6
Ireland	2.6	−0.1	6.3	4.1	12.5	24.3
Israel	5.6	2.5	13.3	9.6	26.5	13.3
Italy	4.8	1.9	8.1	5.4	31.4	23.5
Jamaica	18.3	9.2	26.1	22.2	25.0	24.6
Japan	1.5	-0.4	8.1	4.3	33.1	18.6
Jordan	9.0	3.8	16.8	12.8	14.0	11.5

(continued on next page)

Table A1 (*continued*)

Country	Average Lending interest rate (i_l) 2009–2013[a] (%)	Average Inflation (i) 2009–2013[b] (%)	Nominal Dividends (d_{ec}) (return on equity)[c] (%)	WACC (%)	Tax[d] (%)	Electricity price for domestic segment 2014 (c€/kW h)[f]
Kazakhstan	11.2	6.7	19.0	14.5	20.0	4.5
Kenya	16.3	8.5	22.9	17.5	30.0	13.0
Korea. Dem. Rep.	6.1	0.0	9.5	7.6	25.0	–
Korea. Rep.	5.4	2.6	13.7	9.9	24.0	11.1
Kuwait	5.2	3.7	14.1	10.2	15.0	2.1
Kyrgyz Republic	24.8	8.1	22.5	22.4	10.0	2.0
Lao. PDR	26.0	4.8	18.8	19.3	24.0	4.4
Lebanon	8.0	1.0	14.2	11.1	15.0	5.8
Liberia	13.8	7.5	23.1	17.2	25.0	29.6
Libya	6.0	5.9	17.0	11.9	20.0	1.6
Macedonia. FYR	9.0	2.2	15.3	12.2	10.0	11.7
Madagascar	53.3	8.0	22.9	32.7	20.0	20.1
Malawi	30.4	14.4	31.0	26.2	30.0	3.8
Malaysia	4.9	1.9	13.0	9.3	25.0	10.9
Mali	16.8	2.3	16.4	14.3	30.0	16.9
Mauritania	17.5	4.6	19.1	16.3	25.0	–
Mexico	5.3	4.2	15.8	10.9	30.0	10.0
Moldova	15.4	4.8	14.8	14.2	12.0	4.5
Mongolia	19.0	10.0	23.2	19.0	25.0	–
Morocco	11.5	1.2	13.4	11.1	30.0	10.9
Mozambique	16.6	6.7	22.1	17.1	32.0	5.8
Myanmar	15.3	4.2	14.1	12.9	25.0	–
Namibia	9.3	6.1	19.8	13.8	33.0	11.1
Nepal	8.0	9.6	25.5	17.0	20.0	–
Netherlands	1.9	2.0	9.2	5.0	25.0	19.2
New Zealand	6.1	2.2	10.0	6.7	28.0	17.2
Nicaragua	13.0	6.3	22.8	16.5	30.0	20.3
Niger	16.8	1.4	16.1	14.3	30.0	9.6
Nigeria	17.1	11.4	25.8	19.3	30.0	3.0
Norway	5.7	1.7	9.1	6.2	27.0	18.9
Oman	6.3	3.1	13.9	10.5	12.0	–
Pakistan	13.7	11.4	27.5	18.9	34.0	6.9
Panama	7.3	4.3	16.8	12.0	25.0	16.7
Paraguay	21.6	4.4	19.5	19.5	10.0	6.5
Peru	19.2	2.9	15.0	14.3	30.0	7.2
Philippines	6.9	3.8	17.0	11.9	30.0	17.4
Puerto Rico	5.1	0.0	8.3	6.4	39.0	11.2
Qatar	6.1	−0.1	10.0	8.2	10.0	–
Russian Federation	10.6	7.8	20.1	12.6	20.0	4.3
Rwanda	16.3	5.8	20.4	16.2	30.0	12.7
Saudi Arabia	6.9	4.5	15.3	11.2	20.0	4.2
Senegal	16.8	1.1	14.6	13.3	30.0	15.7
Serbia	16.3	8.1	20.8	17.6	15.0	6.1
Sierra Leone	21.2	13.0	29.4	22.4	30.0	–
Somalia	14.2	0.0	9.5	9.4	35.0	–
South Africa	9.6	5.6	17.1	12.6	28.0	9.0
Spain	4.3	1.7	7.6	5.1	30.0	23.4
Sudan	11.9	24.1	40.2	24.8	35.0	9.9
Suriname	11.7	6.3	20.1	14.5	36.0	19.2
Swaziland	9.5	6.5	20.3	14.3	27.5	8.8
Sweden	3.3	0.9	9.7	5.7	22.0	21.3
Switzerland	2.7	-0.1	6.0	4.0	17.9	16.5
Syrian Arab Republic	9.7	27.2	43.6	26.5	22.0	1.5
Tajikistan	24.1	7.2	22.0	20.1	25.0	0.8
Tanzania	15.2	11.0	26.3	18.9	30.0	6.3
Thailand	6.6	2.3	13.7	10.3	20.0	7.7
Togo	17.5	2.6	16.8	14.8	29.0	13.6
Tunisia	4.8	4.6	16.7	11.3	25.0	8.7
Turkmenistan	27.2	0.0	13.8	17.6	20.0	2.9
Uganda	22.5	11.0	26.4	21.2	30.0	22.2
United Arab Emirates	8.1	1.0	11.2	8.2	55.0	–
United Kingdom	0.5	3.1	10.5	5.1	21.0	18.3
United States	3.3	1.6	10.0	5.5	40.0	9.5
Uruguay	11.8	7.7	21.5	15.8	25.0	26.9
Uzbekistan	27.2	0.0	13.3	19.0	8.0	1.7
Venezuela. RB	17.5	28.6	46.4	29.4	34.0	4.5
Vietnam	12.8	10.1	24.1	13.1	22.0	6.8
Yemen. Rep.	22.7	13.5	28.6	23.5	20.0	4.3
Zambia	16.7	8.4	22.8	17.2	35.0	4.4
Zimbabwe	496.5	2.7	16.4	199.0	25.7	7.5

Sources
[a] [69].
[b] [70].
[c] [71,58].
[d] [72–74].
[f] [25,75,67,76,64,65,77–79].

Table A2
Analysis results.

Country	LCOE of the HCPV systems 2014 (c€/kW h)	Difference between domestic electricity price and LCOE of HCPV systems for 2014 (c€/kW h)	Difference between LCOE of PV and HCPV systems for 2020 (c€/kW h)
Afganistan	15.6	0.9	1.7
Albania	19.0	−7.4	1.2
Algeria	13.4	−10.9	1.4
Angola	21.5	−17.0	0.6
Argentina	20.0	−15.0	1.5
Armenia	23.9	−17.1	0.9
Australia	8.2	3.9	0.7
Azerbaijan	22.8	−20.4	1.0
Bangladesh	21.6	10.9	0.1
Belgium	14.2	8.2	−0.6
Belize	18.1	−2.5	−0.6
Benin	16.1	−2.5	0.5
Bolivia	19.0	−11.2	−0.1
Bosnia-Herzegovina	20.7	−12.6	0.7
Botswana	14.3	−7.3	1.2
Brasil	25.8	−6.8	0.1
Burkina Faso	13.9	6.4	0.6
Burundi	27.5	−23.9	−1.2
Cambodia	18.4	−1.1	−0.2
Cameroon	15.1	−4.8	−0.0
Canada	12.6	−4.3	−0.1
Central African Rep.	15.6	0.0	0.4
Chad	11.4	10.3	1.1
Chile	9.5	4.4	1.2
China	13.1	−1.2	0.6
Colombia	20.9	−10.6	−1.5
Congo Dem. Rep.	36.4	−32.7	−0.9
Congo Rep.	22.7	−16.6	−1.5
Costa Rica	27.5	−14.9	−2.5
Cote d'Ivoire	18.6	−2.3	−0.3
Cuba	14.4	3.6	0.8
Cyprus	9.9	8.6	1.2
Denmark	16.7	13.5	0.2
Djibouti	12.8	–	0.8
Dominican Rep.	18.2	−0.3	0.3
Ecuador	34.2	−25.3	−4.1
Egypt	15.0	−12.8	1.9
El Salvador	15.0	0.8	0.0
Eritrea	11.9	–	0.7
Ethiopia	22.9	−17.8	0.7
Fiji	20.3	−3.5	−0.9
Finland	16.3	−0.3	0.8
France	11.0	4.9	0.0
Gabon	21.2	−6.4	−2.1
Georgia	22.9	–	0.8
Germany	17.3	12.8	−0.9
Ghana	30.8	−23.5	−0.6
Greece	7.2	10.2	0.3
Guatemala	18.3	−2.8	−0.4
Guinea Bissau	24.7	−17.0	0.4
Guyana	18.2	3.9	−0.7
Haiti	15.9	1.4	0.5
Honduras	22.6	−10.0	−0.6
India	19.4	−9.5	0.5
Indonesia	22.3	−15.7	−1.2
Iran	30.0	−24.8	2.1
Iraq	14.9	−13.3	1.5
Ireland	19.3	5.0	−1.5
Israel	10.4	2.9	1.0
Italy	9.2	14.4	0.5
Jamaica	20.9	3.6	1.0
Japan	9.9	8.7	−0.3
Jordan	13.5	−2.0	1.5
Kazakhstan	22.7	−18.2	0.9
Kenya	19.6	−6.5	0.4
Korea Dem. Rep.	10.9	–	0.4
Korea Rep.	15.2	−4.1	0.2
Kuwait	11.7	−9.6	1.1
Kyrgyz Republic	26.9	−24.9	2.3
Lao PRD	29.0	−24.9	−1.2
Lebanon	13.0	−7.2	1.2
Liberia	26.3	3.2	−1.4

(*continued on next page*)

Table A2 (*continued*)

Country	LCOE of the HCPV systems 2014 (c€/kW h)	Difference between domestic electricity price and LCOE of HCPV systems for 2014 (c€/kW h)	Difference between LCOE of PV and HCPV systems for 2020 (c€/kW h)
Libya	11.5	−9.9	1.4
Macedonia FYR	19.9	−8.3	0.8
Madagascar	33.8	−13.7	1.7
Malawi	30.9	−27.1	0.3
Malaysia	15.1	−4.2	−0.8
Mali	13.0	3.9	1.0
Mauritania	15.3	–	1.2
Mexico	11.7	−1.7	0.7
Moldova	28.8	−24.3	−0.3
Mongolia	24.3	–	1.2
Morocco	10.8	0.2	1.1
Mozambique	19.4	−13.6	0.4
Myanmar	17.9	–	−0.1
Namibia	12.0	−0.9	1.2
Nepal	17.9	–	1.1
Netherlands	16.0	3.2	−0.6
New Zealand	13.0	4.2	0.0
Nicaragua	25.1	−4.8	−1.3
Niger	11.2	−1.5	1.3
Nigeria	22.0	−19.0	0.4
Norway	18.8	0.1	0.1
Oman	11.0	–	0.9
Pakistan	19.5	−12.6	1.5
Panama	20.3	−3.6	−1.4
Paraguay	25.6	−19.1	0.3
Peru	20.4	−13.2	−0.8
Philippines	16.8	0.6	−0.6
Puerto Rico	7.0	3.2	0.3
Qatar	10.7	–	0.7
Russian Federation	26.8	−22.5	0.5
Rwanda	24.6	−11.9	−1.4
Saudi Arabia	11.2	−7.0	1.1
Senegal	13.6	2.0	0.5
Serbia	29.5	−23.5	1.0
Sierra Leone	29.2	–	−0.5
Somalia	9.6	–	0.4
South Africa	12.2	−3.2	1.2
Spain	8.2	15.2	0.5
Sudan	25.8	−15.9	1.7
Suriname	19.4	−0.2	−0.6
Swaziland	17.9	−9.1	0.5
Sweden	15.9	5.5	0.5
Switzerland	11.8	4.7	−0.3
Syrian Arab Rep.	37.0	−35.5	2.8
Tajikistan	22.3	−21.5	2.0
Tanzania	22.3	−16.0	0.2
Thailand	15.2	−7.5	−0.4
Togo	17.3	−3.8	0.1
Tunisia	13.0	−4.3	1.2
Turkmenistan	20.1	−17.2	1.8
Uganda	24.2	−2.0	0.3
United Arab Emirates	6.7	–	0.7
United Kingdom	20.2	−2.0	−1.4
USA	8.0	1.5	0.4
Uruguay	20.6	6.3	0.8
Uzbekistan	22.4	−20.7	2.3
Venezuela	45.6	−41.1	−1.6
Vietnam	62.4	−55.6	−2.2
Yemen Rep.	21.2	−16.9	1.8
Zambia	17.2	−12.8	0.8
Zimbabwe	181.4	−173.9	13.4

References

[1] European Photovoltaic Industry Association (EPIA). Global Market Outlook for Photovoltaics 2014–2018 June 2014;Available at: <http://www.epia.org/fileadmin/user_upload/Publications/EPIA_Global_Market_Outlook_for_Photovoltaics_2014-2018_-_Medium_Res.pdf> [accessed December 2014].

[2] International Energy Agency (IEA). Trens 2014 in Photovoltaic Application: Survey Report of Selected IEA Countries between 1992 and 2013. 2014;Report IEA-PVPS T1-25; 2014.

[3] Danchev S, Maniatis G, Tsakanikas A. Returns on investment in electricity producing photovoltaic systems under de-escalating feed-in tariffs: the case of Greece. Renew Sustain Energy Rev 2010;14:500–5.

[4] Spertino F, Di Leo P, Cocina V. Economic analysis of investment in the rooftop photovoltaic systems: a long-term research in the two main markets. Renew Sustain Energy Rev 2013;28:531–40.

[5] Talavera DL, Muñoz-Cerón E, De La Casa J, Ortega MJ, Almonacid G. Energy and economic analysis for large-scale integration of small photovoltaic systems in buildings: the case of a public location in Southern Spain. Renew Sustain Energy Rev 2011;15:4310–9.

[6] Talavera DL, de la Casa J, Muñoz-Cerón E, Almonacid G. Grid parity and self-consumption with photovoltaic systems under the present regulatory framework in Spain: the case of the University of Jaén Campus. Renew Sustain Energy Rev 2014;33:752–71.
[7] Drury E, Denholm P, Margolis R. The impact of different economic performance metrics on the perceived value of solar photovoltaics. October 2011; Technical Report NREL/TP-6A20-52197.
[8] Short W, Packey DJ, Holt T. A manual for the economic evaluation of energy efficiency and renewable energy technologies 1995; NREL/TP–462-5173, National Renewable Energy Laboratory, pp. 1–120.
[9] Branker K, Pathak MJM, Pearce JM. A review of solar photovoltaic levelized cost of electricity. Renew Sustain Energy Rev 2011;15:4470–82.
[10] Fraunhofer Institute for Solar Energy Systems ISE. Levelized cost of electricity renewable energy technologies; November 2013.
[11] Fraisopi F. The CPV Market: An Industry Perspective. GTM Research June 2013; Intersolar München.
[12] Gökçek M, Genç MS. Evaluation of electricity generation and energy cost of wind energy conversion systems (WECSs) in Central Turkey. Appl Energy 2009;86:2731–9.
[13] Desideri U, Campana PE. Analysis and comparison between a concentrating solar and a photovoltaic power plant. Appl Energy 2014;113:422–33.
[14] Hernández-Moro J, Martínez-Duart JM. Analytical model for solar PV and CSP electricity costs: present LCOE values and their future evolution. Renew Sustain Energy Rev 2013;20:119–32.
[15] Díaz G, Gómez-Aleixandre J, Coto J. Dynamic evaluation of the levelized cost of wind power generation. Energy Convers Manage 2015;101:721–9.
[16] Rezaei Mirghaed M, Roshandel R. Site specific optimization of wind turbines energy cost: iterative approach. Energy Convers Manage 2013;73:167–75.
[17] European Photovoltaic Industry Association. Solar Photovoltaics Competing in the Energy Sector: On the road to competitiveness; 2011, Available at: <http://helapco.gr/pdf/tn_jsp.pdf> [accessed December 2015].
[18] Swift KD. A comparison of the cost and financial returns for solar photovoltaic systems installed by businesses in different locations across the United States. Renew Energy 2013;57:137–43.
[19] CREARA ENERGY EXPERTS. PV Grid Parity Monitor Residential Sector, 3nd issue February; 2015. p. 52–72.
[20] Adaramola MS. Techno-economic analysis of a 2.1 kW rooftop photovoltaic-grid-tied system based on actual performance. Energy Convers Manage 2015;101:85–93.
[21] Pedro Pérez-Higueras, Eduardo F. Fernández. High Concentrator Photovoltaic Fundamentals, Engineering and Power Plants 2015. Springer International Publishing: 477-ISBN: 978-3-319-15038-3 (Print) 978-3-319-15039-0 (Online).
[22] Fraunhofer ISE, National Renewable Energy Laboratory (NREL). Current status of concentrator photovoltaic (CPV) technology; September 2015, Version 1.1, TP-6A20-63916.
[23] Nishikawa W et al. LCOE concentrating photovoltaic for CPV. ICSC5 Conference; 2008.
[24] Talavera DL, Pérez-Higueras P, Ruíz-Arias JA, Fernández EF. Levelised cost of electricity in high concentrated photovoltaic grid connected systems: spatial analysis of Spain. Appl Energy 2015;151:49–59.
[25] Breyer C, Gerlach A. Global overview on grid-parity. Prog Photovolt Res Appl 2013;21:121–36.
[26] Rus-Casas C, Aguilar JD, Rodrigo P, Almonacid F, Pérez-Higueras PJ. Classification of methods for annual energy harvesting calculations of photovoltaic generators. Energy Convers Manage 2014;78:527–36.
[27] Leloux J, Lorenzo E, García-Domingo B, Aguilera J, Gueymard CA. A bankable method of assessing the performance of a CPV plant. Appl Energy 2014;118:1–11.
[28] International Electrotechnical Commission (IEC). IEC 61724: Photovoltaic system performance monitoring – Guidelines for measurement, data exchange and analysis; 1998, First edition 1998-04.
[29] Ruiz-Arias JA, Terrados J, Pérez-Higueras P, Pozo-Vázquez D, Almonacid G. Assessment of the renewable energies potential for intensive electricity production in the province of Jaén, southern Spain. Renew Sustain Energy Rev 2012;16:2994–3001.
[30] Drif M, Pérez PJ, Aguilera J, Almonacid G, Gomez P, de la Casa J, et al. Univer Project. A grid connected photovoltaic system of at Jaén University. Overview and performance analysis. Solar Energy Mater Solar Cells 2007;91:670–83.
[31] Mondol JD, Yohanis YG, Smyth M, Norton B. Performance analysis of a frid-connected building integrated photovoltaic system; 2003, ISES Solar World Congress 2003. Göteborg. Sweden.
[32] Šúri M, Huld TA, Dunlop ED, Ossenbrink HA. Potential of solar electricity generation in the European Union member states and candidate countries. Sol Energy 2007;81:1295–305.
[33] Ransome SJ, Wohlgemuth JH, Solar BP. KW h/kWp dependency on PV technology and balance of systems performance. Conf Rec IEEE Photovoltaic Spec Conf 2002:1420–3.
[34] King C. Site data analysis of CPV plants. Photovoltaic Specialists Conference (PVSC), 35th IEEE 2010:3043–7.
[35] Stone Kea. Analysis of five years of field performance of the Amonix High Concentration PV system. In: Proceedings of the Power-Gen Renewable Conference; 2006.
[36] Kinsey GS, Stone K, Brown J, Garboushian V. Energy prediction of Amonix CPV solar power plants. Prog Photovolt Res Appl 2011;19:794–6.
[37] Husna Hea. Impact Of Spectral Irradiance Distribution And Temperature On The Outdoor Performance Of Concentrator Photovoltaic System. AIP Conf Proc 1556; 2013. http://dx.doi.org/10.1063/1.4822243:252-255.
[38] Lecoufle D, Kuhn F. A Place for PV, tracked-PV and CPV. In: 2nd International Workshop on Concentrating Photovoltaic Power Plants, Germany; 2009.
[39] Nishikawa W, Horne S. Key advantages of concentrating photovoltaics (CPV) for lowering levelized cost of electricity (LCOE). In: Proceedings of the 23rd European PV Solar Energy Conference Valencia; 2008. p. 3765–3767.
[40] Verlinden P, Lasich J. Energy rating of Concentrator PV systems using multi-junction III–V solar cells. In: Photovoltaic Specialists Conference, 33rd IEEE; 2008.
[41] Gómez-Gil FJ, Wang X, Barnett A. Energy production of photovoltaic systems: fixed, tracking, and concentrating. Renew Sustain Energy Rev 2012;16:306–13.
[42] Consortium C. Concentrator Photovoltaic (CPV) Workshop. Understanding the Technology and Related Implications for Scaled Deployment. 2011. Dallas: Solar Power International.
[43] King B, Riley D, Hansen C, Erdman M, Gabriel J, Ghosal K. HCPV characterization: analysis of fielded system data. AIP Conf Proc 2014;1616:276–9.
[44] Magpower. Performance in Practice CPV versus PV, 1.5 Year of Operation. In: 3rd Concentrated Photovoltaic Summit USA; 2011.
[45] NASA. Surface meteorology and Solar Energy November 26; 2014, Available at: <https://eosweb.larc.nasa.gov/sse/> [accessed July 2015].
[46] Mints P. The Current Status of CPV 2013; 2013, PV-insider. UK.
[47] IHS. Press Release - Concentrated Photovoltaic (CPV) report -2013. IHS online Press Room Tuesday; December 10, 2013.
[48] Soitec Solar GmbH. Solar Energy – Soitec CPV installations, company brochure distributed at Intl. Conf. Conc. Photovolt, April 7–9; 2014.
[49] Suncore Photovoltaics. In: Company brochure distributed at Intl. Conf. Conc. Photovolt. April 7–9; 2014.
[50] Extance A, Márquez C. The Concentrated Photovoltaics Industry Report; CPV today 2010.
[51] Globaldata. Concentrated Photovoltaics (CPV) – Global Market Size, Competitive Landscape and Key Country Analysis to 2020. 2014; UK.
[52] Haysom JE, Jafarieh O, Anis H, Hinzer K, Wright D. Learning curve analysis of concentrated photovoltaic systems. Prog Photovoltaics Res Appl 2015;23:1678–86.
[53] Prior B. Cost and LCOE by Generation Technology, 2009–2020. GTM Research; November 2011.
[54] Yole Développement. High concentration photovoltaics business and technology update report; April 2013, Available at: <http://www.i-micronews.com/component/hikashop/product/high-concentration-photovoltaics-business-and-technology-update-report.html> [accessed 2015].
[55] European Central Bank. Inflaction in the Euro area; 2014, Available at: <http://www.ecb.europa.eu/stats/prices/hicp/html/inflation.en.html> [accessed July 2014].
[56] Global rates.com. Inflation - summary of current international inflation figures; 2013, <http://www.global-rates.com/economic-indicators/inflation/inflation.aspx> [accessed 2013].
[57] UNEP/BNEF. Private financing of renewable energyd: A guide for policymakers. Sustainable Energy Finance Initiative (UNEP), Bloomberg New Energy Finance (BNEF), Chatham House London; 2009, Available at: <http://fs-unep-centre.org/sites/default/files/media/financeguide20final.pdf> [accessed January 2015].
[58] CDM Executive Board. Guidelines on the assessment of investment analysis:. Bonn: UNFCCC Secretariat; 2011, Available at: <https://cdm.unfccc.int/Reference/Guidclarif/reg/reg_guid03.pdf> [accessed January 2015].
[59] Thonson Reuters. Consulta A.E.A.T. 128308,. IS. Central fotovoltaica. Amortización; 2014 <http://portaljuridico.lexnova.es/doctrinaadministrativa/JURIDICO/77405/consulta-aeat-128308-is-central-fotovoltaica-amortizacion>.
[60] Ministry Economic Spain. Royal Decree 1777/2004; 2004, BOE number 189: 28377–28429.
[61] Jordan DC, Kurtz SR. Photovoltaic degradation rates – an analytical review. Prog Photovolt Res Appl 2013;21:12–29.
[62] Drury E, Lopez A, Denholm P, Margolis R. Relative performance of tracking versus fixed tilt photovoltaic systems in the USA. Prog Photovolt Res Appl 2013.
[63] NREL. Energy Technology Cost and Performance Data for Distributed Generation 2013 (August); 2014, <http://www.nrel.gov/analysis/tech_lcoe_re_cost_est.html>.
[64] WIP – Renewable Energies (WIP). PV parity project. Electricity prices scenarios until at least the year 2020 in selected EU countries. Deliverable 2.2; January 2012, (IEE/10/307/SI2.592205).
[65] Eurostat. Electricity prices for domestic consumers, from 2007 onwards - bi-annual data; 2014, Available at: <http://ec.europa.eu/eurostat/> [accessed January 2015].
[66] UPDEA General Secretariat. Comparative study of electricity tariffs used in Africa; December 2009, Available at: <http://www.updea-africa.org/updea/DocWord/TarifAng2010.pdf> [accessed February 2015].
[67] U.S. Energy Information Administration. Short-Term Energy Outlook. Table 2. U.S. Energy Price; 2014 <http://www.eia.gov/forecasts/steo/tables/?tableNumber=8#startcode=2005> [accessed September 2014].
[68] Fraunhofer ISE. Current and Future Cost of Photovoltaics. Long-term Scenarios for Market Development, System Prices and LCOE of Utility-Scale PV Systems; February 2015, 059/01-S-2015/EN. Study on behalf of Agora Energiewende.

[69] World Bank. Lending interest rate; 2015. Available at: <http://data. worldbank.org/indicator/FR.INR.LEND> [accessed January 2015].
[70] Trading Economics. Inflation Rate -Countries- List; 2015, Available at: <http://www.tradingeconomics.com/country-list/inflation-rate> [accessed January 2015].
[71] Dimson E, Marsh P, Staunton M. Equity Premiums around the World. Research Foundation Publications; 2011: 32–35. Available at: <http://www.cfapubs.org/doi/pdf/10.2470/rf.v2011.n4.5> [accessed January 2015].
[72] Banco Santander. Portal Santander Trade; 2015, Available at: <https://es.santandertrade.com/establecerse-extranjero/espana/fiscalidad> [accessed January 2015].
[73] World Bank Group. Doing Business: Paying Taxes 2014; 2015, Available at: <http://www.doingbusiness.org/data/exploreeconomies/spain/#paying-taxes> [accessed January 2015].
[74] Ernst & Young Global Limited. Worldwide Corporate Tax Guide 2014; 2014; EYG no. DL0917, Available at: <http://www.ey.com/Publication/vwLUAssets/Worldwide_corporate_tax_guide_2014/$FILE/Worldwide%20Corporate%20Tax%20Guide%202014.pdf> [accessed January 2015].
[75] Southern African Power Pool (SAPP). Competitive Electricity Market for Sustainable Regional Development. SAPP Annual Report; 2014, Available at: <http://www.sapp.co.zw/docs/Annual%20report-2014.pdf> [accessed January 2015].
[76] European Commission e. Energy price statistics; 2014, <http://epp.eurostat.ec.europa.eu/statistics_explained/index.php/Energy_price_statistics#Electricity_prices_for_household_consumers> [accessed september 2014].
[77] Organización Latinoamericana de Energía (OLADE). Tarifas Eléctricas en America Latina y Caribe:análisis conceptual y comparativo; 2015, Available at: <http://es.slideshare.net/JoeloRoss/tarifas-electricas-en-america-latina-y-el-caribe-2013> [accessed January 2015].
[78] Regional Center for Renewable Energy and Energy Efficiency (RCREEE). Latest Electricity Price Schemes in RCREEE Member States; 2013; Available at: <http://www.rcreee.org/content/latest-electricity-price-schemes-rcreee-member-states> [accessed January 2015].
[79] International Energy Agency (IEA). Energy prices and taxes -quarterly statistics, first quarter 2013- Paris, France: IEA Publication; 2013.

Solar Energy 155 (2017) 805–815

Contents lists available at ScienceDirect

Solar Energy

journal homepage: www.elsevier.com/locate/solener

Optical modeling of four Fresnel-based high-CPV units

Juan P. Ferrer-Rodríguez [a,*], Hasan Baig [b], Eduardo F. Fernández [a], Florencia Almonacid [a], Tapas Mallick [b], Pedro Pérez-Higueras [b]

[a] IDEA Solar Research Group, Center for Advanced Studies in Energy and Environment (CEAEMA), Universidad de Jaén, Las Lagunillas Campus, Jaén 23071, Spain
[b] Environment and Sustainability Institute, University of Exeter, Penryn Campus, Penryn TR10 9FE, United Kingdom

ARTICLE INFO

Article history:
Received 7 April 2017
Received in revised form 21 June 2017
Accepted 6 July 2017

Keywords:
High concentrator photovoltaics
Optical simulations

ABSTRACT

High Concentrator Photovoltaic (HCPV) units are typically based on the use of Fresnel lenses, refractive secondary optical elements (SOE), and triple-junction (TJ) solar cells. In this work, a detailed optical modeling is applied to analyze the performance of four Fresnel-based HCPV units equipped with different refractive SOEs while considering the subcells current density generation. Wavelength-dependent material properties are utilized while simulating the optical performance. The spectral response of a typical TJ solar cell is also included. This modeling allows to establish the subcell current limitation and the spectral matching ratio, *SMR*, values in each case. The following SOEs have been used for simulating the HCPV units: (i) Dielectric-cross compound-parabolic-concentrator (DCCPC), (ii) (SIngle-Lens-Optical element) SILO-Pyramid, (iii) Refractive truncated pyramid (RTP) and, (iv) Trumpet. Results show that the HCPV units with SOEs RTP and Trumpet, exhibit bottom subcell current limitation and lowest optical polychromatic efficiency, this is partly due to the irradiance absorption in the bottom cell spectral region and longer optical path length of the concentrated rays within the SOE material. In the case of the HCPV unit with the DCCPC SOE, top and bottom subcells limit the current generation alternatively depending on the misalignment angle of the HCPV unit respect to the simulated sunrays. None of the *SMR* parameters are equal to 1 under normal alignment of the HCPV units. The short-circuit current density distributions for each subcell in each case are studied under normal alignment and under 1° of misalignment angle.

1. Introduction

Fresnel-based High Concentrator Photovoltaic (HCPV) devices are typically equipped with secondary optical elements (SOE) in order to improve their performance, since for increased concentrations, the tolerance to misalignment decreases (Pérez-Higueras and Fernández, 2015; Kumar et al., 2015). Some authors (Victoria et al., 2009; Fu et al., 2010; Benitez et al., 2010) have already pointed the advantages of using SOEs, which can be summarized as the increase of: (i) the optical efficiency by collecting more concentrated sunrays, (ii) the acceptance angle, which enhances the energy production and decreases manufacturing, installation and tracker costs, and (iii) the spatial and spectral irradiance uniformity over the multi-junction (MJ) solar cell (Fu et al., 2010). The non-uniform illumination is one of the key issues of the concentrator systems (Victoria et al., 2009; Baig et al., 2012), since the production and collection of the generated current may be altered depending on how uniformly the light is concentrated.

The literature shows detailed studies analyzing the performance of different SOEs under the same primary optical element (POE). Victoria et al. (2009) compared some different SOEs under the same circular plano-convex aspheric lens, results showed that the refractive compound parabolic concentrator (CPC) is more efficient and has a wider acceptance angle than those SOEs based on the SILO (SIngle-Lens-Optical element) design (James, 1989), while, on the other hand, the refractive CPC showed much less irradiance uniformity over the solar cell. Fu et al. (2010) compared three different refractive SOEs made of BK7 or B270 glass under the same Fresnel POE with a geometrical concentration of 800×: kaleidoscope, half-egg and domed kaleidoscope with breaking-symmetry top. They found that the domed kaleidoscope had a better performance, greater irradiance uniformity and acceptance angle. Miñano et al. (2013) presented some free-form Fresnel-Köhler SOE designs achieving relative good irradiance uniformity while avoiding total internal reflection (TIR), and therefore, light leakage between the solar cell and the SOE. Chen and Chiang (2015) showed a "kaleidoscope with equal optical path design (KOD)" SOE based on an ellipsoidal-top, a middle conic section and a bottom region that works under TIR and ends at a square surface. They

* Corresponding author.
E-mail address: jferrer@ujaen.es (J.P. Ferrer-Rodríguez).

http://dx.doi.org/10.1016/j.solener.2017.07.027
0038-092X/

compared the KOD design with other SOEs like the refractive truncated pyramid (RTP), showing higher acceptance angle. The above commented studies are very interesting from both a scientific and an industrial point of view, nevertheless, the refractive index wavelength dependency of the materials simulated is not included in the ray tracing in those works, excepting in that of Chen and Chiang (2015). Moreover, no spectral light absorption inside the materials was simulated or the spectral response of the MJ cell was considered. Among the different studies, only one, in which those last aspects were considered and simulated, has been found. This is the case of Espinet-González et al. (2012), who simulated and compared some refractive SOE, although not under the same POE. They took into account both absorption coefficient and refractive index as a function of the wavelength, and even of the spectral response of the MJ cell, however no related material property data were presented. They showed spatial profiles of the photocurrent density for each subcell, and found the illumination from Fresnel-Köhler design to be the most uniform in comparison to the SILO and the RTP.

An optical modeling intended to improve the approach to real optical phenomena is implemented in this work, including key features, like: (i) standard terrestrial spectrum, (ii) angular distribution of sunrays, (iii) Fresnel POE, (iv) wavelength dependency of refractive index and (v) absorption coefficient for both POE and SOE and for (v) absorption coefficient, and (vi) spectral response of each subcell within the TJ solar cell. This modeling provides the simulated subcell short-circuit currents of a typical TJ solar cell. This allows to know which subcell is limiting the current generation and to properly calculate the optical polychromatic efficiency and spectral matching ratio parameters. These calculations are conducted for normal alignment of the HCPV unit respect to the sunrays and also by different misalignment angles. Moreover, using these results, instead of analyzing the irradiance uniformity on the TJ solar cell, the short-circuit current density uniformity is analyzed for each subcell and for all the misalignment angles.

This modeling is applied in this work to four different Fresnel-based HCPV units equipped with refractive SOEs. These SOEs are designed and their performance analyzed through ray tracing simulations. The materials chosen for the POE and all the SOEs is poly (methyl methacrylate), PMMA, due to its ease of fabrication in a future experimental validation. Both a typical Fresnel lens and a typical triple-junction (TJ) concentrator solar cell are maintained constant for all of the HCPV units while using different SOEs. The different SOEs designed include: (i) Dielectric-Cross Compound-Parabolic-Concentrator (DCCPC), (ii) SILO-Pyramid, (iii) RTP, and (iv) Trumpet.

2. Description of the HCPV units simulated

In this section, the elements configuring the four HCPV units simulated are described. Firstly, the common elements to all the HCPV units, i.e. Fresnel lens POE and TJ solar cell, are detailed. Secondly, the four different SOEs composing the HCPV units are described and briefly explained.

2.1. Primary optics and the TJ solar cell

The primary optical element (POE) used in this study is a typical square Fresnel lens made of PMMA with an effective area of $130 \times 130\ mm^2$ and a focal distance of 152 mm. Its thickness is 1.8 mm and the ring facet spacing is 0.381 mm. F-number is equal to 0.83 and the geometrical concentration ratio between the areas of POE and TJ solar cell, $C_g = A_{lens}/A_{cell}$, is around 559×, since the TJ solar cell is a square of 5.5 mm side. These parameters defining the POE are listed in Table 1.

Table 1
Summary of parameters defining the Fresnel lens simulated.

Parameter	Value
Size [mm^2]	130×130
Focal distance [mm]	152.0
F-Number [–]	0.83
Facet spacing [mm]	0.381
Thickness [mm]	1.8

The solar cell is a typical TJ solar cell made of GaInP/GaInAs/Ge on Ge substrate. It is simulated through the spectral response characteristic of each subcell, top, middle ("mid") and bottom ("bot"), as plotted in Fig. 5 (Section 3). The short-circuit current density values under STC (standard test conditions, AM1.5D, ASTM G173-03, 1000 W/m^2, 25 °C) are simulated to be (Anon., n.d.): $J_{sc,top}{}^{1sun}$ = 15.6 mA/cm^2; $J_{sc,mid}{}^{1sun}$ = 15.7 mA/cm^2; $J_{sc,bot}{}^{1sun}$ = 19.2 mA/cm^2. Whereas for the whole device, $J_{sc}{}^{1sun}$ = 15.6 mA/cm^2, since the subcells are series connected. Table 2 shows the main parameters of the TJ solar cell simulated.

2.2. Four different SOEs

The different SOEs under study are shown in Fig. 1. Parametric optimization is carried out by varying their heights/truncation to reach a trade-off between efficiency and their acceptance angle. Fig. 1 shows a rendering of the four SOEs obtained: (a) DCCPC, (b) SILO-Pyramid, (c) RTP, and (d) Trumpet.

In order to have an idea of the relative SOE sizes to scale, both height and the shape of each SOE are shown in Fig. 2:

For each HCPV unit, the SOE entrance surface is located at the focal distance respect to the POE except for the case of the SILO-Pyramid, which is located 2 mm closer to the POE in order to improve its performance. In the following lines, the different SOEs are explained.

The DCCPC SOE is based on the geometrical principles of the CPC but combining both square entrance and exit surfaces (O'Gallagher, 2008; Cruz-Silva et al., 2016; Cooper et al., 2013). Its exit aperture matches the TJ solar cell area, like in all the SOEs here investigated. The DCCPC SOE here designed is defined by a characteristic axis tilt of the parabola, $\theta_c = 32°$, with a focal distance of $f = 4.2073$ mm and a height $h = 11$ mm. θ_c is close to the maximum angular size of the POE seen from its focal point. The SILO-Pyramid SOE corresponds to a modification of the bottom part of the standard SILO (also called "Dome-B" (Victoria et al., 2009)), which is calculated applying the Fermat's Principle. This modification takes advantage of the TIR at the walls of the pyramid. The resulting SILO-Pyramid SOE has a total height of 10.54 mm, whereas the truncated pyramid bottom part has a height of 3.2 mm and a total virtual entrance square of 10 mm side. The RTP SOE is based on a statistical design approach, as Fu et al. described (Fu et al., 2010), and can be also utilized as homogenizer in a Cassegrain-type concentrator (Shanks et al., 2016, 2017). The resulting design has a height of 17 mm with a square entrance of 12 mm side. The Trumpet SOE here designed is based on the use

Table 2
Summary of parameters defining the triple-junction solar cell simulated.

Parameter	Value
Size [mm^2]	5.5×5.5
Materials (top, mid, bot)	GaInP/GaInAs/Ge
$J_{sc,top}{}^{1sun}$ [mA/cm^2]	15.6
$J_{sc,mid}{}^{1sun}$ [mA/cm^2]	15.7
$J_{sc,bot}{}^{1sun}$ [mA/cm^2]	19.2

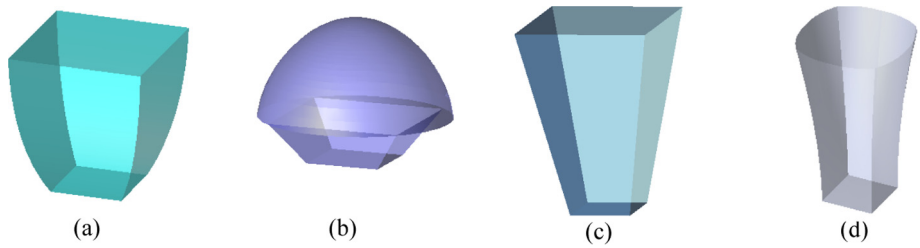

Fig. 1. Not a scale rendering of the different SOE designs simulated: (a) Dielectric-Cross-CPC (DCCPC); (b) SILO-Pyramid; (c) refractive truncated pyramid, RTP; and (d) Trumpet.

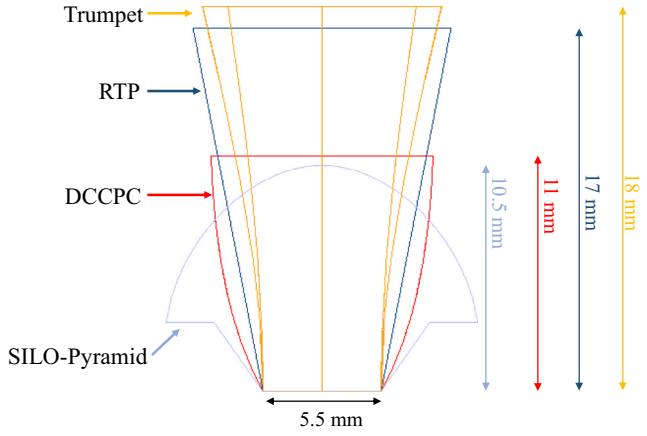

Fig. 2. Layout of the different SOEs profiles to scale with their height specified.

of a total of eight hyperbolic edges (Reddy et al., 2014), four ones for the vertexes of the exit surface and other four ones for the corresponding center of each side. The asymptotes of all of the hyperbolic edges maintain an angle of 15° respect to the symmetry axis of the SOE. The hyperbolic edges are calculated following the description of O'Gallagher for the design of the Compound Hyperbolic Concentrator (CHC) (O'Gallagher, 2008). The solid volume of the Trumpet is built in a CAD environment (SolidWorks) using the hyperbolic edges as guiding curves until reaching a height of 18 mm. The entrance surface is composed by four arcs of circumference whose centers are almost coincident to the center of the entrance surface.

3. Optical modeling

In this section, each feature of the optical modeling implemented in this work is carefully detailed. Moreover, this modeling is compared with other optical modeling works in the literature.

3.1. Description

An original and realistic optical modeling has been developed during this study. This optical modeling includes some non-idealities that are not usually taken into account simultaneously in previous research. These considerations include the use of: (i) standard terrestrial spectrum, (ii) angular distribution of sunrays, (iii) Fresnel POE, (iv) wavelength dependency of refractive index and (v) absorption coefficient for both POE and SOE, and (vi) spectral response of each subcell within the TJ solar cell. Moreover, as a result of those characteristics, this optical modeling provides the next output features –which are not available using a simpler optical modeling: (a) subcell short-circuit current generation, (b) spectral matching ratio analysis, (c) optical polychromatic efficiency, (d) effective acceptance angle calculation, and (e) subcell short-circuit current density uniformity.

3.2. Optical modeling features

(i) Standard terrestrial spectrum and (ii) angular distribution of sunrays

Sunrays are simulated under standard terrestrial direct spectrum ASTM G173-03 within the wavelength range of 0.3 and 2.5 μm. Also, the angular distribution of sunrays (4.7 mrad of angular size) is included in the simulations. See in Fig. 3 both normalized spectra, the one introduced and simulated in the ray tracing software and the standard one, which are almost identical. From here, it will be noted 1 sun = 1000 W/m^2 of standard terrestrial spectrum ASTM G173-03 or, simply, 1 sun of DNI.

(ii) Fresnel POE

The POE is modeled as an aspheric Fresnel lens using conical facets whose angles are calculated in order to focus the light from a point located at the object distance before the lens, to a point located at the image distance after the lens. The facet angle, β, is calculated through Eq. (1) (Leutz and Suzuki, 2001):

$$\tan\beta = \frac{\sin\theta_1 + \sin\theta_2}{\sqrt{(n^2 - \sin^2\theta_1)} - \cos\theta_2} \quad (1)$$

with θ_1 the incident angle of rays on the Fresnel lens, θ_2 the angle of light exiting the Fresnel lens, and n the refractive index of the material. In this work, the object distance is set infinite and the image distance is 152 mm.

(iii) Wavelength dependency of refractive index for POE and SOE

As mentioned above, both POE and SOE are modeled to be made of standard PMMA in each HCPV unit. The correspondent material property is defined through a refractive index, $n(\lambda)$, and an absorption coefficient, $\alpha_P(\lambda)$, for every wavelength, λ, in the range or inter-

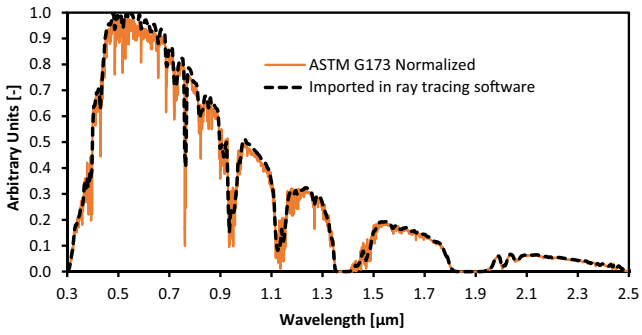

Fig. 3. ASTM G173 and simulated solar spectra, both normalized.

est, in this case, from 0.3 to 2.5 μm. Refractive index values are taken from the model of (Beadie et al., 2015) for PMMA and extended as a constant to the wavelength range mentioned (see Fig. 4). According to the aforementioned refractive index data of PMMA, wavelength-dependent Fresnel reflections and chromatic dispersion are simulated in the ray tracing.

(iv) Wavelength dependency of absorption coefficient for POE and SOE

Concerning the light absorption inside the materials, the Beer-Lambert law of transmission is applied (see Eq. (2)):

$$\Phi_T = \Phi_I e^{-\alpha_P h}, \tag{2}$$

where Φ_T and Φ_I are the transmitted and incident flux respectively, h is the bulk thickness and α_P is the absorption coefficient (for PMMA in our case). Then, the flux absorbed inside the material, Φ_A, is (see Eq. (3)):

$$\Phi_A = \Phi_I(1 - e^{-\alpha_P h}). \tag{3}$$

In this work, absorptance data from (Miller et al., 2011) for standard PMMA for a known bulk thickness are used in order to calculate $\alpha_P(\lambda)$. The resulting $\alpha_P(\lambda)$ values are plotted in Fig. 5. It can be observed that, approximately, the absorption is negligible in the wavelength region where the middle subcell is active. However, $\alpha_P(\lambda)$ is not zero for the whole spectral response region of the TJ solar cell. This may have an impact on the subcell current generated and, consequently, on the performance of each HCPV unit modeled in this work.

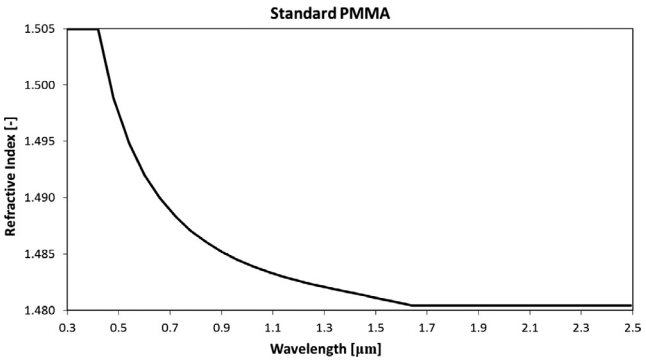

Fig. 4. Refractive index characteristic of standard PMMA used in the simulations.

(v) Spectral response of each subcell within the TJ solar cell

The TJ solar cell is modeled as composed of three different subcells. Each subcell is simulated separately as a surface with an absorption property according to the external quantum efficiency, *EQE*, values of each subcell of a typical TJ solar cell. The typical spectral response data of each simulated subcell surface of a TJ solar cell are plotted in Fig. 5. These plotted values correspond to the spectral response data, $SR_{subcell}(\lambda)$, normalized to the total maximum value of spectral response of the three subcells, which corresponds to around SR_{max} = 0.977 A/W.

3.2.1. Optical modeling output features

(vi) Subcell short-circuit current density generation

The utilization of the $SR_{subcell}(\lambda)$ data allows us to obtain the current density generated, $J_{sc,subcell}$, for each simulated subcell surface. The expression used for calculating the current density generated by each subcell is given by Eq. (4):

$$J_{sc,sub-cell} = \int SR_{subcell}(\lambda) \cdot E(\lambda) \cdot d\lambda = \frac{q}{h \cdot c} \int EQE_{subcell}(\lambda) \cdot E(\lambda) \cdot \lambda \cdot d\lambda, \tag{4}$$

where q is the electric charge, h is the Planck's constant, c is the speed of light in vacuum, $E(\lambda)$ is the spectral irradiance impinging on the solar cell simulated through ray tracing, and $EQE_{subcell}(\lambda)$ is the external quantum efficiency of each subcell in each case.

(vii) Spectral matching ratio analysis

The spectral matching ratio, *SMR*, parameters are related to the current density generated in each subcell. For a TJ solar cell, the next *SMR* parameters can be defined: *SMR*(*top*/*mid*), *SMR*(*top*/*bot*) and *SMR*(*mid*/*bot*). *SMR*(*top*/*mid*) can be defined as (Domínguez et al., 2013):

$$SMR(top/mid) = \frac{J^{conc}_{sc,top}/J^{1sun}_{sc,top}}{J^{conc}_{sc,mid}/J^{1sun}_{sc,mid}} \tag{5}$$

where $J^{conc}_{sc,subcell}$ is the current density generated by the corresponding subcell under concentrated illumination and $J_{sc,subcell}{}^{1sun}$ is analogous to 1 sun of DNI. Similarly, the other spectral matching ratios, *SMR*(*top*/*bot*) and *SMR*(*mid*/*bot*) can be defined just by replacing the corresponding subcell short-circuit density currents in Eq. (5). *SMR*

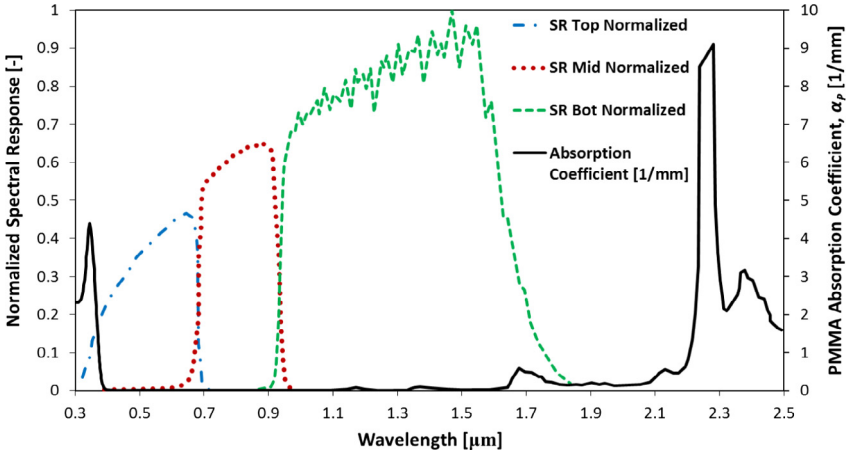

Fig. 5. Absorption coefficient, $\alpha_P(\lambda)$, of standard PMMA and normalized spectral response characteristic of each subcell.

$(top/mid) = 1$ means that the proportion between top and mid subcell photocurrents under concentrated irradiance impinging on the TJ solar cell is the same as compared to standard conditions 1 sun of DNI. In this case, the concentrated spectral irradiance is called equivalent to the standard spectrum with respect to the top and mid subcells. $SMR(top/mid) < 1$ represents a lower irradiance contribution of the top-wavelength region than the mid-wavelength one of the concentrated sunlight on the TJ solar cell when comparing to the case of the TJ solar cell under 1 sun of DNI, i.e. without any concentrator system. And $SMR(top/mid) > 1$ means vice versa. This reasoning is extended to $SMR(top/bot)$ and $SMR(mid/bot)$ by changing the correspondent short-circuit current densities(Rodrigo et al., 2017). The study of these indexes is interesting due to the strong spectral dependence of multi-junction CPV systems in outdoor conditions (Fernández et al. 2014, 2016).

(viii) Optical polychromatic efficiency

Using the $J_{sc,subcell}$ values obtained through ray tracing, the optical polychromatic efficiency, η_{opt}, is calculated through Eq. (6) (Benitez et al., 2010):

$$\eta_{opt} = \frac{J_{sc}^{conc}}{C_g J_{sc}^{1sun}} = \frac{\min\left\{J_{sc,top}^{conc}, J_{sc,mid}^{conc}, J_{sc,bot}^{conc}\right\}}{C_g \min\{J_{sc,top}^{1sun}, J_{sc,mid}^{1sun}, J_{sc,bot}^{1sun}\}}. \quad (6)$$

This definition of the optical efficiency takes into account the series connection of a typical TJ solar cell and how its resulting J_{sc} is obtained. Therefore, it is linked to the solar cell used as target, instead of only considering the optical efficiency as the relation between the output radiant flux over the incoming one to the concentrator system.

(ix) Effective acceptance angle calculation

The angular performance of the different HCPV units is characterized through the acceptance angle, α, where the η_{opt} drops to 90% respect to the maximum. It is also helpful to use the figure of merit effective concentration-acceptance angle product, CAP^*, (Eq. (7)), which cannot be greater than the refractive index of the medium surrounding the TJ solar cell and also takes into account the angular distribution of sunrays (Benitez et al., 2010):

$$CAP^* = \sqrt{C_g} \cdot \sin\alpha \quad (7)$$

(xi) Subcell short-circuit current density uniformity

Instead of analyzing the irradiance distributions over the TJ solar cell, short-circuit current density generated distributions for each subcell under the concentrated irradiance are obtained and analyzed. The normalized $J_{sc,subcell}^{conc}$ spatial distributions for each subcell and for both normal alignment and 1° of tilt angle are shown in Fig. 9 in Section 4.

3.3. Optical modeling in the literature versus present study

Table 3 shows a comparison among different optical modeling works in the literature for concentrator systems that are based on the use of a refractive lens as POE. It can be found that in the majority of the modeling works found, the next features are usually taken into account: (i) standard terrestrial spectrum, (ii) angular distribution of sunrays, (iii) Fresnel POE, (iv) absorption inside dielectric materials and (v) effective acceptance angle calculation. Moreover, the next features are only included in some optical modeling works: (i) wavelength dependency of refractive index for POE and SOE, (ii) wavelength dependency of absorption coefficient for POE and SOE, (iii) spectral response of each subcell within the TJ solar cell, (iv) subcell short-circuit current density generation, (v) optical polychromatic efficiency and (vi) subcell short-circuit current density uniformity. The optical modeling utilized in this work, using a ray tracing software (TracePro), includes all of those features, as can be seen in Table 3. Note that the feature "Absorption inside dielectric materials" is also included since some authors estimate absorption losses without detailing the absorption coefficient of the material.

4. Results and discussion

In this section, the numerical results (quantitative) obtained via simulations are deeply analyzed applying a reasoning derived from the different features of the optical modeling. Additionally, some qualitative results are also analyzed, like the short-circuit current density uniformity of the different subcells.

4.1. Quantitative modeling results

4.1.1. Results under normal alignment and 1° of tilt angle

As commented previously, ray tracing simulations are conducted for the four Fresnel-based high concentrator units. For each unit, the three subcells of the TJ solar cell are simulated obtaining the different short-circuit current densities. A preliminary collection of simulation results of the four HCPV units under normal alignment respect to the incident sunrays is given in Table 4, which shows the resulting short-circuit current density generated of each subcell, the optical polychromatic efficiency and the spectral matching ratios among the three subcells.

Table 3
Summary of different optical modeling works of lens-POE-based systems in the literature.

Feature	Fu et al. (2010)	Benitez et al. (2010)	Espinet-González et al. (2012)	Miñano et al. (2013)	Chen and Chiang (2015)	This work. 2017
Standard terrestrial spectrum	X	X	X	X	X	X
Angular distribution of sunrays	X	X		X		X
Fresnel POE	X	X	X	X	X	X
Wavelength dependency of refractive index for POE and SOE			X		X	X
Absorption inside dielectric materials		X	X	X	X	X
Wavelength dependency of absorption coefficient for POE and SOE			X			X
Spectral response of each subcell within the TJ solar cell		X	X			X
Subcell short-circuit current density generation		X	X			X
Spectral matching ratio analysis						X
Optical polychromatic efficiency		X				X
Effective acceptance angle calculation	X	X		X		X
Subcell short-circuit current density uniformity			X			X

Table 4
Summary of simulation results of subcell short-circuit current density generated, $J_{sc,subcell}^{conc}$, optical polychromatic efficiency, η_{opt}, and spectral parameters under normal alignment of each HCPV unit respect to the sunrays for each Fresnel-based concentrator unit.

Parameter	SILO-Pyramid	DCCPC	RTP	Trumpet
$J_{sc,top}^{conc}$ [A/cm^2]	7.29	7.30	7.31	7.29
$J_{sc,mid}^{conc}$ [A/cm^2]	7.60	7.60	7.60	7.60
$J_{sc,bot}^{conc}$ [A/cm^2]	7.67	7.62	7.15	7.08
Limiting subcell	Top	Top	Bot	Bot
η_{opt} [%]	83.4	83.6	81.8	81.0
η_{opt} [%] ideal case	85.3	84.6	83.2	86.6
SMR(*top*/*mid*) [–]	0.96	0.97	0.97	0.97
SMR(*top*/*bot*) [–]	1.17	1.18	1.25	1.26
SMR(*mid*/*bot*) [–]	1.21	1.22	1.30	1.31

Table 4 shows values of $J_{sc,subcell}^{conc}$ between 7.0 and 7.7 A/cm^2 for all the units and subcells. However, the current limiting subcell varies depending on the HCPV unit. The top subcell is limiting current in the SILO-Pyramid and DCCPC HCPV units, whereas the bot subcell is limiting current in the RTP and Trumpet ones. The optical polychromatic efficiency is greater than 80% for all the HCPV units, specifically between 81.0% (Trumpet HCPV unit) and 83.5% (DCCPC HCPV unit). Moreover, η_{opt} is slightly higher in the top-current-limiting HCPV units than in the bot-current-limiting ones. This last result may be related to the light absorption in the PMMA SOEs within the bot-wavelength region due to the longer optical path way (greater SOE height) of concentrated rays in the RTP and Trumpet SOEs compared to the other units. These η_{opt} results can be compared to those when not considering most of the non-idealities in the optical simulations like: angular and spectral distribution of sunrays, light absorption within POE and SOE and spectral response of the solar cell (just like a perfect absorber). When using a monochromatic source of rays, in this case with a wavelength of 546 nm, the optical efficiency of the HCPV units is simulated to be higher than when considering all those non-idealities, reaching a maximum of 86.6% (Trumpet HCPV unit). These highlight the importance of considering those non-idealities in order to have realistic simulated results of the optical elements designed.

In relation to the *SMR* values under normal alignment, these are globally in the range between around 0.96 and 1.31. Specifically, *SMR*(*top*/*mid*) is between 0.96 and 0.97 for the four HCPV units. Considering *SMR*(*top*/*bot*) values, these are near 1.17 for the SILO-Pyramid and DCCPC HCPV units, and around 1.25 for the RTP and Trumpet ones. *SMR*(*top*/*bot*) values higher for RTP and Trumpet HCPV units are in concordance with the bot subcell current-limitation of both HCPV units. About *SMR*(*mid*/*bot*) values, these are near 1.21 for SILO-Pyramid and DCCPC HCPV units and around 1.30 for RTP and Trumpet ones. Taking into account all the *SMR* values of all the HCPV units, those of the SILO-Pyramid unit are closer to 1, i.e., this HCPV unit concentrates sunrays with the lowest impact on the spectrum in relation to a typical TJ solar cell. This can be related to the lowest SOE height and absence of TIR. On the other hand, the Trumpet HCPV unit corresponds to the case of highest spectral change of concentrated sunrays respect to the standard spectrum. Note that, for all these HCPV units, *SMR* = 1 is not achieved in none of the three versions, so the reference spectrum is distorted by effect of the optical system.

Ray tracing simulations are also conducted under different misalignment angles of the HCPV concentrator unit respect to the incident sunrays. It is worthy to analyze the corresponding simulation results under 1° of tilt angle, which are summarized in Table 5.

Table 5 shows values of $J_{sc,subcell}^{conc}$ between around 6.3 and 7.7 A/cm^2 for all the HCPV units and subcells under 1° of tilt angle. For this tilt angle, it is found that the bot subcell is limiting the current generation in all the HCPV units except for the SILO-Pyramid one (with top subcell current limitation). The optical polychromatic efficiency is between 72.0% (Trumpet HCPV unit) and 78.2% (SILO-Pyramid HCPV unit). This is a reduction of 7% in average in comparison with normal alignment, being DCCPC and Trumpet HCPV units those with highest decrease (around 8%), whereas for SILO-Pyramid and RTP HCPV units it is lowest (around 5%). Note that, for this tilt angle, the top subcell is limiting current only in the SILO-Pyramid HCPV unit and the bot subcell is limiting current in the rest of the cases, whereas under normal alignment, top subcell is limiting in SILO-Pyramid and DCCPC HCPV units. Again, when not considering the non-idealities, the η_{opt} increases, being in this case in the range between around 76% (Trumpet HCPV unit) and 84% (DCCPC HCPV unit).

Considering the *SMR* values under 1° of misalignment, they are found to range between 0.90 and 1.34. More in detail, *SMR*(*top*/*mid*) is between around 0.90 (SILO-Pyramid HCPV unit) and 0.93 (Trumpet HCPV unit). This corresponds to a similar effect described for normal alignment but intensified. In the case of the DCCPC HCPV unit, *SMR*(*top*/*mid*) corresponds to around 0.98, which is a value very close to 1, i.e., near to equivalent conditions to the standard spectrum. *SMR*(*top*/*bot*) values are in the range from around 1.09 to 1.27, being the lowest value that of the SILO-Pyramid HCPV unit. Finally, *SMR*(*mid*/*bot*) values range from around 1.21 (SILO-Pyramid HCPV unit) to 1.34 (RTP HCPV unit). Comparing to the

Table 5
Summary of simulation results of subcell short-circuit current density generated, $J_{sc,subcell}^{conc}$, optical polychromatic efficiency, η_{opt}, and spectral parameters under 1° of tilt angle of each HCPV unit respect to the sunrays for each Fresnel-based concentrator unit.

Parameter	SILO-Pyramid	DCCPC	RTP	Trumpet
$J_{sc,top}^{conc}$ [A/cm^2]	6.84	6.84	6.96	6.36
$J_{sc,mid}^{conc}$ [A/cm^2]	7.60	7.03	7.34	6.86
$J_{sc,bot}^{conc}$ [A/cm^2]	7.69	6.68	6.70	6.30
Limiting subcell	Top	Bot	Bot	Bot
η_{opt} [%]	78.2	76.3	76.6	72.0
η_{opt} [%] ideal case	80.0	83.7	81.5	75.9
SMR(*top*/*mid*) [–]	0.90	0.98	0.95	0.93
SMR(*top*/*bot*) [–]	1.09	1.26	1.27	1.24
SMR(*mid*/*bot*) [–]	1.21	1.28	1.34	1.33

case under normal alignment, on one hand, *SMR*(*top*/*mid*) and *SMR*(*mid*/*bot*) for 1° of tilt angle are further from the value equal to 1. On the other hand, *SMR*(*top*/*bot*) is much closer to 1 for the SILO-Pyramid HCPV unit, whereas it separates from 1 in the rest of the HCPV units.

4.1.2. Results under misalignment angles

Simulated $J_{sc,subcell}^{conc}$ values adding the misalignment are shown in Fig. 6. The subcell that is limiting the current generated is that of the minimum $J_{sc,subcell}^{conc}$ value for each tilt angle. It can be seen, on one hand, top subcell current-limitation in the case of the SILO-Pyramid HCPV unit for all the misalignment angle range except beyond around 1.8°. It is also relative easy to observe the continuous bot subcell current limitation in the case of the RTP HCPV unit. There is also bot subcell current limitation for the whole tilt angle range in the case of the Trumpet HCPV unit. On the other hand, for the DCCPC HCPV unit there is an alternation between the limiting subcells, i.e., there is top subcell current limitation from normal alignment to around 0.8° of tilt angle and from 1.2° and beyond, but there is bot subcell current limitation in the interval between 0.8° and 1.2°.

In order to analyze those spectral differences among the four HCPV units, the three *SMR* plots, (top/mid), (top/bot) and (mid/bot), for each HCPV unit varying the misalignment angle are shown in Fig. 7. These plots present significant differences from each other not only under normal alignment but also under the different tilt angles. On one hand, it can be seen that *SMR*(*top*/*mid*) is lower than 1 (with a minimum of 0.87 at 1.2° for the SILO-Pyramid HCPV unit) in all the cases except for tilt angles greater than around 1.8° for the SILO-Pyramid HCPV unit and Trumpet one. Moreover, it shows a value within 0.87 and 1.09, and is stable in general. On the other hand, *SMR*(*top*/*bot*) and *SMR*(*mid*/*bot*) present a relative higher variation with the tilt angle. For instance, in the case of the DCCPC HCPV unit, these last both *SMR* parameter curves have a peak maximum (with *SMR*(*mid*/*bot*) = 1.29) at around 1.05° and then they decrease rapidly for increased tilt angles until a value of 0.85 at 2.0°, whereas *SMR*(*top*/*mid*) is maintained relative constant (0.96). Something similar occurs in the RTP HCPV unit but with the relative *SMR* maximum (with *SMR*(*mid*/*bot*) = 1.34) of the three parameters at around 1.1–1.2°, while the relative *SMR* minimum for *SMR*(*top*/*bot*) and *SMR*(*mid*/*bot*) is of 1.19 at 2.0°. For this system, *SMR*(*top*/*mid*) is again relative constant (0.97). Considering the cases of the SILO-Pyramid and DCCPC HCPV units, the *SMR* parameter curves change relatively more strongly. In the case of the SILO-Pyramid HCPV unit *SMR*(*top*/*mid*) and *SMR*(*top*/*bot*) present a strong minimum (with *SMR*(*top*/*mid*) = 0.87) at around 1.2°, whereas *SMR*(*mid*/*bot*) is relatively constant near a value of 1.2. As seen in Fig. 7, in terms of the spectral variations, the Trumpet HCPV unit, and especially the RTP one, present lowest dependency with the tilt angle.

Since the η_{opt} values are also calculated including misalignments, it allows for a comparison between all the HCPV units with the different SOEs, including the case of having no SOE (see Fig. 8), to be carried out. This last case is more efficient for normal alignment, since there are no Fresnel losses involved. Nevertheless, its optical efficiency drops relative fast compared to the case of including a SOE. For instance, the η_{opt} of the system without SOE is approximately 0% at around 1.2°, while it is kept within 70–80% for the systems with SOE. The SILO-Pyramid represents the less sensitive SOE design to misalignment for angles between 1.7° and 2.0° among the HCPV units. In general, all these SOE designs present relative similar misalignment performance, although their angular characteristics spread each other for angles

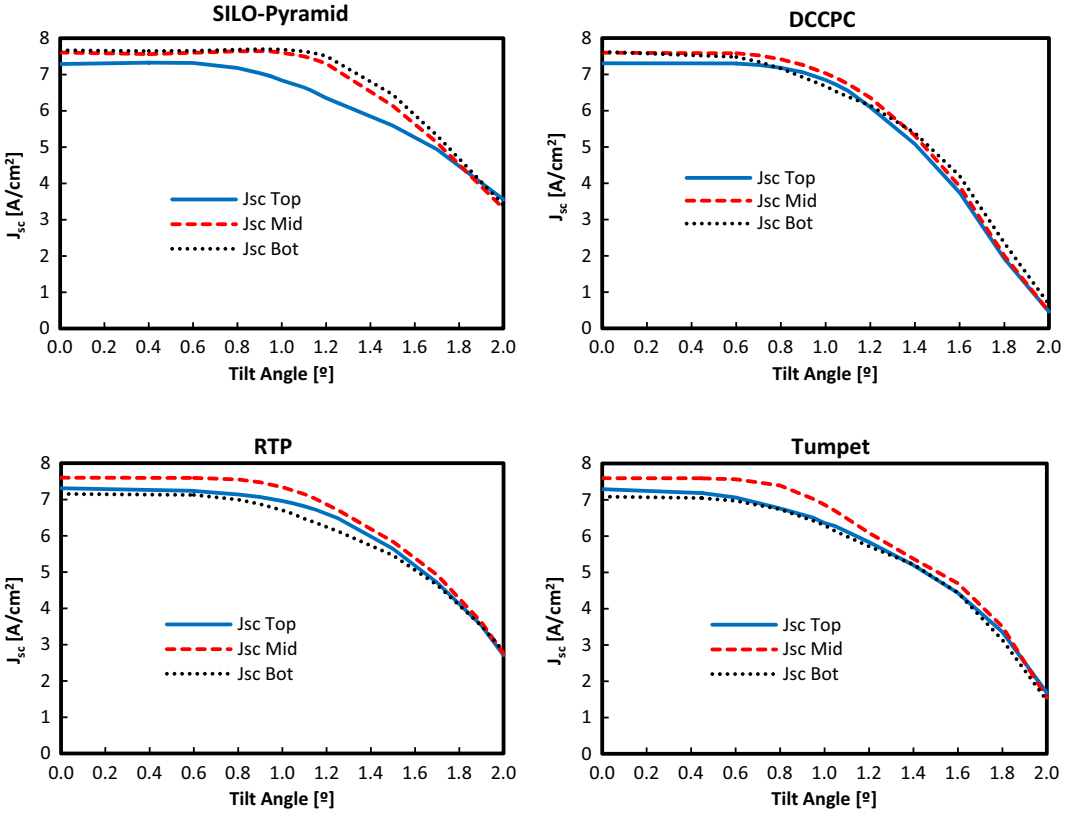

Fig. 6. $J_{sc,subcell}^{conc}$ values of the four Fresnel-based HCPV units for normal alignment and their evolution under the correspondent tilt angle.

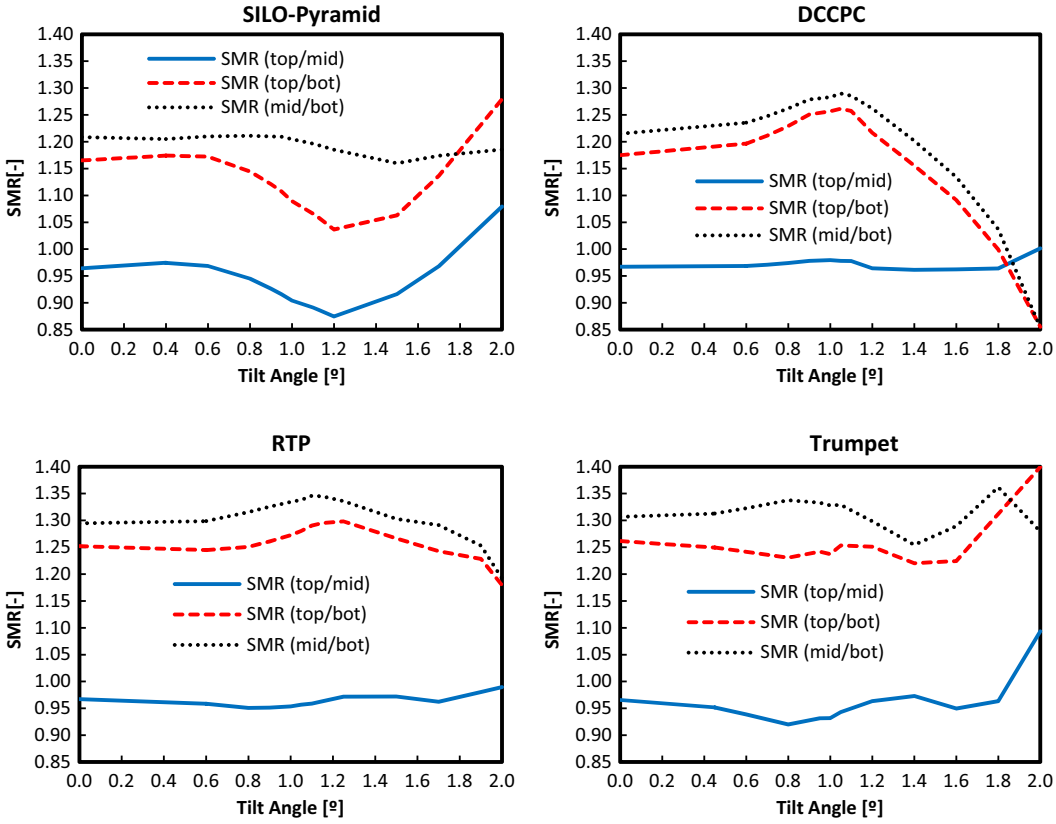

Fig. 7. *SMR* plots, (top/mid), (top/bot) and (mid/bot), for the four Fresnel-based HCPV units for normal alignment and their evolution under the correspondent tilt angle respect to the incident sunrays.

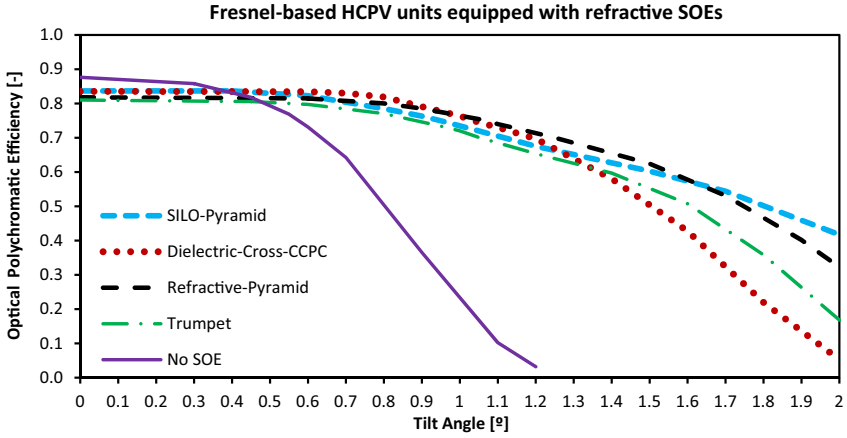

Fig. 8. Optical efficiency versus tilt angle for the four Fresnel-based HCPV units and also including the case of having no SOE (i.e., only POE and TJ solar cell).

Table 6
Summary of main parameters and simulation results.

Parameter	No SOE	SILO-Pyramid	DCCPC	RTP	Trumpet
Optical Polychromatic Efficiency [%]	87.7	83.4	83.6	81.8	81.0
Optical Polychr. Efficiency with AR [%]	–	85.5	87.1	83.5	82.4
Acceptance Angle [°]	±0.50	±1.13	±1.03	±1.11	±0.96
CAP^*	0.21	0.47	0.43	0.46	0.40
Opt. Polychr. Efficiency at Acceptance Angle [%]	78.9	75.3	75.2	73.6	72.9
SOE Volume [mm^3]	–	916	871	1361	1020
SOE Height [mm]	–	10.5	11.0	17.0	18.0

greater than 1.4°. It can be seen that the DCCPC HCPV unit presents variation after 1.4° misalignment.

Table 6 summarizes the values of all parameters for each HCPV unit, and also including the case of having no SOE for comparison reasons. The optical polychromatic efficiency is highest for the HCPV unit with the smallest SOE in terms of optical path length (SILO-Pyramid HCPV unit), with values slightly greater than 83%, which is due to the relative lowest light absorption inside PMMA. The opposite case, with optical efficiency lower than 82%, occurs for the SOE designs of more height: RTP and Trumpet HCPV units. For these two last cases, the bot subcell is limiting the current generated. The effective acceptance angle values of these designs range from ±0.96° (Trumpet HCPV unit) to ±1.13° (SILO-Pyramid HCPV unit). In terms of the effective concentration-acceptance angle product, *CAP**, the best SOE designs correspond to the SILO-Pyramid and the DCCPC HCPV units, with values 0.47 and 0.46 respectively. Applying perfect antireflective (AR) coating on the SOE entrance leads to better efficiency results. These improved optical polychromatic efficiencies range from 82.4% (Trumpet HCPV unit) to a maximum of 87.1% (DCCPC HCPV unit). Obviously, simulating SOEs made of glass (e.g. BK7) and without considering any light absorption inside the materials, may lead to higher performance values. The volume of each SOE in each HCPV unit is also included, since the cost of manufacturing is related to it (Benitez et al., 2010). The RTP SOE has the relative highest material consume, with 1361 mm^3. It is also remarkable the relative reduced volume of the SILO-Pyramid SOE with 871 mm^3.

4.1.3. Uncertainties

The parameters defining both Fresnel lens and TJ solar cell are inherently subject to uncertainties. For example, in a real case, the dimensions of the lens, its focal distance, etc. are measured with a determined uncertainty. In order to analyze the impact of these uncertainties in the simulation results, optical simulations have been conducted with changed dimensions parameters. In this way, POE dimensions, focal length, facet spacing and also solar cell size have been varied and the correspondent $J_{sc,subcell}$, η_{opt} and *SMR* values obtained after optical simulation.

The variation of Fresnel lens parameter with highest impact on the results is its area, with variation in the $J_{sc,subcell}$ lower than 0.11 A/cm^2, lower than 0.23% in η_{opt} and lower than 0.01 in *SMR*. Considering the variation in the TJ solar cell area, concentrated rays would be lost, since the exit surface is defined by that of the SOE. Therefore, a higher reduction of the η_{opt} is expected, and it results to be lower than 6.2%. Nevertheless, $J_{sc,subcell}$ and *SMR* variations are expected to be lower than 0.4 A/cm^2 and 0.03 respectively.

Hence, according to the results above, no substantial changes in the simulation results may be expected as a consequence of the inherent uncertainties related to the simulation parameters.

4.2. Qualitative modeling results

Instead of analyzing the irradiance distributions over the TJ solar cell, short-circuit current density generated, $J^{conc}_{sc,subcell}$, distributions are obtained and analyzed. The normalized $J^{conc}_{sc,subcell}$ spatial

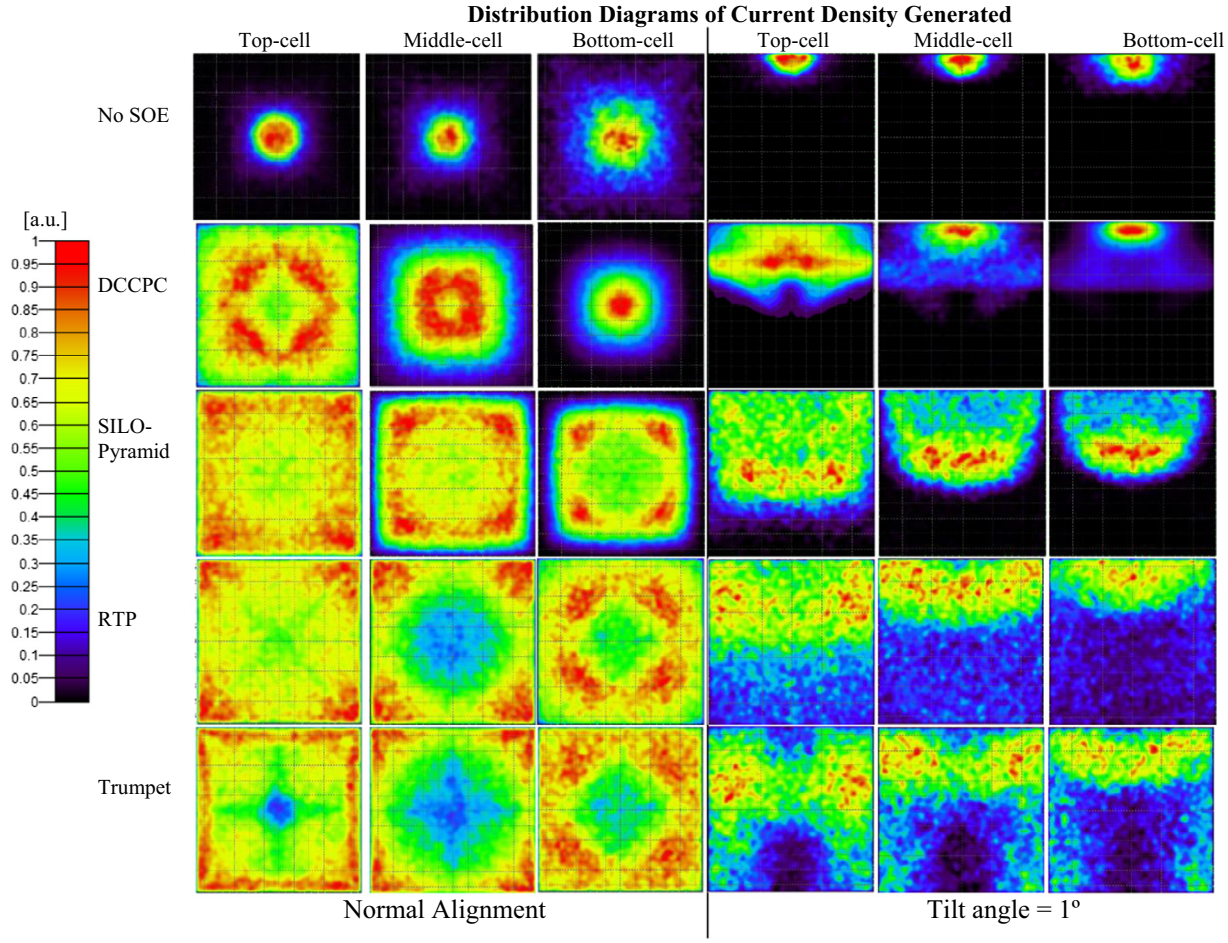

Fig. 9. Normalized short-circuit current density distributions generated by top, mid and bot subcells for normal alignment (left) and for a tilt angle of 1° (right) for the four Fresnel-based HCPV units and, also for the case of the HCPV unit without any SOE.

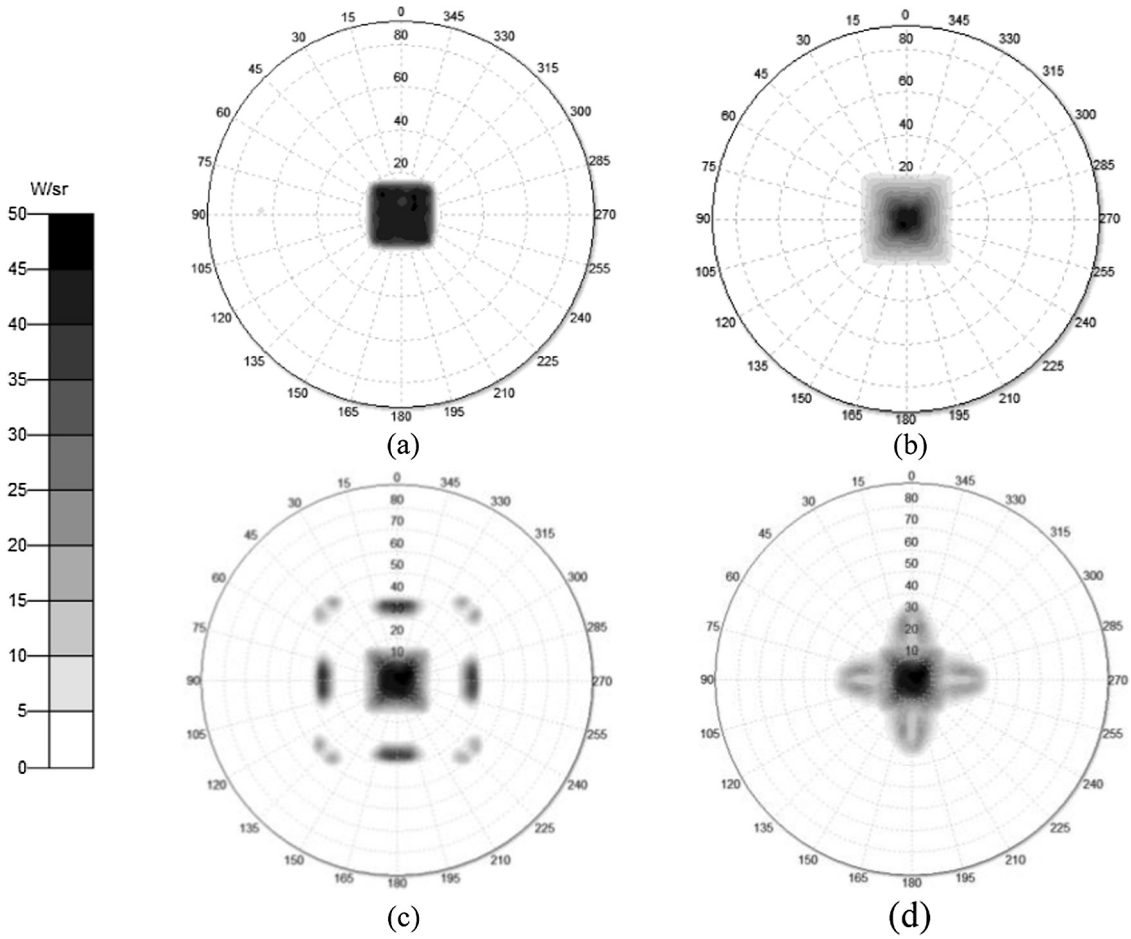

Fig. 10. Polar iso-candela plots for the exit surface of the Fresnel-based concentrator units: (a) DCCPC, (b) SILO-Pyramid, (c) RTP, and (d) Trumpet. Data covers ± 90° from normal to the surface.

distributions for each subcell and for both normal alignment and 1° of tilt angle are shown in Fig. 9 (Baig et al., 2012). Under normal alignment, most of SOE designs for the HCPV units lead to relatively uniform current density distributions as a consequence of rays mixing after TIR on side walls or after refraction on the convex entrance shape in the case of the SILO-based design. The lack of uniformity of the $J_{sc,bot}^{conc}$ distribution in the DCCPC HCPV unit can be observed, this is due to a less interaction with the SOE walls for the rays in the region of the bot cell spectral response. Under 1° of tilted angle, RTP and Trumpet HCPV units are the least sensitive ones to misalignments. This may be due to the TIR effect combined to the higher height of these SOEs compared to the other ones. As from the global results and considering the $J_{sc,subcell}^{conc}$ distribution uniformity, the RTP SOE may have here the best performance although the highest amount of material as commented above.

Not strictly considered as an output of this modeling, since the subcells structure of the TJ solar cell is ignored in this case, the incident angle of rays impinging the solar cell can be however shown through different plots. Fig. 10 shows polar iso-candela plots for the exit surface of each SOE in watts per steradian under normal alignment. The case with less concentrated rays angle respect to the normal of solar cell is that of the SILO-Pyramid HCPV unit, with almost all the rays with less than 20° of incident angle. Among the SOEs based on TIR the maximum incident angle increases due to the multiple reflections on the side walls up to around 50°, which is the case of the RTP HCPV unit. Those rays with more incident angle (e.g. with 50°) may be more difficulty absorbed by the TJ solar cell (García-Linares et al., 2014; Bunthof et al., 2017).

5. Conclusions and future works

We present a complete optical modeling procedure intended to improve the simulation of typical Fresnel-based high concentrator photovoltaic (HCPV) units equipped with a refractive secondary optical element (SOE) and a typical triple-junction (TJ) solar cell. The Fresnel lens (primary optical element, POE) and the SOE are simulated as made of PMMA although any other material can be applied in the modeling. This powerful modeling takes into account some non-idealities for the ray tracing simulations but specially, the wavelength dependency of key material properties are simulated, like: absorption coefficient of the optical materials and the spectral response of the TJ solar cell.

As a consequence of simulating the spectral response of the TJ solar cell, the current density generated by each subcell is also simulated. It allows to calculate the optical polychromatic efficiency, which takes into account the correspondent subcell current limitation. Moreover, the simulation of the current density generation of each subcell allows to determine which subcell is limiting the current generation and to calculate the expected spectral matching ratio (*SMR*) parameters among the three subcells. Plots of current density uniformity generated on each subcell are even provided by this modeling.

Four different HCPV units with the same aspheric Fresnel POE and TJ solar cell, and with four different SOEs are simulated. The design of each SOE is the result of a trade-off between the optical polychromatic efficiency and the acceptance angle of the correspondent HCPV unit.

Among the main results, the HCPV units equipped with higher SOEs, i.e. RTP and Trumpet, exhibit bottom subcell current limitation and lower optical polychromatic efficiency which may be related to the spectral absorption within the PMMA material in the spectral region of the bottom subcell. However, for the other HCPV units with smaller SOEs, i.e. DCCPC and SILO-Pyramid, there is top subcell current limitation and higher optical polychromatic efficiency. Moreover, for a determined HCPV unit, like specifically in the case of the DCCPC SOE, the current limitation can vary among the composing subcells. Specifically, top subcell is limiting for normal alignment and until around 0.8° of misalignment angle of the HCPV unit respect to the incident sunrays and from 1.2° and 2° angle; whereas between 0.8° and 1.2° angle, the bottom subcell is limiting the current generation. Concerning the spectral performance of the four HCPV units, that with the RTP SOE presents the lowest variation of *SMR* with the misalignment angle. Considering extreme values, *SMR*(*mid*|*bot*) is around 1.30 for the HCPV units with RTP and Trumpet SOEs under normal alignment. It is remarkable that, under normal alignment, *SMR* is never equal to 1 in none of its three versions in none of the four HCPV units. About the optical polychromatic efficiency, η_{opt}, and its variation with the misalignment angle, all the HCPV units exhibit similar performance until 1.4° of misalignment angle. They show η_{opt} between 81.0% (Trumpet HCPV unit) and 83.6% (DCCPC HCPV unit) with acceptance angles between ±0.96° (Trumpet HCPV unit) and ±1.13° (SILO-Pyramid HCPV unit)–resulting the effective concentration-angle product between 0.40 and 0.47. However, the HCPV unit equipped with the DCCPC SOE presents little variation after 1.4° of misalignment angle. Taking into account the uniformity of the current generated by each subcell in each HCPV unit, the HCPV units with SOEs based on total internal reflection exhibit an apparent better current density uniformity for a misalignment angle of 1°.

For future works, the validation of this modeling has to be confirmed with experimental data. Moreover, this modeling can be extended to quantify the impact of the uniformity of the current density generated by each subcell in each HCPV unit (Espinet-González et al., 2012). The incident angle of rays and the quantification of its impact on the current generation of each subcell is to be modeled also in future works (García-Linares et al., 2014), like also other non-idealities such as light scattering on the surfaces or light leakage between SOE and TJ solar cell (Baig et al., 2015).

Funding

European Regional Development Fund (ERDF) and Spanish Economy Ministry (ENE2013-45242-R and ENE2016-78251-R); Universidad de Jaén (UJA) and Caja Rural de Jaén (UJA2015/07/01). Financial support provided by the Universidad de Jaén Doctoral School.

Acknowledgments

The authors thank Lambda Research Corporation for its donation of TracePro optical software.

References

Anon., n.d. IEC 62670-1:2013 Concentrator Photovoltaic (CPV) Modules and Assemblies Performance Testing - Part 1: Standard Conditions. s.l.:ISBN 978-2-8322-1120-5.

Baig, H., Heasman, K., Mallick, T., 2012. Non-uniform illumination in concentrating solar cells. Renew. Sustain. Energy Rev. 16 (8), 5890–5909.

Baig, H., Sellami, N., Mallick, T., 2015. Trapping light escaping from the edges of the optical element in a concentrating photovoltaic system. Energy Convers. Manage. 80, 238–246.

Beadie, G. et al., 2015. Refractive index measurements of poly(methylmethacrylate) (PMMA) from 0.4–1.6 μm. Appl. Opt. 54 (31).

Benitez, P. et al., 2010. High performance Fresnel-based photovoltaic concentrator. Opt. Express 18 (S1), A25–A40.

Bunthof, L. et al., 2017. The illumination angle dependency of CPV solar cell electrical performance. Sol. Energy 144, 166–174.

Chen, Y., Chiang, H., 2015. Design of the secondary optical elements for concentrated photovoltaic units with fresnel lenses. Appl. Sci. 5 (4), 770–786.

Cooper, T. et al., 2013. Performance of compound parabolic concentrators with polygonal apertures. Sol. Energy 95, 308–318.

Cruz-Silva, O., Jaramillo, O.A., Borunda, M., 2016. Full analytical formulation for dielectric totally internally reflecting concentrators designs and solar applications. Renew. Energy 101 (804–815).

Domínguez, C., Antón, G., Askins, S., 2013. Current-matching estimation for multijunction cells within a CPV module by means of component cells. Prog. Photovoltaics: Res. Appl. 21 (7), 1478–1488.

Espinet-González, P. et al., 2012. Triple-junction solar cell performance under Fresnel-based concentrators taking into account chromatic aberration and off-axis operation. AIP Conf. Proc. 1477, 81–84.

Fernández, E., Almonacid, F., Ruiz-Arias, J., Soria-Moya, A., 2014. Analysis of the spectral variations on the performance of high concentrator photovoltaic modules operating under different real climate conditions. Sol. Energy Mater. Sol. Cells 127, 179–187.

Fernández, E., Soria-Moya, A., Almonacid, F., Aguilera, J., 2016. Comparative assessment of the spectral impact on the energy yield of high concentrator and conventional photovoltaic technology. Sol. Energy Mater. Sol. Cells 147, 185–197.

Fu, L., Leutz, R., Annen, H., 2010. Secondary optics for Fresnel lens solar concentrators. Nonimaging Optics: Efficient Design for Illumination and Solar Concentration VII 7785, p. 778509–6.

García-Linares, P. et al., 2014. Effect of the encapsulant temperature on the angular and spectral response of multi-junction solar cells. IEEE Photovoltaic Spec. Conf. (PVSC), 3298–3303.

James, L., 1989. Use of imaging refractive secondaries in photovoltaic concentrators, Albuquerque, NM: SAND89-7029.

Kumar, V., Shrivastava, R., Untawale, S.P., 2015. Fresnel lens: a promising alternative of reflectors in concentrated solar power. Renew. Sustain. Energy Rev. 44, 376–390.

Leutz, R., Suzuki, A., 2001. Nonimaging Fresnel Lenses. Springer-Verlag, s.l..

Miller, D., Kempe, M., Kennedy, C., Kurtz, S., 2011. Analysis of transmitted optical spectrum enabling accelerated testing of multijunction concentrating photovoltaic designs. Opt. Eng. 50 (1).

Miñano, J. et al., 2013. Free-form optics for Fresnel-lens-based photovoltaic concentrators. Opt. Express 21, A494–A502.

O'Gallagher, J., 2008. Nonimaging Optics in Solar Energy. Morgan & Claypool Publishers, s.l..

Pérez-Higueras, P., Fernández, E., 2015. High Concentrator Photovoltaics: Fundamentals, Engineering and Power Plants. Springer International Publishing, s.l..

Reddy et al., 2014. Design and optimisation of elliptical hyperboloid concentrator with helical receiver. Sol. Energy 108, 515–524.

Rodrigo, P., Fernández, E., Almonacid, F., Pérez-Higueras, P., 2017. Quantification of the spectral coupling of atmosphere and photovoltaic system performance: indexes, methods and impact on energy harvesting. Sol. Energy Mater. Sol. Cells 163, 73–90.

Shanks, K. et al., 2017. Prototype fabrication and experimental investigation of a conjugate refractive reflective homogeniser in a cassegrain concentrator. Sol. Energy 142, 97–108.

Shanks, K. et al., 2016. Theoretical investigation considering manufacturing errors of a high concentrating photovoltaic of cassegrain design and its experimental validation. Sol. Energy 131, 235–245.

Victoria, M., Domínguez, C., Antón, I., Sala, G., 2009. Comparative analysis of different secondary optical elements for aspheric primary lenses. Opt. Express 17 (8), 6487–6492.

*Manuscript

Development, indoor characterisation and comparison to optical modelling of four Fresnel-based high-CPV units equipped with refractive secondary optics

Juan P. Ferrer-Rodríguez[a,*], Eduardo F. Fernández[a], Hasan Baig[b], Florencia Almonacid[a], Tapas Mallick[b] and Pedro Pérez-Higueras[a]

[a] *Centre for Advanced Studies in Energy and Environment (CEAEMA), IDEA Solar Research Group, Electronics and Automation Department, Universidad de Jaén, Las Lagunillas Campus, Jaén, 23071, Spain, *jferrer@ujaen.es*

[b]*Environment and Sustainability Institute, University of Exeter, Penryn Campus, Penryn, TR10 9FE, United Kingdom*

Abstract

In this work, we compare the optical and electrical performance of a Fresnel-based HCPV system when equipped with different refractive secondary optical elements (SOEs) using both modelling and experiments. These SOEs (designed through a powerful optical model): (i) Dielectric-cross compound-parabolic-concentrator (DCCPC), (ii) (SIngle-Lens-Optical element) SILO-Pyramid, (iii) Refractive truncated pyramid (RTP) and, (iv) Trumpet; are fabricated (made of PMMA) and mounted on commercially available concentrator solar cell assemblies. An indoor characterisation of all these HCPV units, under controlled and repeatable conditions, using a CPV solar simulator "Helios 3198" is performed. The RTP unit shows an optimum performance in terms of overall efficiency and acceptance angle, although this is not necessarily seen in terms of the optical efficiency of the RTP as an SOE. The measured values of optical efficiencies of the SOEs match well the simulated ones, although the performance of a unit at maximum power point is not directly comparable with the optical efficiency of the SOE. The error between the simulations and experiments is less than 3.2% in optical efficiency values of the SOEs. Additionally, the I-V curve parameters and the acceptance angle are measured under varying irradiance and spectral conditions of the incoming light.

Keywords: High concentrator photovoltaics. Indoor characterisation. Secondary optical elements. CPV solar simulator. Optical efficiency. Acceptance angle.

1. Introduction

The photovoltaic (PV) technology presents a great potential for global implementation given the abundance of the solar resourcefreely available. The worldwide installed PV capacity grows constantly, favoured by the nowadays competitive PV production costs. Besides from these factors, different PV technologies compete for lower generation costs of electricity (or specifically, LCOE, levelised cost of electricity). This is the case of the High Concentrator Photovoltaic (HCPV) technology, which aims for the substitution of limited and costly semiconductor material by available and economical concentrator optical systems based on conventional materials. Although the efficiency of concentrator solar cells continues increasing, this technology still has to achieve more competitive LCOE values compared to the conventional PV technology in order to be extensively implemented and to be one of the key components in a possible mix of the electricity generation [1]. Despite the advantages of the HCPV technology, the global installed HCPV power has extremely dropped in the recent years [2]. Its implementation is, however, competitive enough for determined geographic areas with high direct irradiation rates and favourable economic conditions [3]. The relative complexity of the HCPV technology compared to other PV 'technologies is a disadvantage, but also an opportunity for improvement, since the designs and the industrial models can still be highly enhanced. For that, it is necessary to increase the theoretical and practical knowledge of the HCPV technology, which has a rich repertory of physical phenomena involved (light concentration, optical coupling, light interaction with materials, subcell spectral responses of multi-junction cells…).

Attending to the HCPV systems, the typical simple configuration is based on a concentrating Fresnel lens [4] that focuses the sun rays onto a small triple-junction (TJ) solar cell through a secondary optical

element (SOE). The SOEs will provide an increase in the optical tolerance to misalignments (acceptance angle) and improve the light uniformity over the TJ solar cell [29]. SOEs can be reflective or refractive, although the refractive ones allow a higher theoretical maximal concentration [5], thus they are typically utilised in HCPV modules.

Many works analyse the basic configurations of Fresnel-based HCPV systems at simulation level and compare the impact of the different SOEs in their performance [6-8]. Considering experimental works related to that kind of systems, the next publications are a summary of their experimental characterisation. Schmidt et al [9] investigated a typical refractive non-imaging SOE (SILO, SIngle Optical element) in a Fresnel-based concentrator system, using an indoor experimental setup, by characterising the concentration profile at the SOE's exit aperture and proving the high optical tolerances of this kind of SOE. Schmidt et al. [10] analysed the outdoor performance of different types of refractive SOEs made of glass, the SILO SOE and another one with spherical curvature, comparing with optical simulations in terms of short-circuit current generated. They concluded that the SOE with spherical shape was a suitable option for mass production. Herrero et al. [11] investigated Fresnel-based HCPV systems equipped with refractive SOEs focusing the irradiance distribution at the output of the SOE and its effects on the TJ solar cells. They presented a method to estimate the losses caused by non-uniform irradiance patterns on the TJ solar cells. Zamora et al. [12] characterised outdoors two different prototypes of Fresnel-Köhler HCPV concentrators, including a comparison with the optical simulations results of the measured acceptance angle characteristic and illumination uniformity over the TJ solar cell. They showed experimental performance results which confer high potential in the CPV market to the Fresnel-Köhler concentrator. McVey-White et al. [13] developed a technique to measure the influence of the lens temperature of different concentrator prototypes in the irradiance uniformity ant its impact on the subcell current generation. They determined that the Fresnel-Köhler concentrator showed better results than other typical lens-based concentrator systems. Concerning the characterisation method based on subcell current limitation diagrams developed by Domínguez et al. [14], it was applied to analyse the performance of different Fresnel-based HCPV systems, by Herrero et al. [15]. They showed the necessity of SOEs and that, in relation to Fresnel-based systems, chromatic aberrations are dominant respect to spatial optical aberrations. Shanks et al. [16] analysed the theoretical optical efficiency, acceptance angle and irradiance uniformity of a Cassegrain HCPV module equipped with refractive truncated pyramids as secondary optics. They also presented experimental values, using the CPV solar simulator "Helios 3198" at the University of Jaén, of the optical efficiency and acceptance angle characteristic of the system, showing similar acceptance angle values and lower efficiency values (due to a problem with the stiffness of the SOE material). Renzi et al. [17] characterised outdoors different Fresnel-based HCPV mono-modules, equipped with refractive SOEs and a geometrical concentration ratio of 1300×, including the acceptance angle characteristic. They developed a "freeform" lateral profile and hexagonal top surface SOE made of optical glass. Their results showed high-efficiency values for the system formed with the "freeform" SOE.

The work presented here is also related to Fresnel-based HCPV systems (units) with the emphasis on the influence of the refractive SOEs in the electrical performance of the systems. A better understanding of the behaviour of these systems will contribute to an improvement in their design to a higher performance. For that, a Fresnel-based HCPV unit using four different SOE's is characterised under controlled and repeatable indoor conditions and compared to determine the best SOE design. This

characterisation is performed at equivalent standard test conditions of AM 1.5D as well as at conditions far from them, in order to have a wider knowledge of the behaviour of these HCPV units. This knowledge will be useful for understanding the relationship with energy harvesting as a function of the changing outdoor conditions. In our experiments we use a CPV solar simulator "Helios 3198" which has a A+A+A+ rating and allows us to analyse the performance of the units by varying only one parameter (Incoming solar radiation level). On one hand, I-V curve measurements can be acquired under different spectral irradiance conditions, while maintaining constant the irradiance level. This is utilised to know the impact of the spectral change in the acceptance angle and in the electrical parameters, depending on the SOE in the Fresnel-based HCPV unit. On the other hand, I-V curve measurements are possible at different irradiance levels while the spectral conditions are delimited.

The refractive SOE experimentally analysed in this work were previouslyanalysed using a detailed optical simulation methodology including wavelength-dependent properties (implemented in TracePro optical software) [18]. The SOE designs resulted from that optical modelling were later manufactured and have been utilised in this study. The four refractive (as made of PMMA (poly(methyl-methacrylate)) SOEs fabricated are: i) Dielectric-cross compound-parabolic-concentrator (DCCPC, inspired in the SOE of [19] but similar to that of [20]), ii) (SIngle-Lens-Optical element) SILO-Pyramid, iii) Refractive truncated pyramid (RTP) and, iv) Trumpet. The SILO SOE, which works as a lens that images the Fresnel lens on the TJ solar cell, has been deeply analysed in the literature, including design modifications [21]. The other SOEs work under the effect of the total internal reflection (TIR) of light, being the RTP usual in commercial HCPV modules. Besides, an HCPV system without SOE is also mounted and characterised in order to differentiate the impact of the SOEs on the measured performances.

The characterisation includes the influence on each HCPV system performance (though their electrical parameters) of the different irradiance levels and different spectra (monitoring the spectral matching ratio [14, 22]). The acceptance angle characteristic of each HCPV unit is obtained at reference conditions and also at different irradiance and spectral conditions. In addition, this work is useful to improve the optical modelling already developed by comparing the experimental results with those obtained by ray tracing simulations, like all those related with the acceptance angle characteristic, the optical efficiency (obtained through the measured short-circuit current), etc.

Nomenclature

θ	Acceptance angle for I_{sc}	I_{sc}^{conc}	I_{sc} under concentrated illumination
*CAP**	Effective concentration-acceptance angle product	$I_{sc}^{1\ sun}$	I_{sc} at 1 sun of irradiance and reference spectrum
C_{eff}	Effective concentration	LCOE	Levelised Cost Of Electricity
DCCPC	Dielectric-Cross Compound-Parabolic-Concentrator	Mid	Middle subcell of a TJ solar cell
DNI	Direct Normal Irradiance	*n*	refractive index
DNI_{Top}	Effective irradiance for the top subcell	P_{mp}	Power at maximum power point
DNI_{Mid}	Effective irradiance for the middle subcell	PMMA	poly(methyl-methacrylate)
DUT	Device Under Test	V_{oc}	Voltage at open circuit
η	Efficiency	POE	Primary Optical Element
η_{opt}	Optical efficiency	RTP	Refractive Truncated Pyramid
η_{POE}	Optical efficiency of the POE	SCA	Solar Concentrator Assembly
η_{SOE}	Optical efficiency of the SOE	SILO	SIngle Lens Optical element
FF	Fill factor	*SMR*	Spectral Matching Ratio
I-V	Current-voltage	SOE	Secondary Optical Element
I_{sc}	Short-circuit current	TIR	Total Internal Reflection
		TJ	Triple-junction
		Top	Top subcell of a TJ solar cell

2. Description of the high-CPV units

2.1. Main characteristics of the analysed Fresnel HCPV units

The four Fresnel-based HCPV units investigated are equipped with refractive PMMA SOEs. Note that "unit" is used as a synonym of "mono-module" in this work. Besides, they are compared to an equivalent Fresnel-based HCPV unit without SOE in order to analyse the impact of the SOEs. This last unit is called "No-SOE" unit. These units were investigated at optical simulation level in a previous work [18]. As a summary of the characteristics, the Fresnel lens (primary optical element, POE) used is a square of 130 mm side, with 1.8 mm thickness, 152 mm of focal distance, facet spacing of 0.381 mm, and is made of PMMA. It was fabricated by the company ORAFOL Fresnel Optics GmbH [23]. The SOEs are made of PMMA, as commented above, with refractive index n = 1.495 at a wavelength of 540 nm [24]. These SOEs are: i) Dielectric-cross compound-parabolic-concentrator (DCCPC), ii) (SIngle-Lens-Optical element) SILO-Pyramid, iii) Refractive truncated pyramid (RTP) and, iv) Trumpet. Their profiles are sketched to scale in **Figure 1**. On one hand, **Figure 1** (b) shows a photograph of the four SOEs from a side but slight elevation respect to the SOEs. This would be referred, in terms of concentrator optics, as out of the acceptance angle of the SOEs, since the solar cell is not visible through entrance surfaces of the SOEs (applying the principle of reversibility of light). On the other hand, in **Figure 1** (b), the photograph is taken from a position slightly deviated from the zenith of the SOEs with the solar cells visible after a direct refraction on each SOE entrance surface and also after TIR (total internal reflection) on the sides of the RTP, DCCPC and Trumpet SOEs (the SILO-Pyramid SOE does not work under TIR in general). For these three SOEs, it is possible to see a gap between the images of the solar cells. This is due to the optical adhesive spilled over the solar cell and may cause light leakages [25].

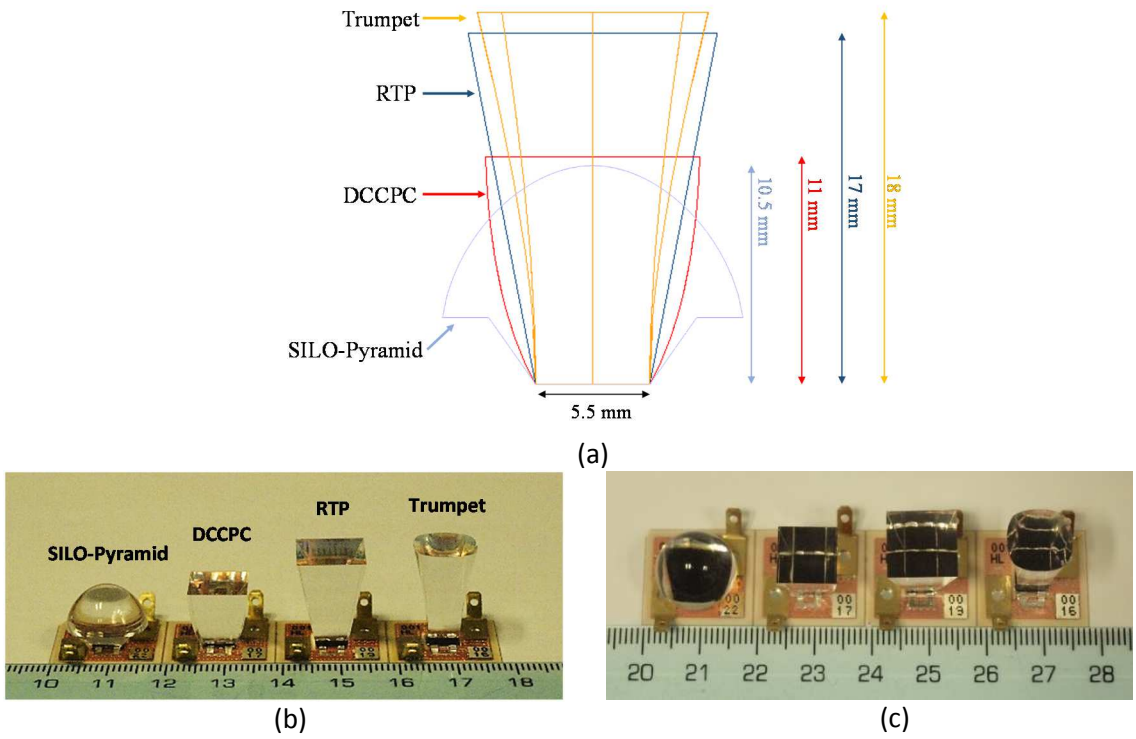

Figure 1. (a) Layout to scale of the four SOEs [18]. (b) Picture of the four SOEs mounted over the correspondent solar cell assemblies (SCAs) near a rule in millimetres. (c) Picture of the four concentrator receivers showing the images of the solar cells from a different position than the zenithally (related to the acceptance angle).

The five triple-junction (TJ) concentrator solar cells (GaInP/GaInAs/Ge) utilised during the experiment are CPV assemblies 3C42A purchased from AZUR SPACE Solar Power GmbH with grid optimised for high concentration and with an antireflective coating adapted to glass [26]. The TJ solar cells are a square of 5.5 mm side. From their datasheet, they have the next averaged values: (short-circuit current) I_{sc} = 2.28 A, (voltage at open circuit) V_{oc} = 3.08 V, (power at maximum power point) P_{mp} = 6.32 W, (fill factor) FF = 0.90 and, (efficiency) η = 41.4 % at 500 suns (1 sun = 1000 W/m^2) of DNI (direct normal irradiance) under the spectral distribution ASTM G173-03. All the relevant parameters concerning the POE and the TJ solar cell are gathered in **Table 1**.

Table 1. Parameters of lens and TJ solar cell assemblies 3C42A (from the datasheet) composing the Fresnel HCPV units.

Fresnel Lens		TJ Solar Cell[a]	
Parameter	Value	Parameter	Value
Size [mm^2]	130 x 130	Size [mm^2]	5.5 x 5.5
Focal distance [mm]	152.0	I_{sc} [A]	2.28
F-Number [-]	0.83	V_{oc} [V]	3.08
Facet spacing [mm]	0.381	P_{mp} [W]	6.32
Thickness [mm]	1.8	FF [-]	0.90
Geometrical concentration [×]	559	η [%]	41.4

[a]Data corresponding at 500 suns of irradiance and ASTM G173-03 spectrum.

In the previous work [18], those different Fresnel optical units were optically modelled and simulated through ray tracing software (including e.g. the spectral response of the TJ solar cell) . Those results will be compared with the experimental results and are summarised in **Table 2**.

Table 2. Summary of simulation results of each Fresnel-based HCPV unit of the previous work [18].

Parameter	No-SOE	SILO-Pyramid	DCCPC	RTP	Trumpet
Optical polychromatic efficiency [%]	87.7	83.4	83.6	81.8	81.0
Acceptance angle [º]	±0.50	±1.13	±1.03	±1.11	±0.96
Concentration acceptance-angle product, *CAP**	0.21	0.47	0.43	0.46	0.40
SOE height [mm]	-	10.5	11.0	17.0	18.0

2.2. Obtaining the different Fresnel HCPV units

Four different CPV assemblies, with TJ solar cells of the same type, are taken. Each SOE is obtained by CNC multiaxis machining from a block of PMMA. Then, the machined parts are polished in order to achieve surfaces with enough optical quality. This procedure allows to obtain these refractive SOEs at low cost. Each SOEs is mounted on one of the TJ solar cell. For that, an optical adhesive (Norland 68TH, n = 1.54 for cured polymer) is used to assure the optical coupling between SOE and TJ solar cell. The curing of the adhesive is achieved through UV illumination, as shown in **Figure 2**, using an UV lamp. Each Fresnel-based HCPV unit has in common the same single Fresnel lens, as their setup are not permanent.

Figure 2. UV curing lamp, used for solidifying the optical adhesive between solar cell and refractive SOE, emitting UV light downwards over the receivers (SCA plus SOE).

3. Experimental set-up

The indoor characterisation is conducted using the CPV Solar Simulator “Helios 3198” (Solar Added Value, SAV S.L.) [27-29]. This is a multi-flash solar simulator that produces collimated light at a maximum of a bit more than 1 sun of irradiation level and with a spectral matching ratio “top/mid” (*SMR(top/mid)*) near to 1 [14, 30, 31], which is defined as (Eq. 1):

$$SMR(top/\,mid) = \frac{I_{sc,top}^{meas} / I_{sc,top}^{1sun}}{I_{sc,mid}^{meas} / I_{sc,mid}^{1sun}} = \frac{DNI_{top}}{DNI_{mid}} \quad (1)$$

where $I_{sc,top}^{meas}$ is the measured short-circuit current of the top isotype-component cell, $I_{sc,top}^{1sun}$ is that at 1 sun of standard spectrum, and DNI_{top} is the top effective direct normal irradiance. It is analogous for the mid isotype-component cell. The laboratory temperature is maintained constant at 25 ºC. The simulated light can be tuned to match *SMR(top/mid)* = 1 at different irradiance levels by using different optical filters, including neutral filters (meshes) of 50% and 30% of transmittance. In the standard configuration, the xenon discharge arc bulb is protected by a glass cover which partially filters UV components the flash light. In addition, that glass cover can be replaced by other one with very less UV filtering. See the transmittance values of the utilised non-neutral filters "SAVF-050" and "SAVF-000", in **Figure 3**, both with lower transmittance at shorter wavelengths.

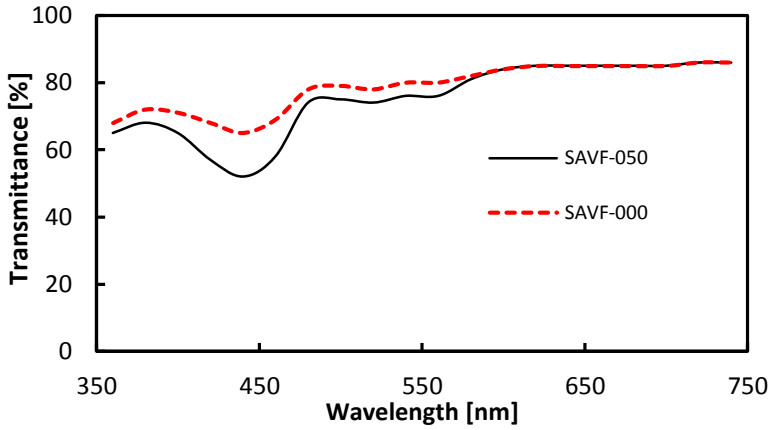

Figure 3. Non-neutral filters utilised (provided by the company Solar Added Value) after the flash lamp in order to tune the spectrum of the light impinging the Fresnel-based HCPV units.

The HCPV devices are mounted on a 2-axis orientable support structure, thus allowing the acceptance angle characterisation of any device under test (DUT). This angular characterisation is performed by using a laser pointer fixed to the support structure. The vertical angle of rotation of the DUT is monitored by measuring the location of the laser spot on a screen at around 7 meters distance. A modelling lamp (halogen lamp), located at the centre of the flash bulb, provides continuous light to be used for the coarse alignment of the DUT with respect to the incoming simulated light. Simultaneously to the I-V curve acquisition, the spectral conditions of the incoming light are monitored by using a Spectroheliometer (isotype component cells) of the company SAV.

For the experiments of this work, a conventional optical breadboard is fixed to the 2-axis orientable support structure. Both Fresnel lens and receiver are mounted on the optical breadboard (see **Figure 4**). The spatial location of the receivers is adjusted by using some rails and also an adjustable mount (standard optomechanical components). Maintaining the Fresnel lens in a fixed position, the receivers are located being the concentrated light spot (lens focus) at the centre of the SOE's surface. A fine adjustment of the receivers is done by maximising the I_{sc} of the measured I-V curves. Then that position of each receiver respect to the Fresnel lens is maintained fixed for the whole characterisation process of each HCPV unit.

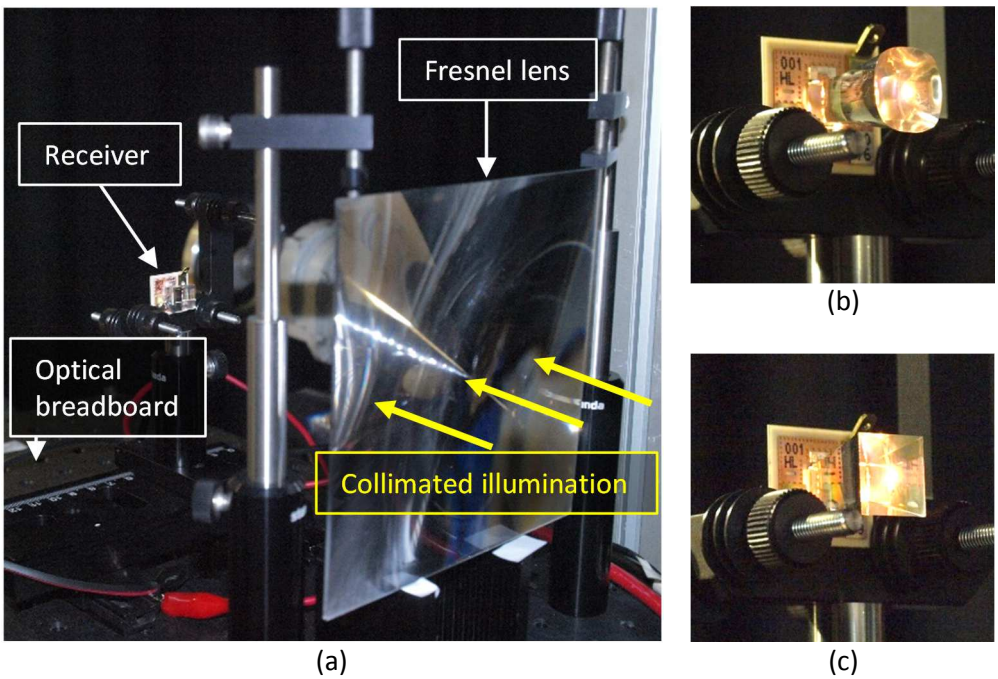

Figure 4. (a) Picture of the experimental setup for the Fresnel-based HCPV units. The spatial location of the receiver is adjustable by using rails and mounts. (b) Detail of the receiver with the Trumpet SOE aligned under the continuous light concentrated into a spot at the centre of the Trumpet's entrance surface. (c) Analogous to (b) but with the RTP SOE.

4. Analysis of results

4.1. I-V characteristics at reference conditions

The I-V curves of all the analysed Fresnel HCPV units at 1000 W/m^2 (1 sun) of irradiance, temperature of 25 ºC and spectral conditions equivalent to AM-1.5D (ASTM G173-03), are plotted in Figure 5. Note that in this work, the temperature of the TJ solar cell is always constant at 25 ºC for the experiments and also for the theoretical considerations. The main important parameters related to those I-V curves are summarised in Table 3. The unit without SOE presents the highest I_{sc} value (2.03 A) since less optical steps are involved, and therefore, less optical losses. The four HCPV units with SOE present I_{sc} values between 1.84 and 1.95 A at 1 sun. Among those HCPV units, the lowest I_{sc} value corresponds to the RTP unit.

It is useful to utilise the concept of effective concentration, C_{eff}, which is useful to know at which concentration the TJ solar cell is really working and is defined as (Eq. 2):

$$C_{eff} = \frac{I_{sc}^{conc}}{I_{sc}^{1sun}} \quad (2)$$

where $I_{sc}{}^{conc}$ formally represents the short-circuit current of the solar cell under concentrated illumination when the HCPV unit is illuminated under 1 sun of *DNI* of standard spectrum, thus the TJ

solar cell is under the concentrated illumination provided by the Fresnel lens, and $I_{sc}^{1\ sun}$ is the short-circuit current of the bare TJ solar cell (no optical system) when it is also illuminated under 1 sun of *DNI* of standard spectrum. Taking into account the I_{sc} values at 500 suns of Table 1, these I_{sc} measured values correspond to effective concentrations between 403 suns (RTP unit) and 427 suns (DCCPC unit).

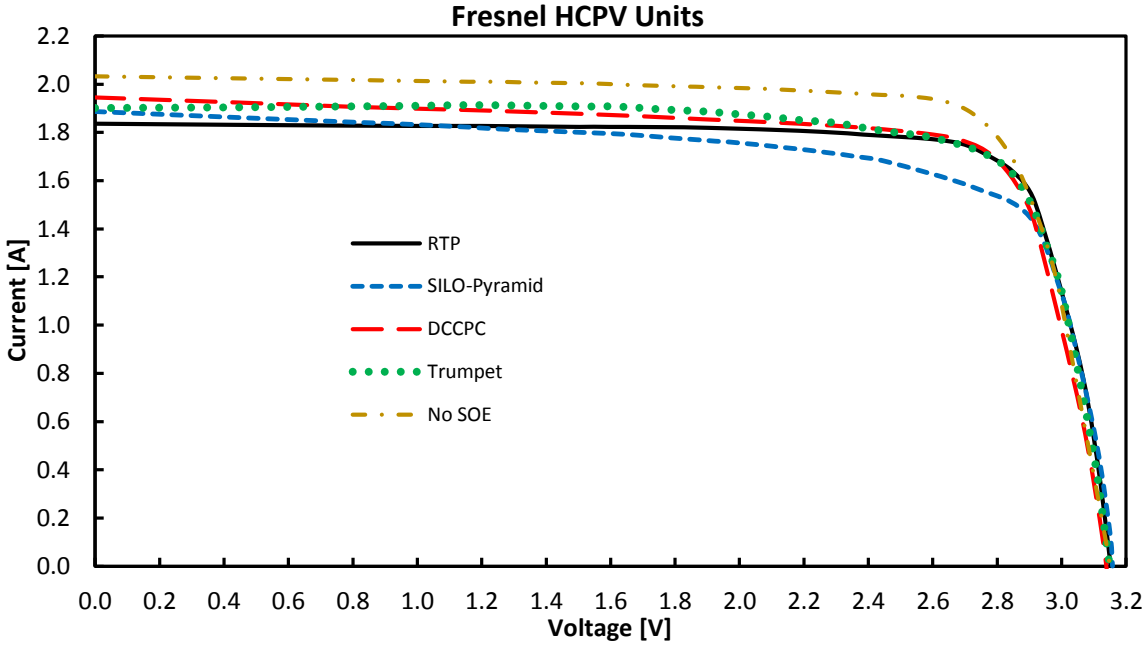

Figure 5. I-V curves of the different Fresnel HCPV units at 1000 W/m^2 of irradiance, temperature of 25 ºC and *SMR(top/mid)* = 1 ± 0.5.

Table 3. I-V curve indoor measurement parameters of the different Fresnel-based HCPV units at *DNI* = 1000 W/m^2.

HCPV Unit	V_{oc} [V]	I_{sc} [A]	P_{mp} [W]	V_{mp} [V]	I_{mp} [A]	*FF* [-]	η [-]	C_{eff} [suns]
RTP	3.16	1.84	4.7	2.76	1.73	0.82	28.0	403
SILO-Pyramid	3.16	1.89	4.3	2.69	1.61	0.72	25.5	414
DCCPC	3.14	1.95	4.8	2.76	1.72	0.78	28.2	427
Trumpet	3.15	1.90	4.7	2.75	1.72	0.79	27.9	417
No-SOE	3.15	2.03	5.1	2.71	1.89	0.80	30.3	446

The V_{oc} values are between 3.14 and 3.16 V. All the units with SOE present P_{mp} values between 4.7 and 4.8 W except for the case of that with the SILO-Pyramid with only 4.3 W. This last case is related to a lower *FF* value, 0.72, for this unit. The reason of this low *FF* could be an imperfect mounting of the SOE on the TJ solar cell. The RTP unit presents the best *FF* with 0.82, even better than the unit without SOE (*FF* = 0.80). In general, the *FF* values lower than expected. This may be due to an effect of the contribution of the I-V curve of the bottom subcell when that is producing similar current than the other subcells, as it is explained in [32]. That situation, with the bottom subcell without an important excess of current generation, could be due to the irradiance absorption within the PMMA material in the infrared range, thus affecting the bottom subcell. The efficiency of the units ranges from a minimum of 25.5% (SILO-Pyramid unit) to a maximum of 28.2% (Trumpet unit). This last value is around 7% lower than

without SOE (30.3%), which supposes a loss of efficiency but a gain in acceptance angle, as it is shown in Section 4.2.

The effective concentration allows to calculate the optical efficiency, η_{opt}, of each unit as (Eq. 3):

$$\eta_{opt} = \frac{C_{eff}}{C_g} = \frac{1}{C_g} \cdot \frac{I_{sc}^{conc}}{I_{sc}^{1sun}} \quad (3)$$

The η_{opt} of the units with SOE is between 72.0% and 76.3%, whereas for the unit without SOE it is 79.8%. η_{opt} can be split into two factors (two optical steps), one of POE and other of SOE (Eq. 4):

$$\eta_{opt} = \eta_{POE} \cdot \eta_{SOE} \quad (4)$$

where η_{POE} is the optical efficiency of the POE and η_{SOE} is that of the SOE. The corresponding values are summarised as in **Table 4**, assuming the same value of η_{POE} since the same single Fresnel lens was used for each HCPV. Thus, the unit without SOE can be used to calculate η_{POE} and then, that value can be used to calculate the correspondent η_{SOE} of each unit with SOE.

Table 4. Summary of measured and simulated optical efficiency values.

Experimental measurements					Optical simulation results [18]		
HCPV Unit	η [-]	η_{opt} [-]	η_{POE} [-]	η_{SOE} [-]	η_{opt} [-]	η_{POE} [-]	η_{SOE} [-]
RTP	28.0	72.0	79.8	90.3	82.0	87.7	93.5
SILO-Pyramid	25.5	74.0	79.8	92.8	83.6	87.7	95.3
DCCPC	28.2	76.3	79.8	95.7	83.7	87.7	95.5
Trumpet	27.9	74.5	79.8	93.5	81.2	87.7	92.6
No-SOE	30.3	79.8	79.8	-	87.7	87.7	-

The measured optical efficiency of the unit without SOE, 79.8%, is much lower than in the optical simulations, 87.7%. This overestimation of the Fresnel lens performance may be due to the difference, related with the manufacturing tolerances, between the geometry of a real lens and that ideal lens simulated through ray tracing [33]. Concerning the η_{SOE} measurement values, these show a good match to those of the optical simulations, and are between 90.3% (RTP unit) and 95.7% (DCCPC unit), with an average of 93.1% (being 94.2% in the optical simulations). The DCCPC unit performs the highest η_{SOE} both in experimental measurements and in ray tracing simulations (95.5%).

It is interesting to compare the cases of the RTP and SILO-Pyramid units. On one hand, the RTP unit shows the lowest η_{SOE} by far (90.3%), although its η is the second best one (28.0%). On the other hand, the SILO-Pyramid unit shows a better η_{SOE} (92.8%), whereas its η is the lowest one (25.5%). This contradictory performance results could be attributed in terms of the *FF* and the illumination uniformity [34], since *FF* is lowest for the case of the SILO-Pyramid unit and highest for the RTP unit. Therefore, the performance of the unit at maximum power point is not directly comparable with the optical efficiency of the SOE.

4.2. Impact of incident angle

In order to obtain the angular performance of these Fresnel-based HCPV units, their acceptance angle characterisation is performed indoors at a simulated irradiance of 1000 W/m^2.

The measured values of I_{sc} acceptance angle and *CAP** (effective concentration-angle product) for all the Fresnel-based HCPV units are gathered in **Table 5**. In addition, in order to compare those results with the optical simulations, both simulated η_{opt} acceptance angle and *CAP** values are also included in **Table 5**. Note that the acceptance angle of the simulated η_{opt} should ideally equal that of measured I_{sc}, since both magnitudes are directly proportional each other (Eq. 3). The effective concentration-angle product is a parameter that, for ideal concentrator systems, equals the refractive index of the medium surrounding the solar cell, and is defined as (Eq. 5) [35]:

$$CAP^* = \sqrt{C_g} \cdot \sin\theta \tag{5}$$

where θ is the I_{sc} acceptance angle (the angle for which I_{sc} is 90% of the maximum value). Note that the term "acceptance angle" is referred to that of I_{sc} if no other specification is denoted.

Table 5. Acceptance angle values of each Fresnel-based HCPV unit by both experimental indoor characterisation and optical simulations.

Experimental measurements			Optical simulation results [18]	
HCPV Unit	I_{sc} acceptance angle [º]	CAP^* [-]	η_{opt} acceptance angle [º]	CAP^* [-]
RTP	±1.09	0.45	±1.11	0.46
SILO-Pyramid	±0.83	0.34	±1.13	0.47
DCCPC	±0.58	0.24	±1.03	0.43
Trumpet	±0.80	0.33	±0.96	0.40
No-SOE	±0.48	0.20	±0.50	0.21

In terms of I_{sc} and considering only the units with SOEs, the lowest acceptance angle value is that of the DCCPC unit (±0.58º), whereas the highest one is that of the RPT unit (±1.09º). The other two units, SILO-Pyramid and Trumpet, show similar θ to each other, roughly ±0.80º. The acceptance angle of the DCCPC unit is clearly lower than expected, maybe due to manufacturing tolerances or errors by hand mounting. The unit without SOE presents the lowest I_{sc} acceptance angle value, as expected since the SOEs are designed to increase de acceptance angle. The measured *CAP** values range from 0.24 (irregular low value for the DCCPC unit) to 0.45 (RTP unit), being 0.20 for the unit without SOE. These *CAP** values of the SILO-Pyramid, RTP and No-SOE units are similar than those presented by Benítez et al. [35]. The RTP unit represents the nearest case to the ideal concentrator among these units.

Comparing with the optical simulation results, the measured acceptance angle and *CAP** values are in general lower than in the simulations for all the units. The RTP unit presents similar values of acceptance angle in both experimental and simulation results (±1.09º and ±1.11º, respectively). Therefore, it shows almost the same values of *CAP** comparing both situations (measured 0.45 and simulated 0.46). The measured acceptance angle of the Trumpet unit is slightly lower than in the simulations (±0.80º and ±0.96º respectively). The SILO-Pyramid unit provides low measured acceptance angle values respect to

the simulation ones (±0.83º and ±1.13º, respectively). In the worst case, the DCCPC unit shows the highest deviation of experimental I_{sc} acceptance angle respect to the simulations (±0.58º and ±1.03º, respectively), and also for *CAP** value (0.24 and 0.43, respectively). Those deviations to the optical simulation results could be explained in terms of manufacturing tolerances or hand mounting errors related, especially for the case of the DCCPC unit. Note that the unit without SOE shows similar results by both experimental and simulations, conferring strength to the experimental method.

The results normalised to the maximum I_{sc} values of each unit constitute their acceptance angle characteristics. They are almost symmetrical with respect to the vertical axis of **Figure 6** (not completely due to defects or imperfections by the manufacturing and assembly of the SOEs) and are bell-shaped. Up to misalignment angles of around ±0.5º, all the units present roughly similar angular performance. However, at misalignment angles of ±1º, there are notable differences among the units with SOEs: the RTP unit shows the highest normalised I_{sc} values; the DCCPC unit shows the lowest values; finally, the Trumpet and SILO-Pyramid units present similar normalised values. The acceptance angle curve of the DCCPC unit presents a fast drop for angles from around ±0.6º to ±1º. This drop is not observed for the other SOE units, and moreover, it was not obtained by the ray tracing simulations (as shown in **Figure 7**). It may be due to manufacturing tolerances. The unit without SOE shows the worst acceptance angle characteristic, as expected.

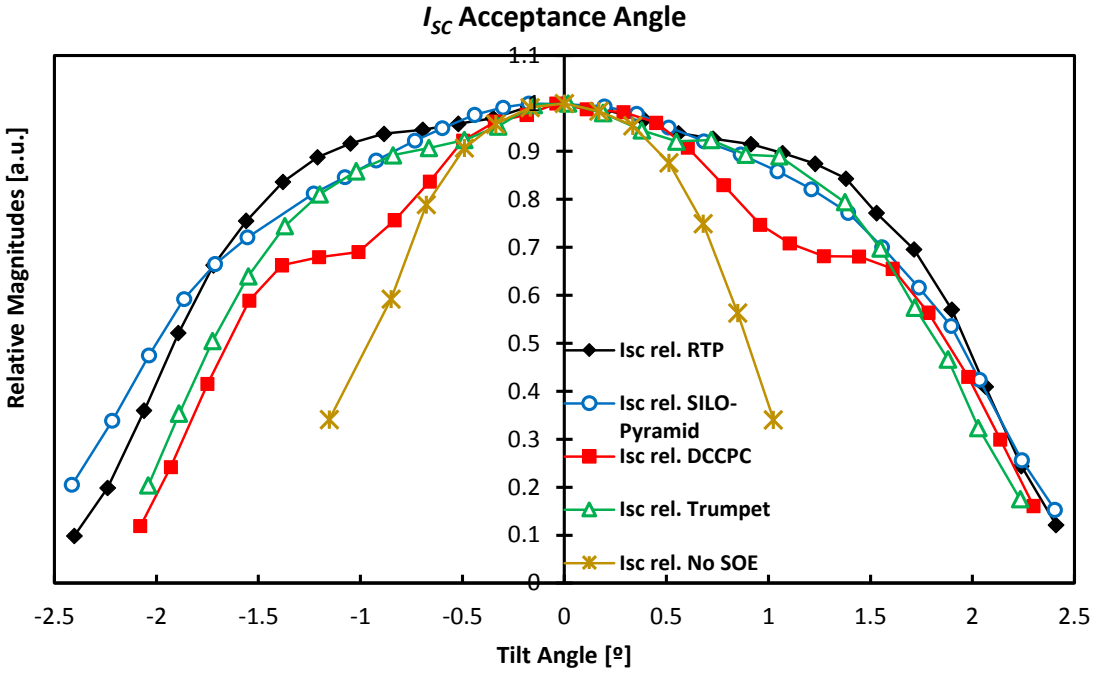

Figure 6. Normalised measured acceptance angle characteristics of the Fresnel-based HCPV units, including the unit without SOE, at 1000 W/m^2.

In order to compare with the results presented in the previous work (optical simulations) [18], the experimental results can be plotted in terms of the measured optical efficiency (**Figure 7**) by using Eq. 7. The measured lower η_{opt} values than in optical simulations can be understood as a systematic underestimation (due to the reduced Fresnel lens η_{opt}). In addition, the general angular behaviour is similar to both measurements and simulations. However, in the case of the DCCPC unit, its measured

angular behaviour is different than in the simulations, as commented above. That may be due to manufacturing errors by the machining of a parabolic shape, since the rays are bouncing off the sides more intensively by misalignment angles. Another difference takes place at misalignment angles greater than around 1.4º, since in the optical simulations, the different optical polychromatic efficiency curves separate each other, whereas in the indoor measurements, they remain together, with very similar values. Note the similar angular behaviour of the unit without SOE within experiment and simulation.

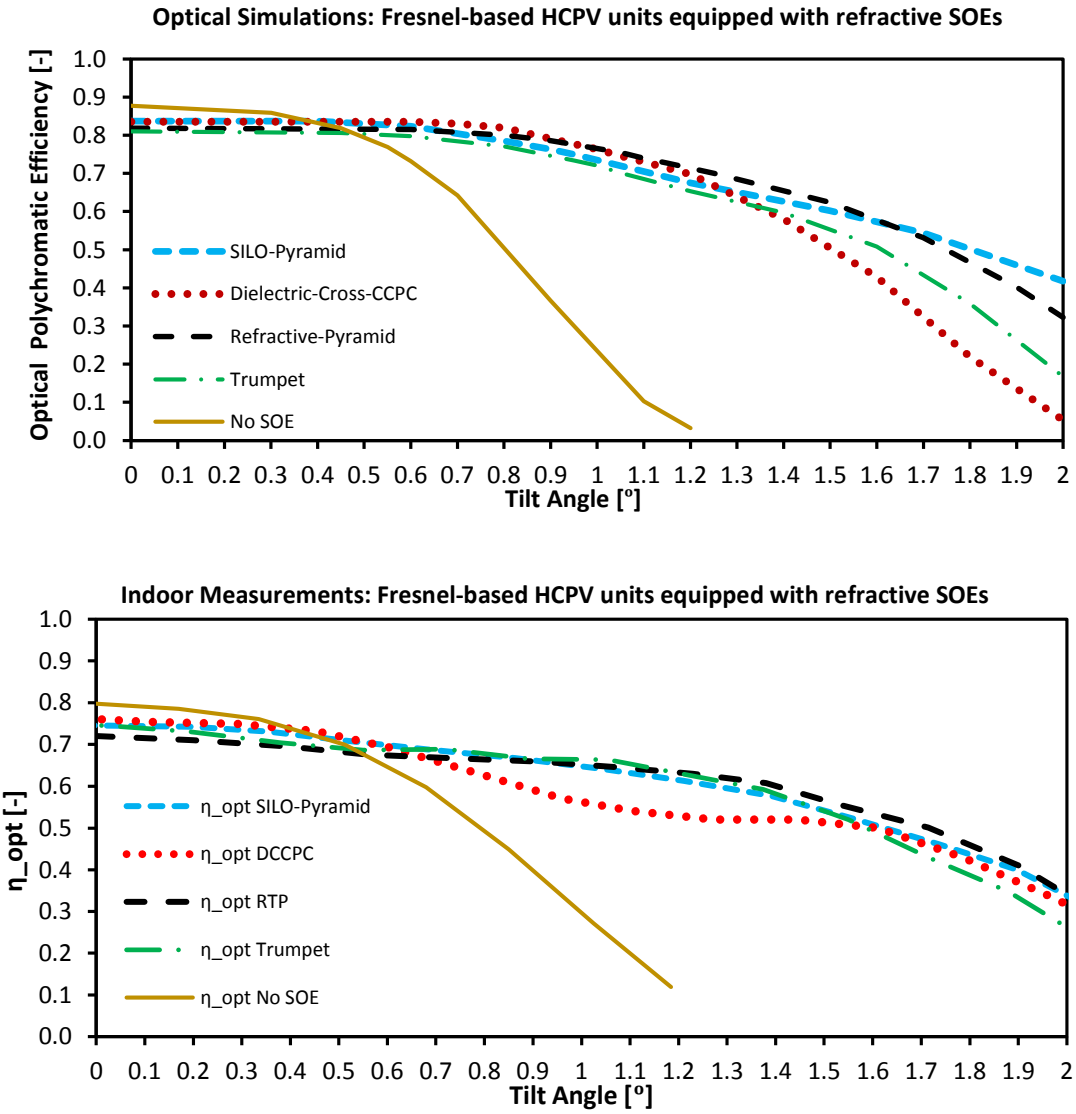

Figure 7. Optical efficiency of all the Fresnel-based HCPV units analysed from both optical simulations (up) [18] and indoor measurements (down).

Concerning the variation of the power of each unit under the changing misalignment angle, P_{mp} acceptance angle values (relative to the angle for which the measured power is 90% of the maximum value) can be obtained (see Table 6):

Table 6. Measured P_{mp} acceptance angle values of all the Fresnel-based HCPV.

HCPV Unit	P_{mp} acceptance angle [º]
RTP	±0.70
SILO-Pyramid	±0.98
DCCPC	±0.61
Trumpet	±0.36
No-SOE	±0.50

The measured P_{mp} acceptance angle values of these units with SOEs range from ±0.36º (Trumpet unit) to ±0.98º (SILO-Pyramid unit). In the case of the Trumpet SOE, it was found that the P_{mp} acceptance angle is much lower than for the unit without SOE as can be seen in **Figure 8**. Note that this last lower value does not imply a low I_{sc} acceptance angle value for the Trumpet unit (±0.80º). The experimental values of acceptance angle for P_{mp} are very different to the I_{sc} acceptance angle values for all the cases [36], except for the DCCPC unit. The only case with P_{mp} acceptance angle clearly superior to that of I_{sc} is the SILO-Pyramid unit (±0.98º and ±0.83º respectively). From the point of view of the energy harvesting, a high P_{mp} acceptance angle value is recommended, since it will suppose that the HCPV system performs with greater tolerance to misalignments. Considering simultaneously these P_{mp} acceptance angle values and the electrical efficiencies of the units (**Table 4**), the RTP unit presents the best trade-off between both magnitudes, with P_{mp} acceptance angle of ±0.70º and η = 28.0%.

Regarding the measured angular characteristic of the normalised P_{mp}, it presents a similar shape to that of I_{sc}, as shown in **Figure 8**, i.e. bell-shaped curves and a different behaviour of the DCCPC unit respect to the other units. In addition, the RTP and Trumpet units show a central peak within the bell-shape curve, much narrower than that of the DCCPC unit. These three units working under TIR, RTP, Trumpet and DCCPC show a similar central peak within the bell-shape acceptance angle curve. That may be caused by the TIR in the SOEs.

In the case of normalised both *FF* and V_{oc}, these parameters are less sensitive to angular misalignments, especially for the case of V_{oc}. See in **Figure 9** the corresponding normalised FF and V_{oc} to with respect to the tilt angle. Normalised *FF* values oscillate although they are greater for increased misalignment angles, with a total relative range of around 20% (SILO-Pyramid unit). Normalised V_{oc} values decrease for increased tilt angles with a very low relative range, with a maximum of 6% (RTP unit). The No-SOE unit presents the fastest reduction of normalised V_{oc}, as expected, due to the lowest acceptance angle.

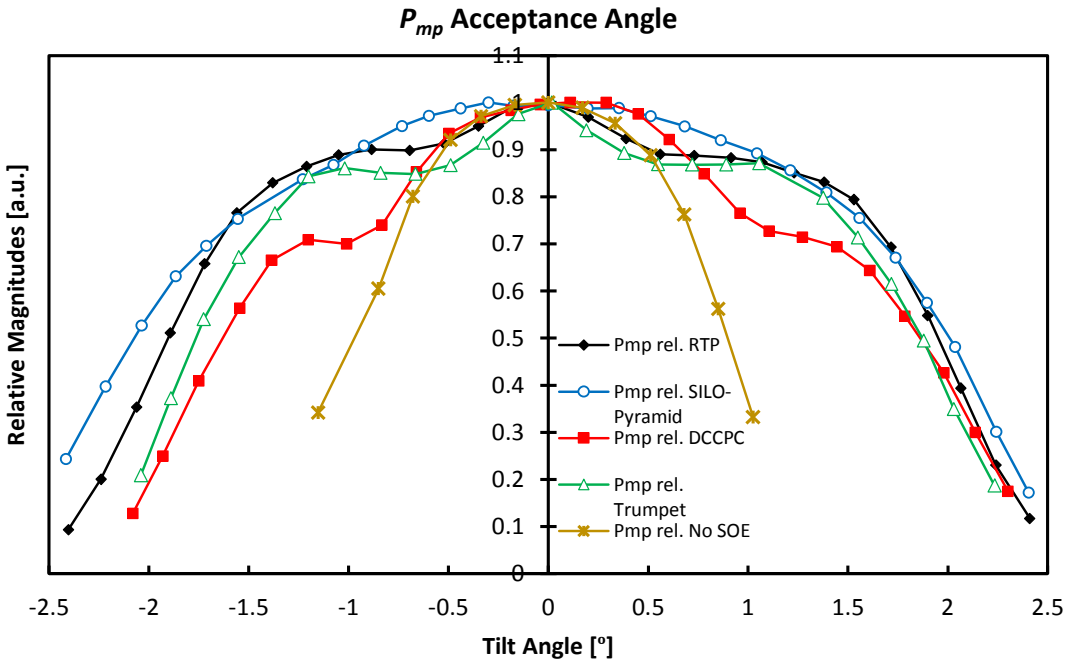

Figure 8. Angular behaviour of the normalised P_{mp} values of all the Fresnel-based HCPV units.

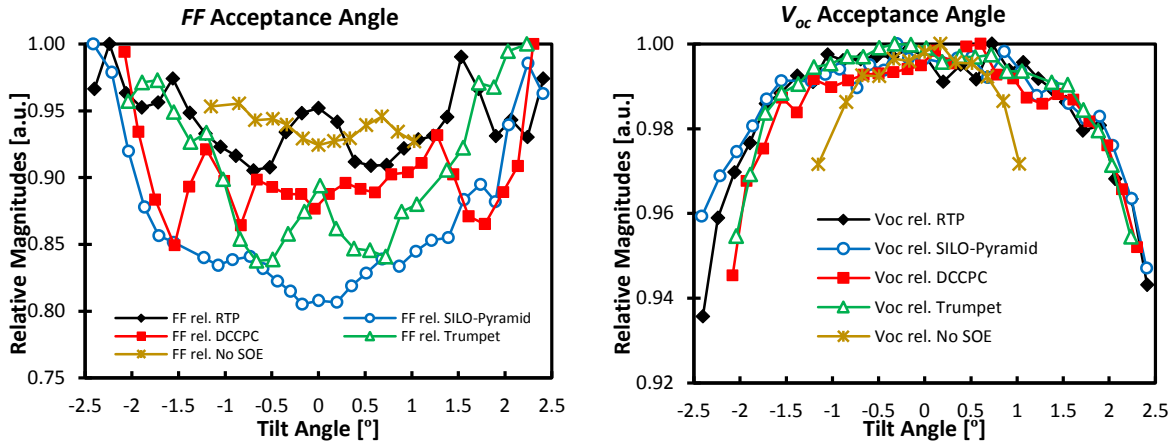

Figure 9. Measured *FF* and V_{oc} normalised (to the maximum values) angular characteristics of all the Fresnel-based HCPV units analysed.

4.3. Impact of DNI

In this section, the experimental results of the four systems are analysed at the irradiance levels (*DNI*) of 450, 650 and 850 W/m^2. In **Figure 10**, the acceptance angle of each Fresnel-based HCPV unit is plotted versus the selected irradiance (in natural logarithmic scale) of the I-V curve measurements involved. Note that all those I-V curves measured to calculate the acceptance angle values were acquired in the range of *SMR(top/mid)* between 0.95 and 1.05, in order to avoid spectral effects. With that restricted spectral conditions, and assuming that I_{sc} grows linearly with the *DNI*, the optical efficiency is maintained constant. Note also that those lines between experimental points are only included to facilitate the visualisation of the results (this is applicable to the rest of the figures of this and the next subsection).

The acceptance angle values range from ±0.55º (DCCPC unit at ln(*DNI*) = 6.48 W/m^2) to ±1.14º (RTP unit at ln(*DNI*) = 6.11 W/m^2), which is a similar range than that presented in **Table 5** (from ±0.58º to ±1.09º). The averaged acceptance angle values are, from lowest to greatest: ±0.57º, ±0.78º, ±0.79º and ±1.06º for the DCCPC, SILO-Pyramid, Trumpet and RTP units, respectively.

In general, all the SOE units present a remarkable constant performance under variations of irradiance with some exceptions. The Trumpet unit shows an acceptance angle value of ±0.65º. The maximum acceptance angle variation (standard deviation over average) is found to be 5.9% (RTP unit) whereas the minimum one is 3.0% (DCCPC unit).

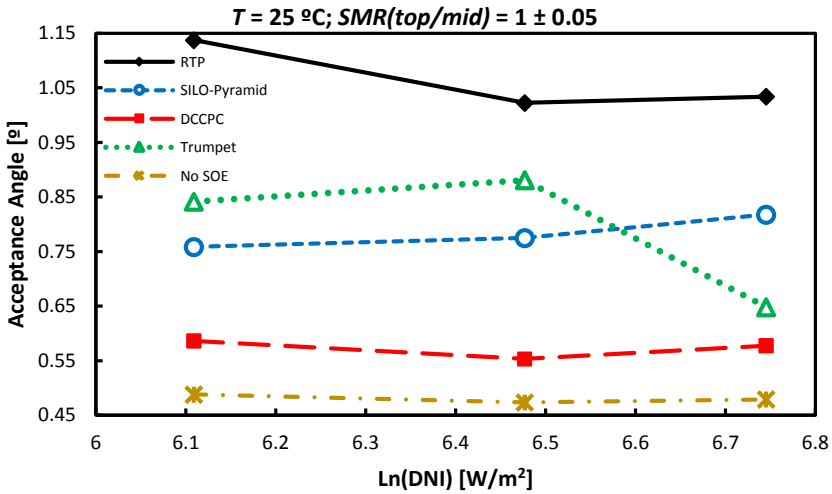

Figure 10. Indoor acceptance angle as a function of the *DNI* for a *SMR(top/mid)* = 1 ± 0.05.

For those same three different irradiance levels, the measured electrical parameters of the Fresnel-based HCPV units, like η, *FF* and V_{oc}, can be analysed under the spectral restriction of *SMR(top/mid)* = 1 ± 0.05. These results are shown in the three plots of **Figure 11**. The V_{oc} values manifest a linear trend versus ln(*DNI*), as expected [27], with determination coefficients R^2 between 0.97 and 0.99, and with slopes as in **Figure 11** between 0.13 and 0.14, with slight variation among the units. Note that these linear fits corresponding to the units with SOEs present similar slope values than that of the No-SOE unit. Thus, the SOEs have no clear effect in the relation of V_{oc} with the irradiance.

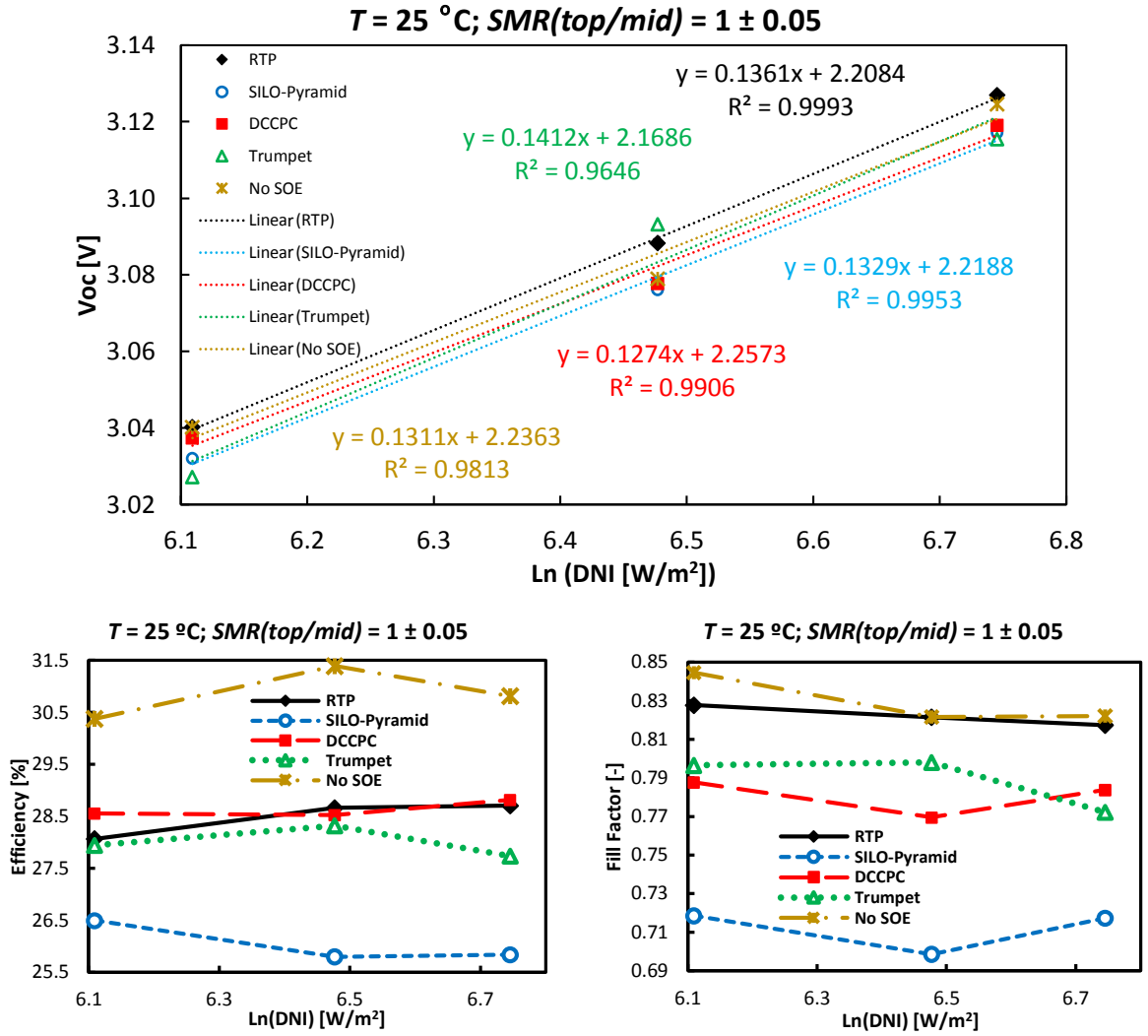

Figure 11. Indoor measured electrical parameters of the Fresnel-based HCPV units analysed as a function of the *DNI* maintaining *SMR(top/bot)* between 0.95 and 1.05: (up) V_{oc}, (down left) η, and (down right) *FF*.

Regarding the efficiency values of the SOE units, these range from a minimum of 25.8% (SILO-Pyramid unit at ln(*DNI*) = 6.48 W/m^2) to 28.8% (DCCPC unit at ln(*DNI*) = 6.75 W/m^2). That range is similar to those values of **Table 4** (from 25.5% to 28.2%). The averaged efficiency values are: 26.04%, 28.00%, 28.48% and 28.63%, for the SILO-Pyramid, Trumpet, RTP and DCCPC unit, respectively. That ranking among the units is not maintained in the case of the DCCPC unit, with an intermediate value between those of Trumpet and RTP units for an irradiance of ln(*DNI*) = 6.48 W/m^2. However, these three units show similar values in general. Taking into account the variability of the efficiency values of each unit, it is very low in general, with a total maximum value of standard deviation over an average of 1.5% (DCCPC unit). With those results, no clear dependence of the efficiency, in general, as a function of the irradiance (ln(*DNI*)) is observed for these units. Comparing with the unit without SOE, with an averaged efficiency of 30.9%, the effect of the SOEs is to reduce the efficiency, as commented in Subsection 4.1. In addition, there is no a different behaviour of the efficiency No-SOE unit, as a function of the irradiance,

respect to the SOE units. Thus, the SOEs do not have an impact on the efficiency of the Fresnel-based HCPV units with the irradiance.

Considering the fill factor values of the SOE units, these range from a minimum of 0.70 (SILO-Pyramid unit at ln(*DNI*) = 6.48 W/m^2) to 0.83 (RTP unit at ln(*DNI*) = 6.11 W/m^2). This range is similar than that of **Table 3** (from 0.72 to 0.82). The averaged *FF* values are: 0.71, 0.78, 0.79 and 0.82, for the SILO-Pyramid, DCCPC, Trumpet and RTP units, respectively. This ranking is maintained in general for the units except for the DCCPC and Trumpet units at ln(*DNI*) = 6.75 W/m^2). The variations in the *FF* values are very low, with a standard deviation over the average values with a maximum of 1.8% for the case of the Trumpet unit. The No-SOE unit shows, in general, a slightly higher FF than the SOE units, with an average of 0.83. Thus, the SOEs may provoke a small reduction of the *FF*, which may be due to the manufacturing errors of them. Therefore, the fill factor exhibits no clear dependence on the irradiance, in the range of this analysis, for these Fresnel-based HCPV units.

4.4. Impact of spectrum

In this subsection, I-V curve electrical parameters and acceptance angle measurements are analysed at different spectral conditions.

In order to analyse the impact of the spectral conditions in the acceptance angle, these correspondent I-V curve measurements are acquired for a fixed *DNI* (in order to avoid any possible impact of the changing irradiance) while *SMR(top/mid)* is changed from around 0.894 to 1.098 (see **Figure 12**). These acceptance angle values range from a minimum of ±0.57º (DCCPC unit, at *SMR(top/mid)* = 0.896) to a maximum of ±1.17º (RTP unit at *SMR(top/mid)* = 0.902), which is a similar range to that of **Table 5** (from ±0.58º to ±1.09º). The averaged acceptance angle values are: ±0.58º, ±0.82º, ±0.85º and ±1.14º, for the DCCPC, SILO-Pyramid, Trumpet and RTP units, respectively. Note that this ranking is maintained in general except for the value of the Trumpet unit, ±0.69º at *SMR(top/mid)* = 0.97. The results present low variability in general, with a maximum standard deviation over the average of 3.8%, except for the case of the Trumpet unit (with a questionable measurement point at *SMR(top/mid)* = 0.97). Considering those results, no clear general dependence of the acceptance angle of the SOE units can be established as a function of the *SMR(top/mid)*. Moreover, the SOEs have no impact on the relation of the acceptance angle with the *SMR(top/mid)*, since there is no clear difference in the behaviour of the SOE units respect to the unit without SOE.

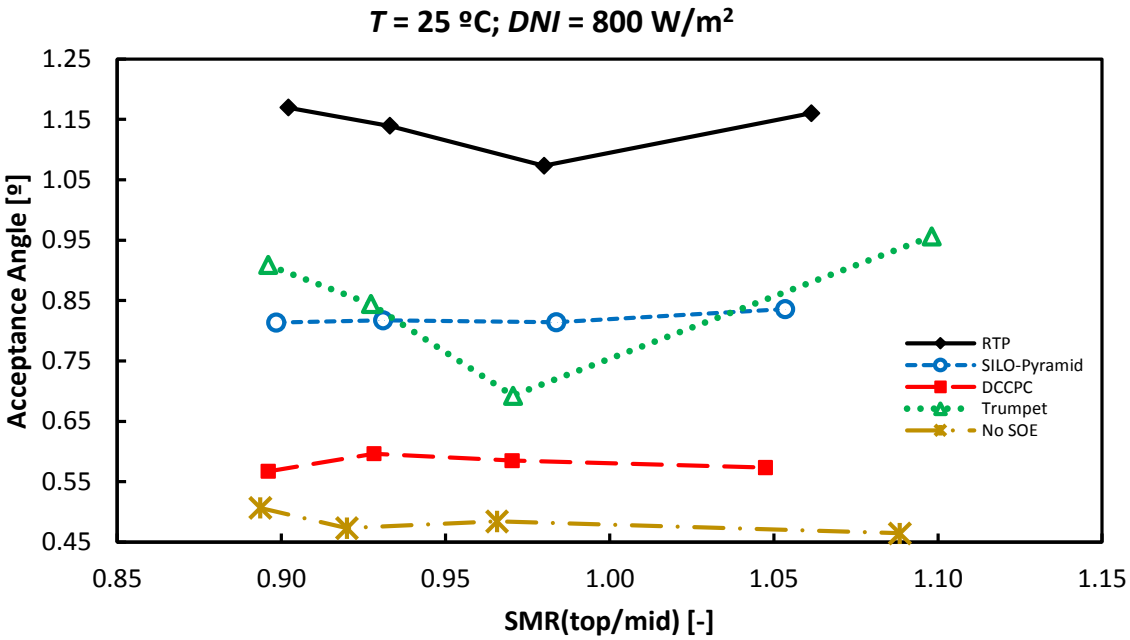

Figure 12. The acceptance angle of the analysed Fresnel-based HCPV units for a fixed *DNI* = 800 W/m^2 at different spectral conditions.

I-V curve electrical parameters, V_{oc}, η and *FF* for a fixed *DNI* = 800 W/m^2 are plotted in **Figure 13** within a spectral range of 0.894 < *SMR(top/mid)* < 1.099. Regarding the V_{oc} values, the range of variation is very low, from 3.10 V (DCCPC at *SMR(top/mid)* = 1.05) to 3.13 V (RTP unit at *SMR(top/mid)* = 0.98), which presents lower absolute values than those at reference conditions (3.14 V to 3.16 V, in **Table 3**). The SOE units do not present a stable ranking of V_{oc} values for the different spectral conditions. Their variability is very low, with standard deviation values over the average no greater than 0.35% (DCCPC unit). No clear dependence of the V_{oc} in the SOE units respect to the *SMR(top/mid)* is found. Thus, no effect of the SOEs is found on the V_{oc} respect to the spectral conditions. In addition, no different behaviour is found for the No-SOE unit, therefore, the SOEs do not alter the V_{oc} values respect to the spectral conditions.

Concerning the efficiency values, these range from 25.2% (SILO-Pyramid unit at *SMR(top/mid)* = 1.05) to 31.14% (DCCPC unit at *SMR(top/mid)* = 0.93). The averaged η values are: 27.1%, 29.1%, 29.4% and 29.8% for the SILO-Pyramid, Trumpet, RTP and DCCPC units, respectively. These last three units show similar values each other for all the spectral range, whereas the SILO-Pyramid unit presents the lowest values for all the *SMR(top/mid)* values. The variability of the results is low, with standard deviation over the average lower than 6.5% (SILO-Pyramid unit). However, the efficiency values tend to be slightly lower (2-3% absolute) at higher *SMR(top/mid)* values than 1.0. In the most extreme case, the SILO-Pyramid unit shows a decrease from 28.9% of efficiency at *SMR(top/mid)* = 0.90 to 25.2% at *SMR(top/mid)* = 1.05, which supposes an absolute reduction of around 3.7% (around 12% in relative terms) of efficiency. Therefore, a general slightly decreasing trend is attributed to the efficiency for *SMR(top/mid)* greater than 1.0. Besides the lower efficiency of the SOE units respect to the No-SOE unit, as commented already, there is no different behaviour for this unit. Thus, no effect of the SOEs can be

established in relation to the behaviour of these Fresnel-based HCPV units with the different spectral conditions.

In relation to the *FF* values of the units with SOE, they range from 0.70 (SILO-Pyramid unit at *SMR(top/mid)* = 1.05) to 0.83 (RTP unit at *SMR(top/mid)* = 0.93), which is a similar range than that of **Table 3** (from 0.72 to 0.82). Three units with SOE present similar average values of *FF*: 0.79, 0.79, 0.82 for the Trumpet, DCCPC and RTP units, respectively. These three units also have similar values each other for the different spectral conditions. Whereas the SILO-Pyramid shows the lowest *FF* average: 0.72, and always the lowest values for the different spectral conditions. The variability is very low, with maximal standard deviation over average lower than 1.8% (RTP unit) and also there is no clear trend in the *FF* values respect to the spectral conditions. Therefore, the SOEs have no impact on the spectral behaviour of the *FF* of these Fresnel-based HCPV units. In addition, the *FF* values of the NO-SOE present no important differences respect to those of the units with SOE. Thus, the SOE's have no impact on the *FF* values, except for the case of SILO-Pyramid unit, which may be due to by hand mounting defect.

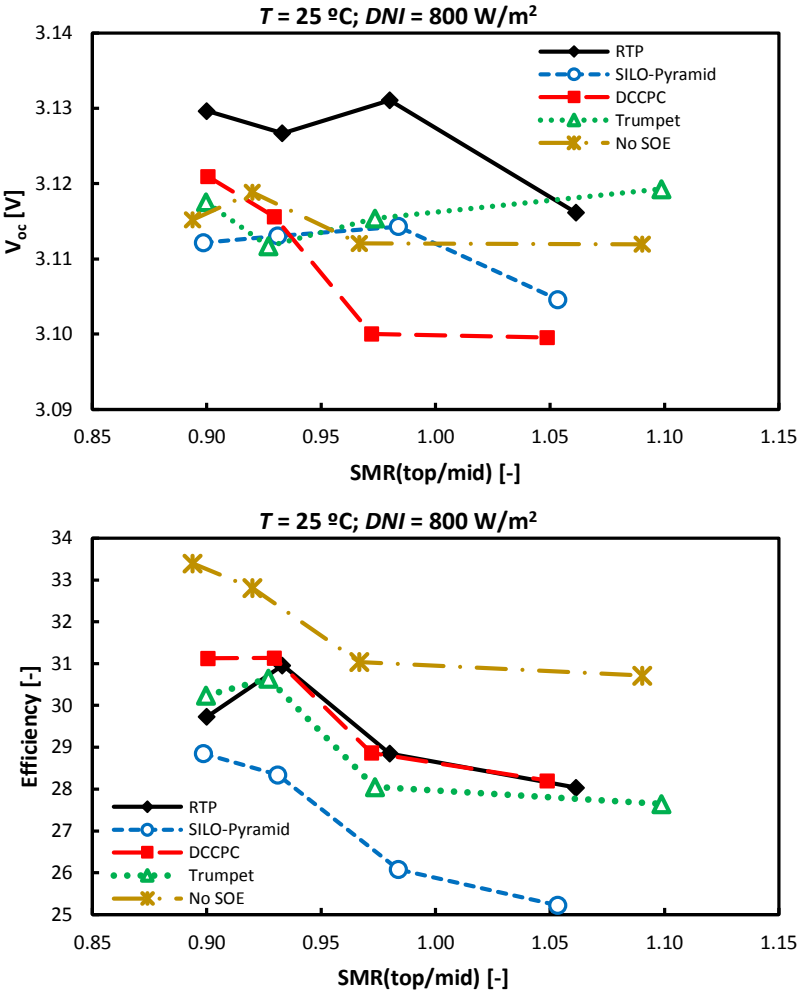

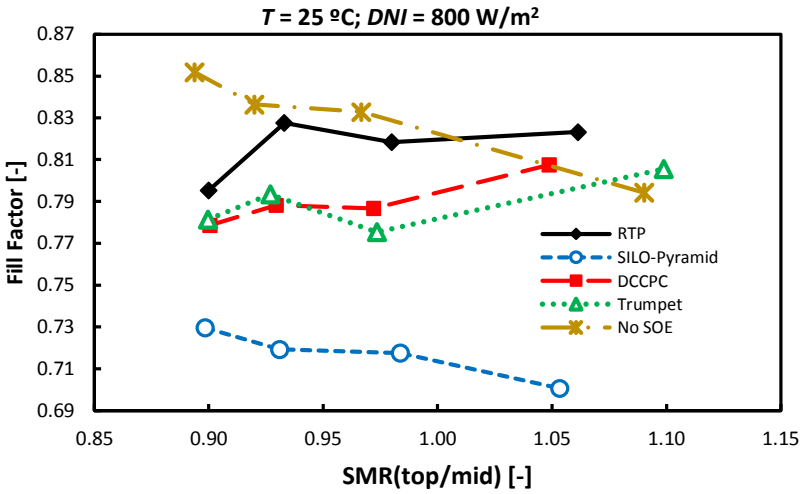

Figure 13. I-V curve electrical parameters of all the analysed units for a fixed *DNI* = 800 W/m^2 versus the spectral conditions.

5. Conclusions and future works

Four different refractive secondary optical elements (SOEs) were manufactured and mounted on commercial Concentrator Photovoltaic (CPV) assemblies to build four Fresnel-based high-CPC (HCPV) units. These SOEs were made of PMMA (poly(methyl-methacrylate)) and glued to the concentrator solar cells by using an optical silicone. These HCPV units were indoors characterised under controlled conditions by using the CPV solar simulator "Helios 3198". In addition a HCPV unit without SOE was characterised in order to differentiate the impact of the SOEs in the measured performances. All the HCPV units were measured at reference conditions (1000 W/m^2 of irradiance, ambient temperature of 25 ºC, and spectral conditions similar to AM1.5D ASTM G173-03). Considering the efficiency and the acceptance angle of the units and the optical efficiency of the SOEs, none of the units showed much better results than the others. For instance, the lowest optical efficiency was given by the RTP SOE, however, the RTP unit achieved the second best efficiency value among the SOE units. On the contrary, the SILO-Pyramid unit yielded the worst efficiency value although the highest SOE optical efficiency. Therefore, the performance of the unit at maximum power point is not directly comparable with the optical efficiency of the SOE. All the SOE units showed a good match with the optical simulations in terms of their optical efficiency (with an average of measured values of around 93%). However, the Fresnel lens performed a much lower optical efficiency (~ 80%) than in the simulations.

Acceptance angle characterisation was performed for all the units and at different irradiance and spectral conditions and plotted for all the basic electrical parameters of the I-V curves (I_{sc}, P_{mp}, FF and V_{oc}). I_{sc} acceptance angle of the RTP unit was in a good match with that of the optical simulations (~ 1.1º), but the rest of the SOE units showed lower acceptance angle values than in the simulations. Regarding the acceptance angle curve of the optical efficiency, all the units provided similar shapes with respect to the tilt angle than in the optical simulations except for the DCCPC unit.

In general, no trend was found for the acceptance angle values measured when varying only the irradiance and when changing only the spectral conditions, for all these Fresnel-based HCPV units, except for the RTP and Trumpet units, with relative minimum acceptance angle values at a spectral matching ratio (*SMR*) (top/mid) of ~ 0.98.

Regarding the electrical parameters, V_{oc}, *FF* and efficiency were also investigated at different irradiance and spectral conditions. No clear trends are found respect to the irradiance, except for V_{oc} with a logarithmic dependence, as well as no trends are found respect to the spectral conditions. However, the efficiency of all the units decreases for *SMR(top/mid)* greater than ~ 1.0. In relation to the general performance of these SOEs, the RTP unit presented the best balanced measured performance when considering its high efficiency and acceptance angle relative to the other units.

For future experimental works, the measurement of the illumination uniformity at the exit surface of the SOEs will help to a better understanding of the performance of the refractive SOEs. Moreover, the found differences in the acceptance angle of many of the SOE units has to be investigated in order to improve both the experimental setup and the optical modelling, as well as in the case of the performance of the Fresnel lens.

6. Funding

European Regional Development Fund (ERDF) and Spanish Economy Ministry (ENE2016-78251-R); Universidad de Jaén (UJA) and Caja Rural de Jaén (UJA2015/07/01).

7. Acknowledgments

The authors thank Lambda Research Corporation for its donation of TracePro optical software.

8. References

[1] M. Yamaguchi, T. Takamoto and K. Araki, “Super high-efficiency multi-junction and concentrator solar cells,” *Solar Energy Materials and Solar Cells*, vol. 90, p. 3068–3077, 2006.

[2] S. Philipps and W. Warmuth, “Photovoltaics report,” Fraunhofer Institute for Solar Energy Systems, ISE, 2017.

[3] D. Talavera, J. Ferrer-Rodríguez, P. Pérez-Higueras, J. Terrados and E. Fernández, “A worldwide assessment of levelised cost of electricity of HCPV systems,” *Energy Convers. Manag.*, vol. 127, p. 679–692, 2016.

[4] D. Miller and S. R. Kurtz, “Durability of Fresnel lenses: A review specific to the concentrating photovoltaic application,” *Solar Energy Materials and Solar Cells*, vol. 95, p. 2037–2068, 2011.

[5] P. Pérez-Higueras and E. Fernández, High Concentrator Photovoltaics: Fundamentals, Engineering and Power Plants, Springer International Publishing, 2015.

[6] M. Victoria, C. Domínguez, I. Antón and G. Sala, “Comparative analysis of different secondary optical elements for aspheric primary lenses,” *Optics Express*, vol. 17, no. 8, p. 6487–6492, 2009.

[7] P. Espinet-González, R. Mohedano, I. García, P. Zamora, I. Rey-Stolle, P. Benitez, C. Algora, A. Cvetkovic, M. Hernández, J. Chaves, J. Miñano and Y. Li, "Triple-junction solar cell performance under Fresnel-based concentrators taking into account chromatic aberration and off-axis operation," *AIP Conference Proceedings*, vol. 1477, pp. 81-84, 2012.

[8] Y. Chen and H. Chiang, "Design of the Secondary Optical Elements for Concentrated Photovoltaic Units with Fresnel Lenses," *Applied Sciences*, vol. 5, no. 4, p. 770–786, 2015.

[9] T. Schmid, T. Hornung and P. Nitz, “Indoor characterization of secondary optical elements,” *AIP Conf. Proc.*, no. 1477, p. 85–88, 2012.

[10] T. Schmid, M. Wiesenfarth, T. Hornung, M. Gremmelspacher, P. Manns and P. Nitz, "Mass manufactured secondary optics for CPV," *AIP Conference Proceedings*, no. 1616, p. 84–87, 2014.

[11] R. Herrero, M. Victoria, C. Domínguez, S. Askins, I. Antón and G. Sala, “Concentration photovoltaic optical system irradiance distribution measurements and its effect on multi-junction solar cells,” *Prog. Photovoltaics: Res. Appl.*, vol. 20, p. 6–11, 2011.

[12] P. Zamora, P. Benítez, R. Mohedano, A. Cvetković, J. Vilaplana, M. Li, M. Hernández, J. Chaves and J. Miñano,

"Experimental characterization of Fresnel-Köhler concentrators," *Journal of Photonics for Energy* , vol. 2, p. 21806, 2012.

[13] P. McVey-White, P. Besson, M. Baudrit, H. Schriemer and K. Hinzer, "Effects of lens temperature on irradiance profile and chromatic aberration for CPV optics," *AIP Conf. Proc.*, no. 1766, p. 0–6, 2016.

[14] C. Domínguez, G. Antón and S. Askins, "Current-matching estimation for multijunction cells within a CPV module by means of component cells," *Prog. Photovoltaics: Res. Appl.*, vol. 21, no. 7, p. 1478–1488, 2013.

[15] R. Herrero, M. Victoria, C. Domínguez, S. Askins, I. Antón and G. Sala, "Understanding causes and effects of non-uniform light distributions on multi-junction solar cells: Procedures for estimating efficiency losses," *AIP Conf. Proc.*, vol. 1679, pp. 50006-1–7, 2015.

[16] K. Shanks, N. Sarmah, J. P. Ferrer-Rodríguez, S. Senthilarasu, K. S. Reddy, E. F. Fernández and T. Mallick, "Theoretical Investigation Considering Manufacturing Errors of a High Concentrating Photovoltaic of Cassegrain design and its Experimental Validation," *Solar Energy*, vol. 131, p. 235–245, 2016.

[17] M. Renzi, L. Cioccolanti, G. Barazza, L. Egidi and G. Comodi, "Design and experimental test of refractive secondary optics on the electrical performance of a 3-junction cell used in CPV systems," *Applied Energy*, vol. 185, p. 233–243, 2016.

[18] J. Ferrer-Rodríguez, H. Baig, E. Fernández, F. Almonacid, T. Mallick and P. Pérez-Higueras, "Optical modeling of four Fresnel-based high-CPV units," *Solar Energy*, vol. 155, p. 805–815, 2017.

[19] N. Sellami and T. Mallick, "Optical efficiency study of PV Crossed Compound Parabolic Concentrator," *Applied Energy*, vol. 102, p. 868–876, 2013.

[20] K. Chong, T. Yew, C. Wong, M. Tan, W. Tan and B. Lim, "Dense-array concentrator photovoltaic prototype using non-imaging dish concentrator and an array of cross compound parabolic concentrators," *Applied Energy*, vol. 204, p. 898–911, 2017.

[21] S. Askins, M. Victoria, R. Herrero, C. Domínguez, I. Antón and G. Sala, "Hybrid dome with total internal reflector as a secondary optical element for CPV," *AIP Conference Proceedings*, no. 1766, pp. 050002-1–050002-6;, 2016.

[22] P. Rodrigo, E. Fernández, F. Almonacid and P. Pérez-Higueras, "Review of methods for the calculation of cell temperature in high concentration photovoltaic modules for electrical characterization," *Renew. Sustain. Energy Rev.*, vol. 38, p. 478–488, 2014.

[23] "Orafol Fresnel Optics GmbH," [Online]. Available: www.orafol.com.

[24] G. Beadie, M. Brindza, R. Flynn, A. Rosenberg and J. Shirk, "Refractive index measurements of poly(methyl-methacrylate) (PMMA) from 0.4–1.6μm," *Applied Optics*, vol. 54, no. 31, 2015.

[25] H. Baig, N. Sellami and T. Mallick, "Trapping light escaping from the edges of the optical element in a Concentrating Photovoltaic system. Energy Conversion and Management," *Energy Conversion and Management*, vol. 80, p. 238–246, 2015.

[26] Azure Space Solar Power GmbH, "Enhanced Fresnel Assembly - EFA Type: 3C42A – with 5.5x5.5mm2 CPV TJ Solar Cell Application: Concentrating Photovoltaic (CPV) Modules," 2014. [Online]. Available: www.azurspace.com/images/products/DB_3988-00-00_3C42_AzurDesign_EFA_55x55_2014-03-27.pdf. [Accessed 27 11 2017].

[27] E. Fernández, J. Ferrer-Rodríguez, F. Almonacid and P. Pérez-Higueras, "Current-voltage dynamics of multi-junction CPV modules under different irradiance levels," *Solar Energy*, vol. 155, p. 39–50, 2017.

[28] C. Domínguez, I. Antón and G. Sala, "Solar simulator for concentrator photovoltaic systems," *Optics Express*, vol. 16, no. 19, p. 14894–14901, 2008.

[29] "Solar Added Value S.L.," [Online]. Available: http://solaraddedvalue.com/en/category/productos/helios-3198/.

[30] P. Rodrigo, E. Fernández, F. Almonacid and P. Pérez-Higueras, "Quantification of the spectral coupling of atmosphere and photovoltaic system performance: Indexes, methods and impact on energy harvesting," *Solar Energy Materials and Solar Cells*, vol. 163, p. 73–90, 2017.

[31] E. F. Fernández, F. Almonacid, J. A. Ruiz-Arias and A. & Soria-Moya, "Analysis of the spectral variations on the performance of high concentrator photovoltaic modules operating under different real climate conditions," *Solar Energy Materials and Solar Cells*, vol. 127, p. 179–187, 2014.

[32] G. Kinsey and K. Edmondson, "Spectral Response and Energy Output of Concentrator Multijunction Solar Cells," *Prog. Photovolt: Res. Appl.*, no. 17, p. 279–288, 2009.

[33] J. Egger, "Use of Fresnel lenses in optical systems: some of some advantages and limitations," *SPIE Optical Systems Enginnering*, vol. 193, p. 63–69, 1979.

[34] H. Baig, K. Heasman and T. Mallick, “Non-uniform Illumination in Concentrating Solar Cells,” *Renewable and Sustainable Energy Reviews*, vol. 16, pp. 5890-5909, 2012.

[35] P. Benitez, J. Miñano, P. Zamora, R. Mohedano, A. Cvetkovic, M. Buljan, J. Chaves and M. Hernández, “High performance Fresnel-based photovoltaic concentrator,” *Optics Express*, vol. 18, no. S1, pp. A25-A40, 2010.

[36] K. Araki, R. Herrero, I. Antón, G. Sala, H. Nagai, K. Lee and M. Yamaguchi, “Why are acceptance angle of P m and I sc different in spite of uniform illumination onto concentrator solar cells ?,” *IEEE Photovolt. Spec. Conf.*, p. 549–553, 2016.

Optics Letters

Optical design of a 4-off-axis-unit Cassegrain ultra-high concentrator photovoltaics module with a central receiver

Juan P. Ferrer-Rodríguez,* Eduardo F. Fernández, Florencia Almonacid, and Pedro Pérez-Higueras

IDEA Solar Research Group, Center for Advanced Studies in Energy and Environment (CEAEMA), Universidad de Jaén, Las Lagunillas Campus, 23071 Jaén, Spain
**Corresponding author: jferrer@jaen.es*

Received 14 March 2016; revised 29 March 2016; accepted 29 March 2016; posted 30 March 2016 (Doc. ID 259645); published 21 April 2016

Ultra-high concentrator photovoltaics (UHCPV), with concentrations higher than 1000 suns, have been pointed out by different authors as having great potential for being a cost-effective PV technology. This Letter presents a UHCPV Cassegrain-based optical design in which the sunrays are concentrated and sent from four different and independent paraboloid–hyperboloid pairs optical units onto a single central receiver. The optical design proposed has the main advantage of the achievement of ultra-high concentration ratios using relative small mirrors with similar performance values of efficiency, acceptance angle, and irradiance uniformity to other designs.

OCIS codes: (080.2740) Geometric optical design; (350.6050) Solar energy; (220.1770) Concentrators; (220.4298) Nonimaging optics; (040.5350) Photovoltaic.

http://dx.doi.org/10.1364/OL.41.001985

Concentrator photovoltaic (CPV) technology presents some advantages with respect to other renewable energy ones (efficiency, etc.), however, CPV systems have to be improved in order to be a more competitive technology [1,2]. Different authors have pointed out the advantages and potential in terms of cost reduction of ultra-high CPV (UHCPV) systems with effective concentration ratios equal to or higher than 1000 suns [3]. Despite such excellent potential, different technological barriers must be eliminated at such elevated concentration levels, namely, (1) to develop solar cells with efficiencies peaking at irradiance values higher than 1000 suns [4], (2) to design a suitable cooling mechanism capable of removing the high heat power density generated by the cells [5,6], and (3) to develop optical designs able to reach UH concentration levels with an adequate optical performance [7]. This Letter is focused on this last concern.

In relation to the optical systems involved in the UHCPV, the use of Fresnel lenses seems to limit the effective concentration ratio at around 1000 suns due to the chromatic aberration [8]. Moreover, the use of mirrors offers a promising alternative solution to get UH fluxes, since they are not limited by the chromatic aberration [9]. However, they have the disadvantage in that large mirrors are usually required [10]. Hence, they are affected by the common problems involved in the fabrication of large reflective optical devices: they are usually expensive and difficult to manufacture [11].

In this Letter, a UHCPV module based on a new optical design that concentrates sunrays from different and independent optical units onto the same single solar cell is proposed. This approach resembles telescopes based on segmented mirrors and is intended to avoid the use of large reflective optical devices. The aim is to offer an alternative optical solution to those currently being discussed in the literature in order to develop successful UHCPV systems [7]. In this work, Cassegrain-based concentrators are considered as concentrators on account of their achromatism and ultra-compactness [12,13]. Other concentrators are also based on using pairs of primary-secondary reflective elements, some of them are compact and reach and maximum performance [14]. Moreover, the design exposed in this Letter utilizes the well-known Köhler technique to produce uniform illumination on a target [15].

The proposed design is based on an adaptation of the Cassegrain concept and consists of a kind of off-axis Cassegrain design. The sunray's concentration is performed after three optical steps in each optical unit [see the two-dimensional (2D) sketch in Fig. 1]. (1) The incoming parallel sunrays reach the primary optics and are reflected on the concave paraboloid of the revolution mirror surface (primary optical element, POE). Since these rays are parallel to the paraboloid's optical axis, then they are focused toward the focus (F). (2) The convex hyperboloid of the revolution mirror surface (secondary optical element, SOE) reflects and focuses the sunrays toward its far focus (G) (it is located inside the homogenizer), since the sunrays of step 1 converge to its near focus (F). The POE and SOE are optically coupled, since both the paraboloid's focus and the near hyperboloid's focus coincide at the same three-coordinate point. (3) The sunrays of step 2 are refracted by the homogenizer (tertiary optical element, TOE) and spread on the cell's

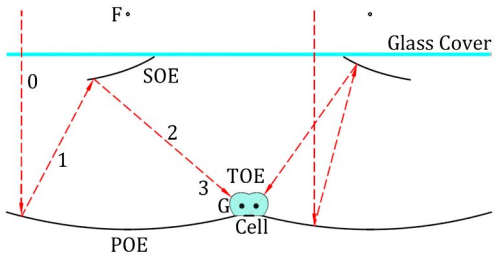

Fig. 1. Two-dimensional sketch of the rays' paths for the transverse section of two optical units through a module's diagonal. (0) Incoming sunrays; (1) reflected rays on the primary optics; (2) reflected rays on the secondary optics; (3) rays transmitted through the tertiary optics and impinging the solar cell. The foci of the two-sheeted circular hyperboloid are (F) and (G), where (F) is also the circular paraboloid's focus.

surface. The homogenizer's optical active surface is a Cartesian oval of revolution optically coupled to the hyperboloid mirror.

The module presented in this Letter is composed of four symmetrical and independent optical units (see Fig. 2) with the axis of symmetry being normal through the center of the solar cell's plane. Each optical unit is based on the adaptation of the Cassegrain design described above (see Fig. 1) and consists of a set of three optical elements: one square paraboloid mirror (POE), one trimmed (resulting in four edges) hyperboloid mirror (SOE), and one Cartesian oval of revolution (TOE). The homogenizer is the assembly of the four Cartesian ovals of revolution (one for each optical unit) and functions as a Köhler integrator, thus, it contributes to spreading out the sunrays onto the solar cell [16] [as it is shown in Fig. 2(b)]. Each Cartesian oval of revolution couples the more external vertex of each secondary mirror with each vertex of the opposite side of the solar cell [17]. In more detail, each POE mirror is based on a circular paraboloid described as

$$\frac{x^2}{24.5^2}+\frac{y^2}{24.5^2}-z=0. \tag{1}$$

Whereas each secondary mirror is based on the open upwards sheet of a two-sheeted circular hyperboloid, which can be described as

$$\frac{x^2}{64.5^2}+\frac{y^2}{64.5^2}-\frac{z^2}{42.5^2}=-1, \tag{2}$$

where x, y, and z are in millimeters. In the case of the design proposed, the SOE's shape has been trimmed by the contour of the light beam that impinges its reflecting surface. The shape of each Cartesian oval of revolution has as the generatrix curve as the locus resulting after solving the differential equation of conservation of the optical path length of any ray trajectory between a vertex of the solar cell and the opposite vertex of the correspondent secondary mirror. The generatrix curve is then revolved around the axis defined between the two vertexes. The height of each individual solid Cartesian oval of revolution along its longitudinal axis is chosen to be 20 mm from its basis—the basis matches the correspondent solar cell vertex. The location of the far focus of the SOE mirror has as relative positive Cartesian coordinates, with respect to the solar cell surface's center (which is 10 mm over the plane, defined by the centers of the POE mirrors), the next values: $(x, y, z) = (3.54, 6, 3.54)$ mm. The module has symmetry around the normal at the solar cell's center in steps of 90°, i.e., each of the four optical units corresponds to an identical quadrant portion of the module. For the simulations, a glass frontal exterior covering, needed to protect the module against soiling, water, etc., is also included. The SOE mirrors can be fixed to the interior side of the glass covering by adding a small support like a cylinder.

The geometrical concentration ratio is $C_g = 2304X$, since the cell is of 5 × mm × 5 mm and each paraboloid mirror is of 120 × mm × 120 mm. Each paraboloid is of 150 mm focal distance. For each hyperboloid, the far focus is at 120 mm in front of the mirror (front focal distance) and the near focus is 35 mm back from the mirror (back focal distance). The module has a depth of 123 mm.

The optical simulation was performed by simulating the solar ray's source, taking into account the solar angular profile (4.65 mrad) and also, the solar spectral distribution of energy (for simplicity, extra-terrestrial spectrum ASTM E-490-00). For both optical design and simulations, the software TracePro was used. Figure 2 shows the ray tracing and the sunray's concentration from the four different optical units to the same target. The planar frontal glass covering is simulated as fused silica. All the mirrors have been simulated as "standard mirror" in TracePro. It corresponds to a surface with the next flux coefficients: absorptance = 0.05, specular reflectivity = 0.949, and integrated bidirectional reflectance distribution function (BRDF) = 0.001324 using the ABg scatter model. The homogenizer is simulated as if made of B270 glass and the solar cell as the perfect absorber.

From the optical simulation, the optical efficiency of this design, defined as the ratio between the power reaching the solar cell over the module's incoming power, results $\eta = 73\%$, resulting an effective concentration ratio of 1682 suns. If the

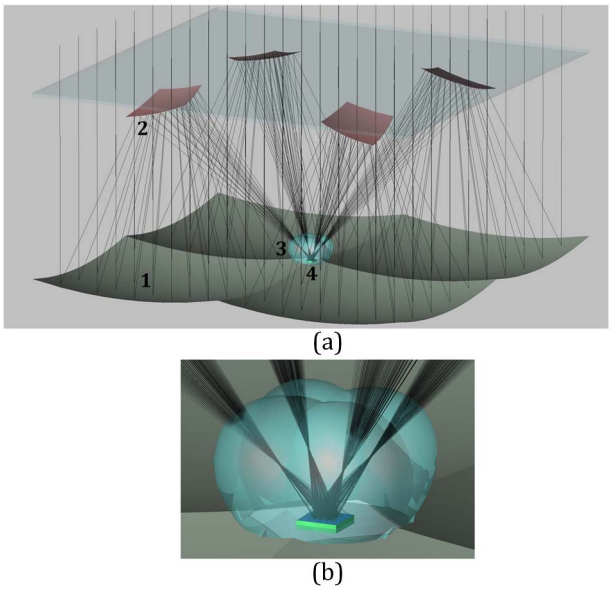

Fig. 2. (a) Model and ray tracing of the Cassegrain 4-optical-unit module with the central receiver. The elements are marked: (1) paraboloid mirrors (POE), (2) hyperboloid mirrors (SOE), (3) homogenizer (TOE), and (4) solar cell. (b) Detail of ray tracing at the central receiver.

glass covering is not considered, the calculation of the efficiency increases up to 79%. The 3D irradiance map on the cell is not completely uniform and has a relative small "hole" (less irradiance in the cell's center than in its surroundings, see Fig. 3). The irradiance distribution on the solar cell reaches a maximum of 5480 suns and has an average value of 1682 suns; when simulating an incoming power of 1000 W/m^2–the maximum value is around 3.3 times higher than the average one. Each of the four rays' beams is impinging on the solar cell with an average angle of approximately 30° with respect to the normal at the solar cell's surface.

In Fig. 4, the effective acceptance angle characteristic (considering the finite angular aperture of the sun) of the whole optical system is presented. The relative transmission efficiency of 0.9 (relative to the maximum optical efficiency value) corresponds to a misalignment angle of 0.61°. From this value, the effective concentration-acceptance angle product (CAP*) can be calculated, resulting 0.51.

The summary of the simulation results of this 4-optical-unit design module and its geometrical parameters are presented in Table 1.

The values shown in Table 1 are similar compared to the optical performance results of other Cassegrain designs [18–22] for which the optical efficiency ranges from 0.62 [18] to 0.85 [21], CAP* values vary from 0.36 [18] to 0.47 [21], and the geometrical concentration ratio is between 500× [21] and 1057× [19]—much lower than in the design proposed. In relation to the irradiance distribution over the solar cell, the two best designs, among the above cited ones, are a two-mirror Köhler-based design with a cell's irradiance maximum over average value near to 2.6 [22], and a Cassegrain-based design with a kaleidoscope homogenizer with a value near to 1.4 [21].

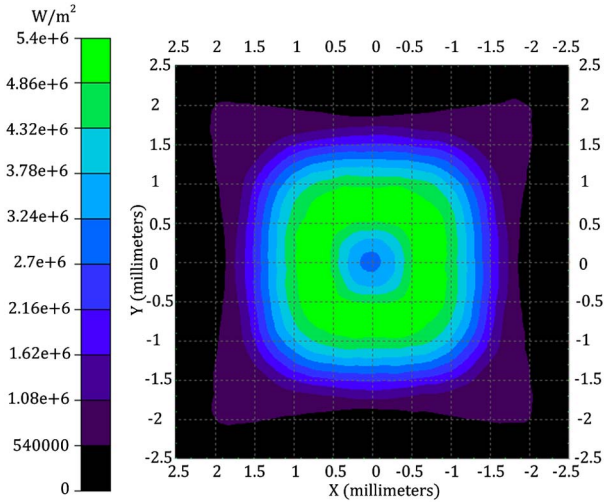

Fig. 3. Irradiance map of the incident rays on the solar cell.

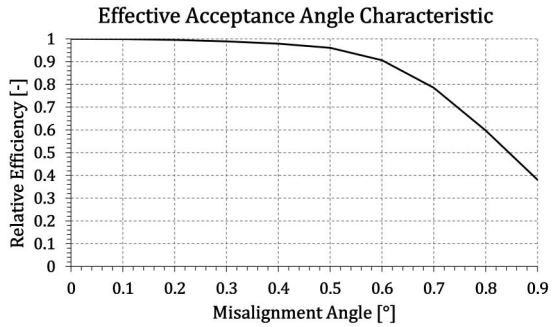

Fig. 4. Effective acceptance angle characteristics of the design.

Table 1. Summary of Geometrical and Simulation Parameters

Magnitude	Value
Geometrical Concentration Ratio [–]	2304
Optical Efficiency [–]	0.73
Effective Concentration [suns]	1682
Effective Acceptance Angle [°]	0.61
Effective Concentration-Angle Product [–]	0.51
Optical Efficiency without Glass Covering [–]	0.79
Cell's Irradiance Maximum [suns]	5480
Cell's Irradiance Maximum over Average [–]	3.3

Concerning the optical efficiency of the design, the global optical efficiency losses are explained in terms of the next factors: (1) transmission through the planar frontal glass covering, (2) the shadow of the SOE and (3) TOE, (4) the metallic reflection on the POE and (5) SOE, and (6) the transmission through the TOE. For each loss factor, an optical efficiency, η_i, and the associated optical losses, $\text{Losses}_i = 1 - \eta_i$, can be defined. The global optical efficiency, η_{global}, can be expressed as

$$\eta_{\text{global}} = \prod_{i=1}^{i=6} \eta_i = 0.73, \tag{3}$$

where $i = 1$ to 6 corresponds to each loss factor item in Table 2. The global losses can be calculated as $\text{Losses}_{\text{global}} = 1 - \eta_{\text{global}} = 0.27$. The correspondent optical efficiencies for each loss factor, and the associated optical losses, are listed in Table 2.

Both the SOE and TOE shadowing are shrinkable. Reducing the near focal distance of each SOE, the useful mirror area will decrease. Nevertheless, due to the conservation of the étendue, the sunrays' focalization at the SOE's far focus will be worse, and this has to be considered as a trade-off between both characteristics. Concerning the TOE shadowing, the size of each Cartesian oval of revolution can be reduced in the trade-off with the acceptance angle characteristic of the module.

It is important to note that, although the proposed design may be relatively complex due to the relatively high number of optical elements needed, it offers some important opportunities. This design is a way of reaching UH concentration ratios

Table 2. Detailed List of Optical Losses

	Optical Efficiency [–]	Optical Losses [%]
1. Glass Cover Transmission	0.931	6.9
2. SOE Shadowing	0.925	7.5
3. TOE Shadowing	0.991	0.9
4. POE Reflectance	0.949	5.1
5. SOE Reflectance	0.949	5.1
6. TOE Transmission	0.955	4.5
Global	0.73	27

while avoiding the use of large concentrating mirrors which are, apparently, more expensive and difficult to fabricate than smaller ones, as previously stated [10,11]. Moreover, the height of the POE is reduced 75% (36 mm) when compared with having only one single parabolic mirror of the same focal distance. Furthermore, since the POE and SOE are quadric surfaces, they may be easier to be manufactured, in general, than freeform surfaces if these last do not have a symmetry axis [23]. Another opportunity of this design is derived from the use of a Köhler-based homogenizer, which provides more degrees of freedom in the optical design.

In analyzing the compactness of this design, the more compact this design is the higher the incident angle of rays over the cell, and therefore, Fresnel losses on the cell are higher. However, the relative low rays' incident angle on the solar cell's plane is a guarantee of not having significant Fresnel reflecting losses at the solar cell's surface [24]. Another limitation is related to the conservation of the étendue, since it contributes to spread out the concentrated sunrays. This is more evident if the design is tuned to reduce the size of the SOE mirrors in order to decrease the shadowing losses.

Considering the maximum concentration value over the solar cell (see Fig. 3), it does not represent a problem for up-to-date HCPV solar cells in terms of their reliability which some authors demonstrated by measuring triple-junction cells at very high concentration ratios, even up to around 1×10^4 suns [25]. The maximum irradiance value of the proposed design results in less than four times the average irradiance on the solar cell, a value that is slightly higher than other designs, as it was mentioned above. This value should be improved in future designs, since it may have an impact on the fill factor of the solar cell's I–V curve, and therefore, reduce the efficiency of the whole concentrator module [26]. As can be seen in Fig. 3, the irradiance pattern on the cell's surface has a 90° step symmetry, since the four irradiance patterns of the four optical units are summed on the solar cell's surface. The impact of the shadow of each SOE on the total irradiance distribution leads to a central region with lower values than its surroundings [16].

In order to improve the optical performance of this design, different variations of primary and secondary mirrors' focal distances can be explored. Also, the calculation of the homogenizer can be varied, due to the degrees of freedom existing in the design, in searching for an improvement of both irradiance uniformity and acceptance angle.

In conclusion, a new UHCPV (i.e., effective concentration higher than 1000 suns) module design based on the Cassegrain design (pair paraboloid–hyperboloid) with four optical units around a central receiver has been designed. Each one of these optical units is an adaptation of the conventional Cassegrain design in order to send the sunrays out of the axis defined by the paraboloid mirrors (primary optics). The effective CAP* of the design is relatively good at 0.51 with an effective acceptance angle of 0.61°. The optical efficiency is 73%, the geometrical concentration ratio is 2304×, and the effective concentration value is 1682 suns. Without considering the covering glass, the optical efficiency is 79%. These simulation results assure the optical feasibility of the design concept implemented in this Letter. The UHCPV module's proposed optical design represents a good trade-off between the acceptance angle and irradiance uniformity, having similar optical performance values to other designs, while avoiding the use of relatively large concentrating mirrors.

Funding. European Regional Development Fund (ERDF) and Spanish Economy Ministry (ENE2013-45242-R); Universidad de Jaén (UJA) and Caja Rural de Jaén (UJA2015/07/01).

Acknowledgment. The authors thank Lambda Research Corporation for its donation of TracePro optical software. The authors also thank Dr. Miguel A. Rubio-Paramio for his collaboration.

REFERENCES

1. P. Pérez-Higueras and E. F. Fernández, *High Concentrator Photovoltaics: Fundamentals, Engineering and Power Plants* (Springer, 2015).
2. D. Talavera, P. Pérez-Higueras, J. Ruíz-Arias, and E. F. Fernández, Appl. Energy **151**, 49 (2015).
3. C. Algora and I. Rey-Stolle, in *Next Generation of Photovoltaics* (Springer, 2012), pp. 23–60.
4. E. F. Fernández, A. García-Loureiro, and G. Smestad, in *High Concentrator Photovoltaics: Fundamentals, Engineering and Power Plants* (Springer, 2015), pp. 9–37.
5. L. Micheli, E. F. Fernández, F. Almonacid, K. Reddy, and T. Mallick, AIP Conf. Proc. **1679**, 130003 (2015).
6. L. Micheli, E. F. Fernández, F. Almonacid, K. Reddy, and T. Mallick, in *42nd IEEE Photovoltaic Specialist Conference (PVSC)* (IEEE, 2015), pp. 1–6.
7. K. Shanks, S. Senthilarasu, and T. K. Mallick, Renewable Sustainable Energy Rev. **60**, 394 (2016).
8. F. Languy, K. Fleury, C. Lenaeerts, J. Loicq, D. Regaert, and T. Thibert, Opt. Express **19**, A280 (2011).
9. K. Shanks, S. Senthilarasu, and T. Mallick, in *High Concentrator Photovoltaics: Fundamentals, Engineering and Power Plants* (Springer, 2015), pp. 85–113.
10. K. Lovegrove, G. Burgess, and J. Pye, Sol. Energy **85**, 620 (2011).
11. D. Malacara and B. J. Thomsom, *Handbook of Optical Engineering* (CRC Press, 2001).
12. R. Winston and J. M. Gordon, Opt. Lett. **30**, 2617 (2005).
13. K. Shanks, N. Sarmah, J. P. Ferrer-Rodriguez, S. Senthilarasu, K. S. Reddy, E. F. Fernández, and T. Mallick, Sol. Energy **131**, 235 (2016).
14. A. Goldstein, D. Feuermann, G. Conley, and J. Gordon, Opt. Lett. **36**, 2836 (2011).
15. R. Wiston, J. Miñano, and P. Benítez, *Nonimaging Optics* (Elsevier, 2005).
16. R. Winston and W. Zhang, AIP Conf. Proc. **1407**, 105 (2011).
17. M. Hernandez, A. Cvetkovic, P. Benitez, and J. Minano, Proc. SPIE **7059**, 705908 (2008).
18. C. Liang and J. Lin, Sol. Energy **122**, 264 (2015).
19. M. Dreger, M. Wiesenfarth, A. Kisser, T. Schmid, and A. Bett, in *Proceedings of CPV-10 Conference* (2014), Vol. **177**.
20. P. Benitez, A. Cvetkovic, R. Winston, L. Reed, J. Cisneros, A. Tovar, A. Ritschel, and J. Wright, in *Conference Record of the 2006 IEEE 4th World Conference on Photovoltaic Energy Conversion* (IEEE, 2006), pp. 690–693.
21. K. Shanks, N. Sarmah, K. Reddy, and T. Mallick, AIP Conf. Proc. **1616**, 211 (2014).
22. R. Winston, P. Benitez, and A. Cvetkovic, Proc. SPIE **6342**, 634213 (2006).
23. M. Nijkerk, O. Van der Togt-Marinescu, and G. Gubbels, "Freeform design and fabrication : where the proof of the pudding is in verification," in *International Conference on Space Optics*, Rhodes, Greece, 2010.
24. A. Bäuerle, A. Bruneton, J. Wester, J. Stollenwerk, and P. Loosen, Opt. Express **20**, 14477 (2012).
25. J. Gordon, E. Katz, D. Feuermann, and M. Huleihil, Appl. Phys. Lett. **84**, 3642 (2004).
26. H. Baig, K. Heasman, and T. Mallick, Renewable Sustainable Energy Rev. **16**, 5890 (2012).